EXPERIMENTAL STUDY ON THERMO-HYDRO-MECHANICAL BEHAVIOUR OF COMPACTED KAOLIN CLAY

BY

OGECHI CHINONYE MARY ILEME

Submitted for the Degree of Doctor of Philosophy
(Civil Engineering)

School of Energy, Geoscience, Infrastructure and Society

Heriot-Watt University

June, 2017

ABSTRACT

Several engineering problems are associated with unsaturated soils that are subjected to high temperature due to the environments where they are located or activities around them. Typical examples include upper layers of soils in tropical regions, soils around geothermal structures, landfill liners and clay barriers around nuclear waste repository systems. Previous researchers have reported that variations in stress, suction and temperature affect the mechanical behaviour of unsaturated soils. Notwithstanding already existing studies, the influence of temperature on some unsaturated soils is still a challenge relative to saturated soils, as the results from these existing studies are soil specific and cannot be inferred as the behaviour of all unsaturated soils. A sound understanding of the behaviour of unsaturated kaolin clay without a hydraulic history under temperature and suction variation is still required.

The main objective of this study was to investigate the influence of temperature variations on the volumetric and water retention behaviours of statically compacted kaolin clay. Statically compacted samples at a dry side of optimum were tested at different temperatures, using standard and suction controlled oedometer cells, to investigate the influence of temperature on volumetric behaviours. The tests were carried out considering various stress paths. Additionally, pressure plate and vapour equilibrium tests were carried out following a drying path at two temperatures and void ratios to investigate the influence of temperature and densities on the water retention of statically compacted kaolin clay. Complimentary tests were carried out to investigate the effect of temperature variation on overall volume and suction, through the filter paper method.

Either collapse or expansion occurred on wetting, depending on the density of the sample. Compressibility was found to increase with an increase in temperature. For tests at constant suction, increase in temperature was found to increase compressibility at low suction, but compressibility was unaffected by temperature at high suction. The results when presented in the light of LC model, indicated a shift of the LC curve to the left at high temperature. The study demonstrated that temperature variation alone was sufficient to vary suction and volume. Features captured on other soils were also identified; for example, yield stress was found to increase with suction. Water retention was observed to decrease with an increase in temperature and increase with void ratio (along the capillary fringe). Good fits were observed, when pertinent soil water retention models were fitted to the obtained water retention data. The study noted that the hydro-mechanical behaviour of a sample prepared at the wet of optimum water content is significantly different from dry of optimum sample and this should be considered when predicting soil behaviour. The study also demonstrated that increase in temperature will affect samples without hydraulic history differently. Further work is still required on an extended range of temperature and suction.

To my Lord and my God

ACKNOWLEDGEMENT

This research was supported by the School of Built Environment, Heriot-Watt University.

I would like to express my sincere gratitude to my supervisors, Dr. Gabriela Medero and Professor P. K. Woodward, for giving me the opportunity to work with them and for their immense support throughout the research period. I am very appreciative of their patience with me, especially during the birth of my child.

I am immensely grateful to Professor John McCarter for taking time to read part of the thesis and for giving useful feedback.

Special thanks to Dr J. Sun and Dr A. Cuthbertson for their feedbacks.

I am indebted to the staff members of the School of Built Environment, particularly the technicians: Alastair, for your encouragement and immense support, especially with calibration of equipment; Tom and David for helping with the oedometer cell and fabricating auxiliary equipment needed for the experimental programme. Special thanks are due to the SBE research team for their help regarding administrative issues.

I would also like to acknowledge other researchers linked to the unsaturated soils network: particularly Gilbert Kasangaki, your explanations and discussions on experimental procedures were greatly valued; Menan, for the useful discussions, particularly on the experimental programme.

Special thanks to my colleagues and friends: Faidess, Poja, Ipshita, Isaac, Jurbe, Nawras, Solomon, Gbenga, Shei, Linda, Gom, Judith, Ikenna, Amaka, Nkechi, and Ann. Your words of encouragement were greatly appreciated.

My heartfelt gratitude to my family: sisters, brother and parents for their love, support and constant prayers. To my mum, I owe you the world for your invaluable support. Finally, my immense gratitude goes to my dearest husband Vitus Ileme and my beloved children Judith and Anthony for their sacrifices, patience, unceasing love, support and encouragement throughout the course of the study. I could not have done it without your support.

ACADEMIC REGISTRY

Research Thesis Submission

Name*:*	OGECHI CHINONYE MARY ILEME		
School/PGI:	EGIS		
Version: *(i.e. First, Resubmission, Final)*	Final	Degree Sought (Award **and** Subject area)	PhD Civil Engineering

Declaration

In accordance with the appropriate regulations I hereby submit my thesis and I declare that:

1) the thesis embodies the results of my own work and has been composed by myself
2) where appropriate, I have made acknowledgement of the work of others and have made reference to work carried out in collaboration with other persons
3) the thesis is the correct version of the thesis for submission and is the same version as any electronic versions submitted*.
4) my thesis for the award referred to, deposited in the Heriot-Watt University Library, should be made available for loan or photocopying and be available via the Institutional Repository, subject to such conditions as the Librarian may require
5) I understand that as a student of the University I am required to abide by the Regulations of the University and to conform to its discipline.

* *Please note that it is the responsibility of the candidate to ensure that the correct version of the thesis is submitted.*

Signature of Candidate*:*		Date:	10/07/2017

Submission

Submitted By *(name in capitals):*	ANTHONY OKWANANKE
Signature of Individual Submitting:	
Date Submitted:	

For Completion in the Student Service Centre (SSC)

Received in the SSC by *(name in capitals):*			
Method of Submission *(Handed in to SSC; posted through internal/external mail):*			
*E-thesis Submitted (**mandatory for final theses)***			
Signature:		Date:	

TABLE OF CONTENTS

LIST OF TABLES

LIST OF FIGURES

LIST OF ACRONYMS AND SYMBOLS

Notation	Description	Unit
Acronyms		
A	Area	m^2
A_f	Fitting parameter for Fredlund and Zing equation	-
A	Fitting parameter related to air entry value	-
a_g	Fitting parameter for Gardener's equation	-
a_m	Fitting parameter for Mualem's model	-
a_{bc}	Fitting parameter for Brooke and Corey SWRC model	-
B	Mankoc et al. (2007) fitting parameter	-
c	Apparent cohesion	kPa
c'	Effective cohesion	kPa
C	Coefficient of uniformity	-
CWC	Constant water content	-
C_Z	Coefficient grading	-
$C(\psi)$	Correction factor for Fredlund and Zing model	-
CWC	Constant water content	-
d_p	Particle size	mm
DO	Double oedometer	-
D_{10}	Particle size for which 10% is finer (effective size)	mm
D_{30}	Particle size for which 30% is finer	mm
D_{50}	Mean particle size (Particle size for which 50% is finer)	mm
D_{eq50}	Equivalent mean spherical particle diameter	mm
D_{60}	Particle size for which 60% is finer	mm
e	Void ratio	-
e_0	Initial void ratio	-
e_{ic}	Void ratio after isotropic compression	-
e_{peak}	Void ratio after isotropic compression	-
E_m	Young's modulus of elasticity for the membrane	kPa
F_s	Bonding force between particles	kPa
g	Acceleration due to gravity	ms^{-2}
h	Height of the capillary rise	m
h_s	Hydrostatic pressure head	m
k	Alonso et al. (1990) parameter describing cohesion increase with ψ	-
k_{sat}	Saturated coefficient of permeability	ms^{-1}

k_w	Coefficient of permeability	ms^{-1}
K	Lateral pressure coefficient	-
K_0	Lateral pressure coefficient at rest	-
K_a	Active lateral pressure coefficient	-
L	Separation distance between any two spheres	m
M	Critical state stress ratio (also known as slope of critical state line)	-
M_a	Critical state stress ratio with respect to $(p - u_a)$	-
M_f	Fitting parameter for Fredlund and Zing equation	-
M_b	Critical state stress ratio with respect to $(u_a - u_w)$	-
M_s	Saturated critical state stress ratio	-
m	Mass of a single particle	g
m_{vG}	Fitting parameter for van Genuchten SWRC model	-
m_m	Fitting parameter for Mualem's model	-
n	Porosity	-
n_f	Fitting parameter for Fredlund and Zing equation	-
n_{bc}	Fitting parameter for Brooke and Corey SWRC model	-
n_{vG}	Fitting parameter for van Genuchten SWRC model	-
n_m	Fitting parameter for Mualem's model	-
n_g	Fitting parameter for Gardener's eqn	-
p	Mean total stress equal to $(\sigma_1 + 2\sigma_3)/3$ for triaxial tests	kPa
p_0	Yield stress	kPa
p^c	Mean stress at which one may reach the saturated virgin state through suction unloading involving only elastic swelling	kPa
p_o*	Pre-consolidation mean stress for saturated conditions	kPa
q	Deviator stress $(\sigma_1 - \sigma_3)$	kPa
R	Universal gas constant	$Jmol^{-1}K^{-1}$
R_h	Relative humidity $(100u_v / u_{v0})$	%
r	Alonso et al. (1990) parameter defining the maximum soil stiffness	-
r_s	Radius of capillary tube	m
R_s	Radius of curvature	m
R_1, R_2	Radius of curvatures for menisci between two irregular soil particles	m
SO	Single oedometer	-
S_r	Degree of saturation	%
S_{r0}	Initial degree of saturation	%
S_{ric}	Degree of saturation after isotropic compression	%

S_{rpeak}	Degree of saturation at peak deviator stress	%
SSA	Specific surface area	cm^{-1}
T	Relative temperature in Celsius scale/absolute temperature	$^oC/K$
T_r	Reference temperature	^oC
t	Time	Sec
t_m	Membrane thickness	mm
T_s	Surface tension	Nm
u_a	Pore air pressure	kPa
u_w	Pore water pressure	kPa
$(u_a - u_w)_b$	Bubbling pressure (also known as air-entry value)	kPa
Δu	Pressure difference across the air-water interface	kPa
u_v	Partial pressure of pore water vapour	kPa
u_{v0}	Saturation pressure of water vapour over flat surface of pure water	kPa
V	Volume	m^3
w	Gravimetric water content	%
w_{opt}	Optimum moisture content	%
w_r	Residual gravimetric water content	%
w_s	Saturated gravimetric water content	%
w_w	Gravimetric water content corresponding to ψ_w	%

Notation	**Description**	**Unit**
Greek Symbols		
α	Contact angle	^{o}
α_d	Desorption (drying) contact angle	^{o}
α_w	Wetting contact angle	^{o}
α_{vG}	van Genuchten (1980) fitting parameter related to air-entry value	kPa^{-1}
β	Parameter that controls rate of increase of soil stiffness	-
β_T	Empirical coefficient fits relative viscosity data over a temperature range	
ε_a	Axial strain	%
ε_v	Total volumetric strain	%
ϑ	Parameter that controls rate of increase of soil stiffness with ψ_m within virgin state	-
$\lambda(0)$	Compressibility coefficient for saturated state along virgin loading	-
$\lambda(\psi)$	Compressibility coefficient for increments of net normal stress for	

	virgin state	-
λs	Stiffness parameter for changes in mean net stress	-
λ_ψ	Compressibility coefficient for increments of suction for virgin states	-
κ	Elastic stiffness parameter for changes in net normal stress	-
κ_ψ	Elastic stiffness parameter for changes in suction	-
κ_Θ	Shear strength envelope fitting parameter with respect to Θ	-
μ	Coefficient of friction	-
μ_w	Absolute viscosity	-
ϕ	Friction angle	o
ϕ'	Effective angle of friction	o
ϕ^b	Angle of friction with respect to matric suction	o
ϕ_w	Angle of wall friction	o
φ	Filling angle with respect to liquid bridge between particles	o
π	Osmotic suction	kPa
ρ	Density	Mgm^3
ρ_b	Bulk density	Mgm^{-3}
ρ_d	Dry density	Mgm^{-3}
ρ_s	Particle density	Mgm^{-3}
ρ_{dmax}	Maximum dry density	Mgm^{-3}
ρ_{max}	Maximum density	Mgm^{-3}
ρ_{min}	Minimum density	Mgm^{-3}
ρ_w	Density of water	Mgm^{-3}
ρ^c	Critical density	Mgm^{-3}
σ	Total normal stress	kPa
σ_{con}	Consolidation stress	kPa
σ_c	Unconfined yield strength	kPa
σ_{crit}	Critical unconfined yield strength	kPa
σ_n	Normal stress	kPa
σ_v	Vertical stress	kPa
σ_1	Total major principal stress	kPa
σ_3	Total cell pressure (total minor principal stress)	kPa
$\sigma_3 - u_a$	Net normal stress	kPa
σ'	Vertical effective stress ($\sigma - u$)	kPa
θ	Water content	%

Θ	Normalised volumetric water content	-
θ_r	Residual water content	%
θ_s	Saturated volumetric water content	-
τ	Shear Strength	kPa
υ	Angle of dilation	^{o}
ν	Specific volume	-
ν_{w0}	Specific volume of water ($1/\rho_w$)	Mgm^3
ω_v	Molecular mass of water vapour	$kgmol^{-1}$
ψ	Total suction	kPa
ψ	Matric suction	kPa
ψ_a	Air-entry value	kPa
ψ_r	Residual value	kPa
ψ_w	Water-entry value	kPa
ψ *	Matric suction in excess of ψ_a , $[(u_a - u_w) - \psi_a]$	kPa
ψ_0	Hardening parameter of the suction increase yield curve	kPa
χ	Effective stress parameter related to the degree of saturation	-
ξ	Gallipoli et al. (2003) bonding parameter	-

LIST OF PUBLICATIONS

Ileme, O. M., Medero, G. M, Kane, D., Arouto, J. & Woodward, P. K. (2013). Effect of temperature on collapse potential. In: *Proceedings of the Infrastructure and Environment Scotland, p*p. 53 – 57.

Ileme, O. M., Medero, G. M. & Woodward, P. K. (2016). Effect of temperature on volume change behaviour of statically compacted kaolin clay. In: *Proceedings of 3rd European Conference on Unsaturated soil, Paris.*

CHAPTER ONE

1 INTRODUCTION

1.1 BACKGROUND

Current engineering practices involve some applications where soils or earthen structures are subjected to elevated temperature. A notable example is the disposal and storage of high level radioactive wastes in repositories. In this case, compacted clays are used as backfill to seal the waste and prevent the migration of radionuclides to environments where the public can get in contact with them (Westsik et al., 1983). Other applications where elevated temperature is relevant are in undergrounding of high voltage cables, clay liner used around landfill waste and pavement-soil system in arid and semi-arid regions. The backfill materials around the high voltage cables and nuclear wastes/clay liners are subjected to high temperature because of heat emitted from the flow of electricity and decomposing wastes respectively. Water also infiltrate into these materials over time. This may likely lead to changes in soil properties such as permeability, compressibility and soil structure (Romero et al., 2005). The main uncertainty associated with the use of these materials is their long-term stability under expected conditions such as temperature and stress. To ensure the optimal performance of these systems, it is important to understand to what extent elevated temperature among other variables will affect the mechanical and hydraulic behaviour of these soils.

The influences of temperature on soils have been actively studied in the past with so much focus on saturated soils (e.g. Hueckel and Baldi,1990; Towhata et al., 1993; Tanaka et al., 1997; Delage et al., 2000; Sultan et al., 2002). A general understanding is that the effect of temperature on the volume change of saturated soils is dependent on the over-consolidation ratio. Heavily over-consolidated soils expand on heating (Sultan et al., 2002), while normally consolidated soils typically show contraction when heated. In contrast, limited number of researches have been carried out regarding thermal effects on the mechanical and hydraulic behaviour of unsaturated soils (e.g. Romero, 1999; Romero et al. 2003; Romero et al., 2005; Folly, 2001; Francoise, 2008; Haghighi, 2011; Tang et al, 2008; Ye et al., 2012; Cui & Tang, 2013; Uchaipichat and Khalili). Because experimental studies on unsaturated soils are generally expensive and time consuming, existing experimental data are usually used to predict soil behaviour. Results obtained from the existing studies have shown that the influence of elevated temperature on

unsaturated soils is dependent on the soil type, initial conditions and stress path. For instance, regarding volumetric behaviour, Romero et al. (2003) studied the effect of temperature (up to 80^{o}C) and suction (up to 0.45MPa) on the volumetric behaviour of statically compacted Boom clay and reported that the influence of temperature was significant on compressibility associated with loading as well as swelling strain observed on wetting. The swelling strain of high density sample (16.7kN/m^{3}) was observed to be larger at 80^{o}C than at 22^{o}C, while compressibility increased with increasing temperature. Similar pattern of behaviours regarding increased compressibility and swelling strain with temperature were also reported by Tang et al. (2008) and Romero et al. (2005) respectively. However, Romero et al. (2005) presented experimental data on FEBEX clay tested at 80 and 22^{o}C that was not in agreement; smaller swelling strain was observed on high density sample (16.0kN/m^{3}) at 80^{o}C than at 22^{o}C. Francoise (2008) observed that the compressibility of silty-sand was unaffected by an increase in temperature.

In term of the relationship between temperature and yield stress which is an important parameter used for modelling deformation problems, Folly (2001); Romero et al. (2005) on Boom clay; Tang et al. (2008); Haghighi, (2011) have shown that the yield stress will reduce with increasing temperature. An exception to this is the study of Romero et al. (2005) on FEBEX, in which an increase in yield stress was reported with an increase in temperature. In fact, this difference in behaviour has been linked to the complex stress paths which the soil has been subjected to before heating (Ileme et al., 2016). A typical scenario usually witnessed in the field is a situation where the backfill is subjected to heating and cooling in the as placed condition. Regarding this type of scenario, while Tang et al. (2008), Ye et al. (2012) have shown that the strain behaviour on heating is influenced by the suction level, Cui & Tang (2013) reported that it is linked to OCR.

The mixed findings in the existing literature are not surprising as different soils under different conditions have been used. And soils, unlike other materials such as metals, are complex and vary considerably in their structures. From the existing literature, it appears that the influence of temperature on the volumetric strain of unsaturated soil is unique for each soil type. And for this reason, the result obtained from one soil cannot be used to predict precisely the expected strain on another soil. It has been observed that most reported evidences on the influence of temperature on kaolin clay have been based on samples with a hydraulic history and water content at wet of optimum (e.g. Folly, 2001; Haghighi, 2011). In the real sense, most backfills are placed as compacted soils at either optimum water content or at dry of optimum water content. In such a case, the soil does

not have a hydraulic history. Compaction of clayey soil to wet of optimum is difficult to achieve in the field. There are evidences in the literature that wet and dry of optimum samples exhibit entirely different structure and fabric (Leroueil & Vaughan, 1990; Fredlund, 2002) resulting in significantly different volumetric and water retention behaviours; variation of the normal compression lines under loading and wetting (Gens et al., 1995; Wheeler & Sivarkumar, 1995; Sivakumar & Wheeler, 2000; Gao et al., 2016). Soils with water content at the dry side of optimum exhibit bimodal pore size distribution while soils at wet-side of optimum generally exhibit unimodal pore size distribution (Lloret et al., 2003; Thom et al., 2007; Farulla et al., 2010; Koliji et al., 2010; Monroy et al., 2010, Gao et al., 2016). Consequently, existing study is relevant on soils with hydraulic history. The use of data obtained from existing study in the prediction of the behaviour of compacted soil will result in wrong estimation. Thus, data on the influence of temperature on kaolin clay without a hydraulic history is required to predict precisely the influence of temperature on volumetric behaviour of compacted kaolin soils. This research experimentally studied the thermo-hydro-mechanical behaviour of kaolin clay under unsaturated conditions. The research is an extension of work undertaken by Haghighi (2011). Unlike other studies on kaolin, this study considered complex stress paths usually encountered in the field. The experimental data from SWRC were used with existing hydraulic models for unsaturated soil to identify the influence of temperature on hydraulic conductivity. Additionally, the influence of temperature on soil water retention curve was studied on a continuous primary soil water retention curve, rather than on the scanning curve. The research hypothesis is "the influence of elevated temperature up to 50^{o}C on the compressibility and water retention behaviour of kaolin clay with a hydraulic history will differ from the influence on the same soil without a hydraulic history".

1.2 AIMS AND OBJECTIVES

The aim of this study was to investigate the effect of temperature variation on the volume change, compressibility properties, suction change and water retention of compacted kaolin clay without a hydraulic history. The questions are; will change in temperature affect the magnitude of volume change under a specific stress path; is the influence of elevated temperature on soil water retention curve of compacted soils with hydraulic history the same as reported influence on soils without hydraulic history? To answer

these questions, the study specifically investigated the influence of temperature on the compressibility parameters, compressibility, slope of the normal compression line and the effect of temperature on stress path dependence characteristics of soil volume change. Additionally, the effect of elevated temperature on the water retention and hydraulic characteristics of compacted kaolin clay were investigated by comparing results obtained at 50^{o}C with results obtained at 25^{o}C considering a drying soil water retention path. Data regarding the influence of temperature cycles on overall volume and suction were obtained. This will try to fill the knowledge gap on the influence of the thermal cycle on the magnitude of suction.

The study will add to the body of existing knowledge on the thermo-hydro-mechanical behaviour of compacted clay and is of relevance to areas where unsaturated inactive clays are subjected to temperature variations. Kaolin clay has been used in this study and is a benchmark soil used by many geotechnical researchers to predict the behaviour of inactive clay soils. Consequently, the study will be of interest to soil mechanics research community.

1.3 THESIS OUTLINE

The thesis consists of eight chapters.

A review of the conceptual and theoretical background of unsaturated soils, water retention properties of different soils, hydraulic models and influence of temperature on mechanical and hydraulic properties of unsaturated clay soils is presented in Chapter two. Also, presented in Chapter two is a review of experimental techniques and procedures used in testing unsaturated soils, specifically fine-grained soils.

Physical properties of the soil used in this study are presented in Chapter three. Among the properties presented are Atterberg limits, specific gravity, compaction characteristics and particle-size distribution. Also, presented in Chapter three is a detailed explanation of sample preparation method used in the experimental programme; all the experimental works carried out, together with testing procedures. The equipment used and the different techniques adopted, are also explained in this Chapter.

In Chapter four, results and discussions of preliminary tests carried out to observe the hydro-mechanical behaviour of compacted kaolin are presented.

Experimental results were presented in Chapters five and six. Data include the influence of temperature and suction on compressibility, post-compressibility parameters, water retention, hydraulic conductivity and the influence of temperature cycles on volume and suction. In Chapter seven, the main findings were discussed.

Finally, conclusions drawn from the study and recommendations for further works are presented in Chapter eight followed by references.

CHAPTER TWO

2 LITERATURE REVIEW

INTRODUCTION

Presented in this chapter is a review of literature on the physical properties, mechanical behaviour and modelling of unsaturated soils. This provides an understanding of the conceptual framework and behaviour of unsaturated soils. In addition, current state of knowledge on temperature effect on clay soils is reviewed and presented in this chapter, which helped in identifying the knowledge gaps.

2.1 UNSATURATED SOIL

Soils are made of particulate materials with voids in-between the particles. When these voids are completely filled with water, the soil is said to be saturated with positive pore water pressure. On the other hand, when the voids are partially filled with water or filled with a mixture of gas (air in most cases) and water, the soil is said to be unsaturated and the pore water pressure is negative. Special cases of unsaturated soils can occur when soils contain more than two fluid media (water, oil and gas). Typical examples are hydrocarbon-bearing soils (Raveendiraraj, 2009). Unsaturated soils can occur naturally or be man-made as explained below.

2.2 OCCURRENCE OF UNSATURATED SOILS

2.2.1 Naturally occurring unsaturated soils

a) Soils above water table

Soils above the water table are considered unsaturated, due to the voids being filled with air and water. They are commonly seen in the arid and semi-arid regions where soils de-saturate to a considerable depth below ground level because of excessive evaporation and evapo-transpiration (Freudlund & Rahardjo, 1993). The depth of unsaturated soil could be many meters below ground level. In such circumstances, heavy rainfall may temporarily produce a saturated zone at the ground surface (due to infiltration) and then unsaturated conditions at some depth above the ground water table. Changes in climatic

conditions subject soils in these regions to cycles of saturation and de-saturation, resulting in the formation of different soil fabrics during each cycle (Zakaria, 1994).

The major factor that distinguishes unsaturated from saturated soils is the negative pore water and pore air pressure sustained by unsaturated soils. The pore air pressure is generally greater than the pore water pressure. The difference between the two pressures results in suction. The value of suction that can be sustained in natural soils largely depends on grain sizes. For instance, clay soils with grain size usually less than 0.002mm will sustain higher suction than sandy soils (Barbour, 1998). This phenomenon will be discussed in detail later in this chapter.

b) Gassy soils

Soils that have organic contents in them tend to emit gases e.g. methane, nitrogen or carbon dioxide, during the decomposition of the organic materials. Typical examples include some soils forming seabed and some soils at landfill sites (Wheeler, 1988). The emitted gases, in the form of discrete bubbles, occupy some of the water-filled voids without affecting the soil skeleton. Barden & Sides (1970) explained that gases can only occur as discrete bubbles if the soil is above a critical degree of saturation; usually above 85% (Spark, 1963). Although these soils are reported to have a high degree of saturation, however, they are treated as unsaturated soils. In the analysis of such soils, both the principles of saturated and unsaturated soil are employed. The effective stress principles are applied in analysing the compressibility of the entire soil, while the principles of unsaturated soils are adopted in the analysis of the additional compressibility arising from compression of the occluded bubbles (Vanoudheusden et al., 2003).

2.2.2 Man-made unsaturated soils

a) Compacted fills/soil

Compacted soils are used in many civil engineering projects e.g. dams, roads, embankments and as engineered barriers in nuclear waste isolation systems. The soil is first placed as 'fill' in the construction site and then compacted to engineering specification to increase the strength and stiffness. Compacted soils, by their very nature, are typically unsaturated because of the method of formation; the fill is placed in layers, with air entrapped in-between the layers, and then compacted. Thus, even when excavated in a saturated state, they become unsaturated by the time they are transported

and compacted in their new state due to entrapment of air during excavation, transportation and placement.

2.3 STRUCTURE/FABRIC OF UNSATURATED SOILS

The behaviour of an unsaturated soil is greatly influenced by the soil structure, made of a combination of different fabrics (geometrical arrangement of soil particles). Soil structures vary considerably and are influenced by the following: modes of formation, stress state, compaction method, applied stress and wetting path (Wheeler, 1988; Monroy et al., 2010). The structures of each group of unsaturated soil are discussed in subsequent sections of this chapter.

2.3.1 Structure of natural unsaturated soils

As discussed in Sec. 2.2.1, unsaturated soils occur naturally in soils above the ground water table. A typical soil profile above the water table is usually made up of three distinct zones as shown in Fig. 2.1 depending on the depth of the water table (Wroth & Houlsby, 1985; Fredlund, 2000). Each zone depicts a unique soil structure. The different structures, as shown in Fig. 2.2, are based on the continuity of air and water phases, hence, the degree of saturation.

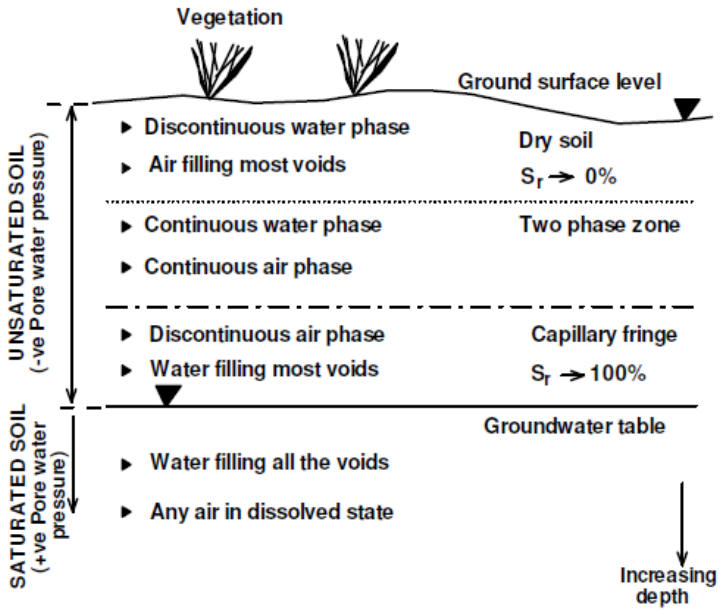

Figure 2-1 Different zones found in a naturally occurring unsaturated soil (Kasangaki, 2012)

The zone immediately above the ground water table is known as the capillary fringe zone, and may also be called the continuous water zone (Fig. 2.1). The degree of saturation is high, up to 100% (Fredlund, 2000). The air phase is in the form of occluded bubbles and is discontinuous, as shown in Fig. 2.2c. However, the pore water pressure is negative, while the pore air pressure is greater than the pore water pressure, though not necessarily zero. According to Terzaghi (in Barbour, 1998), this zone occurs as a result of capillary forces which counteract gravitational forces. If gravitational forces alone acted on soils, there would be a clear boundary between saturated and unsaturated soil.

The zone above the capillary fringe zone is called the two-phase zone. This type of soil structure is found when the air and water phases are continuous (see Fig. 2.2b). Usually, the degree of saturation is intermediate and ranges between 20 – 80% (Fredlund, 2000). The pore water pressure is negative with the pore air pressure zero, relative to atmospheric pressure. The theories of unsaturated soils were developed based on this zone (Fredlund, 1985), but evidence has been shown that the theories can also be applied successfully to other zones (Fredlund & Rahardjo, 1993).

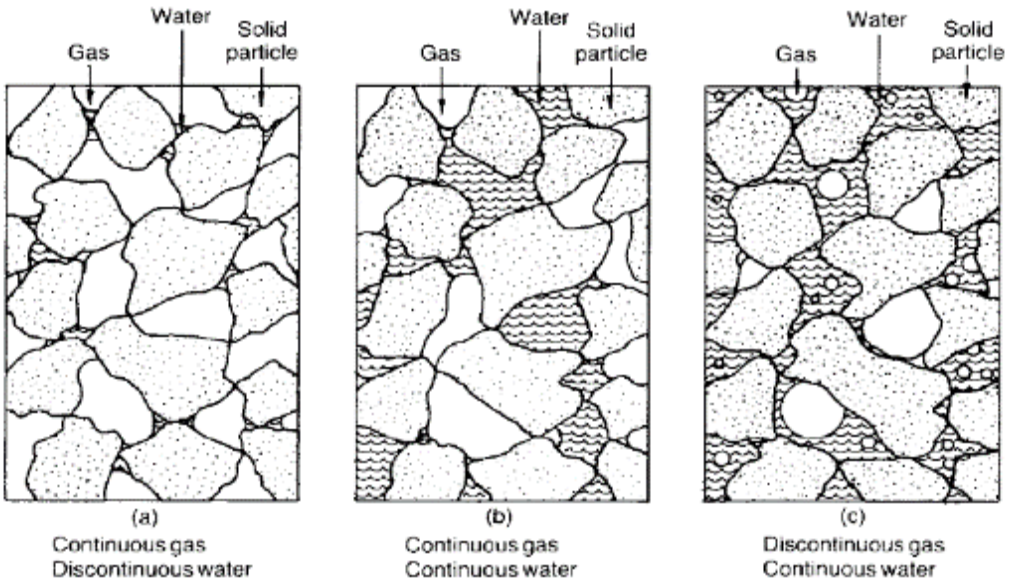

Figure 2-2 Structure of an unsaturated soil showing the three distinct zones (Wheeler, 1988)

The final zone is the dry zone, in which the air phase is continuous while the water phase is discontinuous as shown in Fig. 2.2a. This type of fabric is usually seen near ground

surfaces, especially during dry seasons and has a low degree of saturation. In this case, the pore water pressure is negative while the pore air pressure is atmospheric.

2.3.2 Structure of gassy soils

Gassy soils like natural soils have different structures that exhibit different pattern of behaviours, especially volume change. The type of structure depends on the sizes of the gas bubbles relative to the sizes of the soil particles. It is worth mentioning that gassy soils herein are limited only to soils with discrete bubbles. One type of structure is similar to that shown in Fig. 2.2c, but the gas in this case is not air. The bubbles are smaller than the normal size of soil particles and void spaces, hence the bubbles fit well into the void spaces without affecting the soil skeleton. Fig. 2.3a illustrates another type of structure, with bubbles much larger than the soil particles. In such a case, the gas bubbles are not considered as occluded bubbles within the pore water (Wheeler, 1988). To aid in the analysis of this soil type, Wheeler (1988) proposed a continuum model as shown in Fig. 2.3b, in which the gas bubbles were idealised as spherical cavities within a continuum of saturated soil. This type of structure is commonly found in fine-grained seabed soils.

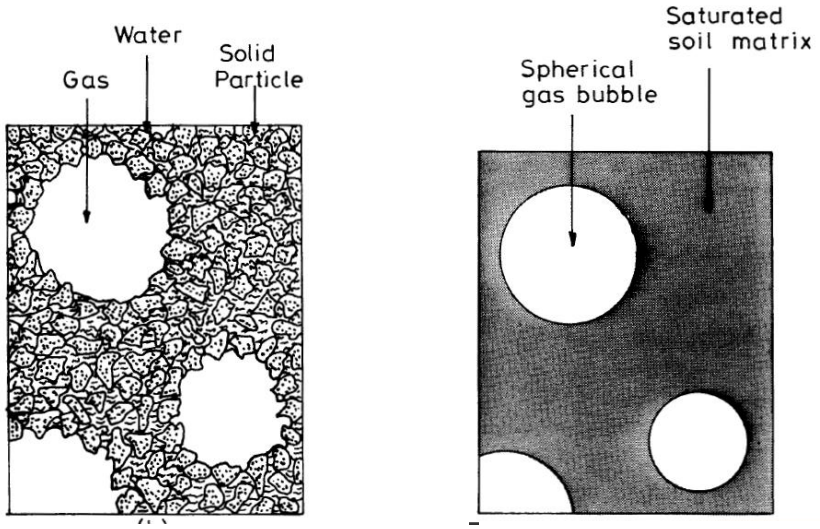

a) Soil structure **b) continuum model**

Figure 2-3 Structure of gassy soils with gas bubbles larger than the soil particles and void spaces (Wheeler, 1988)

2.3.3 Structure of compacted soils

In the literature, compaction of soils is considered as a fabrication process (Tarantino & De Col, 2008). Compacted clay soils exhibit a double structure made of saturated packets

containing small water filled voids (intra-aggregate voids) separated by larger unsaturated voids (inter-aggregate voids), as shown in Fig. 2.4 (Brackley, 1975; Delage & Lefebvre, 1984). Double structure in compacted clay soils was also confirmed by Romero et al. (1999), Pusch & Moreno (2001), Alonso (2005) and Monroy et al. (2007).

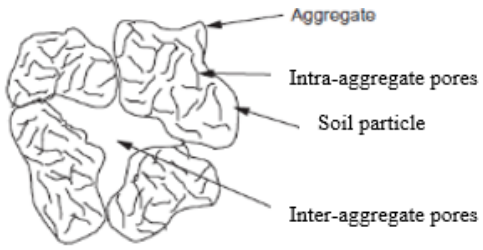

Figure 2-4 Structure of a compacted soil (After Thom et al., 2007)

The structure of compacted soils is further classified into microstructure and macrostructure (Gens & Alonso, 1992) based on the relative size of pores. The fabric within the saturated packet is called microstructure, while the entire arrangement of packets with large inter aggregate voids is called macrostructure. The double structure in compacted clay soils makes the microstructural study complex, since the intra-aggregate voids in the microstructure are usually saturated unless a high suction is imposed and the principle of effective stress applies. The inter-aggregate voids in macrostructure, on the other hand, are usually unsaturated and the principle of unsaturated soil applies (Lloret et al., 2003). The pore water in the intra-aggregate voids are usually influenced by particle surface forces, whereas the pore water in inter-aggregate voids is influenced by capillary forces (Alonso et al., 1990).

The initial degree of saturation or water content affects the relative size and distribution of the pore spaces. When clay soils are compacted dry of optimum, flocculated structures are formed with bimodal pore size distribution or double porosity fabric (Lloret et al., 2003; Thom et al., 2007; Farulla et al., 2010; Koliji et al., 2010; Monroy et al., 2010). Conversely, dispersed structures with unimodal pore size distribution are formed when clay soils are compacted wet of optimum (Thom et al., 2007, Gao et al., 2016). In bimodal pore size distribution, two peak pore sizes are observed: intra-aggregate and inter-aggregate pores (see Fig. 2.5). Unimodal pore size distribution has a single peak pore size which is mainly micro pores (Koliji et al., 2010). Additionally, variation in compaction water contents will result in soils with different fabrics and different

mechanical behaviour (Gens et al., 1995; Wheeler & Sivarkumar, 2000). Alonso et al. (1987) explained that an increase in compaction water content will affect the overall volume of macro-pores through the reduction of larger pores associated with macro-pores. On the contrary, Thom et al. (2007) reported based on their study on specwhite kaolin clay, that the micro-pores are affected by changes in compaction water content rather than macro-pores. They observed a decrease in micro-pores with increasing compaction water content and an increase in some cases. Some researchers (e.g. Gens et al., 1995; Wheeler & Sivarkumar, 1995; Gao et al., 2016) have provided evidence to show that the mechanical and hydraulic behaviour of sample prepared wet of optimum is significantly different from dry of optimum samples due to the different fabrics. Wheeler & Sivarkumar (1995) observed that the normal compression line of compacted sample of kaolin at zero suction fell below the normal compression line of the reconstituted kaolin at corresponding suction. The slopes of the two compression lines were also observed to be different, indicating different soil fabric in the samples. Gao et al. (2016) conducted water retention and triaxial tests to study the effect of fabrics resulting from different sample preparation methods (reconstituted and compacted samples) on the hydro-mechanical behaviour of unsaturated clayey silt. The results indicated that the air-entry value of reconstituted specimen is higher than that of the compacted specimen for the same void ratio. At the same density, they observed that the shear strength of the reconstituted specimen was higher that the shear strength of compacted specimen, under the same confining net pressure and suction.

Soil fabrics are influenced by changes in applied stress and compaction effort. Numerous studies have shown that macro pores are greatly affected during loading by a reduction in their volume, resulting in an increase in the population of microspores as loading advanced (Delage & Lefebvre, 1984; Romero et al., 2003; Cuisiner & Laloui, 2004; Lloret & Villar, 2007). Regarding the influenced of compaction effort on soil fabric, Lloret et al. (2003) observed, in their study on two statically compacted bentonites at dry densities of 1.5Mg/m^3 and 1.8 Mg/m^3, a decrease in the relative size of macro-pores due to increase in dry density achieved from increasing compaction effort. The sample compacted at a dry density of 1.8 Mg/m^3 had dominant macro-pores of 10μm while the sample at 1.5Mg/m^3 had dominant macro-pores of 40μm as shown in Fig. 2.5. Thom et al. (2007) investigated the effect of different methods of compaction, post compaction wetting, compaction effort and compaction water content on bimodal distribution of pore sizes. Samples of specwhite kaolin clay were prepared and compacted dry of optimum

using three different compaction methods namely; isotropic compression, static compression and dynamic compaction. Mercury intrusion porosimetry (MIP) was then used to study the pore size distribution in each of the samples. The researchers reported that bimodal structure was not broken down by compaction. Both micro-pore and macro-pore volumes were affected by an increase in compressive pressure. Reduction of micro-pores was observed in statically compressed samples at all values of water contents. Samples compressed isotopically showed similar behaviour as statically compacted samples, though the reduction was insignificant at higher water content. Wetting of samples compressed to 400kPa and 800kPa resulted in a reduction of inter-aggregate volume and an increase in the percentage of intra-aggregate pores, but bimodal pore size distribution was retained. Monroy et al. (2007) conducted a series of tests on statically compacted London clay (dry density = 1.384Mg/m^3) to show evidence of changes in micro-fabric following reduction in matric suction. Changes in soil fabrics were observed following reduction in matric suction under a constant applied load of 7kPa. Reduction in suction to 470kPa and 150kPa did not result in any change in fabric. However, reduction in suction to 40 and 0kPa resulted in a change from bimodal pore size to a unimodal pore size distribution contrary to the observations of Thom et al. (2007). The peak reduced from 17,440nm before saturation to 1,730nm after saturation. Both inter-aggregate and intra-aggregate pores were affected by wetting.

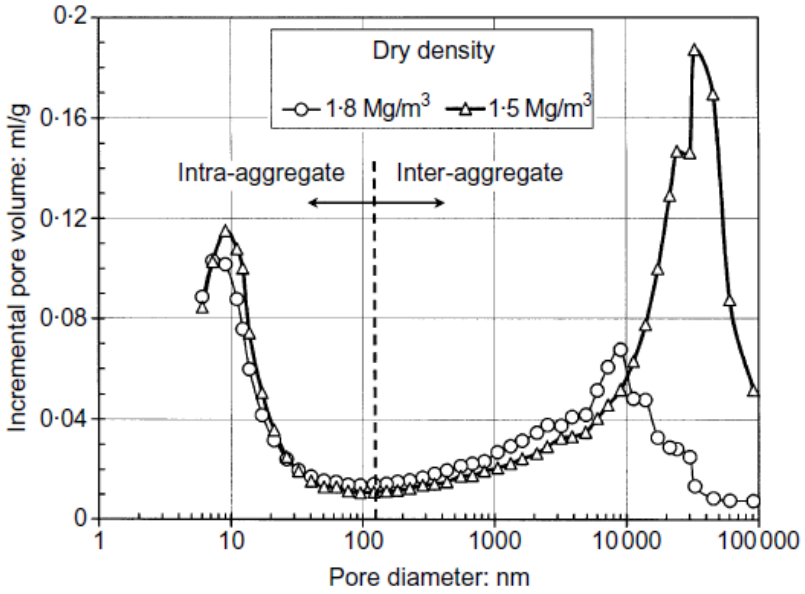

Figure 2-5 Distribution of incremental pore volume for two compacted bentonite samples at different densities (Lloret et al., 2003)

Increase in temperature has also been reported to affect soil fabric. Studies by Romero et al. (2005) observed macrostructural rearrangement of Boom clay on heating which was not reversible on cooling.

2.4 PORE WATER IN UNSATURATED SOILS

2.4.1 Bulk, meniscus and adsorbed water

There are generally three forms of pore water within the voids of unsaturated soils: bulk water, meniscus water and adsorbed water (Karube et al., 1996). When soils undergo drying, the water filled voids empty progressively, with the larger voids emptying first. The voids do not completely dry up; small lenses of water are left around soil particle contacts surrounding the emptied void in an identical manner to water in a capillary tube (Ridley & Wray, 1995). These small lenses of water are called meniscus water, while water within the water-filled voids is called bulk water (see Fig. 2.6). Adsorbed water is tightly bound to the soil particles and considered part of the soil skeleton (Kato et al., 1995). This type of pore water is associated with residual degrees of saturation, which is typical of soils dried under high suction values.

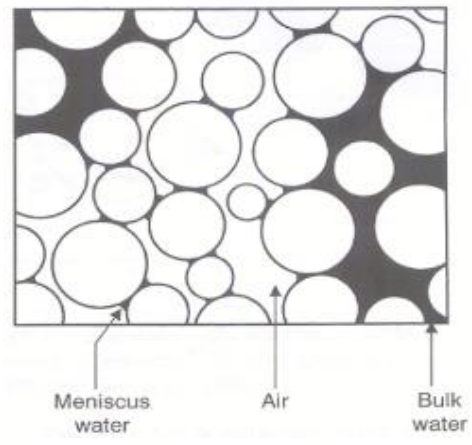

Figure 2-6 Bulk water and meniscus water (Wheeler & Karube, 1995)

A general understanding is that meniscus water introduces additional normal force at particle contact where it is formed, which increases elastic deformation of soil particles at soil contact (Wheeler & Sivarkumar, 1990; Wheeler & Karube, 1995). Another interesting effect of meniscus water on unsaturated soil is that it reduces plastic deformation. The explanation for this is that the normal force tends to push the soil

particles firmly together, thereby preventing slippage and increasing shear strength in unsaturated soil (Wheeler & Karube, 1995). Bulk water produces the same effect as pore water in saturated soils; producing normal and tangential forces at inter-particle contact, except that in case of unsaturated soils the forces act only in the flooded voids.

2.5 PORE PRESSURES AND SUCTION IN UNSATURATED SOILS

2.5.1 Pore pressures

An unsaturated soil is comprised of three phases of matter: liquid phase, gaseous phase and solid phase. The solid phase is made of incompressible soil particle, which may form compressible mass due to aggregation (Matyas & Radhakrishna, 1968). The gaseous and the liquid phases are air and water respectively that occupy the voids between soil particles. As a result of air and water in the voids of unsaturated soils, two pressures exist: pore air pressure (u_a) and pore water pressure (u_w). Surface tension develops on the surface of the air-water interface (contractile skin) due to imbalanced molecular forces acting on the molecules of water. The molecular forces acting at the air-water interface are different from those acting at the interior of the water. Molecules of water at the interior experience equal forces in all directions, whereas molecules at the interface skin experience forces only from the interior of the water, as shown in Fig. 2.7a. The shortage of force at the exterior result in surface tension developing along the contractile skin to bring the system to equilibrium. The tensile pull exerted by the surface tension makes the contractile skin behave like an elastic membrane with radius of curvature R_s (see Fig. 2.7b). This property decreases with temperature. Davies & Rideal (1963) suggested that the contractile skin should be considered as an additional phase in an unsaturated soil. For a portion of a mixture to qualify as an independent phase, it must have different properties from the contiguous material (Fredlund et al., 2012). Contractile possess a tensile pull different from the property of the bounding water, making it meet the requirement for the designation as a phase. However, in terms of volume-mass relationship, unsaturated soil can be considered as a three-phased system because the volume of contractile skin is negligible, with the mass considered as part of a mass of water. But in terms of stress analysis, the contractile skin could be considered as an additional phase (Fredlund & Rahardjo, 1993).

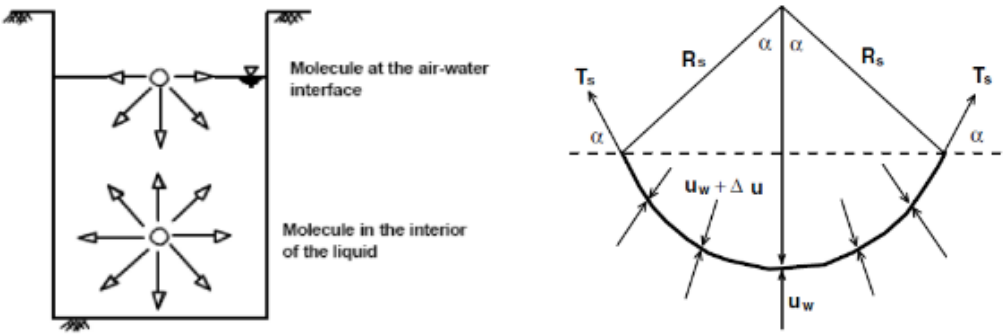

Figure 2-7 (a) Intermolecular forces at the air-water interface; (b) surface tension and pressures on the curved interface (Fredlund & Rahardjo, 1993)

The pore air pressure is not equal to pore water pressure. If the pore air pressure and pore water pressure were equal, force equilibrium would be achieved with a flat (planar) air-water interface (Wheeler, 2010). The curved nature of air-water interface is linked to the difference between the two pressures. For the curved interface, the face fluid at lower pressure is on the convex side of the interface like an inflated balloon. Water is generally considered to be at lower pressure than air hence, water is on the convex side while air is on the concave side. The reason for this consideration is that the contact angle θ between the interface and particle when measured from the water side, is assumed to be small, tending towards zero. This implies that the interface must be concave on the air side for the contact angle to be zero (see Fig. 2.8).

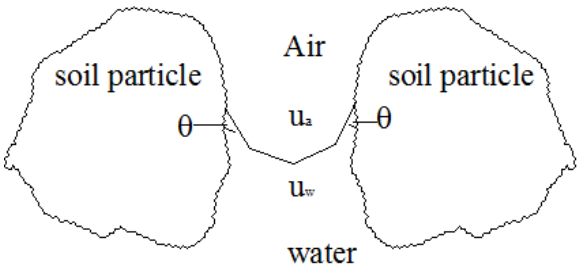

Figure 2-8 Air water interface with contact angle tending to zero

The air phase is connected to the atmosphere and u_a is taken as zero. Therefore, if u_a is greater than u_w, then u_w will have a negative value since it is smaller than u_a. This means that unsaturated soils have affinity for free water at atmospheric condition.

2.5.2 Suction in unsaturated soils

Soil suction is classified into two groups; matric and osmotic suction. The difference in pressure $u_a - u_w$ is known as matric suction and is linked to capillary and adsorption forces (Fredlund et al., 2012). At high suction and low water content, the mechanism responsible for soil suction is adsorption and is peculiar to soils with high electro-chemical activities such as clay minerals. At low suction and high water content, capillary action controls the soil suction. For a curved interface having a radius of curvature R_s, the matric suction is given by Eq. 2.1 and is for a pair of particle.

$$u_a - u_w = \frac{2T_s}{R_s} \qquad \textbf{2-1}$$

Where R_s is radius of curvature of the interface, T_s is surface tension; (T_s = 73.75mN/m at 20^{o}C).

In a case where the water meniscus is bounded by irregular solid surfaces resulting in different radii of curvatures R_1 and R_2, the matric suction is given by Eq. 2.2. Both Eq. 2.1 and Eq. 2.2 show that matric suction increases as the radii of curvature (R_s) of the interfaces decrease. Ideally, increase in matric suction produces additional normal force at inter particle contact because of increase in meniscus water. However, this does not increase indefinitely. Fisher (in Wheeler, 2010) explained the effect of inter-particle normal forces increases with suction, but reaches a limiting condition as suction tends to infinity.

$$u_a - u_w = T_s\left(\frac{1}{R_1} + \frac{1}{R_2}\right) \qquad 2\text{-}2$$

Osmotic suction (π) is associated with dissolved salt in the soil which influences the relative humidity (Freudlund & Rahardjo, 1993; Lu & Likos, 2004). For instance, at high concentration of dissolved salt, the relative humidity is reduced, thereby increasing the osmotic suction. The effect of osmotic suction is difficult to identify and is always assumed to be constant unless the concentration of solute changes (Lu & Likos, 2004; Leong et al., 2007). The tendency for unsaturated soils to draw water is not only dependent on the negative value of u_w, but also on the difference in osmotic potential between the soil water and free water in the air.

Total suction (ψ) is the addition of matric and osmotic suction $\psi = \pi + (u_a - u_w)$. In thermodynamic term, total suction is equated to the suction measured from the partial pressure of water vapour in equilibrium with the soil-water, relative to the partial pressure of water vapour in equilibrium with free pure water. This relationship is defined mathematically using Kelvin's equation as shown in Eq. 2.3 below:

$$\boldsymbol{\psi} = -\frac{\boldsymbol{RT_K}}{\boldsymbol{v_{w0}w_v}}\mathbf{ln}(\frac{\boldsymbol{u_v}}{\boldsymbol{u_{v0}}}) \qquad \textbf{2-3}$$

where R is universal gas constant (8.3143J/molK), T is absolute temperature, v_{w0} is the specific volume of water, ω_v is the molecular mass of water vapour, u_v is the partial pressure of pore water vapour, u_{v0} is saturated pressure of water vapour over a flat surface of pure water at the same temperature, and u_v/u_{vo} is the relative humidity. All the components of total suction (matric and osmotic) are usually considered in flow processes of unsaturated soils; however, in the mechanical behaviour of unsaturated soils, only matric suction is usually considered. This is because most engineering problems in unsaturated soils are associated by the matric suction component, thereby rendering osmotic suction insignificant (Fredlund & Rahardjo, 1993).

2.6 STRESS STATE VARIABLES

The stress state of saturated is based on the principle of effective stress. Terzaghi (1936) explained that changes in volume and shear strength of saturated soils are due to changes in effective stress. For unsaturated soils, however, earlier attempt by Bishop (1959) to extend and validate the use of effective stress in unsaturated soils through Eq. 2.4 was unsuccessful.

$$\boldsymbol{\sigma' = \sigma - u_a + \chi(u_a - u_w)} \qquad \textbf{2–4}$$

where σ' is effective stress, σ is total stress, χ is a parameter which is dependent on the degree of saturation S_r, soil structure and stress path on wetting /drying of the soil. The parameter χ ranges between two extremes of 0 and 1, for completely dry soil and fully saturated soil, respectively. At any of the extremes, Eq. 2.4 reduces to an effective stress equation for saturated soil. The dependence of χ on *Sr* was supported by the studies of Bishop & Donald (1961). However, the studies by Jennings & Burland (1962); Wheeler

& Sivarkumar (1995) invalidated the use of effective stress equation for unsaturated soils. In the former study, the behaviour of partially saturated soil under an applied load was compared with the behaviour of saturated soil under the same load following a wetting path. The result of the test showed collapse on wetting for the partially saturated soil. They argued that collapse on wetting could not be justified by Eq. 2.4, pointing out that if the principle of effective stress was true for unsaturated soils, the soil would have increased in volume on wetting, since wetting increases pore water pressure and decreases in effective stress. Wheeler & Sivakumar (1995) provided evidence, based on the critical state of compacted kaolin, to invalidate the use of single effective stress for unsaturated soils. In their work, two samples A and B at suction of 200kPa and 0kPa respectively, were observed to have the same shear strength, indicating equal values of effective stress in both samples. However, sample B was observed to reach a critical state at a lower value of void ratio than sample A. A third sample C (at a suction of 0kPa), which reached the critical state at the same void ratio as A, was observed to have a much lower shear strength than A. This shows that the same value of effective stress cannot be assigned to A and B, such that A behaves like B in all respects. Burland & Ridley (1996), pointed out that changes in suction and applied stress result in totally different soil responses. Whereas suction acts at inter-particle contacts and stabilizes the soil, applied stress results in grain slippage and therefore should not be combined into a single equation, but dealt with separately. Gallipoli et al. (2003) and Taratino & Tombolato (2005) explained that the bonding water menisci was responsible for the failure of effective stress in unsaturated soils. The additional normal force provided by the bonding water menisci at particle contacts prevent relative slippage between particles. This is like a decrease in effective stress. On the other hand, meniscus water also causes elastic deformation, which is like an increase in effective stress in saturated soils. This means that the presence of meniscus water in unsaturated soils acts like an increase in effective stress in some cases and a decrease in effective stress in other cases. For these reasons, a single effective stress equation cannot be used in unsaturated soils (Wheeler & Karube, 1996; Wheeler, 2010).

Several researchers (e.g. Bishop & Blight, 1963; Burland, 1964) suggested the use of two independent stress variables. Finally, Fredlund & Morgenstern (1977) proposed the following independent stress variables for unsaturated soil $(\sigma - u_a)$, $(u_a - u_w)$, $(\sigma - u_w)$. They suggested that any of the following combinations could be used in defining the stress state in unsaturated soils; $(\sigma - u_a)$ and $(u_a - u_w)$; $(\sigma - u_w)$ and $(u_a - u_w)$ or $(\sigma - u_a)$ and $(\sigma - u_w)$. However, it is more realistic to select either $(\sigma - u_a)$ and $(u_a - u_w)$ or $(\sigma - u_w)$

and (u_a - u_w), because a combination of ($\sigma - u_a$) and ($\sigma - u_w$) might not give useful results. In fact, the stress variables ($\sigma - u_a$), known as *net stress*, and (u_a - u_w) known as *matric suction*, are usually adopted because u_a is zero in the field relative to atmospheric pressure, which reduces the variables to total stress and negative pore water pressure, thereby making it easier to handle (Wheeler & Karube, 1996).

Recently, some researchers (e.g. Khalili et al., 2004) reintroduced the concept of effective stress in unsaturated soils, by displaying supporting evidence on the appropriateness of Bishop's effective stress equation. Notwithstanding, the two stress state variables have been used in this research.

2.7 SOIL WATER RETENTION CURVE

The relationship between gravimetric water content *w* or volumetric water content θ or degree of saturation *Sr* and suction/water potential is known as the soil water retention curve (SWRC) or the soil water characteristic curve (SWCC) (Fredlund & Xing, 1994; Leong & Rahardjo, 1997; Barbour, 1998; Pham et al., 2003; Baker & Frydman, 2009). In a fully saturated soil, the degree of saturation is 1 and all the voids are filled with water. As the soil dries up, water in the voids retreat into the smaller voids, thereby increasing the curvature of the air-water interface (Wheeler, 2010). The pore water pressure becomes more negative as drying proceeds which results in an increase in suction and a continuous drying curve. On the other hand, suction decreases as the soil saturates from a dry state, yielding a continuous wetting curve. This implies that a typical soil water retention curve follows two distinct paths: drying and wetting paths. These paths can also be referred to as desorption and sorption curves, respectively. The two paths, as shown in Fig. 2.9, will be discussed later in this section. Only the drying path is shown in most of the SWRC studies reported in literature (Fredlund et al., 2011). This lack of diversity is due to the difficulties associated with experiments involving the wetting path.

The SWRC may be likened to a consolidation curve in saturated soils, because it provides a framework for predicting the response of unsaturated soils (Barbour, 1998). Most unsaturated soil functions like the permeability function, coefficient of volume change and shear strength, can be evaluated from SWRC (Fredlund, 2000).

A typical SWRC has three distinct zones, as shown in Fig. 2.10; namely the capillary zone, the transition zone and the residual zone. In the capillary zone, the soil is in a

saturated state with a continuous water phase, due to capillary forces. As suction increases, the soil continues to be saturated until a point is reached at which the applied suction overcomes the capillary force and air begins to enter the pores. At this suction, which is called the air-entry ψ_a suction, drainage of the soil pores begins, as observed by Barbour (1998).

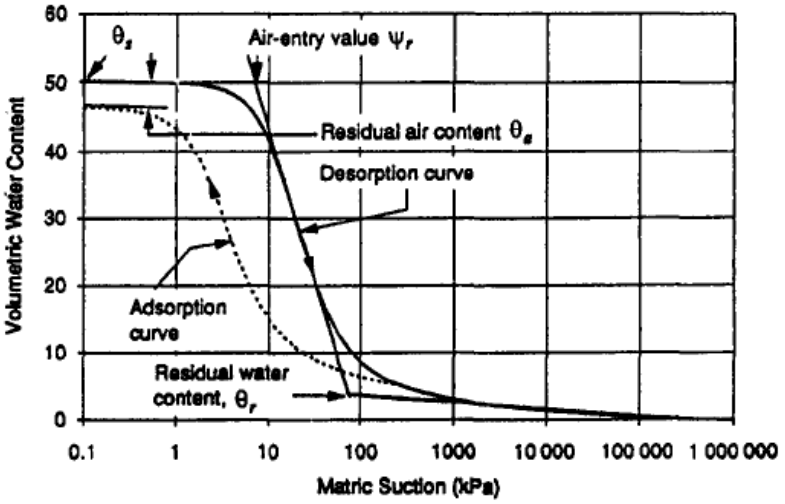

Figure 2-9 SWRC with the primary drying and wetting curves (Fredlund & Xing, 1994)

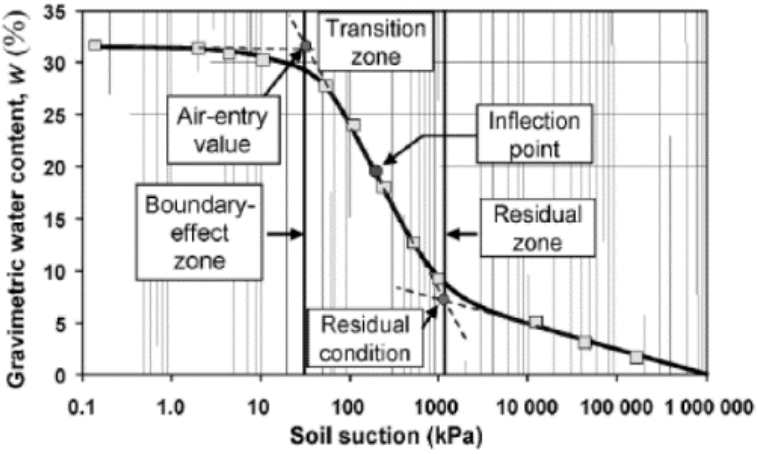

Figure 2-10 The different zones on a SWRC (Fredlund & Houston, 2009)

The capillary zone is marked by a near horizontal curve (Fredlund et al., 2001; Barbour, 1998; Yang et al., 2004), showing that water content remains almost constant, with increasing suction until air-entry suction is reached. This is usually more pronounced in plastic soils because they can sustain high tensile pull without air entering the voids (Fredlund & Xing, 1994). Immediately after the air-entry suction is the transition zone. In this zone, the rate of desaturation of the pores with suction is high, until the residual suction ψ_r is reached. This is evident from the steep nature of the curve along this zone. The last zone is the residual zone with discontinuous water phase. The suction at the start of this zone is known as residual suction ψ_r, while the corresponding water content is known as residual water content θ_r. At the residual suction, water becomes tightly absorbed by the soil particles and is usually said to be chemically bonded. Drainage through liquid flow becomes difficult and removal of water from the pores occurs only through vapour migration (Fredlund et al., 1996; Barbour, 1998).

2.7.1 Hysteresis in the soil water retention curve

The value of matric suction in a SWRC is not uniquely defined by the value of water content, but by the history of drying and wetting (Croney, 1952; Fredlund, 2002; Pharm et al., 2003; Yang et al., 2004; Tarantino, 2009). For instance, at a specific water content, the value of suction is more on drying than on wetting as can be seen from Fig. 2.11. This phenomenon is known as hysteresis (Fredlund, 2000; 2002). This is attributed to the difference in size between the primary pores and connecting pore throat, an effect known as the ink bottle effect (Tinjum et al., 1997; Gallage et al., 2013). Considering the primary pore "A" in Fig. 2.12, when the pore is drying from a fully saturated state, the pore begins to drain when the suction exceeds $(u_a - u_w)_r = 2T_s/r$. At this point, the menisci are at the narrow entry points of the pores with small radii of curvature r as shown in Fig. 2.12. For the same pore to refill, the suction must be below $(u_a - u_w)_R = 2T_s/R$. In this case, the menisci are well inside the pores with larger radius R. Since $R > r$, it then follows that the suction on drying $(u_a - u_w)_r$ is greater than the suction on wetting $(u_a - u_w)_R$. This implies that drying depend on the radii of the connecting pore throat, whereas wetting depends on the radius of the primary pores. This also affects the equilibrium height of water as shown in Fig. 2.12. The implication of this is that the height of the capillary fringe zone explained in Sec. 2.3.1 for a specific soil will vary depending on if the soil is undergoing wetting or drying.

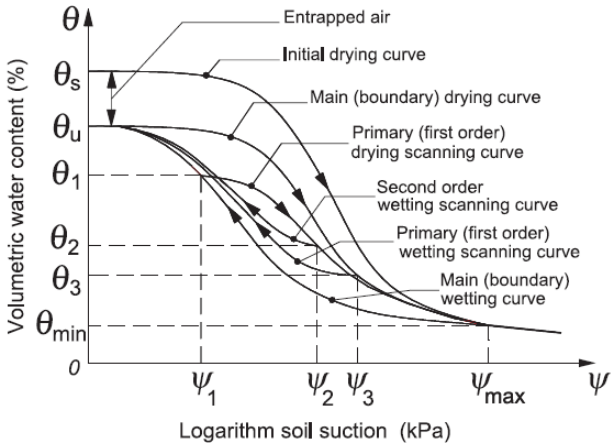

Figure 2-11 Hysteresis in the soil water retention curve (Pham et al., 2005)

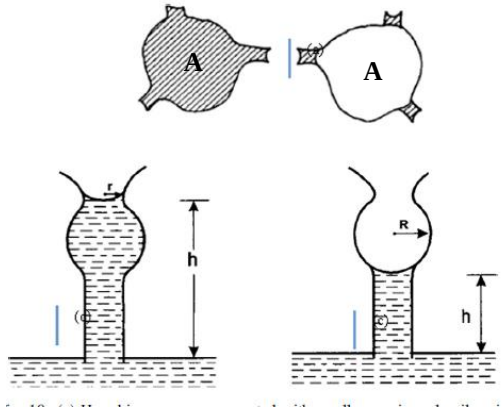

Figure 2-12 Ink bottle effect (Gallage et al., 2013)

Other factors that are linked to hysteresis are contact angle and the entrapped air effect. The contact angle, as well as the radius of curvature, is greater in an advancing meniscus than a receding one. Thus, the suction for a water content on drying will be higher than that on wetting (Ng & Menzie, 2007; Wheeler, 2010).

The drying and wetting curves from fully saturated and dry states respectively form the main boundaries of the SWRC as shown in Fig. 2.11. Primary curves are obtained when the soil is either wetted from an intermediate point on the boundary drying curve to zero suction, or dried from an intermediate point on the boundary wetting curve to maximum suction. Numerous studies have shown that there are also uncountable numbers of intermediate drying and wetting curves within the bounding curves; these intermediates being called scanning curves, as shown in Fig. 2.11 (Fredlund, 2000; Pham et al., 2003). The stress state of soil determines the position of a soil on the SWRC. For instance, if a

soil that was initially undergoing drying from a fully saturated state did not reach the residual zone before undergoing wetting, the position of the soil at the onset of wetting will lie somewhere along the scanning curve before connecting the main wetting curve as shown in Fig. 2.13. The complexities of hysteresis have been pointed as the main reason why in-situ suction cannot be evaluated using the SWRC (Fredlund, 2002). For example, when a soil is sampled from the field, it is usually difficult to determine whether the soil is on the wetting or drying path, because a specific water content can correspond to a suction ranging from 10 to 1000kPa, depending on the path followed.

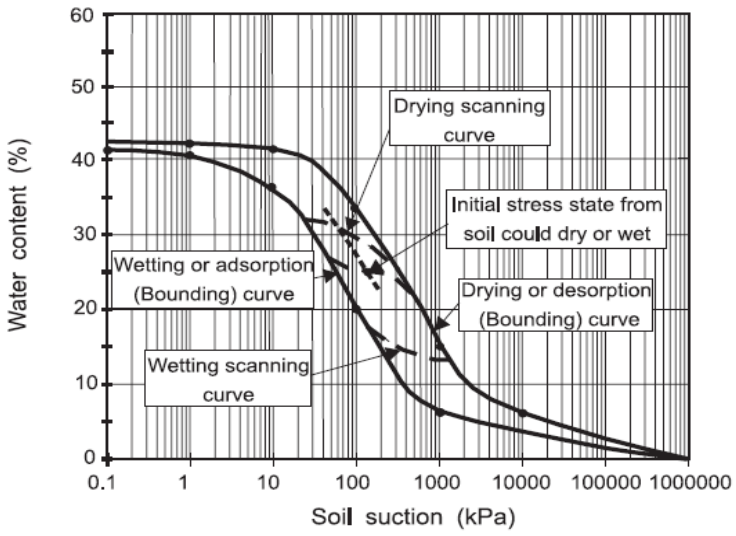

Figure 2-13 Scanning curves within boundary drying and wetting SWRC (Fredlund, 2000)

2.7.2 Methods of determining the soil water retention curve

The soil water retention curve is normally determined by a pressure plate test using the axis-translation technique which will be discussed in Chapter 3. Common procedures involve saturating the sample first, then increasing suction in steps to obtain the drying curve. The sample is then re-saturated from a dry state by decreasing suction in steps to obtain the wetting curve. Cavitation, which is usually associated with an axis-translation technique, limits the range of suction that can be imposed with pressure plate, to about 1500kPa (Fredlund, 2000; Yang, et al., 2008). Suction greater than 1500kPa is usually imposed using an osmotic or vacuum desiccator through relative humidity control (Fredlund, 2000; Vanapalli et al., 1996). In the relative humidity method, a small piece of sample is allowed to come to equilibrium with a salt solution. The water content

corresponding to an imposed suction is measured. Vanapalli et al. (1996) noted that samples for an osmotic test should be obtained from the remnants of pressure plate tests, to ensure a continuous curve along the same path. The major difference between data obtained from the relative humidity method and the axis-translation method is that matric suction is imposed with axis-translation, while total suction is imposed with relative humidity. A Tempe cell has also been used by some researchers to establish SWRC, though for low values of suction like with pressure plate (Yang et al., 2004). With the use of a pressure plate or desiccator, the stress state of a sample is usually not known. Some researchers (Lloret et al., 2003) have used oedometer and triaxial cells to establish a SWRC. In such tests, the stress state and deformation of the soil were accounted for.

Additionally, SWRCs have been determined empirically from grain size distributions using Eq. 2.5 (Fredlund et al., 1997). The limitation of the equation is that it can only be used on a narrow range of soils (i.e. used for soil which it has been validated on).

$$\boldsymbol{P(d) = \frac{1}{ln\left[\exp(1)+\left(\frac{g_a}{d}\right)^{g_n}\right]^{g_m}}\left\{1-\left[\frac{ln\left(1+\frac{d_r}{d}\right)}{ln\left(1+\frac{d_r}{d_m}\right)}\right]^{7}\right\}} \qquad \textbf{2-5}$$

where *P(d)* is the percentage passing a particular grain size, *d*(mm), g_a is the fitting parameter corresponding to the initial break in the grain size distribution curve, g_m is the fitting parameter corresponding to the curvature of the particle size curve, g_n is the fitting parameter corresponding to the maximum slope of the particle size distribtion curve, d_r is the residual particle diameter and d_m is the minimum particle diameter (mm).

Another empirical equation (Eq. 2.6) was proposed by Feng & Fredlund (1999) for establishing the hysteresis curve. Again, this model depends on experimental data to establish full wetting and drying curves, although only limited data is required for the model. As per Pham et al. (2003), the model works well for low swelling soils.

$$\boldsymbol{w(\psi) = \frac{w_u b + c\psi^d}{b+\psi^d}} \qquad \textbf{2-6}$$

where *c* is the water content at relatively high suction, *d* and *b* are fitting parameters and control the air entry value when w_u and *c* are constant.

2.7.3 Factors that affect the SWRC

The shape of the soil water characteristic curve is affected by grain size/soil type, stress history, void ratio, compaction and compaction effort. In case of grain size, the slope of the SWRC increases with increasing grain size. For instance, the slope of a sandy soil is steeper than that of a clay, as shown in Fig. 2.14a; a relationship which is evident from the studies by Barbour (1998) and Yang et al. (2004). Their studies showed that, as you move from coarse grain to fine grain, the slope of the curve gets flatter and the air entry value, as well as the residual suction increases. This phenomenon is linked to reduction in the pore sizes as you move from coarse to fine grained soil. Additionally, the capillary regime is usually larger in clay soils, indicating that clay soils can sustain higher tension. This is attributed to the geometrical constraints imposed by the clay network and physio-chemical forces (Baker & Frydman, 2009).

An increase in consolidation/ dry density also affects the SWRC by shifting the position of the curve to the right; thereby resulting in an increase in the air entry value as shown in Fig. 2.14b (Huang, 1994 in Barbour, 1998; Yang et al., 2004). This has also been attributed to the reduction in the size of the largest pores with consolidation resulting in menisci with smaller radii of curvature. Similar findings were also made by Karube & Kawai (2001). They reported a decrease in air entry value with an increase in void ratio.

Furthermore, an increase in compaction water content and compaction effort affects the shape of SWRC. Soils compacted wet of optimum have a higher air entry value with a steeper slope than soils compacted dry of optimum (see Fig. 2.15). This is also due, in part, to changes in soil structure with change in compaction water content, as previously explained in Sec. 2.3.3.

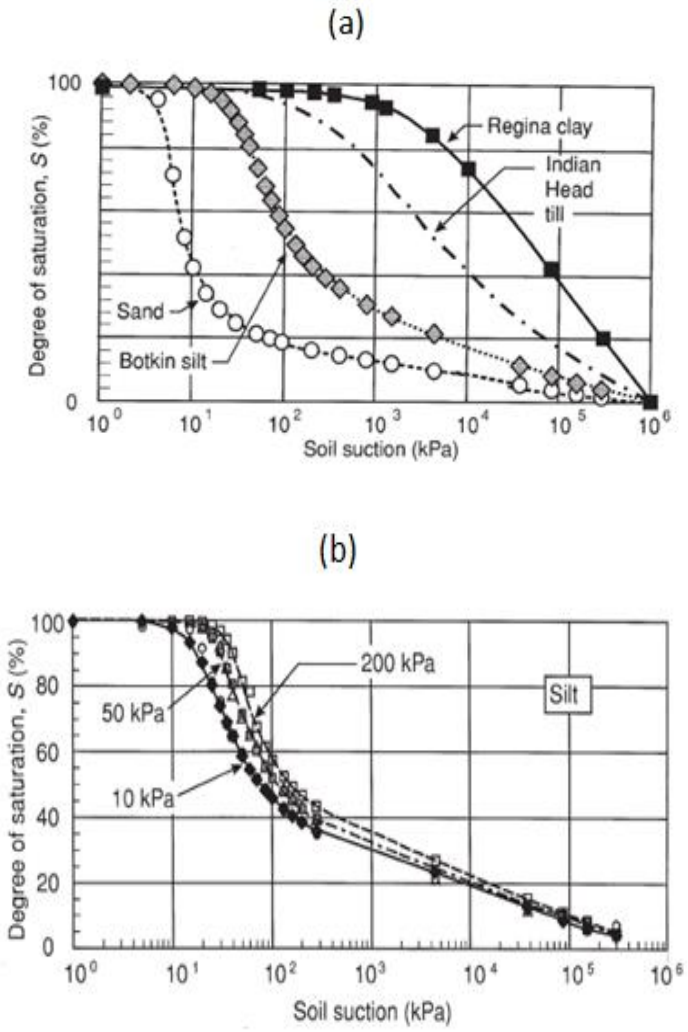

Figure 2-14 Influence of (a) soil texture (b) consolidation on the SWRC (Barbour, 1998)

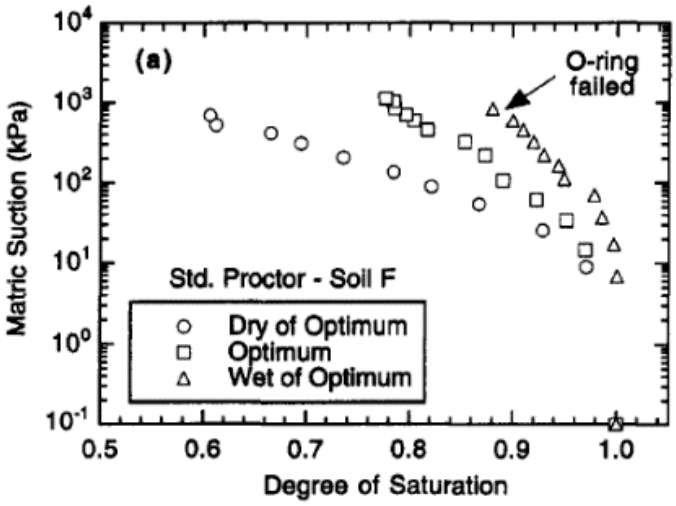

Figure 2-15 Effect of compaction water content on SWRC (Tinjum et al., 1997)

Soils compacted at the dry of optimum water content have bimodal pore size distribution, resulting in formation of macro-pores between particles that are remoulded during compaction, while soils, compacted at the wet of optimum have unimodal pore-size distribution with micro-pores (Tinjum et al., 1997). The formation of macro pores, when soils are compacted at the dry of optimum, results in a decrease in air entry value because the sizes of the pores are large and cannot sustain high suction along the capillary zone. Also, an increase in compaction effort affects the shape of the SWRC. Soils compacted with high compaction pressure have higher air entry values, as observed by Tinjum et al. (1997), owing to the reduction in the sizes of larger pores associated with increased compaction effort and thus an increase in the relative number of pores associated with capillarity.

2.7.4 Mathematical models for the SWRC

Unsaturated soil parameters for constitutive models are evaluated from the SWRC. However, long testing times required in establishing a full and continuous SWRC are limiting the development of these models (Fredlund et al. 2012). Several mathematical models, e.g. Eq. 2.7 (Gardner, 1958), Eq. 2.8 (Brooks & Corey, 1964), Eq. 2.9 (Mualem, 1976), Eq. 2.10 (van Genuchten, 1980) and Eqs. 2.11 & 2.12 (Fredlund & Xing, 1994) have been formulated and are used in fitting experimental data to obtain full and continuous SWRCs. Fredlund & Xing (1994) suggested an additional equation (see Eq. 2.13) with the residual water content as a fitting parameter.

$$w = w_r + \frac{w_s - w_r}{1+\left(\frac{\psi}{a_g}\right)^{n_g}} \quad \textbf{2-7}$$

$$w = w_r + (w_s - w_r)\left(\frac{a_{bc}}{\psi}\right)^{n_{bc}} \quad \textbf{2-8}$$

$$w = w_r + \frac{w_s - w_r}{\left[1+\left(\frac{\psi}{a_m}\right)^{n_m}\right]^{m_m}} \quad \textbf{2-9}$$

$$w = w_r + \frac{(w_s - w_r)}{[1+(\alpha_{vg}\psi)^{n_{vg}}]^{m_{vg}}} \quad \text{2-10}$$

$$w = C(\psi)\frac{w_s}{[\ln(e+(\frac{\psi}{a_f})^{n_f})]^{m_f}} \quad \textbf{2-11}$$

$$C(\psi) = \left[1 - \frac{\ln\left(1+\frac{\psi}{\psi_r}\right)}{\ln\left(1+\frac{1000000}{\psi_r}\right)}\right] \quad \textbf{2-12}$$

$$w = w_r + \frac{w_s - w_r}{\left\{ln\left[e+\left(\frac{\psi}{a_f}\right)^{n_f}\right]\right\}^{m_f}} \quad \textbf{2-13}$$

In the equations listed, m, n and a; are fitting parameters; w_s is the saturated water content, w_r is the residual water content. Fredlund & Xing (1994) and van Genuchten (1980) explained that the fitting parameters can be obtained graphically or through least square fitting method. Leong & Rahardjo (1997) explained that most of the SWRC models are formulated from a single generic equation with seven parameters (see Eq. 2.14).

$$a_1\Theta^{b_1} + a_2\exp\left(a_3\Theta^{b_1}\right) = a_4\Psi^{b_2} + a_5\exp\left(a_6\Psi^{b_2}\right) + a_7 \quad \text{2-14}$$

where a_1, a_2, a_3, a_4, a_5, a_6, b_1, b_2 are constants, Ψ = suction pressure and Θ = normalized/dimensionless volumetric water content $(w_w - w_r)/(w_s - w_r)$, where w_w = volumetric water content, w_r = residual water content and w_s = saturated water content. The dimensionless water content is usually equivalent to degree of saturation provided the volume change of the soil structure is negligible as suction changes (Fredlund et al., 2012). It is used to reference the water content range to saturated water content.

The models from Gardner, Mualem and van Genuchten appear to be similar, except for the fact that Gardner's model is a two-parameter model, while Mualem and van Genuchten models are three parameter models, when the m parameter (a parameter related to the slope of the SWRC) is not fixed. Manipulation of corresponding fitting parameters in both Fredlund & Xing and van Genuchten models affects the shape of the curves in a likely manner, as shown in Fig. 2.16 (Leong & Rahardjo, 1997). From Fig. 2.16, it could be observed that the SWRC shifts to the left with increasing "parameter a" (which is a fitting parameter related to air entry suction). This is because the pore size distribution function that formed the basis of FX model is a modification of van Genuchten's pore size distribution function.

The general shape for most SWRCs is sigmoidal (Leong & Rahardjo, 1997). But this depends on the equation used to fit the experimental data, as some equations (e.g. Gardner, 1958; Brooks & Corey, 1964) will not give sigmoidal curves and hence will not produce a good fit. Based on this and earlier discussions, further discussions will be on the Fredlund & Xing and van Genuchten models.

van Genuchten (1980)

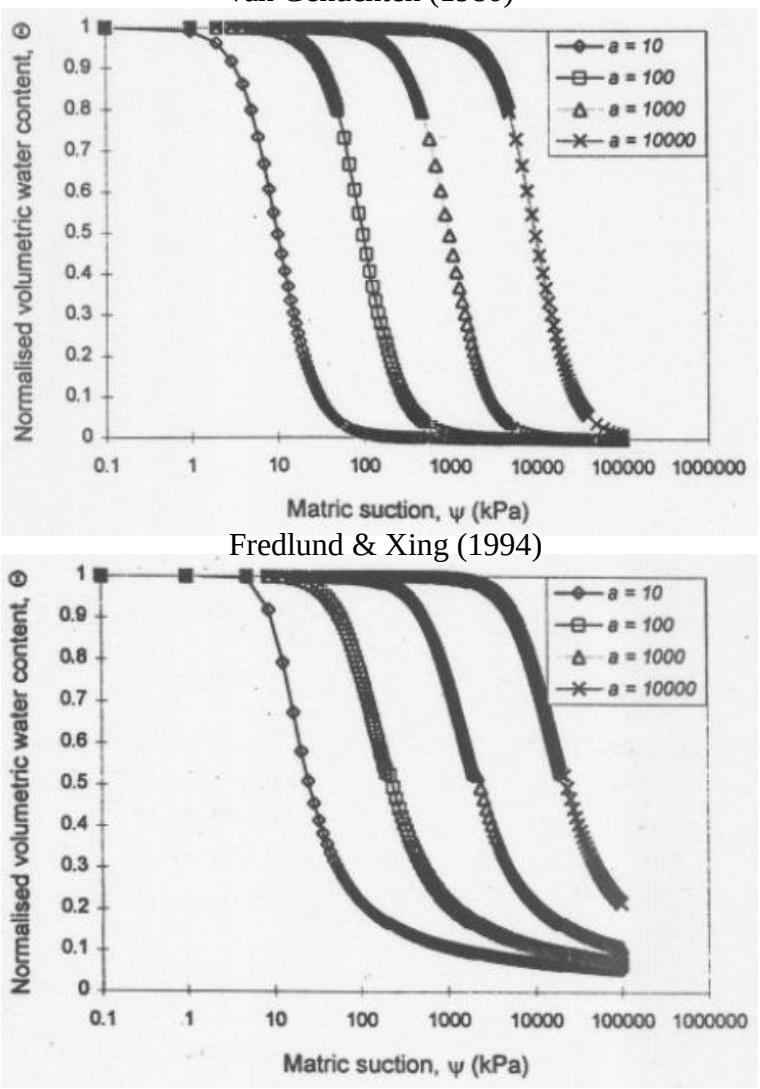

Fredlund & Xing (1994)

Figure 2-16 Effect of fitting parameter "a" on the shape of van Genuchten (1980) and Fredlund & Xing (1994) soil water retention models (Leong & Rahardjo, 1997)

van Genuchten's model is formulated from Mualem's model and is a three-parameter model, when w_r is known. However, the m parameter can be fixed by relating m to n through the equation: m = 1-1/n that then reduces the model to a two-parameter model. Fredlund & Xing's model assumes that the shape of the SWRC is dependent on the pore

size distribution of soils. A correction factor C (ψ) is introduced (Eq. 2.12) in the model that forces the curve to pass through zero water content at a suction of 1000000kPa. The assumption of 1000000kPa suction for the residual water content is based on the evidence produced by Coleman & Croney (1961 in Leong & Rahardjo, 1997) which showed that soil water content approaches zero at a soil suction of 1000000kPa. This is also supported by thermodynamics relationship Eq. 2.3 (Kelvin's equation). From Eq. 2.3, at a temperature of 20^{o}C and relative humidity of 0.01%, the total suction is approximately 1000000kPa. However, at 50^{o}C which is the temperature used in this study, suction value of about 1300000kPa is estimated at the same relative humidity of 0.01%.

Some of the models have been shown to perform better than the others. The number of parameters has also been linked to the performance of the models. Leong & Rahardjo (1997) reported that the more the number of a model's parameters, the better its performance. In addition, some models have been reported to be satisfactory for specific soils, while others are suitable for all soils. Among all the models, Fredlund & Xing (1994) Eq. 2.11 and 2.12 have been rated best for fitting all soil types, especially when the correction factor C(ψ) is set to a value of one (Leong & Rahardjo, 1997). The same two equations have also been reported to fit satisfactorily over the entire range of suction (Fredlund & Xing, 1994). This is followed by the van Genuchten (1980) Eq. 2.10, which fits well at high and medium water content; Eq. 2.13 from Fredlund & Xing (1994) is optimal with residual suction.

2.8 MECHANICAL BEHAVIOUR OF UNSATURATED CLAY SOILS

2.8.1 Shear strength of unsaturated clay soils

Shear failure occurs in soils when the shear stress is more than the shear strength of the soil. Many geotechnical problems such as bearing capacity, lateral earth pressures, slope stability are based on the shear strength of soils (Fredlund & Rahardjo, 1993). Like deformation problems, shear strength is also related to the stress state variable.

Although the failure of effective stress principle in unsaturated soils is mainly associated with volume change. An equation based on the independent stress variables was also proposed for shear strength (Fredlund et al., 1978) see Eq. 2.15.

$$\tau = c' + (\sigma - u_a) \tan\phi' + (u_a - u_w) \tan\phi^b \qquad \textbf{2-15}$$

Where τ is the shear strength, c' is the cohesion, ϕ' is the friction angle, ϕ^b is the friction angle in relation to suction. The dependence of shear strength on suction was studied by Wheeler & Sivakumar (1995). In their study, they realized that shear strength increases with an increase in suction; an effect attributed to increase in meniscus water as the soil dries up (suction increase), resulting in additional normal forces that binds the soil particles together. This was supported by Tarantino & Tombolato (2005), but they also pointed out, that the ultimate shear strength of unsaturated soil is not only controlled by suction and net stress, but also by the degree of saturation. The discussion on shear strength will not be detailed as the research focus is on volume change.

2.8.2 Volume change of unsaturated soils and constitutive models

Following on the formulation of independent stress variable for unsaturated soils, Matayas & Rahardshinka (1968) explained the volume change behavior of unsaturated soil using the formulated stress variables. They proposed equations for defining the state function in unsaturated soils under isotropic and k_o conditions using the proposed independent stress variables. The equations define the stress dependent state parameters; void ratio *e* and degree of saturation S_r under triaxial condition as shown in Eq. 2.16 & 2.17.

$$\boldsymbol{e = F(P - u_a, q, \psi, e_o, S_{ro})} \qquad 2\text{-}16$$

$$\boldsymbol{S_r = \emptyset\left(P - u_a, q, \psi, e_o, S_{ro}\right)} \qquad 2\text{-}17$$

Where P_a, q & ψ are stress parameters, e_0 *and* S_{ro} are state parameters; initial void ratio and initial degree of saturation respectively. They explained that the state of a soil can be described by the stress state, void ratio e, degree of saturation *Sr* without reference to its previous structure. Furthermore, the state histories of different test paths were then presented as state surface on a (σ, e, u_a - u_w) or (σ, Sr, u_a - u_w) space as shown in Fig. 2.17. The surface for void ratio and suction are wrapped. The shape of the surface is greatly influenced by the initial void ratio, soil type, initial suction and degree of saturation.

Matayas & Rahardshinka (1968) observed that compressibility was greatly influenced by suction as also observed by Barden & Sides (1970). Higher suction will result in more rigid and less compressible soil structure. Wetting at constant applied stress could result in either swelling or collapse depending on the magnitude of applied vertical stress and

the density of the soil. These behaviours were also confirmed by Lloret &Alonso (1980); Alonso et al. (1987); Lawton et al. (1989), Wheeler & Sivakumar (1995). Usually, the swelling on wetting is limited to a low value of vertical applied stress. For the soils tested by Matayas & Rahardshinka (1968), collapse behaviour was observed on wetting at low value of vertical stress for isotropic tests while swelling was observed in the soil tested under k_o condition. Lloret &Alonso (1980) explained that the direction of volume changes on wetting (collapse or swell) is greatly influenced by the clay content and initial structure. Potentially unstable soils and soils with low clay content will experience collapse, while soils with high clay content will experience swell. Matayas & Rahardshinka (1968) pointed out that changes in void ratio appeared to be independent of the path followed, i.e. two samples that followed different testing paths finally arrived at the same void ratio. This agreed with the finding of Barden & Sides (1970), but they noted that this was only true for the same saturation process, reversal in direction of saturation will lead to stress path dependence.

For highly expansive clays, Pousada (1984 in Faruella et al. 2010), Alonso et al. (1995), Al-Homoud et al. (1995) reported shrinkage or swelling accumulation during cycles of wetting and drying. Farulla et al. (2010) also reported shrinkage accumulations on compacted scaly clay during cycles of wetting and drying, which increased with vertical net stress. They explained that most of the accumulated shrinkage strain occurred during the first cycle and then the soil tends to reversible and elastic strain on subsequent cycles.

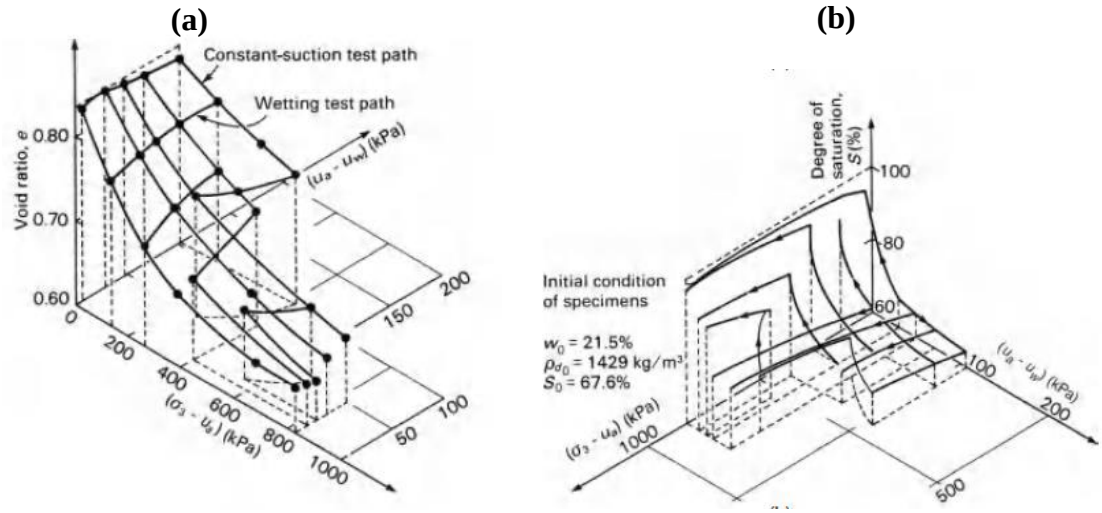

Figure 2-17 (a)Variation of void ratio and (b) degree of saturation in e, σ, *Sr* and ψ space (Matayas & Radharshinka, 1968)

Incidentally, some factors limited the use of state surface proposed by Matayas & Rahardshinka (1968) for all soils. First, the state surface for k_o and isotropic paths is unique only if the imposed path involves a non-decreasing degree of saturation, but for other stress paths and expansive soils, lack of uniqueness was found. Second, different criteria proposed for finding the swell pressure of expansive soils led to different values. Hence, swell pressure is path dependent and should not be viewed as a fundamental property of expansive soils. Third, change in suction under specific applied load results to irreversible volume change.

To establish a unified and consistent way of thinking, Alonso et al. (1987) proposed the concept of the yield curve. The yield curve in *suction (ψ): yield stress(p)* plane could explain the occurrence of yielding, plastic compression and elastic swelling during loading (increase in p) and wetting (decrease in s) see Fig. 2.18. The curve predicts irreversible and reversible compressive strain for any stress path within the plastic and elastic zone respectively. For instance, in Fig. 2.18, an increase in *p* or a decrease in *s* will reposition the yield surface from A_1B_1 to A_2B_2. During the transition, some irreversible and plastic compressive strain will be induced after the yield surface A_1B_1. The curve A_1B_1 predicts that the yield stress p_o increases with an increase in suction on loading (path L) and the magnitude of collapse associated with wetting increases with applied stress p (path C). Hence, the curve is named "Loading-Collapse" curve.

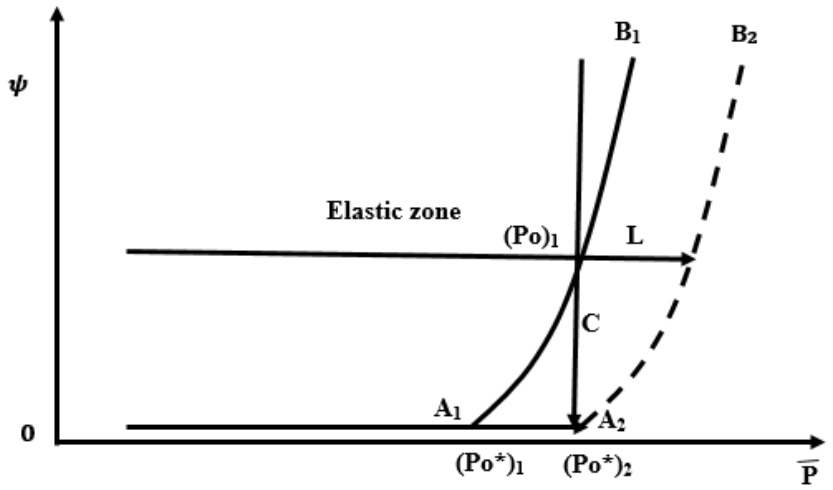

Figure 2-18 Proposed yield curve showing loading and collapse paths (after Alonso et al., 1987)

Alonso et al. (1987) explained that an increase in suction beyond the suction previously reached by an unsaturated soil will induce an irrecoverable volumetric strain. Thus, an additional yield curve SI is introduced, depicting maximum applied suction, beyond which plastic volumetric strain is induced. Both SI and LC curves bounds the elastic region in the (ψ: p) plane. Some degree of coupling exists between suction increase and loading collapse surfaces. An increase in suction across the yield surface will affect the response of a soil to loading along p and repositions the yield surface to the right.

They also reported that the shape and position of the LC curve is greatly influenced by compaction energy and initial fabric induced by compaction. For example, increase in compaction energy will result to a denser sample and higher pre-consolidation pressure, thereby shifting the LC curve to the right. This was supported by the study of Sivarkumar & Wheeler (2000) on compacted kaolin clay; an increase in compaction energy resulted in an expansion of the yield curve while an increase in compaction water content affected the initial state of the soil through the initial value of suction and the position of the normal compression line. They emphasized that, soils compacted at different water content can be treated as fundamentally different soils.

For expansive soils, an additional yield surface SD in form of a straight line was introduced as shown in Fig. 2.19 to represent increase in volume/swell on wetting. A decrease in suction below SD (SD_1 - SD_2) surface will result in an irreversible swell and a shift of the LC (LC_1 – LC_2) surface to the left, indicating an apparent reduction in pre-consolidation pressure.

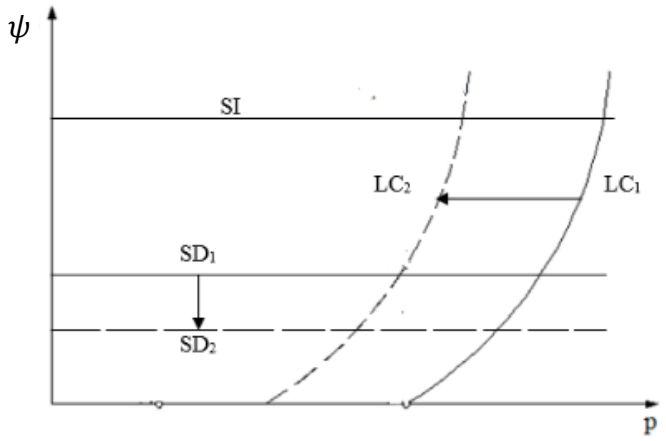

Figure 2-19 Yield surface SD for expansive soils (after Alonso et al., 1987)

Furthermore, Alonso et al. (1990) extended the works of Alonso et al. (1987) by formulating an equation for the constitutive model. This was based on two stress state variables and hardening plasticity law which reduces to critical state at full saturation. The model could explain in a unified and consistent approach, many of the features of unsaturated soil behavior treated separately, including the stress path dependence which other models have failed to explain.

Alonso et al. (1990) proposed mathematical expression for the LC yield using the equation of a virgin compression line (for isotropic state) and for unloading curve, see Eq. 2.18 and 2.19 respectively.

$$\boldsymbol{v = N(\psi) + \lambda(\psi) ln \frac{p}{p^c}} \qquad \textbf{2-18}$$

$$\boldsymbol{dv = k \frac{dp}{p}} \qquad \textbf{2-19}$$

where p is the net mean stress, p^o is the pre-consolidation stress, po^* is the pre-consolidation stress for saturated condition, p^c is the reference stress, $N(\psi)$ is the specific volume at $p = pc$, $\lambda(\psi)$ is the stiffness parameter for changes in net mean stress of the soil, k is elastic stiffness parameter for changes in mean net stress, υ is specific volume.

The proposed expression relates the behaviour of two samples at different suction $\psi = 0$ for saturated condition and $\psi = \psi$ for higher suction. The sample at $\psi = \psi$ will yield at a higher stress po, while $\psi = 0$ will yield at po* as shown in Fig. 2.20. Both stress paths are presented in a (p, ψ) by relating the N(s) at point 1 and 3 through a path that involves unloading at constant suction from p_o to p_o^* and then reduction in suction from ψ to 0 at constant po* (path 1-2-3). Since wetting at constant po* (path 2-3) is inside the yield surface, it is elastic and is considered as reversible swelling ΔVs. This was represented by Eq. 2.20. Note that p_{at} has been added to ψ in Eq. 2.20 to avoid infinite values as ψ approaches zero.

$$dv = -k_s \frac{ds}{(\psi + p_{at})} \qquad \textbf{2-20}$$

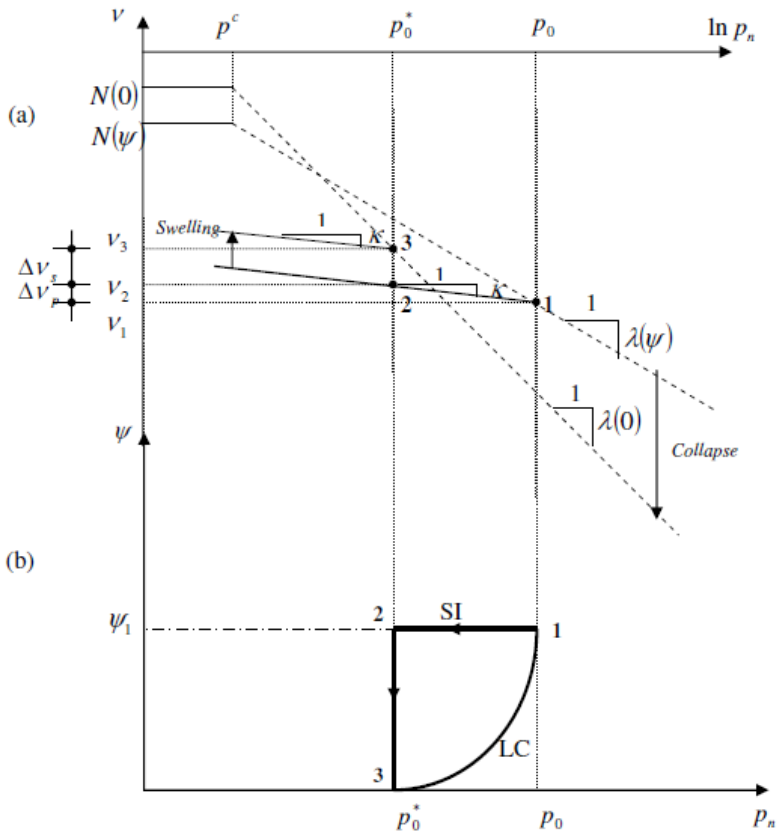

Figure 2-20 Relationship between pre-consolidation stresses Po and Po*: (a) compression curves for saturated and unsaturated soils (b) stress path and yield curve in (p, ψ) space (Alonso et al., 1990)

Alonso et al. (1990) proposed Eq. 2.21 and Eq. 2.22 to explain the increase in yield stress with suction as well as collapse observed on wetting. For stress paths involving initial decrease in suction and then loading at constant suction, the final specific volume for the stress state is given was explained by Eq. 2.23. Additionally, they proposed mathematical relationship between stiffness and suction was also formulated as given by Eq. 2.24.

$$N(\psi)-\lambda(\psi)\ln\frac{p_o}{p_o*}+k\ln\frac{p_o}{p_o*}+k_\psi\ln\frac{\psi+p_{at}}{p_{at}}=N(0)-\lambda(0)\ln\frac{p_o*}{p^c} \qquad \textbf{2-21}$$

$$\frac{p_o}{p^c}=\left(\frac{p_o*}{p^c}\right)^{[\lambda(0)-k]/[\lambda(s)-k]} \qquad \textbf{2-22}$$

$$v(p,\psi)=v(p^c,\psi_i)+\Delta v(p^c)\Big|_{\psi i}^{\psi}+\lambda(\psi)\ln\frac{p}{p^c} \qquad \textbf{2-23}$$

$$\lambda(\psi) = \lambda(0)\left[(1-r)\exp\left(-\beta_{\psi}\right)+r\right] \qquad \textbf{2-24}$$

Where r is a constant related to maximum stiffness of the soil (for an infinite suction), $r = \lambda(\psi \rightarrow \infty)/\lambda(0)$ and β is a parameter which controls the rate of increase of soil stiffness with suction. For simplicity $\psi = \psi_0$ is assumed as a constant. Where ψ_0 is the maximum past suction ever experienced by the soil and bound the transition from elastic to plastic state (virgin state) due to an increase in suction.

For hardening law, the plastic volumetric deformation due to increase in p and ψ on reaching the yield curves is given by Eq. 2.25 & Eq. 2.26 respectively.

$$\frac{dp_o}{p_o *} = \frac{v}{\lambda(0)-k} d\varepsilon_v{}^p \qquad \textbf{2-25}$$

$$\frac{d\psi_0}{\psi_0 + p_{at}} = \frac{v}{\lambda_{\psi} - k_{\psi}} d\varepsilon_v{}^p \qquad \textbf{2-26}$$

Where ε_v is total volumetric strain

In summary, the model assumes that $\lambda(\psi)$ decreases with increasing suction, implying that the collapse potential on wetting would increase indefinitely with increasing net vertical stress and as a result, the maximum collapse potential could not be accounted for by the model. At the reference pressure *pc* the loading collapse yield curve LC is a vertical straight line in the *suction versus mean net stress* plane.

The model of Alonso et al. (1990) is valid for a limited range of net vertical stress and suction depending on the material. Subsequently, Josa et al. (1992) extended the model of Alonso et al. (1990) to account for maximum collapse potential and larger stress range. Wheeler & Sivarkumar (1995) proposed an alternative model that assumes that virgin compression takes place only when the applied stress is greater than the yield stress or maximum collapse potential. In their work, they postulated a state boundary hypersurface joining the critical state and normal compression hyper-lines (previously proposed by Alonso et al. 1990). The hypersurface is defined by $v = f_4(p,q,\psi)$. Elastic behaviour is exhibited by a soil with its state lying inside the hypersurface. When the state transverses the hypersurface, the behaviour becomes plastic, which then leads to expansion of the yield surface as shown in Fig. 2.21.

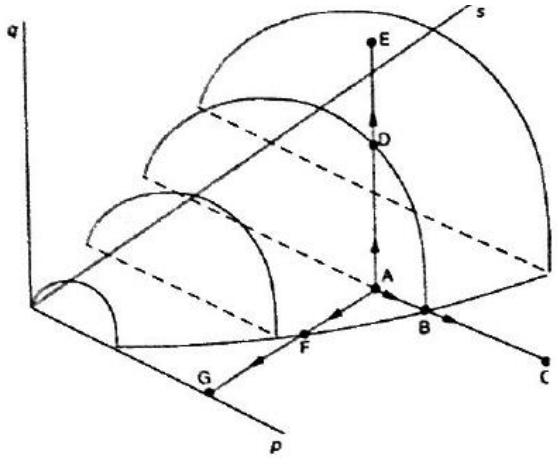

Figure 2-21 Yield surface for unsaturated soils (Wheeler & Sivakumar, 1995)

Based on series of triaxial tests following ramped consolidation, Wheeler & Sivarkumar (1995) observed that the soil state once the yield is exceeded is along a normal compression line defined by $v = N(\psi) - \lambda(\psi)\, ln(p/p_{at})$; where N($\psi$) and $\lambda(\psi)$ are intercept and slope (stiffness parameter) of the normal compression lines respectively. From their triaxial tests, they observed that N(ψ) and $\lambda(\psi)$ increase with increasing suction as shown in Fig. 2.22b, in contrast to Alonso et al. (1990), but consistent with Josa et al. (1992). From the stress path shown in Fig. 2.22, they derived an equation for the LC yield curve (see Eq. 2.27) by relating change in specific volume Δv due to changes in stress from A to C in Fig. 2.22a through the swelling indices k and k_s.

$$(\boldsymbol{\lambda(\psi) - k})\ \mathbf{ln}\left(\frac{\boldsymbol{P_o}}{\boldsymbol{P_{at}}}\right) = (\boldsymbol{\lambda(0) - k})\ \mathbf{ln}\left(\frac{\boldsymbol{P_o(0)}}{\boldsymbol{P_{at}}}\right) + \boldsymbol{N(\psi) - N(0) + k_{\psi}}\ \mathbf{ln}\left(\frac{\boldsymbol{\psi + P_{at}}}{\boldsymbol{P_{at}}}\right) \quad 2\text{-}27$$

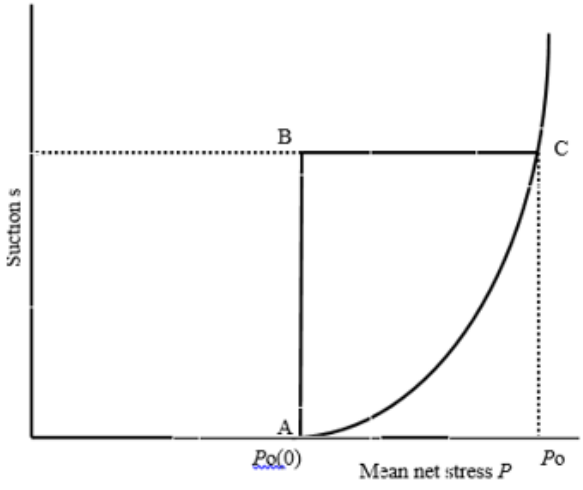

(a)

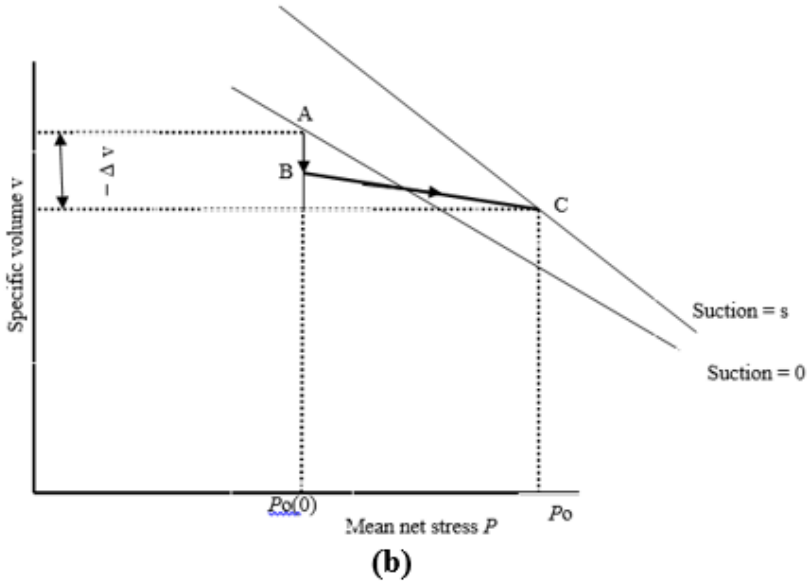

Figure 2-22 Diagrammatical representation of LC yield curve (Wheeler & Sivakumar, 1995)

P_{at} is included in Eq. 2.27 to enable the equation to be used at zero suction. The equation is assumed to describe the shape of the yield curve for all values of *Po(0),* which is considered as an advantage relative to the model of Alonso et al. (1990) because it is easier to obtain $N(\psi)$ (for different suction values) experimentally than to measure Pc for the reference pressure.

The work of Wheeler & Sivarkumar (1995) validated the assumption that the plastic compression due to collapse on wetting and that due to loading can be described by a single unique surface because they are of the same process.

Gallipoli et al., (2003) proposed an elasto-plastic model which builds on Bishop's effective stress model to explain the processes through which suction affects the mechanical behaviour of unsaturated soils and how the processes are influenced by degree of saturation. The processes include; change in the average soil skeleton stress resulting from changes in the average fluid pressure acting on the soil pores and provision of additional normal force at the inter-particle contact. The degree of saturation influences the area over which the air and water pressures act, as well as the capillary action at inter-particle forces. Gallipoli et al., (2003) explained that the use of average skeleton stress alone in constitutive models cannot account for some of the key features of unsaturated soils (e.g. collapse on wetting and increase in pre-consolidation pressure on drying). In

order to account for these features, Gallipoli et al. (2003) proposed a model of the form $\xi = f(\psi)(1\text{-}Sr)$ where ξ is a variable that accounts for the magnitude of inter-particle bonding due to water menisci and is a product of degree of saturation of air $(1\text{-}Sr)$ and the function of suction, $f(\psi)$ as shown by the model. The model in addition to average skeleton stress accounts for additional normal force at the inter-particle contacts using ξ which is related to the number of water menisci per unit volume of the solid fraction and the intensity of the stabilising normal stress exerted at the inter-particle contact by a single water meniscus. The term $(1\text{-}Sr)$ is related to the number of water menisci per unit volume of solid fraction. It tends to zero when the soil is saturated and increases as the number of menisci increases. The term $f(\psi)$ on the other hand varies between 1 and 1.5 for suction values ranging between zero and infinity respectively.

2.8.3 Expansive and collapsible soils

Natural deposits of unsaturated soils experience swell or collapse on wetting. These soils are often named after their behaviour; expansive soils (for swelling clays) and collapsible soils (for collapsing soils). Elementary clay arrangements previously discussed in Sec. 2.3 are dominant in expansive soils, whereas grains bonded with clay particles are dominant in collapsing soils (Alonso et al., 1987).

Expansive soils experience large volume change (swelling) due to wetting. This behaviour is usually linked to high content of swelling clay minerals such as montmorillonite and smectite (Al Rawas, 1999; Jones & Jefferson, n.d.). The mode of swelling in expansive clays is known as intra-crystalline swelling (Grim, 1962). Weak bonds exist between the molecular layers that make up a crystal of montmorillonite and smectite. On wetting, water enters the crystals as well as the unit layers that make up the crystals, thereby causing expansion of the soil. For soils with these clay minerals, high magnitude of swelling is usually encountered on wetting and it is this aspect of behaviour that made soils with the clay minerals useful as a barrier for nuclear waste isolation (Yong, 1999; Delage et al., 2010). The swelling on wetting leads to self-healing of cracks and fissures left after placement and compaction. Expansive soils can also collapse on wetting depending on the position of the wetting path on the LC yield curve. This is usually at high values of applied net stress. Several studies have also shown that compacted non-expansive clay soils can also undergo swelling on wetting when compacted to high density (e.g. Lawton et al., 1992; Sivarkumar & Wheeler, 2000). In this case, the mechanism of swelling on wetting is categorised as inter-crystalline swelling

(Grim, 1962). The soil particles are initially held together by water under tension due to capillary forces. On getting access to free water, the capillary forces relax on absorption of water, causing expansion of the soil. The water absorption is limited to only the void spaces and external crystal surfaces unlike in expansive soils where water enters in-between the crystals.

Collapsible soils, e.g. loess experience collapse on wetting, even though they commonly exhibit high shear strength and stiffness in their natural state (Houston et al., 2001, Liu et al., 2016). Deposits of loess are found widely around the world, especially in arid regions where there is little rainfall and much evaporation (Liu et al., 2016). These soils are usually alluvial, colluvial and windblown with high void ratio and dried clay in-between particles (Houston et al., 1988). Rogers (1995) explained that in natural soils, collapsible soils are often associated with the young geological deposits. Collapsible soils have high suction at inter-particle contacts that produces bonding like effect. On wetting, the high suction at inter particle contact is reduced, and the bonding material weakens resulting in collapse (Barden et al., 1973). In fact, four conditions are required for collapse to occur as explained by Barden et al. (1973); Mitchell (1976 in Lawton et al., 1992).

- An open potentially unstable unsaturated structure.
- A high value of applied stress to develop a metastable condition.
- A high value of suction or other bonding agents to stabilize intergranular contacts which collapses on wetting.
- Addition of water to the soil, which reduces the bonding agent or suction and causes shear failure at the inter-particle contacts.

Alonso et al. (2010) noted that in some cases, the self-weight of the soil is enough to trigger the collapse on wetting. In a case where the soil has been previously wetted, they explained that the collapse will occur at a stress level higher than that at which the soil has been previously wetted.

2.8.4 Methods of determining collapse potential

The double oedometer tests proposed by Jenning and Knight (1957) are mostly used in quantifying the amount of collapse on wetting. Other tests used in quantifying collapse are; single oedometer tests (Houston et al., 1988) and single point multiple specimen test procedure (Noorany, 1992). In the double oedometer, two tests are performed with identical samples; constant water content test and saturated test (also known as free swell

test). The first test involves loading at constant water content, giving the constant water content compression curve. In the second test, the sample is loaded after saturation (usually saturated under a small sitting load) and the saturated compression curve is obtained from this test. The collapse potential is then obtained from the difference in void ratio between the saturated and constant water content tests at each value of applied stress. In the single oedometer test, a soil sample is loaded to a vertical stress of 200kPa and then saturated under this value of applied stress. In this case, the collapse potential is calculated from the change in void ratio when water was introduced to the sample. For the single point, multiple specimen tests, different samples of the same initial conditions are loaded to different values of vertical stress and then each sample is saturated under its applied stress. A whole range of vertical stress is usually covered, this way, the saturated compression curve can be traced. Lawton et al. (1989) noted that the collapse potential obtained from double oedometer test at each value of vertical stress will correspond to that obtained from single point test.

2.9 INFLUENCE OF TEMPERATURE ON THE BEHAVIOUR OF UNSATURATED SOILS

The effect of temperature on soil properties is a subject of interest to Geotechnical engineers due to numerous Geo-mechanical applications involving temperature variations. Regarding saturated soils, the effect of increasing temperature on the mechanical behaviour and properties of saturated soils has been researched by many authors, (e.g. Campanella & Mitchell, 1968; Baldi et al., 1988; Cekerevac & Laloui, 2010). The major conclusions drawn from most of the studies are;

a) Heating induces expansion under high over-consolidation ratio (at low vertical net stress) and contraction under low OCR. The thermal expansion observed on heating at low vertical net stress is attributed to expansion of soil constituents; water and solid, whereas thermal contraction on heating at high vertical net stress is ascribed to weakening of contacts between aggregates (Cui et al., 2000).
b) Contraction on heating under low OCR results in densification/thermal hardening thereby causing heat induced over-consolidation.

On the contrary, the effect of high temperature on unsaturated soils especially under non-isothermal condition is not yet well established for all soils, due in part to the mixed

findings by different researchers. The conflicting findings might be due to the different mineralogical compositions and initial conditions of the soils used in the individual studies, as well as complexities associated with unsaturated soils. Consequently, literature on the subject will be grouped under expansive soils and non-expansive soil as well as the testing path followed.

2.9.1 Influence of temperature on mechanical behaviour of expansive soils

Stress path: wetting and drying at constant vertical stress and temperature (isothermal wetting)

For this testing path, a sample at a specified temperature is brought to the required vertical net stress on a loading path, and then subjected to wetting through suction reduction and then drying through increasing suction. As explained in Sec. 2.8.3, expansive soils undergo substantial swelling on wetting (usually at low applied stresses). It has been reported that an increase in temperature on wetting either enhances or reduces the swelling property of expansive clays (Romero et al., 2003; Romero et al., 2005; Gens et al., 2007). In the studies of Romero et al. (2005) on Boom clay subjected to wetting at constant vertical net stress, additional swelling was observed due to an increase in temperature from 22^{o}C to 80^{o}C. The observed swelling was evident at low values of vertical net stress (between 0.025MPa – 0.3MPa). However, Villar & Lloret (2004); Romero et al. (2005), Lloret & Villar (2007) reported a decrease in the swelling property of saturated FEBEX with an increase in temperature (see Fig. 2.23). In this case, the reduction in swelling observed with an increase in temperature was less evident at high value of vertical net stress (3MPa) as shown in Fig. 2.23. Villar & Lloret (2004) postulated that the process that enhances swelling at high temperature is hindered when the vertical net stress is increased. As discussed earlier in Sec. 2.8.3, it is already well established that swelling on wetting occurs at low values of applied stress (Lawton et al., 1992; Sivakumar & Wheeler, 2000). Thus, an increase in temperature cannot enhance swelling at high applied stress, since the behaviour usually observed is not swelling. Expansive soils compacted to low density usually exhibit collapse on wetting at high vertical stresses and swelling at low vertical stresses. Romero et al. (2003) observed that temperature does not enhance the behaviour of this group of sample on wetting, but rather increases the compressibility associated with loading at constant suction. Drying of heated sample is associated with high shrinkage (Romero et al., 2003).

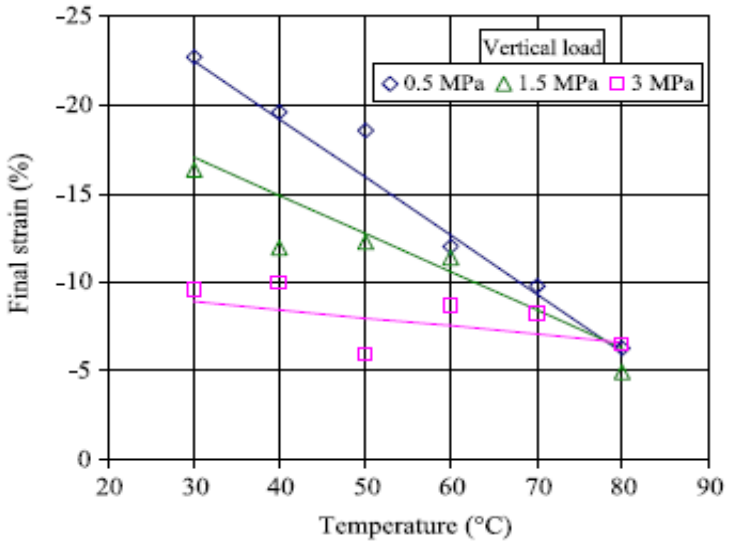

Figure 2-23 Reduction in swelling strain with increasing temperature (Villar & Lloret, 2004)

Loading and unloading at constant suction and temperature

The testing path follows an increasing or decreasing vertical net stress at constant suction and temperatures. Apparently, the compressibility parameters are obtained following this type of stress path. The influence of high temperature on compressibility has been claimed to be dependent on factors such as over-consolidation ratio, plasticity, expansibility and compaction water content/ initial suction (Villar & Lloret, 2004; Tang et al., 2008). For instance, Romero et al. (2003); Lloret & Villar (2007); Tang et al. (2008) demonstrated that an increase in temperature during loading will increase the compressibility associated with loading and reduce the yield stress, thereby reducing the size of the elastic domain. However, Romero et al., (2005) reported an increase in yield stress with an increase temperature to 40^{o}C and 60^{o}C on compacted FEBEX bentonite under a loading path at constant suction. It is worth noting that the samples were first subjected to cycles of wetting and drying before undergoing loading and unloading and that the result may have been influenced by this initial stress path.

There have been conflicting findings from different authors regarding the influence of high temperature on the compressibility parameters. Romero et al. (2005), Tang et al. (2008) demonstrated that the compressibility parameters are insensitive to temperature. Romero et al. (2003) however, reported that the pre-yield parameters are insensitive to temperature, but the post-yield compressibility parameters (stiffness parameter and slope

of the normal compression line) are temperature sensitive; they increase with temperature. On the contrary, Ye et al. (2012) reported a decrease in the slope of the normal compression line with increasing temperature for GMZ01.

Stress path: Heating and cooling at constant suction

The stress path involves heating and cooling of a sample brought to a constant suction through wetting. Increase in volumetric strain with increasing temperature, coupled with strain accumulation has been observed by some researcher under this stress path (Romero et al., 2003; Romero et al., 2005). The direction of volumetric strain usually depends on the initial behaviour of the sample on wetting, which can be linked to the OCR. For instance, if a soil swells on wetting, increasing temperature in the sample will result in increased swelling strain. Romero et al. (2003) also observed that the magnitude of swelling decreases with increasing temperature as suction increases. However, the observations of Tang et al. (2008), Ye at al. (2012) contradicted this assertion. Both observed that samples of MX80 and GMZ01 bentonite expanded on heating at relatively high suction (113 and 39MPa) at both low and high applied stress. In the study of Tang et al. (2008), samples of MX80 bentonite heated to 70^{o}C at a constant suction of 113 and 39MPa and vertical stress of 0.1MPa experienced expansion heating. However, the sample tested at low suction (9MPa) under the same value of applied vertical stress (0.1MPa) experienced contraction on heating. In this case the direction of volumetric strain was dependent on suction value. The sample with high suction value expanded on heating, whereas sample at low suction contracted on heating.

Further on, Romero et al. (2003) demonstrated that the behaviour of samples under thermal actions is stress path independent by comparing results obtained under a thermal cycle at constant suction and those obtained under isothermal wetting as shown in Fig. 2.24. It could be observed from the figure that similar volumetric strains were obtained at 80^{o}C along a wetting path and thermal cycle path. Cooling was associated with an irreversible volumetric strain which reduced on subsequent cycles. Romero et al. (2003) explained that the thermally induced irreversible strain associated with cooling is because of structural rearrangement of particles at the macro-structural level due to thermal expansion at the microstructure.

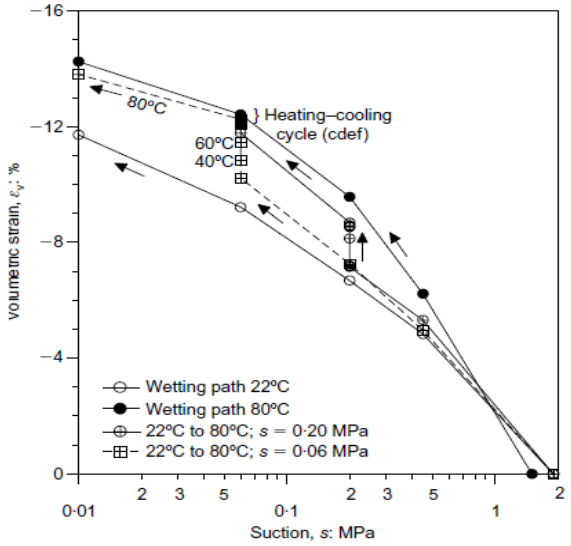

Figure 2-24 Comparing results of isothermal wetting and non-isothermal tests to show stress path independence of thermal behaviour (Romero et al., 2003)

Stress path: Wetting and drying at constant volume, at different temperatures

This type of stress path is usually followed to determine the swelling pressure of a sample. With this stress path, a sample is restrained from changing volume on wetting. Unanimous observations have been made by different researchers regarding the influence of temperature on swelling pressure. Romero et al. (2003), Villar & Lloret (2004), Lloret & Villar (2007) all reported reduction in swelling pressure with an increase in temperature.

2.9.2 Influence of temperature on the mechanical behaviour of unsaturated non-expansive soils

In terms of the influence of temperature on non-expansive unsaturated soils, only limited studies have been carried. Most of the existing studies were carried out under simple stress paths, without considering complex stress paths usually encountered in most scenario.

Folly & Rees (2001) studied the effect of temperature on the volume change behaviour of speswhite kaolin under a loading path at constant temperature and suction. The study was carried with a suction and temperature controlled oedometer cell. Vertical stress was applied through an air pressure controlled loading ram. The saturated samples were

prepared from slurry and then subjected to vertical stresses up to 0.8MPa at two constant temperatures; 25^{o}C and 60^{o}C and three constant suction values 0, 100, 300kPa. Folly & Rees (2001) demonstrated that samples at high temperature exhibited higher compressibility on loading, though at low vertical stress < 400kPa. An increase in temperature caused the softening of the soil. However, at high vertical stress, compressibility seems not to be affected by temperature; convergence of the compression curves was observed at both temperatures as shown in Fig. 2.25. Similar finding was also made by Haghighi (2011) on compacted kaolin subjected to loading at constant matric suction (100, 300 and 500kPa) and temperatures (10^{o}C and 50^{o}C). Haghighi (2011) observed an increase in compressibility and soil softening with an increase in temperature at all values of imposed suction.

Uchaipichat & Khalili (2009) observed from a temperature and suction controlled loading test that the compressibility parameters of silty clay samples were insensitive to temperature. Although they observed softening of the silty soil due to an increase in temperature, they reported a decrease in pre-consolidation pressure with increasing suction at high temperatures (60 and 40^{o}C). The reverse (increase in pre-consolidation pressure with an increase in suction) was observed at 25^{o}C especially for suction values less than the air entry suction. This contradicted other finding in literature (e.g. Alonso et al., 1990; Wheeler & Sivakumar, 1995) in which the pre-consolidation pressure increased with suction. Uchaipichat & Khalili (2009) attributed this difference to the sampling-induced structure. Although sampling induced structure may have caused the difference, the use of single effective stress principle the may be another reason for the difference.

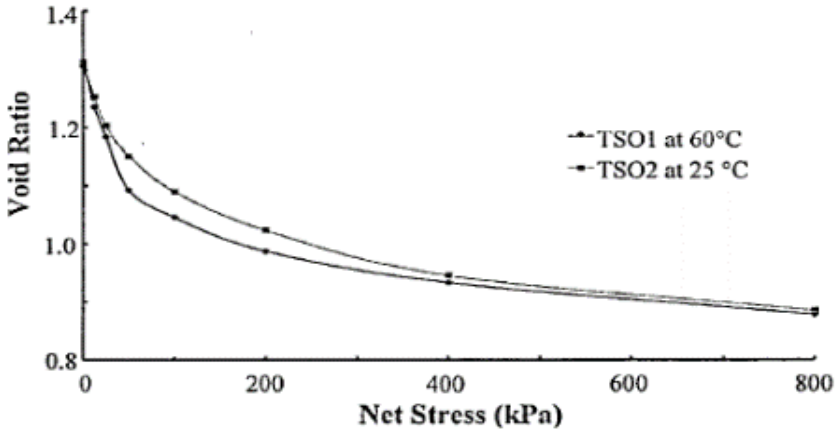

Figure 2-25 Effect of temperature on the compressibility of kaolin (Folly and Rees, 2001)

2.9.3 Influence of temperature on hydraulic behaviour of soils

The effect of temperature on hydraulic properties of saturated soil has long been established. A unanimous observation is that an increase in temperature increases the hydraulic conductivity of saturated soils (Pusch, 1980; Towhata et al., 1993; Cho et al., 1999). Pusch (1980) observed an increase in the hydraulic conductivity of bentonite up to one order of magnitude as a result of an increase in temperature to 70^{o}C. Cho et al. (1999) observed three times increase in the hydraulic conductivities of compacted bentonite samples (1.4Mg/m^3, 1.6Mg/m^3, 1.8Mg/m^3) when heated from 20^{o}C to 80^{o}C. Cho et al. (1999) explained that the absorbed water is changed into bulk water as the soil heats up, this increases the volume of bulk water, thereby increasing permeability. Similarly, the hydraulic conductivity/permeability of unsaturated soils increases also with an increase in temperature (Delage et al., 2000; Romero, et al., 2001; Villar & Lloret, 2004; Zhang et al., 2013). The influence of temperature on saturated permeability is based on the relationship between relative viscosity and temperature. Usually, an empirical relationship with a fitting parameter β_T relating viscosity to temperature is used to fit the experimental data. Most saturated permeability studies at different temperature agree with the relationship. For instance, Towhata et al. (in Romero, 2001) obtained $\beta_T = 0.042K^{-1}$ on kaolinite-clay at 90^{o}C, Cho et al. (1999) obtained $\beta t = 0.022K^{-1}$ on saturated bentonite clay at 80^{o}C, indicating a reasonable fit to the model. Romero et al. (2001) formulated an equation for unsaturated soils based on this relationship at constant void ratio *e* and water content *w* as shown in Eq. 2.28

$$\left|\frac{k_w(e,w,T_r)}{k_w(e,w,T)}\right|_{e,w} = \frac{\rho_w(T)\mu_w(T_r)}{\rho_w(T_r)\mu_w(T)} \approx 1 + \beta_T(T - T_r) \qquad \textbf{2-28}$$

where ρ_w, is the density of water, μ_w, the absolute viscosity and β_T = 0.030K-1 (for a reference temperature T_r = 22°C) an empirical coefficient that fits the relative viscosity data over a temperature range 22 – 80°C, k_w is permeability.

With Eq. 2.28, Romero (2001) obtained β_T = 0.005K^{-1} on unsaturated Boom clay tested at 80°C and at high water content (S_r = 95%). However, at low water content (S_r = 75%), Romero (2001) reported $\beta_T \rightarrow 0$ at the same temperature. This indicates that the influence of temperature on the permeability of the unsaturated soil is pronounced at high water content (low suction), with the predominance of bulk water than at low water content. This observation is consistent with the observation of Zhang et al. (2013) on GMZ bentonite tested at 20 and 40°C. However, Ye et al. (2014) reported significant temperature dependence of unsaturated permeability at high suction (≥ 20MPa) based on permeability test on compacted GMZ01 bentonite at 20, 40 and 60°C. For saturated soils, temperature effect on permeability can be explained by the change in the viscosity of water with temperature, intrinsic permeability and the density of water. Of all the factors, Cho et al. (1999) observed that viscosity is the most sensitive to temperature and contributes greatly to temperature dependence of permeability. For unsaturated soils, temperature dependence on permeability is lower than would be predicted from the influence of temperature on the viscosity of water (Romero, 2001; Zhang; 2013). Other possible factors suggested for unsaturated soils include; alteration of clay fabric due to thermo-chemical interactions and porosity redistribution (Romero, 2001).

Regarding the influence of temperature on SWRC, many studies on unsaturated soils (e.g. Romero et al., 2001, 2005; Villar & Lloret, 2004; Lloret &Villar, 2007; Akasson et al., 2009; Uchaipichat & Khalili, 2009) demonstrated that increase in temperature reduces the water retention/storage capacity (see Fig. 2.26). The authors observed low storage capacity in heated samples of Boom clay, FEBEX bentonite, MX80 bentonite and kaolin during a stress dependent soil water retention test. Some studies, e.g. Romero et al. (2001), Uchaipichat & Khalili (2009) have shown that the air entry value decreases with an increase in temperature as can be seen in Fig. 2.27. The effect of temperature on the hydraulic properties of unsaturated soils has been linked to surface tension dependence on temperature as an increase in temperature reduces the surface tension. Romero et al. (2001) explained that the influence of temperature on soil water retention could also be

because of thermal alteration of clay fabric and intra-aggregate fluid chemistry. Bachmann et al. (2002) observed much more dependency of soil water retention on temperature greater than would be expected from change in surface tension alone. They suggested variation in contact angle and possibly liquid gas interfacial tension due to the solute effect as other possible influences. Ma & Hueckel (1993 in Villar et al., 2004) suggested that the transfer of tightly bound intra-aggregate water to free inter-aggregate water due to an increase in temperature can also play a role in temperature dependence of soil water retention.

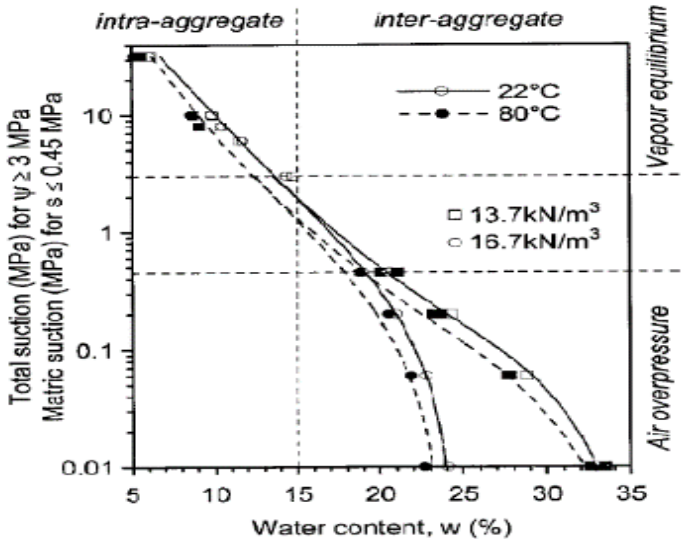

Figure 2-26 Influence of temperature on SWRC (Romero et al., 2001)

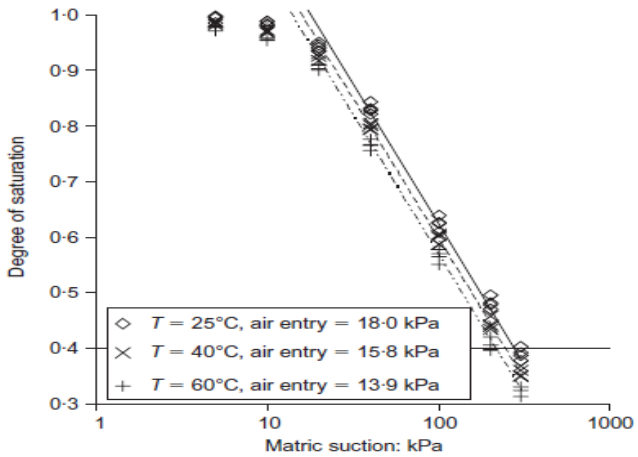

Figure 2-27 Influence of temperature on air entry value (Uchaipichat & Khalili, 2009)

CONCLUSION

Relevant literature on the current study have been reviewed, particularly on the principles and properties of unsaturated soils, the thermal, mechanical and hydraulic behaviour of clay soils. Based on the reviewed literature, a change in temperature influences the mechanical and hydraulic behaviour of unsaturated soil. Unanimous findings were reported on some topics like thermal effect on hydraulic and water retention properties. Notwithstanding, contradictory findings have been reported regarding temperature effect on mechanical behaviour, especially on the compressibility parameters. This has been attributed to factors like stress path and soil structure, etc. For deformation, several studies demonstrated that deformation is more dependent on soil suction and applied stress than on temperature.

Based on the existing literature on non-expansive clay soils, thermal effects on the mechanical and hydraulic behaviour of non-expansive clay soil without a hydraulic history have not yet be systematically studied. Additionally, complex stress path (e.g. non-isothermal path) identical to scenario encountered in the field needs to be considered to have a complete understanding of thermal effects on unsaturated clay soils.

3 PHYSICAL PROPERTIES OF MATERIAL AND EXPERIMENTAL PROGRAMME

INTRODUCTION

Presented in this Chapter are details of the studied material and the key physical properties: specific gravity (GS), liquid limit (LL), plastic limit (PL) and plasticity index (PI). In addition, detailed explanation of experimental procedure and sample preparation methods are presented.

3.1 MATERIAL SELECTION

Speswhite kaolin clay, with a 42% clay fraction (Haghighi, 2011) was adopted in this research. Kaolin clay has been adopted as opposed naturally occurring non-expansive clay because it is industrially manufactured with known chemical and mineralogical composition. Thus, factors that can influence the expected results are known and influence can be easily predicted. The use of natural soil on the other hand might require additional studies outside the scope of this research to understand the chemical compositions and other factors that can influence the results. Result obtained from kaolin can be used to predict the behaviour of some non-active clays with similar initial conditions, whereas result from a natural clay soil can only be used to predict the behaviour of the same soil. Kaolin clay has a moderate swelling behaviour which makes it suitable considering the scope of the study. Additionally, this research builds on the investigation of thermo-hydro-mechanical behaviour of kaolin clay developed by Haghighi (2011) and for continuity, the same soil is used in this research. The rate of consolidation is fast; hence, testing time will be short relative to some natural clay soils. Considerable work on the hydro-mechanical behaviour of kaolin clay has been done (e.g. Wheeler & Sivakumar, 1995) which can be used for analysis. In terms of application for the study, kaolinite is used to enhance compacted clay liners and have been reported to perform better than bentonite enhanced clay liners due to their long-term durability (Sullivan & Quigley, 2003).

Speswhite kaolin is an industrially manufactured fine-grained soil with particle sizes ranging between 0.001- 0.02mm with 42% by weight less than 0.002mm and 58% less than 0.02mm (Haghighi, 2011), as presented in Fig. 3.1. The powdered kaolin was supplied by Whitfield and Son Ltd. In a dry state, the kaolin clay powder is white in colour; however, at a water content above 10%, its colour changes to whitish grey. The

hygroscopic water content in equilibrium with the laboratory atmosphere is 0.23%. The mineralogical composition was obtained by Hagihigi (2011) through X-ray diffraction and is presented in Table 3.1.

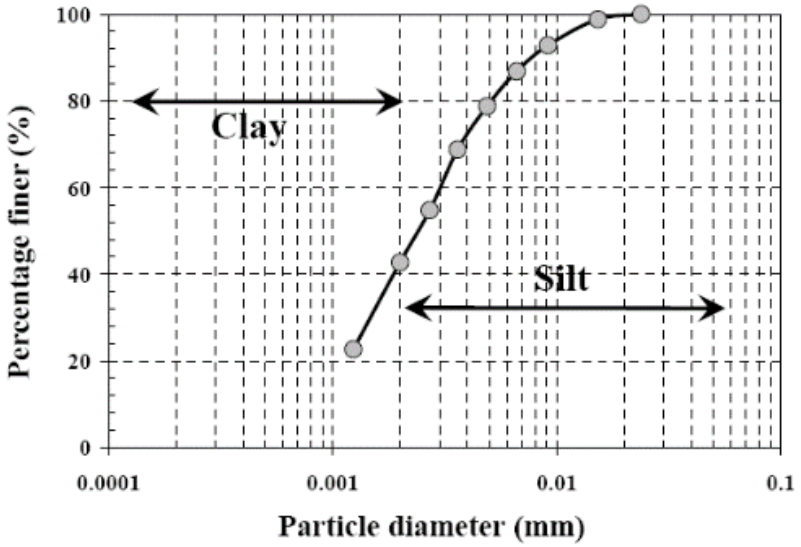

Figure 3-1 Particle size distribution curve of the tested kaolin clay (Haghighi, 2011)

Table 3-1 Mineralogical compostion of the tested kaolin clay (Haghighi, 2011)

Mineral	***Percentage composed (%)***
Kaolinite	82
Illite	3
Quartz	15

As stated above, the soil grains are predominantly kaolinite; hence, it is envisaged that the engineering behaviour of the soil will be mainly influenced by the properties of kaolinite. Kaolinite is a 1:1 clay mineral, one silica layer is bonded to one alumina layer (Hu & Liu, 2003; Mirand-Trevino & Coles, 2003). Unlike other clay minerals, such as montmorillonite, the silica-alumina layers in kaolinite crystals are held together by a strong hydrogen bond which is difficult to separate by water molecules. Thus, hydration does not occur in-between the layers, but occurs at the surface and edge of the soil structure (Mirand-Trevino & Coles, 2003). Because of this characteristic, kaolinite has a

low swell-shrink tendency, as water cannot be accommodated in-between the layers during hydration or expelled from the layers during dissipation.

3.2 PHYSICAL CHARACTERISATION OF THE STUDIED MATERIAL

3.2.1 Particle size distribution

As observed from the particle size distribution curve Fig. 3.1, the Speswhite kaolin clay used in this study is made of silt and clay. The curve shows that silt predominates in the material.

3.2.2 Specific gravity

The small pyknometer method, as recommended for particles finer than 2mm (BS 1377: Part 2: 1990) was used to obtain the specific gravity values at three different temperatures; 50°C, 25°C and 10°C (see Fig. 3.2). Each test point was performed three times and an average of the three was taken. From Fig. 3.2, it can be observed that specific gravity increases non-linearly with temperature.

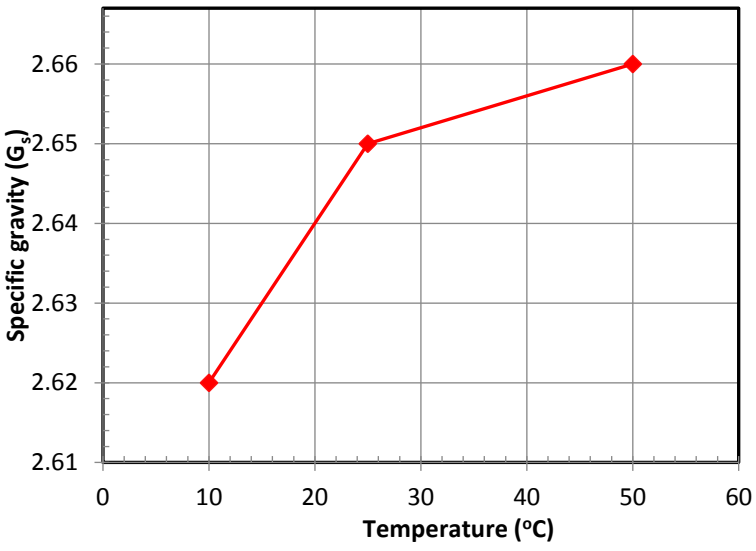

Figure 3-2 Specific gravity of kaolin at different temperatures

The increase in Gs with temperature increase could be attributed to thermal expansion of water. Increase in temperature will cause an increase in volume of water, hence through

mass volume relationship, the density will reduce. On heating a mixture of soil and water, the volume of soil particles will remain unchanged, but the volume of water will increase. The density of soil particles will be unaffected by increases in temperature, while the density of water decreases with temperature. If these assumptions follow, then through the relationship $Gs = \rho_s/\rho_w$, the specific gravity of the same soil will be higher at higher temperatures, since the density of water will decrease with temperature.

From Fig. 3.2, the *Gs* at 25ºC is 2.65. Kim (1996) and Haghighi (2011) reported *Gs* values of 2.61 and 2.64 respectively at room temperature. The value obtained by Hagihighi (2011) is close to the value obtained in this study at 25ºC.

3.2.3 Atterberg limits

The liquid limit was obtained in accordance to BS 1377: Part 2: 1990 using the cone penetration method. Three sets of tests were performed. The water content at 20mm penetration was obtained in each test and an average of 59.1% for the three tests was obtained, which is the liquid limit (see Table 3.2). This value falls within the range (40% to 60%) of liquid limit reported for pure kaolinite (Head, 2006). Liquid limit value of 55.0% was reported by Haghighi (2011).

The plastic limit of the material was obtained by the rolling method, in accordance with BS1377: Part 2: 1990. The plastic limit as shown in Table 3.2 is 34.1%. The plasticity index of the material, estimated from the difference between liquid limit and plastic limit, is 26.3% (see Table 3.2). Thus, the material is plastic at water contents between 33% and 59%. Below 33% water content, the material is semi-solid and above 59%, the material will flow. Based on the liquid limit and plasticity index, the material falls under CH in the 'Unified Soil Classification System'; meaning clay of high plasticity. The implication of this is that when the soil is at a water content within the plastic range, substantial time will be taken for the soil to consolidate under load on dissipation of excess pore water pressure (Carter & Bentley, 1991).

The activity of the material estimated as the ratio of plasticity index to percentage of material finer than 2μm is 0.78. This estimation seems reasonable as the material is not solely composed of kaolinite, but contains both kaolinite and illite. The activity of kaolinite ranges between 0.3-0.5, while that of illite is 0.9. Thus, an activity in-between the values recommended for kaolinite and illite is considered reasonable. Based on Skempton's measure of activity of clay soils, the material is a normally active clay

(Skempton, 1985) indicating that it has moderate swelling and water absorption tendencies.

Table 3-2 Physical properties of kaolin clay

Classification	
Soil	Industrially manufactured kaolin clay
Liquid limit (%)	59.1
Plastic limit (%)	34.1
Plasticity index (%)	25
Activity	0.78
USCS	CH

CH- Clay of high plasticity, USCS- Unified Soil Classification System

3.2.4 Compaction characteristics

Although static compaction method was used during sample preparation, as will be shown in Sec.3.2.4, the standard Proctor method, based on dynamic compaction, was used to establish the compaction characteristics. The compaction test was carried out in accordance to BS 1377 recommendation for a sample passing through a 20mm sieve (with 27 blows of 2.5kg rammer falling through a height of 300mm). From the test result, a plot of dry densities versus water content was made to establish the compaction curve as shown in Fig.3.3. From Fig. 3.3 the optimum water content (w_{opt}) was estimated as 27% and the maximum dry density ($\rho_{D\max}$) was estimated as 1.41Mg/m^3 (see also Table 3.3) corresponding to a void ratio of 0.88.

Table 3-3 Compaction characteristics of kaolin clay

Compaction characteristics	
Specific gravity (25^{o}C)	2.65
Maximum dry density (Mg/m^3)	1.41
Optimum water content (%)	27

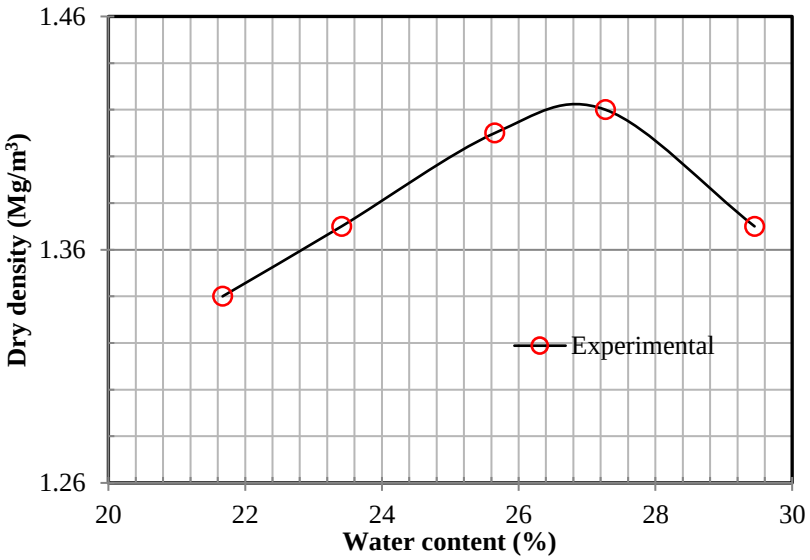

Figure 3-3 Compaction curve for kaolin clay

3.2.5 Sample preparation method

Different samples (size and initial configuration) were prepared for each set of experiments. In each experiment, the samples were divided into Group A and B samples, with void ratios (*e*) 1.0 and 1.5 respectively. For each void ratio, samples were prepared at three different degrees of saturation (*Sr*) (60%, 30% and 15%) by mixing oven dried soil thoroughly with the required quantity of distilled water to achieve the desired water content (*w%*), based on *Sr* and *e*. Thereafter, the materials were passed through a sieve of 1.18mm aperture except for the material for preparing sample at a degree of saturation of 60% and void ratio of 1.5, which was passed through a sieve of 2.8mm aperture. This size of sieve was used because the material was slightly sticky and difficult to pass through smaller sieves. Passing the materials through sieves will produce samples with macro pores of 1.18mm and 2.8mm, which were considered adequate, as the minimum sample height used during the experiments was 19mm. Samples produced from material passed through the 2.8mm sieve apertures were similar to aggregated samples described by Koliji et al. (2010). The sieved materials were then transferred into an airtight plastic container, sealed and left for 24hrs for uniform distribution of water. Afterwards, the samples were statically compacted in two layers using a loading frame into oedometer rings of sizes; ϕ =75mm and H = 19mm for standard oedometer tests and ϕ = 50mm and H = 20mm for suction controlled oedometer tests. Ideally, dynamic compaction should have been used, since the compaction curves were established with dynamic compaction. However, static compaction was used to ensure repeatability of the prepared samples and

to achieve uniform density (Venkatarama & Jagadish, 1993; Sivarkumar, 1993). According to Sivakumar & Wheeler (2000), similar compressibility parameters will be observed from samples compacted by either dynamic or static compaction methods, as long as the initial conditions are the same. Lawton et al. (1989) observed that better correlations emerge from statically compacted samples, rather than from dynamically compacted samples, due to lesser chance of random variation during static compaction. Thus, the use of static compaction is considered appropriate.

Samples were compacted to attain the volume of the ring. This way, the required void ratio was achieved. Different compaction efforts were used to compact each of the samples to achieve the desired void ratio. Since the loading frame is not a digital system, several trials were made first to obtain the compaction effort for each sample. This was done by trying different weights and monitoring the volume of sample achieved, until the weight that compresses the required mass of soil to attain exactly the volume of the mould was obtained. The compaction stresses and the initial conditions of the samples after compaction, are shown in later chapters. One of the challenges encountered during sample preparation was evaporation, which significantly affected the proposed initial condition. Samples were prepared quickly and at 1% water content higher than originally proposed, in order to overcome this problem. In spite of this, water content measured after moisture equilibration was still slightly less than anticipated.

3.3 EXPERIMENTAL EQUIPMENT, LAYOUT AND TESTING PROCEDURES

The equipment used during testing, their layouts and the testing techniques adopted are explained in this section. Among the main equipment/apparatus are a standard oedometer cell, a suction controlled oedometer cell and its subsidiary equipment, pressure plates, apparatus used for filter paper and for vapour equilibrium tests. The equipment was all calibrated to give credence to the results and the calibration methods are presented. Also, described in this chapter are the testing procedures for all the tests carried out.

3.4 STANDARD OEDOMETER TESTS

A series of standard oedometer tests, without suction control, was performed at different temperatures and void ratios. The aim of these tests was to gain understanding of the volumetric response of the selected material at different temperatures; and to then use that data as a guide in the selection of suitable initial conditions (void ratio, water content) for the main experiments.

A standard oedometer apparatus is described in most soil mechanics text books; thus, a description of the apparatus has been excluded. However, the testing procedures, as well as calibration details, are presented.

3.4.1 Calibration of standard oedometer apparatus

Calibration of the oedometer apparatus, involving load frame and cell, was carried out using a dummy sample, in a similar manner to the standard oedometer test. Deformation of apparatus Δa was obtained for each load step. The calibration was repeated twice and an average of the results was used. Three oedometer presses A, B and C, were calibrated at room temperature, while an additional press, D, that was used for tests at elevated temperatures, was calibrated at 50^{o}C. During analysis, cumulative deformation of the apparatus Δa for each load step was subtracted from cumulative deformation of the sample ΔH to obtain the exact deformation of the sample.

3.4.2 Testing procedure for standard oedometer test

Double and single oedometer tests, introduced by Jennings & Knight (1957), were performed at laboratory temperature and 50^{o}C using fixed ring oedometers with dual drainage. The temperature in the laboratory was controlled and the average temperature was 19^{o}C. Soil samples were compacted directly into the oedometer ring. For the sake of clarity, each sample tested has been named according to the initial condition and testing regime. The names are explained together with the obtained results in Sec.4.2 to aid an understanding of the results. Vertical stresses were applied through a mechanical lever arm system capable of applying vertical stress up to 800kPa. For all the performed tests, each loading and wetting stage lasted for 24 hours, in accordance to BS 1377, to ensure full consolidation. The vertical displacement ΔH of the samples was recorded at the end of each consolidation stage, using a dial gauge which had been calibrated for testing at room temperature.

The temperature controlled tests were set up in a temperature chamber, with an operating temperature between 0°C - 50°C. Vertical displacements were recorded by a 10mm range linear displacement transducer with an operating temperature range of 20°C - 125°C. Void ratio e, for each loading/wetting step, was computed from Eq. 3.1(Head, 2006) while the collapse potentials were obtained from Eq. 3.2 (Jennings & Knight, 1957)

$$e = eo - \left(\frac{1+eo}{Ho}\right)\Delta H \qquad 3\text{-}1$$

$$CP = \frac{e_i - e_f}{e_o + 1} \qquad 3\text{-}2$$

where e_i and e_f are, void ratios obtained at constant water content and on saturation respectively, under the same value of vertical net stress. The difference $e_i - e_f$ corresponds to the change in void ratio due to saturation (Medero et al., 2009). e_o is the initial void ratio and *Ho* is the initial height of the sample.

One dimensional oedometer tests are done under k_o condition; in other words, lateral displacement is not allowed. This condition was achieved with the use of the confining ring, which is designed to restrain the sample from lateral displacement. Since an increase in temperature might cause lateral expansion of the confining rings by an increase in diameter, resulting in lateral displacement of the samples, the thermal expansion of the rings at 50°C was calculated using the coefficient of linear expansion of stainless steel. The value obtained was thought to be insignificant, hence thermal expansion of the ring was considered negligible.

3.5 SUCTION CONTROLLED OEDOMETER TESTS

3.5.1 Justification for the use of a suction controlled oedometer

Volume changes in soils can occur as a result of a change in suction, vertical net stress (Matyas & Radhakrishna, 1968) or temperature (Romero, 1999, Hagihighi, 2011). For compressible soils, an increase in vertical net stress, without suction control, will result the decrease of void ratio. This decrease in void ratio translates to an increase in the degree of saturation (*Sr*), a condition known as mechanical wetting (Tarantino, 2009) and a corresponding decrease in suction. To avoid these coupled phenomena and to control each parameter independently, a suction and temperature controlled oedometer was

adopted for testing. A suction controlled triaxial cell can also be used to control the parameters independently (Romero, 1999). Such a cell has the great advantage of controlling the stress path in the sample, but the volume changes are determined indirectly and are subjected to calibrations (Francois, 2008). Details of the suction controlled oedometer and the auxiliary equipment are presented in the section below.

3.5.2 Cell layout

The suction controlled oedometer cell used in this research was designed and fabricated by Hagihighi (2011). As shown in Figs. 3.4a & 3.4b, the cell is made of two main parts, all constructed from stainless steel: 1) the cell cover 2) the cell body with the base and an internal chamber for the sample. The cell body has an external and internal diameter of 101mm and 51mm respectively, with a height of 70mm. Inside the internal chamber is a 50mm x 20mm stainless ring, with diameter to height ratio of 2.5:1, that retains and prevents the sample from lateral deformation. A 5mm thick porous stone, with a diameter slightly less than the diameter of the ring, sits on top of the sample during testing. Pore air pressure is applied to the sample through this porous stone. At the base of the cell is a high air entry ceramic disc, which acts as an interface between the soil and the water reservoir beneath the ceramic disc. The ceramic disc was used for imposing pore water pressure, and acts as a link between the pore water pressure and the water in the measuring system. Two recesses fitted with valves are located at the base of the cell; one for water inlet into the reservoir and the other for water outlet and flushing the cell.

The cell cover is fitted with a 1mm flat diaphragm, attached without gap to a loading cap. The loading cap transmits load evenly on the sample by means of air pressure acting on the diaphragm. The diaphragm acts as an interface between the diaphragm chamber and the internal chamber of the cell and can withstand temperature up to 150^{o}C (Haghighi, 2011). A hollow stainless piston of 13mm external diameter passes through the centre of the loading cap, diaphragm and the cell cover, where it is then soldered to the lower end of the loading cap. The upper end of the piston is fitted with a valve through which connection is made to the air pressure system for applying pore air pressure. The flat edge of this valve provides a base for the anvil of a linear variable displacement transducer (LVDT), which is used for monitoring the displacement in the sample. Connection of the cell to the air pressure system, in order to impose suction, was made through a valve on the piston using rubber tubing with a permissible pressure limit of 1000kPa. The air pressure system is fitted with regulators, manifolds and certified pressure gauges with a

maximum working pressure of 600kPa. Air pressure was supplied from a compressor with maximum working pressure of 1000kPa. Two upper recesses are located on the cell cover, one of which is used for connection to the air pressure system for applying the diaphragm pressure. Holes for screws are located around the circumference of the cell cover as well as the cell body and are used for securing the cover and the main cell. Prior to testing, the equipment was set up and pressure tested to identify and seal points of leakage in the system. The cell and the auxiliary equipment were also calibrated before testing. The calibration details are explained later in the chapter.

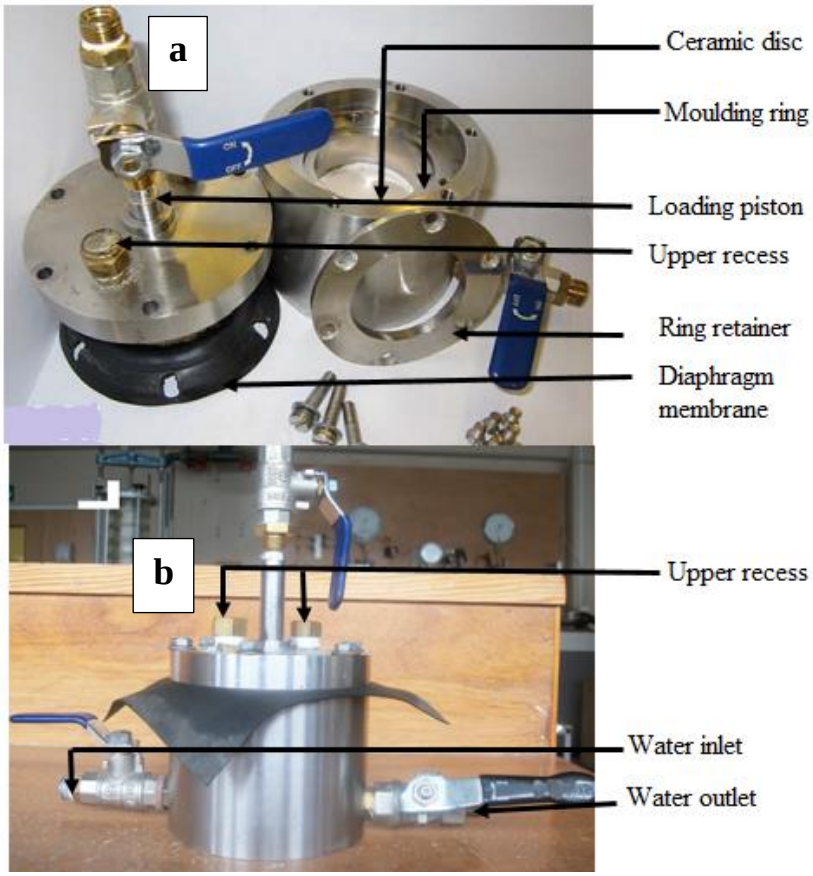

Figure 3-4 (a) Components of suction controlled oedometer cell (b) assembled cell

3.6 REVIEW OF DIFFERENT METHODS OF CONTROLLING AND IMPOSING SUCTION

The major difficulty associated with testing unsaturated soil samples is the measurement of suction. In the field, pore air pressure is zero while pore water pressure has a negative

value (Fredlund, 2012). In the laboratory, however, negative pore water pressure will cause cavitation resulting in errors in the values of pore water pressure (Fredlund & Rahardjo, 1993; Ng & Menzie, 2007). Consequently, different methods have been devised for controlling suction to prevent this problem, as well extend suction measurements to high values. They include;

- Axis translational technique
- Osmotic technique
- Relative humidity control using salt solution technique

The methods are grouped under direct and indirect methods (Tarantino & Mongiovi, 2001). Direct methods measure actual values of negative pore water pressure in the soil while indirect methods measure either water content or relative humidity and then the corresponding suction is evaluated from a calibration curve. The axis translation technique is classified as direct method, while the osmotic and relative humidity techniques are classified as indirect methods.

3.6.1 Axis translation technique

The axis translation technique was developed to solve the problem of cavitation in the laboratory due to negative pore water pressure (Hilf, 1956). This is achieved by raising the pore air pressure (u_a) from zero to a positive value, which results in the transition of (u_w) by the same amount, thereby maintaining a constant suction regardless of the transition of u_a and u_w. The working principle of axis-translation technique is clearly explained in Marihno et al., (2008) as shown in Fig. 3.5. In Fig. 3.5a, a capillary tube with pore air pressure $u_{a0} = 0$ (atmospheric) and negative capillary water pressure ($u_{w0} < 0$), is shown to have matric suction $u_{a0} - u_{w0}$. When the air pressure in the tube was increased to a positive value $(u_{a)AT} > 0$ as shown in Fig. 3.5b, the capillary water pressure was raised to a positive value $(u_{w)AT} > 0$ an equal amount of pressure as $(u_a)_{AT}$. Thus, the matric suction in (b) and (a) were maintained equal $[(u_a)_{AT} - (u_w)_{AT} = u_{a0} - u_{w0}]$. The technique assumes that water and solid boundaries are incompressible to not modify the curvature of meniscus on application of pore air pressure. Marihno et al., (2008) explained that an increase in pore air pressure will translate to an equal increase in pore water pressure, so long as the curvature of meniscus is not altered. The technique is suitable in soils with continuous air-water phase, typically at Sr < 90% (Vanapailli et al., 2008). At Sr > 90%, measured suction can be overestimated due to entrapped air. The meniscus of the entrapped air deforms on application of pore air pressure u_a, resulting in

an increase in the curvature of meniscus of the external air-water interface and resultant increase in measured matric suction (Marihno et al., 2008). Romero (2001) explained that this can be avoided by slow application of the pore air pressure or by adopting the air-over pressure method.

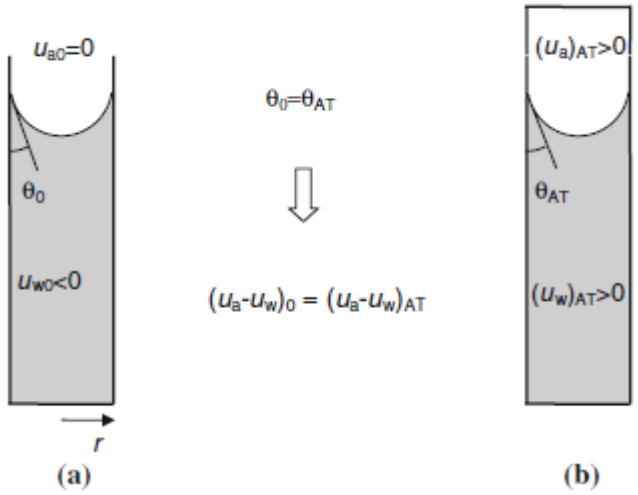

Figure 3-5 The working principle of axis-translation technique (Marihno et al., 2008)

High air entry ceramic disc (HAE) is used in this technique for controlling the water pressure. It acts like an interface between the air and water phase (Vanapalli et al., 2008, Marihno et al., 2008). By saturating the HAE disc and placing the sample in contact with it, the continuity of water between the disc and soil sample is ensured. The air entry value of the ceramic disc is usually greater than the suction to be imposed, to prevent air from entering the water compartment beneath the disc (Lu & Likos, 2004). The maximum air entry value of a ceramic disc is dependent on the effective pore size of the ceramic disc, which influences the surface tension (Fredlund & Rahardjo, 1993). When the HAE disc is saturated, surface tension develops in the pores of the material at the air-water interface, this helps to sustain pressure difference between the liquid and the air phase. At equilibrium, the water in the pores of the HAE disc will be in pressure equilibrium with the pore water pressure in the soil sample, while the air in the pores of the porous stone will be in pressure equilibrium with the pore air pressure in the sample. This technique could impose suction between 0 -1500kPa (Fredlund & Rahardjo, 1993; Romero et al., 2003). The axis translation technique is normally used in a pressure plate apparatus, although many researchers have used it in other apparatus such as triaxial cell, direct shear

box and oedometer cell, (e.g. Fredlund & Rahardjo, 1993; Wheeler & Sivakumar, 1995; Romero et al., 2003; Navaneethan et al., 2005; Kim et al., 2010).

The axis translation technique has the following limitations;

- The suction imposed by this method depends on the air-entry value of the ceramic disc, thus, it applies a limited range of suction. The highest air entry value that is obtainable is 1500kPa (Marihno et al., 2008; Vanapalli et al., 2008).
- The influence of cavitation on pore water is prevented by elevating the pore water pressure from a negative to positive value; this condition is different from the condition in the field (Vanapalli et al., 2008; Baker & Frydman, 2009).
- Diffusion of air pressure into the ceramic disc is usually encountered during testing, especially as suction increases. This influences the water measurement in and out of the sample and can be solved by measuring diffused air volume and correcting the pore water volume change (Vanapalli et al., 2008).

The major source of error in this technique is associated with the presence of occluded air at high degree of saturation, resulting in wrong estimation of matric suction (Romero, 2001; Cunningham et al., 2003).

3.6.2 Osmotic method

The osmotic method of imposing suction on the soil was developed by biologists and then adopted by Geotechnical engineers (Cui & Delage, 1996). In this method, the soil sample is placed in contact with a semi-permeable membrane (usually cellulose acetate) and then an aqueous solution of polyethylene glycol (PEG) is circulated. Exchange of water between the soil and the osmotic solution occurs through the semi permeable membrane, which allows only the passage of water. Thus, through the principle of osmosis, water moves from the soil to the PEG solution since it is usually at a higher concentration when imposing suction. As water is drawn from the soil, matric suction is imposed on the soil sample like the axis-translation technique. At equilibrium, the energy potential of the soil water becomes equal to that of the solution, hence, the suction in the soil becomes equal to that in solution (Ng & Menzie, 2007). The concentration of PEG solution controls the value of applied suction, with high concentration resulting in high suction value up to 10MPa (Delage, 1998; Blatz et al., 2008).

Since this method is an indirect method of controlling suction, PEG solution is first calibrated using either pychrometer or tensiometer to establish a relationship between

osmotic suction and the concentration of PEG solution. An outstanding advantage of this method is that it can be used to impose a high range of suction up to 10MPa (Delage et al., 1998). Unlike the axis-translation technique, similar condition of soil suction obtained in the field is reproduced with the osmotic method, especially at high degree of saturation where the air phase is usually discontinuous. The equilibration time for the osmotic method is short compared to the vapour equilibrium method, since liquid water is exchanged rather than water vapour (Delage et al., 1998).

Notwithstanding the advantages, the osmotic method has one major disadvantage; the ability of the method to impose high suction depends on the semi-permeable membrane used and its ability to withstand a high concentration of PEG. Most membranes experience chemical breakdown at high concentration of PEG (Tarantino & Mongiovi, 2000). As a result, PEG solution can infiltrate into the sample resulting in wrong suction estimation. This is the major source of error associated with the osmotic method (Tarantino & Mongiovi, 2000).

3.6.3 Humidity control technique/vapour equilibrium method

In this method, suction is imposed by controlling the relative humidity using an aqueous solution (Romero, 1999; Fredlund & Rahardjo, 1993; Lu & Likos, 2004). The soil sample and an aqueous solution (sulphuric acid or sodium chloride) are placed in a sealed container. The aqueous solution imposes relative humidity to the environment by migration of water molecule through the vapour phase until equilibrium is achieved. Total suction is imposed to the soil sample when equilibrium is achieved. A humidity probe is used to measure the imposed relative humidity which is converted to the corresponding suction using Kelvin's equation (Equation 2.3). The value of suction applied depends on the aqueous solution used as well as the concentration of the solution. This method has been used in numerous works to impose suction on soil samples and has been reported to be effective (e.g. Delage et al., 1998; Romero et al., 2003; Cuisinier & Masrouri, 2005; Blatz et al., 2008; Pintado et al., 2009).

A notable advantage of this method is that it could be used to impose very high suction between 3 - 1000MPa (Romero, 1999; Delage & Cui, 2000; Villar, 2000), although adequate care needs to be taken to ensure steady temperature. Small variation in temperature affects the imposed suction (Delage et al., 1998).

Long testing time required for the sample to reach equilibrium limits the use of this method. Esteban & Saez (1988 in Delage et al., 1998) observed a testing period of several months with the use of vapour equilibrium. Delage et al., (1998) explained that the long equilibration time is due to the very low kinetics of gas transfer. Cunningham (2000) suggested that regulated air could be circulated through the sample to reduce the testing time. But this can be used for drying or maintaining constant suction. Cui et al. (2002) observed a reduction in the testing time by circulating humid air at the base of the sample. Additionally, vapour equilibrium method is not suitable at low suction values (Delage et al., 1998). This is attributed to the nonlinear relationship between relative humidity and suction at low suction. The source of error associated with this method is temperature fluctuation. Krahn & Fredlund (1972) reported that temperature fluctuation needs to be maintained within ±0.001 to measure total suction at an accuracy of ±10kPa.

3.6.4 Methods of measuring suction

The following devices are used for measuring suction; filter paper, tensiometer, thermocouple psychrometer and thermal conductivity sensor. Like previously discussed methods, these methods are grouped into direct and indirect measurement methods. The direct measurement method includes the use of tensiometer, while the indirect methods are; filter paper and thermocouple psychrometer.

3.6.5 Filter paper method

Another indirect method of estimating soil suction is by the filter paper method. Although simple and inexpensive (Chandler & Gutierrez, 1986; Houston et al., 1994; Bulut, 2001; Bulut, 2008), its accuracy is user dependent and based on the accuracy of the calibration curve used. The use of filter paper is based on the principle that filter paper will absorb water in liquid phase from soil sample placed in contact with it or in vapour phase when separated from the soil by a vapour barrier, until it reaches a water content in equilibrium with the soil (Chandler & Gutierrez, 1986). Different suction (total or matric) can be measured depending on the contact established between the filter paper and the soil. When the filter paper is placed in intimate contact with the soil, water flows from the soil to the filter paper until equilibrium is reached, thus, water absorbed by the filter paper has the same concentration as the soil water and matric suction is measured (Marinho & Oliveira, 2006). However, when the filter paper is suspended above the soil, water vapour flows from the soil to the filter paper until equilibrium is reached; in this case, total suction is measured. To evaluate the suction in the soil, the water content of the filter paper at

equilibrium is correlated with water content from a previously established calibration curve.

Among the commonly used filter papers are Whatman No. 42 and Schleicher & Schuell No. 589-WH. Each filter paper has its unique properties, thus, different calibration curve has been developed for each filter paper. To ensure accurate result, appropriate curve developed for a specific batch of filter paper should be used (Navaneethan et al., 2005). There are usually discrepancies in the value of suction inferred from different calibration curves for the same type of filter paper (Navaneethan et al., 2004). These differences have been attributed to different source of suction and equilibration time used by the different authors during calibration (Houston et al., 1994; Bulut et al., 2001; Leong et al., 2002). Therefore, it is important to take these factors into consideration while selecting the calibration curve to be used.

Filter paper can be used to measure a wide range of suction. Chandler & Gutierrez (1986) reported suction values between 80kPa and 6000kPa. Chandler et al. (1992) extended the suction range below 80kPa. Ridley et al. (2003) reported a maximum suction value of 30000kPa while Haghighi (2011) reported that filter paper can measure all suction values. Houston et al. (1994) reported that low values of matric suction is easily measured using filter paper. In fact, it appears that the maximum range of suction measured by filter paper depends on the calibration equation used.

As mentioned earlier, this method is user dependent and requires utmost care to overcome the challenges associated with the method. The challenges include; ensuring intimate contact between the filter paper and the soil (Bulut, 2008). If this is not ensured, total suction can be measured instead of matric suction. The influence of poor contact between the sample and filter paper was observed by Fredlund &Rahardjo (1993) when they compared results obtained from filter paper methods and thermocouple pyschrometer to check the validity of the filter paper method. Close agreement was observed between pyschrometer method and the non-contact filter paper method but great difference was observed in the contact method. This difference was attributed to lack of intimate contact between the soil and the filter paper, probably, total suction has been measured instead of matric suction. Another challenge with the use of filter paper method is loss of water when transferring filter paper into a weighing tin to obtain the filter paper water content. This should be done instantly to limit the loss of water. Chandler & Gutierrez (1986) reported a 10% loss in filter paper water content after leaving an initially wet filter paper

for two and a half minutes (see Fig. 3.6). They recommended that weighing is done within 30sec. Also, Navaneethan et al. (2005) reported a 10% increase in measured suction for one min delay.

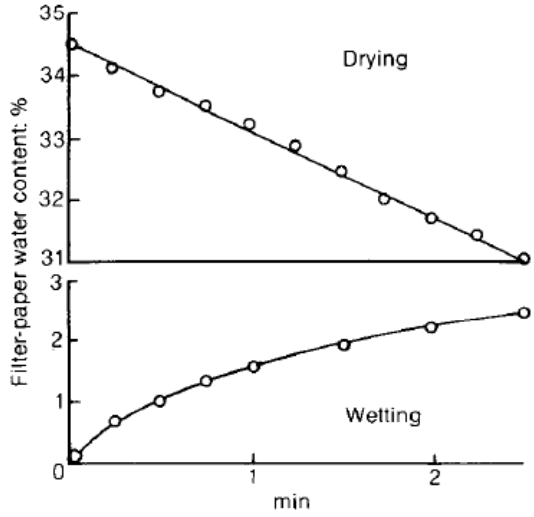

Figure 3-6 Loss of filter paper water content with time (Chandler & Gutierrez, 1986)

Temperature gradients affect the accuracy of the filter paper method, especially total suction measurement. Bulut and Leong (2008) stated that the sensitivity of filter paper to temperature is critical at very high relative humidity and recommended that temperature fluctuation should be limited to ±0.1^{o}C.

Sources of error in filter paper method

- Water is lost or gained between the filter paper and the surrounding atmosphere during the transfer/handling of the filter paper. The transfer should be done as fast as possible to minimize this error.
- Temperature variations during equilibration. To minimize this error, temperature should be maintained constant within +/-1^{o}C during equilibration.
- Not using filter papers from the same brand and/or batch can also cause some errors. Filter papers from the same brand are said to be identical because they have the same calibration curve.

3.6.6 Tensiometer

Tensiometer is a direct suction measuring device. It measures negative pore water pressure directly from the soil at atmospheric pore air pressure. Conventionally, tensiometers are made of high air entry filters attached through a small tube to pressure measuring devices. The working principle of tensiometers is like that of the axis-translation technique which is matric suction generation due to pressure difference at air-water interface (Marinho et al., 2008). But unlike the axis-translation technique, most conventional tensiometers measure limited range of suction (0 - 80kPa) due to unmanageable cavitation at higher suction. However, Ridley & Burland (1993, 1995) developed high capacity tensiometer (HCT) capable of measuring higher suction values up to 1500kPa (see Fig. 3.7). The high suction capacity was achieved by using high air-entry ceramic filter (1500kPa) and by avoiding heterogeneous cavitation of water in the device. This was achieved through the reduction in volume (about 3mm^3) and surface area of the water reservoir (Ridley & Burland, 1993). Additionally, materials that are possible sources of nucleation e.g. O-rings and elastomers were avoided to increase the measurable suction (Ridley & Burland, 1995; Take, 2003).

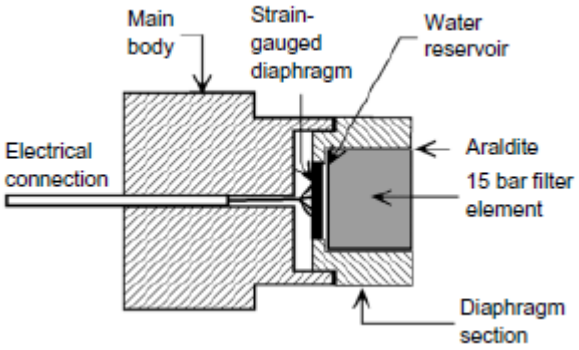

Figure 3-7 High capacity tensiometer developed by Ridley & Burland (1995)

Accurate measurement of suction with tensiometer depends on successful saturation and calibration of the high air-entry filter (Lourenco et al., 2008; Toll et al., 2013) and the contact established between the device and the soil. Tarantino & Mongovi (2001) explained that full saturation can be attained by subjecting the high air-entry filter to cycles of cavitation and high water pressure. This forces any entrapped air to dissolve in water (Toll et al., 2013). However, Take & Bolton (2003) observed that a single cycle is adequate for low air-entry filters (10 - 30kPa). To overcome the problem of contact,

Marihno et al. (2008) suggested that a small amount of slurry should be placed at the tip of the tensiometer before inserting it into the soil.

The challenges associated with the use of tensiometer are interpretation of the measured suction data and long term measurement of suction. There is usually no distinction between a good and bad measurement of negative pore water pressure (Tarantino, 2004), as it is always difficult to identify when the tensiometer has stopped recording true suction value. The error associated with the method is linked to cavitation of negative pore water pressure. This limits the range of suction that can accurately be measured with tensiometer.

Table 3-4 Summary of different methods of measuring and controlling suction

Method	Suction component	Range of suction (kPa)	Limitations
Axis translation	Matric suction	0-1500	Suction imposed is limited by the air entry value of the porous material.
Osmotic technique	Matric suction	10MPa (Delage et al, 1998)	The semi permeable membrane experience chemical breakdown, hence, maximum suction imposed by this method is limited to the performance of the semi-permeable membrane (Tarantino and Mongiovi, 2000). Suction cannot be applied in a continuous manner since change in suction is applied by changing the concentration of PEG solution.
Humidity control technique	Total suction	Up to 1000MPa	Like osmotic method, suction cannot be imposed in a continuous manner. It is time consuming. Accuracy of the method is dependent on temperature, as slight fluctuation in temperature affects the result.
Filter Paper (contact method)	Matric suction	Entire range of suction (Haghighi, 2011)	The accuracy of the contact method depends on the quality of contact between the filter paper and the soil sample. The accuracy of the method is user dependent.
Filter paper (Non-contact method)	Total suction		
Psychrometer	Total suction	100 – 8000	Like the humidity technique, it is affected by temperature fluctuation.
Tensiometer	Matric suction	0-80 Up to 1500 for HCT	It measures small range of suction due to the problem of cavitation. Accuracy of measured suction depends on the contact between the soil and the device.

3.7 TEST SET-UP AND TECHNIQUES USED DURING SUCTION CONTROLLED ODEOMETER TESTING

Three parameters were controlled during testing: suction, temperature and vertical net stress. The fourth parameter (displacement) was measured. Different techniques were adopted to control/impose these parameters. The techniques are discussed in the following sections.

3.7.1 Test set up for axis-translational technique

The axis-translation technique was adopted for imposing matric suction on the samples. As explained in Sec. 3.6.1, this technique is based on controlling the pressure difference between air and water pressures above a high air entry ceramic disc (HAE). In this research, pore water pressure was maintained at a constant positive value (20kPa) during testing, while the air pressure was varied depending on the value of suction to be achieved. The water and air pressure control systems connected to the cell were used in achieving this technique. One of the underlying principles of this technique is separation of air and water phases using the HAE that is made of very tiny pores (Lu & Likos, 2004). On saturation, contractile skin is formed on the surface of the pores of the disc, thereby developing surface tension. The formation of surface tension allows the passage of water into the water measuring system (GDS volume/ pressure controller), without the passage of air. The surface tension helps the disc to sustain the pressure difference, and collapses when the pressure difference exceeds the air entry value of the disc. When the air entry value is exceeded, the pores of the ceramic disc are filled with air, which gradually penetrate the water measuring device as the air builds up. This results in erroneous measurements of the imposed suction (Fredlund & Rahardjo, 1993). The size of pores influences the air entry value of a disc; the smaller the diameter, the higher the air entry value (Lu & Likos, 2004). To ensure the accuracy of suction, a 1500kPa ceramic disc was used for testing; thus, the maximum suction that could be sustained during testing with the axis translation method is 1500kPa. However, matric suction ranging between 0kPa - 400kPa was imposed during testing, which is lower than the air entry value. Although matric suction values less than the air entry value were adopted during testing, significant amounts of air still diffused into the water reservoir especially while testing at 50^{o}C. However, the water compartment was flushed every 24 hours to ensure that any diffused air is removed from the system (Ng & Zhou, 2014). It is worth mentioning that the volume of diffused air was not measured during testing, as the water pressure line was

not fitted with a diffused air volume indicator. The method adopted for flushing will be explained later in this chapter.

Continuity of water between the soil and ceramic disc is essential during testing. To ensure this happens, the ceramic disc was kept saturated and a water pressure of 20kPa was always maintained, to avoid de-saturation of the stone, as well as to impose the required suction. GDS volume-pressure controller, capable of controlling pressure up to 200kPa, was used to control the pore water pressure and was connected to the cell through the water inlet port, using a rubber tubing with permissible pressure limit of 1000kPa (See Fig. 3.8). Care was taken when filling the tubing, to ensure that air bubbles were not formed, as this will also result in discontinuity between the water in the pores of the disc and the water measuring system, resulting in a wrong estimation of matric suction (Romero, 1999). The GDS consists of four main parts: i) a digital pressure and volume control panel, ii) a water cylinder, iii) a piston and iv) a stepper motor. When a pressure value is keyed into the control panel, the stepper motor pushes the piston forward, which then compresses the water in the cylinder to give the required pressure. One step of the motor results in the displacement of $1mm^3$ of water. Output pressure, targeted pressure and the volume of water in the cylinder are displayed on a dashboard adjacent to the control panel. This makes it easier to estimate the volume of water displaced or taken up by the soil sample during testing.

a) Calibration of GDS pressure and volume controller

Prior to use, the GDS pressure and volume controller was calibrated up to 200kPa against a Budenberg gauge; a dead weight gauge tester. Additional calibration for low pressure (10kPa) was done using a hydrostatic water column (Kasangaki, 2012), as the Budenberg gauge is not suitable for low pressures (< 20kPa).

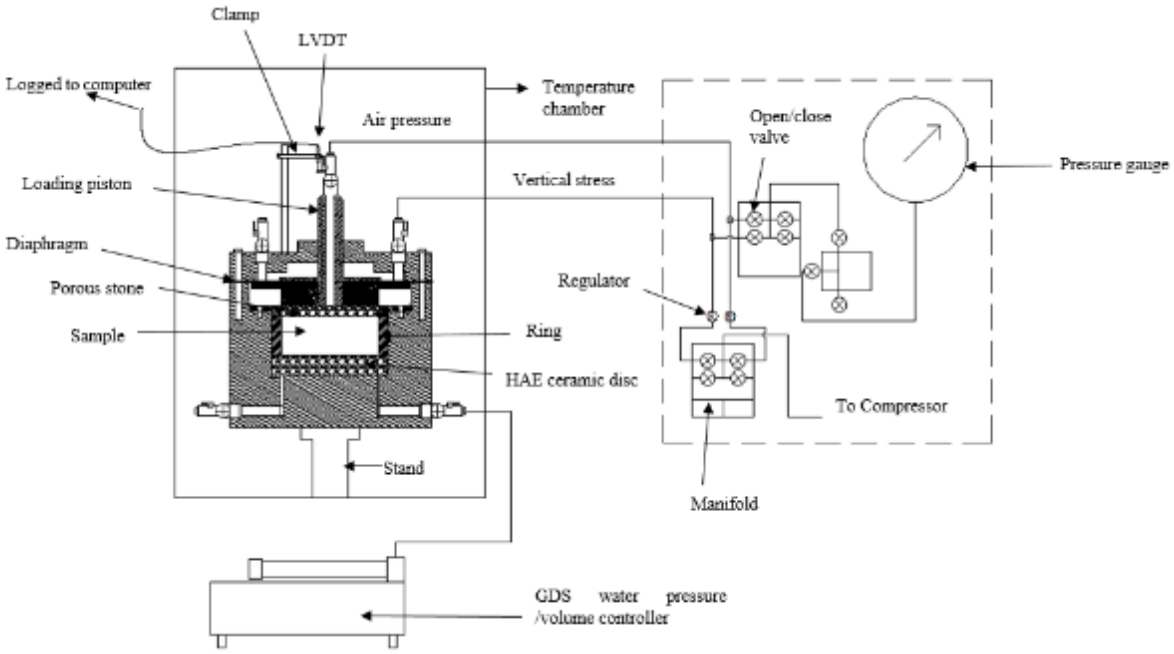

Figure 3-8 Set-up of suction controlled oedometer test

b) Fixing and saturation of ceramic discs

The ceramic disc was fixed to the base of the cell with a silicon seal which was then allowed to set for 6 hours. This was done at a temperature of 50^{o}C to get rid of any air trapped in the seal (Romero, 1999). Special care was taken when applying the silicon seal to ensure that the seal did not cover the part of the ceramic disc where the sample sits. This was done by using the sample mould as a barrier for the seal; this way the area of the ceramic disc not covered by the seal was slightly greater than the area of the sample. It was observed during set-up that the seal breaks at water pressure higher than 30kPa, thereby pushing the stone upwards and flooding the cell with water. In order to avoid this problem, water pressure of 20kPa was used in all suction controlled tests.

Before the start of any test, the ceramic disc was saturated. The cell and water line were filled with water, ensuring that air bubbles were eliminated. The water line was then connected to the cell through the central conduit and a water pressure of 140kPa was applied. Under the applied pressure, the inlet and outlet valves were closed and left for 48 hours to allow any trapped air to dissolve in water. The system was then flushed to get rid of the dissolved air by opening the outlet valve and allowing water to flow under pressure for 24 hours. The whole process was repeated twice, but the pressure was maintained for 24 hours during the second and third cycle. The volume of water

discharged from the outlet valve per hour was determined in the third cycle. Full saturation was achieved when the flow was about 2 to 3 drops per minute (Sivakumar, 1993). Prior to saturation of the ceramic disc, the pressure/volume controller and the water pressure lines were flushed 3 times to ensure that there was no entrapped air in the system.

c) Pneumatic loading technique with diaphragm membrane

As stated in Sec. 3.5.2, vertical net stress was imposed on the sample, through the loading cap by means of air pressure acting on the diaphragm. On application of air pressure, the diaphragm expanded, exerting force on the loading cap, which was then transmitted to the sample. As the sample deforms, the piston moves downward causing compression of the anvil of the linear variable displacement transducer (LVDT) and this was recorded as displacement of the sample. The cell was calibrated to determine the actual pressure transmitted to the sample for each value of diaphragm pressure. This was done using a calibrated proven ring with a load factor of 1.21N. The cell was calibrated at different values of air pressure that make up the predetermined suction values to be used during testing. During calibration, it was noted that the air pressure required to impose each suction value generated a force that acts in an opposite direction to the diaphragm pressure. This force was always exceeded to ensure the transmission of the required force to the sample.

The cell was calibrated for four values of pore air pressures: 50kPa, 70kPa, 120kPa and 230kPa, which correspond to the values of air pressure required for imposing suction values of 30kPa, 50kPa, 100kPa and 210kPa during testing. The calibration procedure described in Haghighi (2011) was used during the calibration. Pore air pressure was first applied and maintained at a constant level, then the movements of the LVDT and the dial gauge of the proven ring due to the applied pressure were read off. The diaphragm pressures were then applied incrementally up to 500kPa. The gauge and LVDT readings were taken for each increment. Care was taken during calibration to ensure that no gap existed between the diaphragm and loading cap prior to application of diaphragm pressure, as this would have resulted in the movement of the piston and error in the calibration data (Romero, 1999). The cell was calibrated at 25^{o}C and 50^{o}C. Similar results were obtained from the calibrations done at both temperatures, indicating that the expansion of the diaphragm was unaffected by an increase in temperature to 50^{o}C. The calibration results are presented in Fig. 3.9.

Additional calibration was done for cell deformability at 50°C and 25°C. This was done by inserting a 20mm high stainless disc in place of the sample. Cycles of vertical net stresses were applied and the cell deformation on application of each stress value was recorded by a linear displacement transducer clamped to the piston. The data obtained was used to correct the test result, to ensure that actual deformation of samples on loading was obtained. This was done by subtracting the cell deformation from the total deformation obtained from the sample. The LDVTs used for both testing and calibration of the cell were also calibrated against a certified micrometre screw gauge at laboratory temperature.

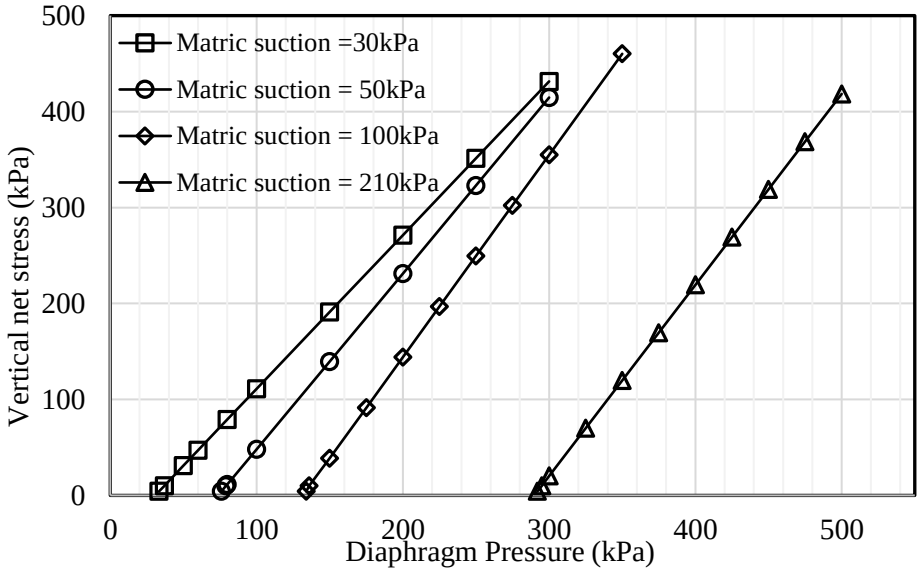

Figure 3-9 Diaphragm pressure versus vertical net stress for the calibration of a suction controlled oedometer cell

d) Technique used to regulate temperature in the sample

Temperature imposition was carried out via a calibrated digital temperature chamber, capable of maintaining temperatures ranging between 0°C and 50°C. Temperature controlled experiments were set up in the chamber and the required temperature was set using a digital control. Considerable time was required for samples to reach thermal equilibrium with the atmosphere of the chamber. The time required for thermal equilibrium was assessed by burying a calibrated thermocouple (logged to a computer) at the centre of a compacted sample placed in the cell (see Fig. 3.10a). With the cell closed, the whole assembly was placed inside the temperature chamber and different temperature

values were imposed on the sample. Three temperature steps were considered: 25, 35 and 50°C. The soil temperature evolution is shown in Fig. 3.10b. It could be observed from the figure that at 35°C and 50°C, temperature rose slowly in the sample and became constant within 5 hours. Based on this, an equilibration time of 5 hours was adopted in all temperature controlled oedometer tests. It is worth mentioning that this assessment procedure was carried out on one sample with a set of initial conditions (e_0 = 1.5, *Sr* = 30%). The initial condition was chosen because most of the suction and temperature controlled experiments were carried out at that initial condition. However, it is envisaged that samples at other initial conditions might have different thermal equalisation time. Nonetheless, 5 hours were used for all the tests and assumed to be adequate for all samples.

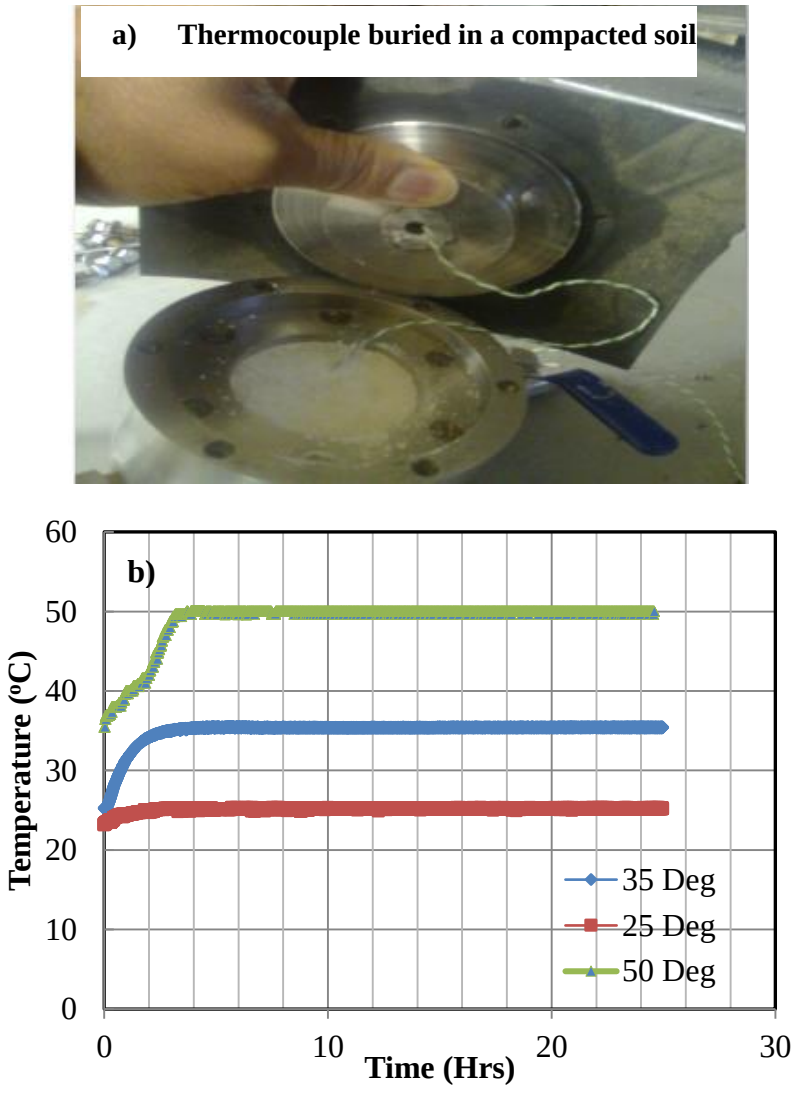

Figure 3-10 Temperature versus time taken for sample to attain thermal equilibrium

e) Calibration of temperature chamber

The temperature chamber was calibrated for the temperature range of 5 – 50°C (see Fig. 3.11). Appropriate corrections were adopted when required, according to the calibration. During testing, a calibrated thermocouple probe was always inserted in the temperature chamber. This was used as a check to relate the temperature reached by the chamber with the pre-set value, and to ensure that a steady temperature was maintained during testing.

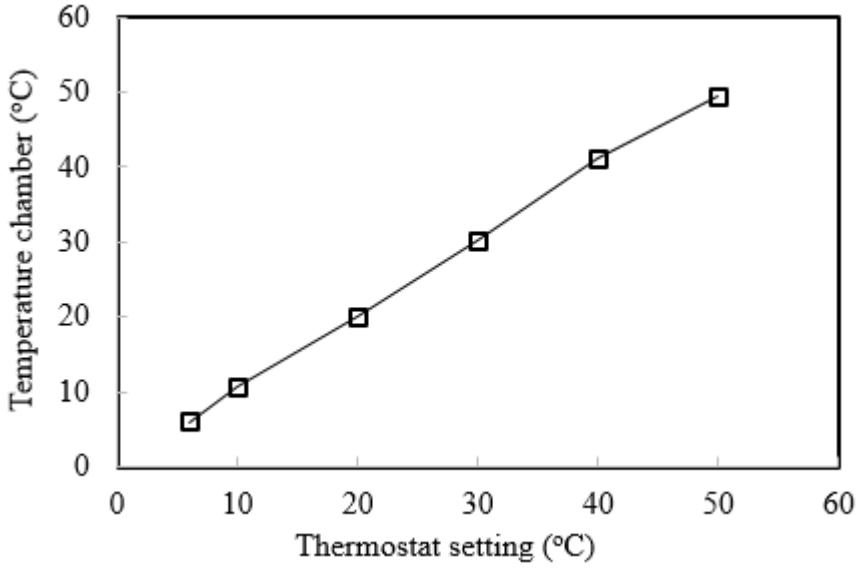

Figure 3-11 Calibration curve for the temperature chamber

3.7.2 Sample set-up for suction controlled tests

Samples for suction controlled oedometer tests were statically compacted into the oedometer rings of diameter 50mm and height 20mm. The compaction was done externally with the standard oedometer and then transferred into the suction controlled oedometer cell for testing. The conditions of the tested samples are shown in Table 3.5.

3.7.3 Testing procedure for suction and temperature controlled oedometer tests

Three sets of tests were carried out under controlled suction, temperature and vertical net stress. The sets involved: i) a non-isothermal test involving a thermal cycle at constant suction and vertical net stress, ii) a loading test at constant temperature and suction, and iii) a test at constant vertical net stress and temperature with increasing suction. Details of the tests are shown in Table 3.5.

a) Heating and cooling test at constant suction and stress (non-isothermal test)

Thermal cycle tests at constant suction and vertical net stress (non- isothermal tests) were carried out on two sets of samples, with an initial void ratio of ≈1.5 and two different degrees of saturation *Sr* (≈ 60% and 30%), as shown in Table 3.5; Test c. The aim was to observe the influence of thermal cycles on the volume change of compacted kaolin samples under constant matric suction and vertical net stress. The stress paths followed during testing are shown in Fig. 3.12. Pore water pressure was set at 20kPa, taking into consideration the elevation difference between the GDS pressure/ volume controller and water inlet port of the cell. This value of pore water pressure was also maintained during setting up, to prevent de-saturation of the high air entry ceramic disc. A compacted sample was then placed on top of the saturated ceramic disc and the cell was quickly assembled to prevent the sample from taking up water from the stone. The LVDT was clamped in position with the spindle not fully released and then logged to a computer. Initial suction was applied by opening the air pressure valve and setting the pressure gauge to the required value. Tests $NI1_{30}$, $NI1_{100}$, $NI2_{30}$ and $NI2_{100}$ were carried out at two different values of suction; 30kPa and 100kPa. The selection of the suction values was based on the outcome of preliminary tests and on the fact that an increase in suction results in increased stiffness (Alonso et al., 1990). Hence, it was envisaged that any significant change in volume on heating and cooling might not be observed at a suction value higher than 100kPa. A total of 14 days was allowed for suction equalisation, to be consistent with the equilibration time for kaolin clay (Hagihighi, 2011). Hagihighi (2011) monitored water volume movement in compacted kaolin clay on reducing suction to 0kPa. He observed that the rate fell to less than 0.015/day after 14 days and then proposed 14 days as the equilibration time for kaolin. Once equilibrium was attained, a vertical net stress of 55kPa was applied and maintained for 24 hours. Again, this value of vertical net stress was adopted, based on the outcome of preliminary tests. Tests with similar samples at a vertical net stress of 120kPa and 110kPa resulted in negligible volume change on thermal loading. As a result of this data, a vertical net stress of 55kPa was adopted. Thermal loading was imposed thereafter under the imposed suction and vertical net stress, following three temperature steps: 25^{o}C, 35^{o}C and 50^{o}C. For each step, temperature was increased via several sub steps at a rate of 2^{o}C per hour; a process requiring 5 hours to move from 25^{o}C to 35^{o}C and 7.5 hours from 35^{o}C to 50^{o}C. Francois (2008) explained that adopting small temperature steps will reduce the build-up of excess pore water pressure that may result in over-consolidated behaviour of the sample. In his study of

thermal behaviour of silty clay, he observed that temperature steps at a rate of 3.4°C per hour were suitable. In this study, each step was maintained for 24 hours to ensure full consolidation.

At high temperature, provision was made for bleeding off air; the cell was slightly tilted and the outlet valve was slightly opened, while the GDS pressure/volume controller settings were adjusted to maintain the required water pressure (Kasangaki, 2012). Since air is lighter than water, any diffused air would stay on top of water, hence moving towards the elevated side and then escaping through the provision made in the outlet valve.

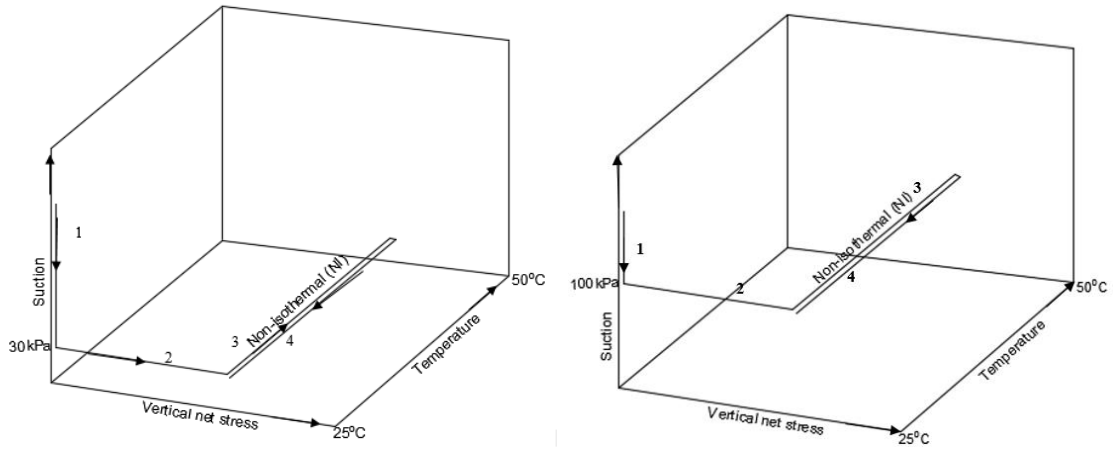

(a) **(b)**

Figure 3-12 Stress path for non-isothermal test (a) 30kPa matric suction (b) 100kPa matric suction

b) Loading at constant temperature and suction

Five loading tests ($L1_{(25)}$, $L1_{(25)}$, $L1_{(50)}$, $L2_{(25)}$ and $L2_{(50)}$) at constant imposed suction and temperature (one duplicate test to ascertain repeatability) were carried out on samples prepared at the same initial conditions (e_0 = 1.5, Sr = 30%) as shown in Table 3.5, test d. The samples were loaded at two constant temperatures (25°C and 50°C) and two constant suctions (30kPa and 210kPa). The stress paths are shown in Fig. 3.13. In the compacted state, the sample was placed on top of the saturated HAE ceramic disc. The desired temperature and suction were imposed simultaneously and 14 days allowed for thermal and suction equalisation. Displacement of the sample due to suction and temperature

increase was measured by LVDT logged to a computer. Thereafter, vertical net stresses were applied incrementally up to 415kPa with five loading steps. A period of 24 hours was allowed after each load increment. It was assumed that five loading steps were enough to prevent significant pore pressure re-distribution. As reported by Uchaipichat & Khalili (2009), an increase in vertical net stress causes re-distribution of pore water pressures. This implies that adequate time should be allowed for re-equalisation of suction to ensure that the imposed suction is maintained. There was initial concern on allowing 14 days for suction re-equalisation for each increment of vertical net stress, due to time limits. According to Folly (2001), the equilibration time on application of vertical net stress, temperature or suction should be obtained by monitoring the time taken for the vertical displacement of the sample to reach equilibrium. This is in a case where deformation of the sample is of interest. Since the parameter monitored in the test was volume change, deformation of the sample on application of a vertical net stress of 100kPa at 50^{o}C was monitored for 24 hours. It was observed that change in vertical displacement fell to less than 0.004mm per hour after about 17 hours, as shown in Fig. 3.14. Consequently, the need to allow 14days equalisation time for each increment of vertical net stress was ruled out to save time. A period of one day was adopted, irrespective of pore pressure re-distribution, since volume change was the main concern; the preliminary tests indicated 17 hours to be suitable to obtain equalisation.

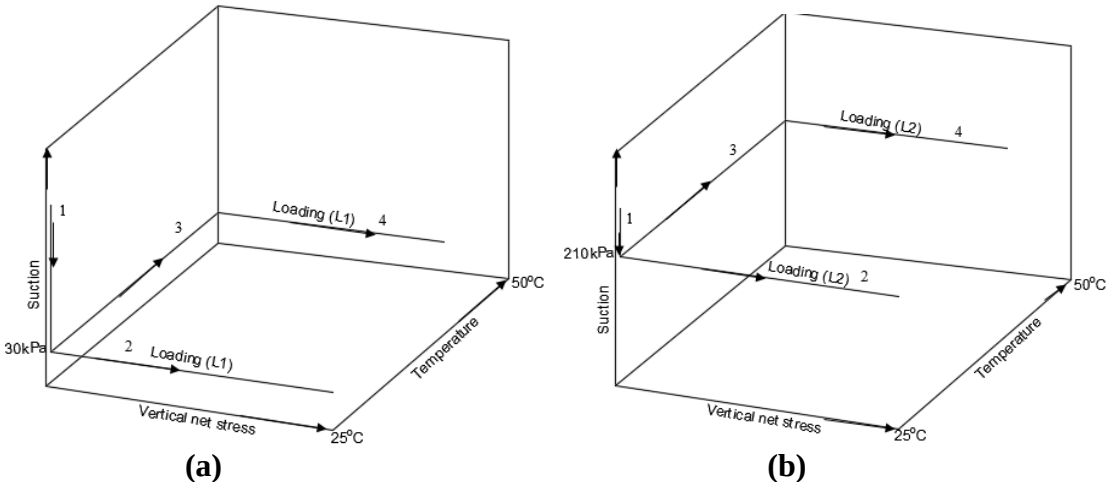

Figure 3-13 Stress path for loading at constant temperatures and matric suction (a) 30kPa matric suction (b) 210kPa matric suction

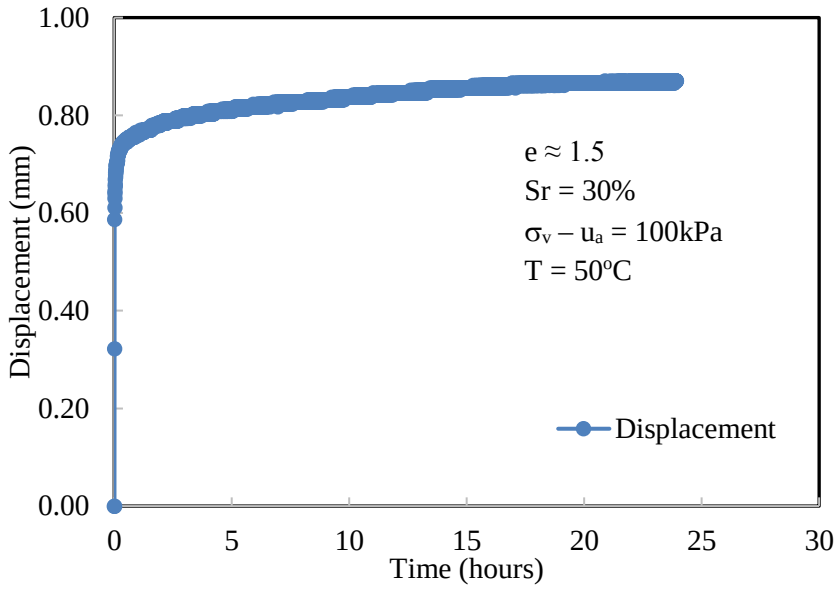

Figure 3-14 Displacement of sample with time

c) Suction increase at constant vertical net stress and temperature

The tests ($D1_{50}$ and $D1_{25}$) involved increases in suction under constant vertical net stress (55kPa) and constant temperatures of 25°C and 50°C (see Fig. 3.15 for stress path and Table 3.5 Test e for the test conditions). The test starts at a compacted condition with an initial suction value of 286kPa. In that condition, the kaolin clay sample was placed on a HAE ceramic disc, and matric suction was set to 30kPa, reducing it from an initial value of 286kPa. To achieve this, the air pressure was set up to 50kPa and the water pressure was maintained at 20kPa. The required temperatures of 25°C and 50°C, and vertical net stress of 55kPa, were then applied under the reduced matric suction. Thereafter, the matric suction was increased in steps (from 30 - 100 - 210kPa) and a period of 14 days was maintained in-between each step for initial suction equalisation. Deformation of the sample at each suction step was recorded by LDVT logged to a computer.

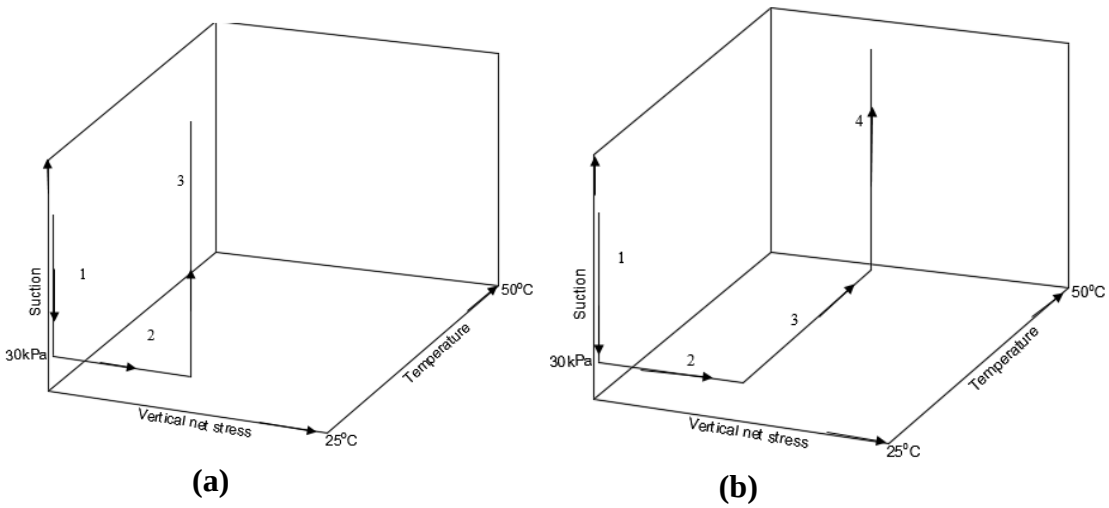

Figure 3-15 Stress path for increasing suction at constant temperature and vertical net stress (a) 25°C (b) 50°C

Table 3-5 Test conditions and summary of all the tests carried out

Type of apparatus	Test	Proposed Initial condition		Description	No. of tests carried out
		≈ e_0	≈ Sr (%)		
Standard oedometer	a) Standard oedometer tests at room temperature and 25°C	1.0	60, 30, 15	Wetted at 25kPa, 50kPa, 100kPa, 200kPa	10
		1.5		Constant water content	16
				Wetted at 5kPa	10
	b) Standard oedometer tests at 50°C	1.0	30	Wetted at 200kPa	4
		1.5	60, 30	Constant water content	3
				Wetted at 5kPa	4
Suction controlled oedometer	c) Thermal cycle test	1.5	30 60	Test at constant vertical net stress (55kPa), constant suction (30kPa and 100kPa) and varying temperature (25°C – 50°C – 25°C)	5
	d) Loading at constant temperature and suction	1.5	30	Test at two constant temperatures (25°C and 50°C) and two suction (30kPa and 210kPa) respectively, then varying load (4.5kPa - 415kPa)	5

	e) Increasing suction at a constant vertical net stress and temperature	1.5	30	Test at two constant temperatures (25°C and 50°C) and vertical net stress (55kPa) and increasing suction from 30kPa – 210kPa	2
Pressure plate + filter paper + NaCl for vapour equilibrium	f) Pressure plate test			Tests following a drying path from a saturated state (0kPa) to 400kPa at two temperatures; 25°C and 50°C.	36
	g) Vapour equilibrium test	1.0 1.5	45 30	Test following a drying path from 400kPa to 3000kPa, 4000kPa and 5000kPa at two temperatures, 25°C and 50°C.	14
	h) Filter paper test			Tests following a drying path from a saturated state (0kPa) to 5000kPa at two temperatures; 25°C and 50°C	15
Filter paper	Cycles of heating and cooling tests	1.0	60 30 15	Subjecting samples to a thermal cycle (10°C-25°C-50°C-25°C) and then measuring suction and volume changes after each cycle.	30
		1.5	60 30 15		30
Falling head permeameter	Permeability test	1.0	45	Saturated permeability tests on samples pre-heated at 25°C and 50°C.	3
		1.5	30		3

3.8 SOIL WATER RETENTION TESTS

Soil water retention tests following a drying path were performed to determine the effect of temperature on the water retention properties (e.g. air entry value, residual suction and slope of the SWRC) of compacted kaolin clay. Three different methods: i) pressure plate, ii) filter paper and iii) vapour equilibrium were adopted to establish a complete SWRC, because a full curve cannot be obtained from only one method. Each of the methods has drawbacks that limit the achievable suction value as discussed in Sec. 3.6. The equipment and testing procedures are described in the following sections.

3.8.1 Pressure plate tests for SWRC (low suction values)

a) Equipment

Unlike the conventional pressure plate, the pressure plate used for testing in this study is relatively small, with an internal diameter of 76mm and an external diameter of 102mm. The cell can only accommodate one sample at a time. As a result, three cells were used simultaneously during testing to reduce the testing time (Hagihighi, 2011). The cell is made of stainless steel with two essential parts; the cell body and cover (see Fig. 3.16).

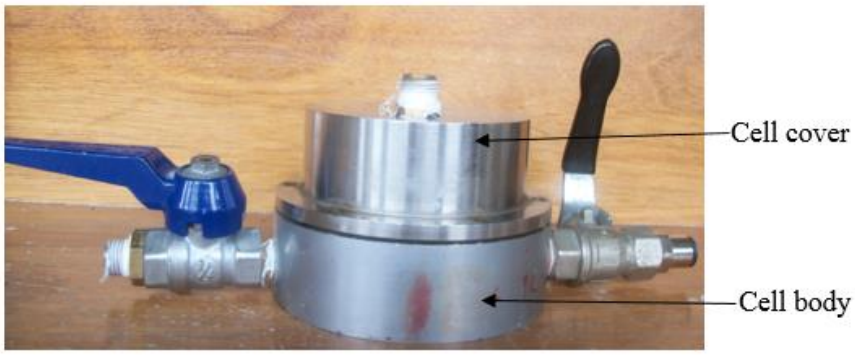

Figure 3-16 Pressure plate

The cell body is fitted with a 15 bar HAE ceramic disc at the base which was saturated in a similar process as explained in Sec. 3.7.1b. The three cells were connected in series, during set up and saturation, as shown in Fig. 3.17 and 3.18. At the lower sides of the cell body are recesses fitted with valves for flushing and applying pore water pressure during testing. A central recess, fitted with a connector, is located on top of the cell cover and is used for connecting to the air pressure system. Ordinarily, an air humidifier is fitted to the air pressure line to humidify the dry air and reduce evaporation, especially when testing at high temperature (Romero, 1999; Folly, 2001; Francois, 2008). The maximum temperature used during testing was 50^{o}C; evaporation was assumed to be minimal and negligible at this temperature.

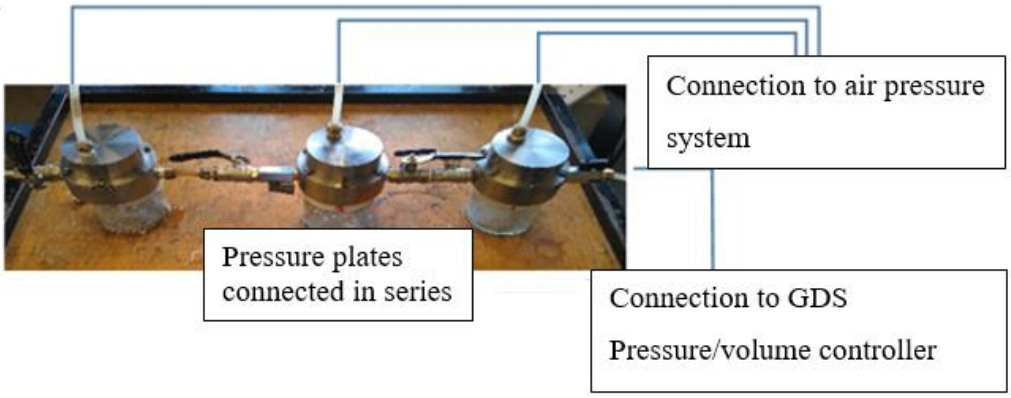

Figure 3-17 Experimental set-up of pressure plate test (After Hagihighi, 2011)

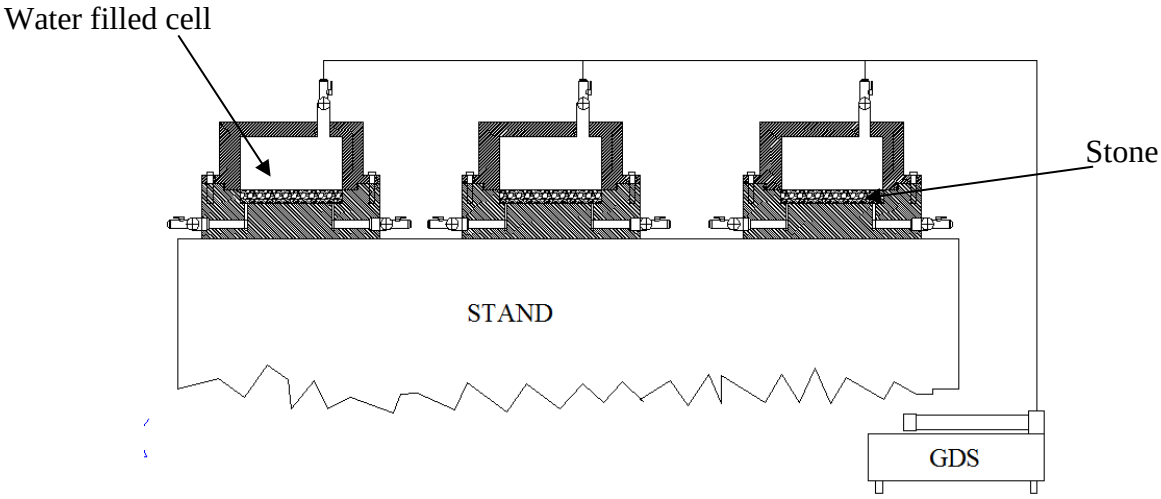

Figure 3-18 Saturation of the HAE ceramic discs

A diffused air volume indicator was not fitted to the water pressure line; hence, the volume of diffused air through the ceramic disc during testing, especially at high temperature, was not accounted for. For this reason, the SWRC has been established in terms of gravimetric water content, rather than volumetric water content (Kasangaki, 2012). A calibrated temperature chamber, with a temperature range between 0^{o}C – 50^{o}C, was used for imposing temperature on the samples.

b) Sample set-up for the pressure plate tests

Samples for the SWRC tests were prepared in a similar manner to the samples used for the oedometer tests (see Sec. 3.2.5). The difference is that the samples for the drying

SWRC tests were compacted in smaller moulds (50mm x 19mm) and then transferred to the pressure plates for saturation and testing.

c) Sample saturation

Saturation of the samples was done by flooding the cell with 20mls of water and allowing each sample to imbibe water. The water pressure was maintained at 20kPa during saturation and samples were left for 24 hours to ensure full saturation. The path followed by samples on saturation is explained by Fredlund (2000). According to Fredlund (2000), compacted samples, or in-situ samples, have their matric suction located somewhere along a scanning curve. When saturated, the matric suction is relaxed and the stress state falls along the wetting path, before proceeding on the drying path with increasing suction.

d) Testing procedures for the primary drying curve using pressure plate

A total of 36 tests were performed on two groups of samples; e_0 = 1.0 and 1.5. Testing was done at two constant temperatures; 25^{o}C and 50^{o}C (see Table 3.5) and suction up to 400kPa was imposed. The stress paths followed during testing are shown in Fig. 3.19. A destructive method, involving destroying each sample at the end of each test to determine water content, was used as it was not possible to measure the volume of water leaving the sample continuously. Hence, the curve was presented in terms of gravimetric water content. All tests were carried out following the drying curves. The wetting path was not obtained, due to the size of the pressure plate and the length of time needed to obtain each point on the SWRC. The pressure plate can take only one sample at a time, and a period of 14 days was required for each point on the SWRC. The wetting path of the primary SWRC will require drying the samples first, and then following a wetting path.

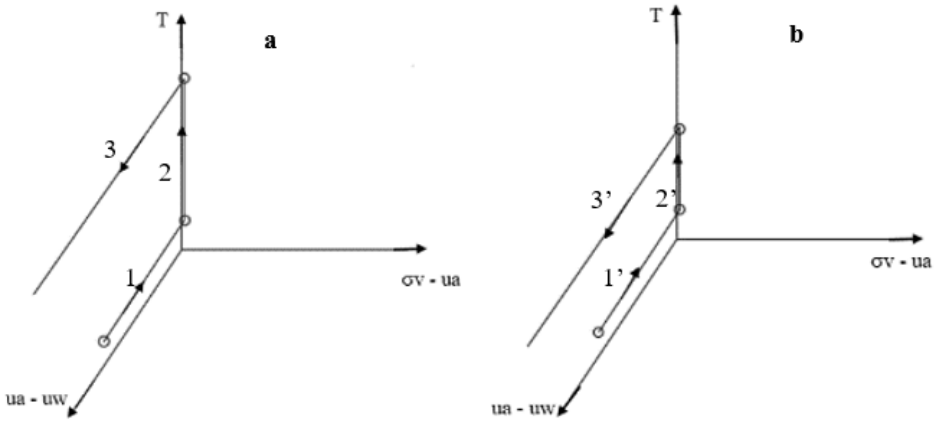

Figure 3-19 Stress path for the primary drying SWRC (a) 50^{o}C (b) 25^{o}C

The test starts from a saturated state corresponding to an initial suction value of 0kPa. In that state, the temperature was increased to the desired value (25^{o}C or 50^{o}C) and a period of 5 hours was allowed for thermal equilibrium between the sample and the environment of the chamber. Thereafter, suction was imposed in steps from 10kPa to 400kPa. A period of 14 days was allowed after each step of suction increment for equalisation. On application of suction, drainage of water from the sample was observed through the water volume controller. It was found that the water volume change became negligible even before the 14days equalisation time, though this depends on the suction value. This indicates that 14 days was adequate for suction equalisation. The cell and the water lines were flushed periodically, especially when testing at high temperature to get rid of diffused air and ensure continuity of water between the soil and water measuring system. When testing at high temperature (50^{o}C) and high suction (400kPa) the observed rate of diffusion increased significantly, compared to tests at low suction < 400kPa. To solve this problem, the outlet valve was slightly opened to create an escape for air while maintaining the required air pressure. Once the sample reached equilibrium, the cells were opened and the water content of the sample determined.

3.8.2 Filter paper method for the primary drying curve

As mentioned previously, it was not possible to use only one method to establish a full SWRC, due to the different limitations of each of the methods. The maximum suction achieved with the pressure plate was 400kPa. Higher suction was not achievable due to uncontrollable diffusion of air into the water compartment; hence the contact filter paper method was adopted to extend the curve beyond 400kPa.

a) Equipment and sample

Whatman No. 42 filter paper, 200ml glass jar, PVC tapes, tweezers, drying tins and cling film comprise the equipment used for the filter paper method; the technique used, being similar to that used by Bulut et al. (2001).

Since this is an extension of the SWRC similar samples, with the same initial conditions, as used for the pressure plate tests were used. Special care was taken during compaction to achieve samples with flat smooth surfaces, to ensure good contact between the sample and the filter papers. If good contact is not achieved, total suction rather than matric suction might be measured (Marinho & Da Silva Gomes, 2012). Care was also taken to

ensure that the filter papers were not compressed, as this will have a similar effect as would a lack of contact (Chandler & Gutierrez, 1986).

Whatman No. 42 was chosen, in part, because it is rated highly among other filter papers due to its thickness and small pore sizes (Chandler & Gutierrez, 1986). Furthermore, the calibration equation adopted was established with Whatman No. 42 filter paper.

b) Testing procedure for SWRC using filter paper method

Filter paper tests were performed at 25^{o}C and 50^{o}C to establish a SWRC following a drying path. Samples were first saturated with 20ml of water, after compaction, to relax the matric suction, ensuring that the same path taken during pressure plate testing was maintained. The saturated samples were then placed inside a temperature chamber set at 25^{o}C or 50^{o}C. The points on the SWRC were achieved by allowing the samples to lose water through evaporation. The evaporation times were altered to cover from 1 - 48 hours, to obtain each point on the curve. After exposing samples for the specified time, they were removed from the chamber, then three dry untreated Whatman No. 42 filter papers (two big protective papers and a small paper for actual suction measurement) were sandwiched between two samples that were exposed for evaporation for the same length of time and at the same temperature (see Fig. 3.20). The protective filter papers were used to prevent the small paper from coming in contact with the soil samples and so becoming contaminated (Walker et al., 2005).

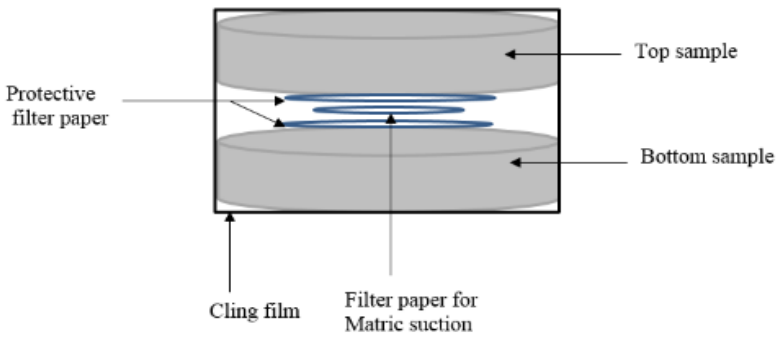

Figure 3-20 Arrangement of filter papers for suction measurement (After Bulut et al., 2001)

Note: Samples and filter papers were in close contact during testing. The space shown in the diagram is to help in labelling the filter papers.

To ensure constant water content, or minimal loss of water, through evaporation during suction equalisation, the samples with the sandwiched filter papers were wrapped with several layers of cling film, placed inside a jar, and finally sealed with cling film and tapes. The jar was then returned to the temperature chamber and left for 14 days for suction equalisation, in line with the equilibration time for the calibration equation, as proposed by Haghighi (2011). Temperature fluctuation was observed as $\pm 0.1^{o}C$ in line with that specified in the literature. Once equilibrium was attained at the end of 14 days, the water contents of the inner filter papers, as well as those of the samples, were determined. Equivalent suction values were calculated from the calibration equation proposed by Haghighi (2011).

3.8.3 Vapour equilibrium method for the primary drying path at high suction values

The water retention result obtained with the filter paper method, when compared with the result from the axis-translation technique, was found to vary significantly. This was linked to different phenomena through which water was removed from the sample. In the filter paper test, water was removed from the sample through evaporation, whereas in the axis-translation technique, water drained from the sample on application of suction. There was doubt regarding the filter paper results. Consequently, the relative humidity control/ vapour equilibrium method was adopted to extend the SWRC to high suction value (3000 - 5000kPa). In the vapour equilibrium technique, soil suction is imposed to a soil through the movement of water molecules in the vapour phase from a reference salt solution to the soil pores, or vice versa. The movement ceases once equilibrium is achieved (Freundlund & Rahardjo, 1993). When this technique is used to impose suction, the soil sample exchanges pure water with the reference salt solution until equilibrium is established with the vapour pressure of the salt solution (Romero, 1999). The amount of water exchanged depends on the vapour pressure of the salt solution, which is controlled by the concentration of the solution.

In this work, NaCl was used to impose three suction values (3000, 4000 and 5000kPa). Different solutions were prepared for each suction value. The quantity of solute (NaCl) was varied in each solution to obtain the concentrations required to achieve the predetermined total suction. A relationship between total suction, the activity of NaCl and temperature was adopted from Romero (1999) and was used to evaluate the concentration of each solution for a predetermined suction value (see Eq. 3.3).

$$\varphi = -465.17\,(T + 273.15)e^{-4.5731\,X10^{-4}\,T} ln a_1 \qquad \textbf{3-3}$$

Ψ is total suction, a_1 activity of the solution, T (^oC) is temperature.

$$a_1(m,T) = 1 - 0.035m - m(m-3)(1.9772 \times 10^{-3} - 1.193 \times 10^{-5}T) \qquad \textbf{3-4}$$

Valid for m ≥ 3.0mol/kg.

where m is molality in mol/kg, u_v/u_{vo} is relative humidity.

A plot of total suction versus molality at different temperatures, is shown in Fig. 3.21 (Romero, 1999). The molality of NaCl at temperature T was calculated from Eq. 3.4 (Romero, 1999). The concentrations required to obtain total suction values of 3000kPa, 4000kPa and 5000kPa, with the corresponding masses of NaCl, are shown in Table 3.6. By multiplying the required moles of NaCl for each concentration, with the molecular mass of NaCl, the weight of solute in grams was obtained. Fig. 3.21 was used to confirm the calculated values. Since the vapour equilibrium method was adopted to extend the SWRC beyond 400kPa, offcuts from samples used for the pressure plate tests at 400kPa were used. The reason for this is to ensure continuity in the stress state of the water retention curve. The size of sample, specifically the height, was reduced to approximately 10mm to decrease the equalisation time. Each of the samples was placed in a cup, weighed and accommodated inside a glass jar filled with the desired concentration of NaCl, while leaving an air volume of about 100 x $10^3 mm^3$. Thereafter, the samples were left to equilibrate in the temperature chamber at 25°C or 50°C for 14 days, to be consistent with the equilibration time used by Romero et al. (2001). Once equilibrium was achieved, the samples were weighed and their water contents determined.

Table 3-6 Mass of solute and corresponding suction

Temperature (°C)	Suction Ψ (kPa)	Molality m (mol/kg)	Mass of NaCl (g)
25	3000	0.6692	39.2
	4000	0.8824	51.6
	5000	1.0911	63.8
50	3000	0.6260	36.6
	4000	0.8260	48.3
	5000	1.0219	59.8

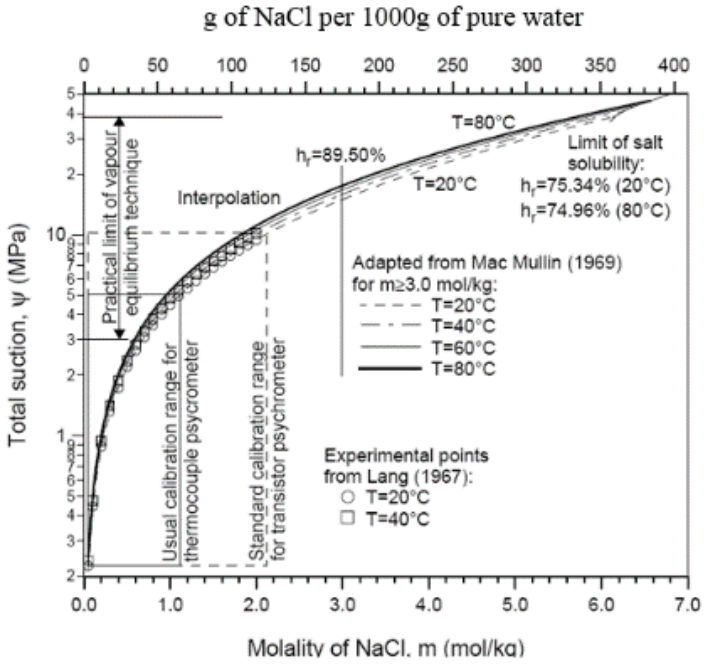

Figure 3-21 Total suction versus molarity of NaCl at different temperatures (Romero, 1999)

3.9 TESTS TO DETERMINE THE INFLUENCE OF THERMAL CYCLES ON SUCTION AND VOLUME CHANGES

The aim of the tests was to observe the influence of temperature cycles on the value of measured suction and volume changes.

3.9.1 Testing procedure for the influence of thermal cycle on volume and suction

The experimental programme involves subjecting compacted samples of kaolin clay to thermal cycles and evaluating both matric and total suction through the filter paper method. Volume changes in the samples were measured using a Vernier calliper.

The procedure described by Bulut et al. (2001) was adopted, but Whatman No. 42 filter paper was used. Changes in matric suction and total suction, as well as volume change with temperature, were measured in two groups of samples, with void ratios of 1.5 and 1.0. The samples were prepared at different degrees of saturation (60%, 30%, 15%) as shown in Table 3.5, dividing the samples into 6 sub-groups; e_0 = 1.0 (Sr = 60%, 30%, 15%) and e_0 = 1.5 (Sr = 60%, 30%, 15%). The samples were also subjected to four

temperature steps (10ºC- 25ºC-50ºC-25ºC). Eight sets of samples were used for each sub group; two for each temperature step.

After compaction, the initial dimensions of the samples were measured using a Vernier calliper. Thereafter, filter papers were sandwiched between two disc samples of the same initial condition, ensuring good contact between the filter papers and the samples. The top and bottom samples were sealed together with a tape. With the help of PVC discs, filter papers for total suction measurement were suspended on top of the samples as shown in Fig. 3.22. Afterwards, the samples with the filter papers were placed in glass jars and then sealed with layers of cling film to prevent exchange of moisture between the air inside and outside the glass jars. All the samples were then placed inside a temperature chamber and subsequently subjected to temperature cycles, as mentioned previously. Under each temperature step, the samples were allowed to equilibrate for 14 days. At the end of each equilibration period, two glass jars from each sub group were removed from the temperature chamber. The testing paths are shown in Fig. 3.23. With utmost care and speed, the filter papers for matric and total suction were removed from the samples using tweezers and transferred into drying tins for moisture content estimation. Suction values were evaluated from the calibration equation proposed by Haghighi et al. (2011). Final dimensions of the samples were taken after each temperature step. Unfortunately, most of the samples were destroyed at this stage of measurement as it was difficult to ensure good contact between the Vernier calliper and the sample without damaging the sample. Final water contents of the samples were determined after the final measurements.

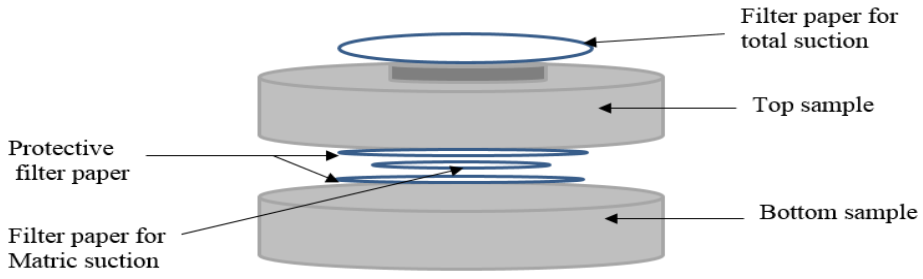

Figure 3-22 Arrangement of sample and filter paper during testing (After Bulut et al., 2001)

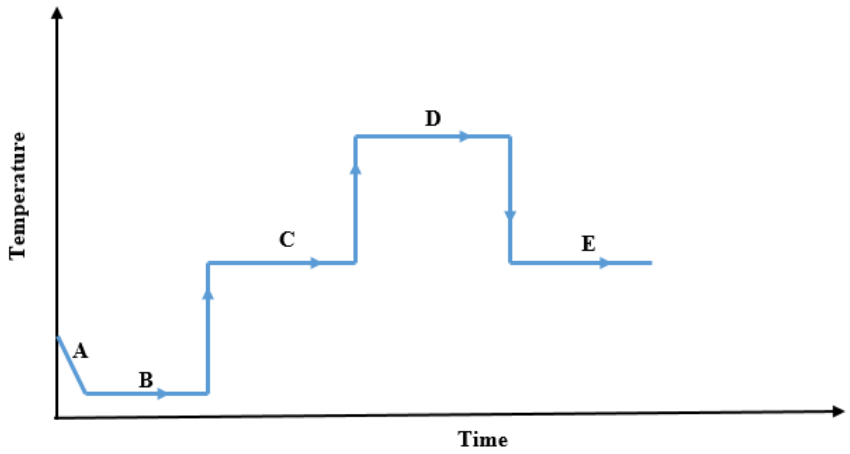

Figure 3-23 Testing paths for thermal cycle tests

3.10 SATURATED PERMEABILTY TESTS ON PRE-HEATED SAMPLES

Falling head permeability tests were conducted on samples with void ratios of 1.0 and 1.5 and a degree of saturation of 30%. The samples were pre-heated to 25°C and 50°C before carrying out the falling head permeability tests. The results from the tests were used to complement the SWRC, to predict the unsaturated permeability function.

In contrast with other sample preparation methods, dynamic compaction (tamping) was adopted for the sample preparation; hence the compaction effort was not evaluated. Based on the studies by Sivakumar & Wheeler (2000), it was assumed that the compaction method did not have any significant effect on the soil fabric, since utmost care was taken to achieve similar initial conditions, as achieved with static compaction. The samples were compacted directly into the permeameter moulds. After compaction, each sample was pre-heated, then saturated by imbibing it in water. Full saturation was achieved by applying a vacuum pressure of 20mmHg. During testing, great care was taken to ensure that the sample was always saturated and in contact with the mould (Head, 1994). The stand pipes were filled with water to a given level h_1. Water was then allowed to flow through the sample until water in the standpipe reaches an indicated lower level h_2. The time required for water to drop from h_1 to h_2 was recorded. The permeability of the sample K_T (m/s) was then calculated using Eq. 3.5 (Head, 1994).

$$K_T = 3.84 \frac{aL}{At} Log_{10}\left(\frac{h_1}{h_2}\right) * 10^{-5} \qquad \text{3-5}$$

where a (mm^2) is the cross-sectional area of the standpipe, L (mm) is the height of the permeameter mould, A (mm^2) is the cross-sectional area of the mould and t (sec.) is the time taken for the water level to fall from h_1 to h_2.

3.11 LIMITATIONS OF THE STUDY

Very high temperature values, up to 100^oC, are experienced around most geo-thermal structures (Cekerevac, 2003). However, in this study, the temperature has been limited to a maximum of 50^oC due to the limited temperature range of the testing equipment. Additionally, for temperature controlled loading tests at constant suction, the suction imposed on samples using the axis-translation technique was limited to 210kPa. This is due, in part, to limited capacity of the compressor used to supply air pressure, and due to the maximum suction, that was attainable during calibration for vertical net stress.

CHAPTER FOUR

4 HYDRO-MECHANICAL BEHAVIOUR OF KAOLIN CLAY AT ROOM TEMPERATURE

4.1 INTRODUCTION

In this chapter, details of an investigation into the hydro-mechanical behaviour of compacted kaolin clay, through single and double oedometer tests, are presented. The aim of the tests was to understand the volumetric behaviour of different samples with predefined initial conditions. Several authors (e.g. Barden & Seed, 1970; Barden et al., 1973; Sivarkumar & Wheeler, 2000) have reported that changes in the compaction water content of clay soils may result in soils with different fabric, potentially leading to different soil behaviour and compressibility parameters thus, cannot be modelled as change in initial state. However, Tarantino & De Col (2008) pointed out that a soil compacted at dry side of optimum but at different water contents might be modelled with a single set of parameters provided the effect of compaction induced void ratio on water retention is accounted for. Based on these studies, samples at 60%, 30% and 15% degrees of saturation and void ratios of 1.0 and 1.5 have been investigated, to understand their volumetric behaviour and to determine if different initial degree of saturation can be modelled as change in initial state. Tests were undertaken at room temperature (18^{o}C – 20^{o}C). Results from these tests were used as guidelines for the definition of initial conditions for tests detailed in Chapters 5 and 6.

4.2 STUDIED SAMPLES AND TEST CONDITIONS

Two groups of samples, A and B, were used in the study, with approximate void ratios of 1.0 and 1.5 respectively. Initial states of the samples prior to testing are shown in Table 4.1, as well as the test conditions. The samples were named according the void ratio (group A or B), degree of saturation 1, 2, 3 (1→ 60%, 2→30%, 3→15%) and the test type SO, DO_{CWC} and DO_5 (SO → single oedometer, $DO\text{-}_{CWC}$→ double oedometer at constant water content, $DO\text{-}_5$ →double oedometer at saturated condition). For instance, the name $A1_{(SO)}$ is explained below:

where A – is the group (A→ e_0 = 1.0)

No. 1 - is the degree of saturation 60%

SO – is the test type (SO → single oedometer test)

The samples for CWC and SO tests were sealed during testing to minimise moisture loss through evaporation and to maintain constant water content. All samples were loaded in steps: 5, 10, 25, 50, 100, 200 and 400kPa. Single oedometer tests ($B2_{(SO-25)}$, $B2_{(SO-50)}$, $B2_{(SO-100)}$) were wetted at constant vertical stresses of 25, 50 and 100kPa, to investigate the effect of hydraulic path on the compressibility of samples with an initial void ratio of 1.5 as shown in Table 4.1, column 3. Initial matric suction values were measured for each of the samples using the filter paper method (see column 5, Table 4.1).

Furthermore, tests were performed to show the influence of matric suction on the volumetric behaviour of the soil samples. Two sets of samples were prepared at the same initial state (e_0 = 1.48, S_r = 29%), as shown in Table 4.2 (columns 2, 3 and 4) and then wetted with different volumes of water (see column 5, Table 4.2) to change the hydraulic history of each sample. Matric suction was estimated from the first set of samples using the filter paper method, while the second set was used for testing. The variations of the matric suction with pre-test water content and degree of saturation are shown in Fig. 4.1. The curves have a similar trend, showing that the variation of degree of saturation is because of variation in water content of the sample. Table 4.2 (columns 6 - 9) shows the estimated matric suction values and pre-test conditions. Following wetting, the samples were left for 14days for equalisation. During the equalisation of suction, a load of 5kPa was applied on the samples to avoid shrinkage of those samples.

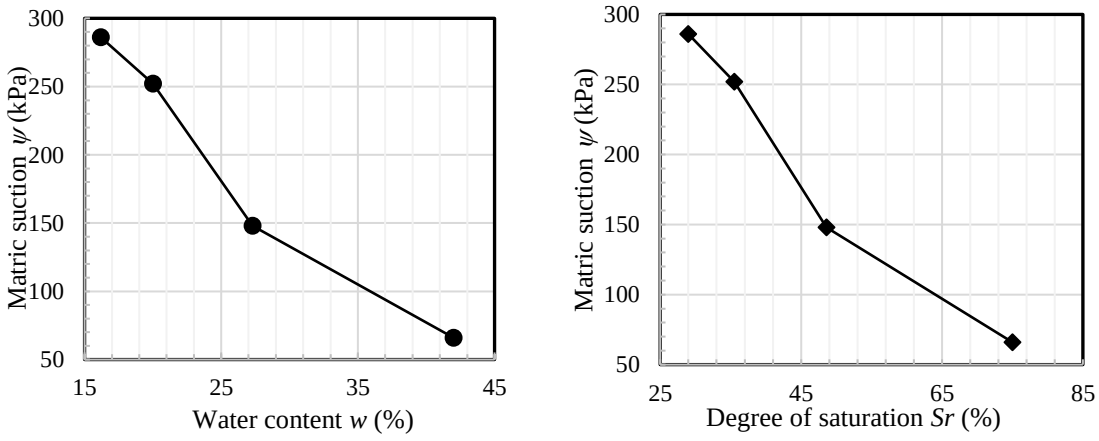

Figure 4-1 Variation of matric suction with water content and degree of saturation

Table 4-1 Initial state of samples for single and double oedometer tests after static compaction

Tests	Initial states					Test details Single oeometer (SO) Double oedometer (DO)	No. of tests
	Water content w (%)	Void ratio e_0	Degree of saturation S_r (%)	Initial matric suction (kPa)	Compaction pressure (kPa)		
$A1_{(SO)}$	21.5	0.98	58.0	212	679	Wetted at 200kPa (SO)	2
$A1_{(DO\text{-}cwc)}$	21.5	0.99	57.6			Constant water content (DO)	2
$A1_{(DO\text{-}5)}$	21.5	0.98	58.0			Wetted at 5kPa (DO)	3
$A2_{(SO)}$	9.9	0.98	26.8	628	939	Wetted at 200kPa (SO)	2
$A2_{(DO\text{-}cwc)}$	10.1	0.98	27.3			Constant water content (DO)	2
$A2_{(DO\text{-}5)}$	10.1	0.98	27.2			Wetted at 5kPa (DO)	2
$A3_{(SO)}$	5.3	1.00	14.2	1112	999	Wetted at 200kPa (SO)	1
$A3_{(DO\text{-}cwc)}$			14.2			Constant water content (DO)	1
$A3_{(DO\text{-}5)}$			14.2			Wetted at 5kPa (DO)	1
$B1_{(SO)}$	32.2	1.47	58.0	109	57	Wetted at 200kPa (SO)	1
$B1_{(DO\text{-}cwc)}$	32.7	1.48	58.6			Constant water content (DO)	1
$B1_{(DO\text{-}5)}$	32.8	1.48	58.8			Wetted at 5kPa (DO)	1
$B2_{(SO)}$	16.6	1.49	29.5	286	180	Wetted at 200kPa (SO)	1
$B2_{(DO\text{-}cwc)}$	15.7	1.48	28.1			Constant water content (DO)	1
$B2_{(DO\text{-}5)}$	15.9	1.48	28.5			Wetted at 5kPa (DO)	1
$B3_{(SO)}$	7.7	1.47	13.9	691	280	Wetted at 200kPa (SO)	1
$B3_{(DO\text{-}cwc)}$	8.0	1.49	14.2			Constant water content (DO)	1
$B3_{(DO\text{-}5)}$	8.0	1.49	14.2			Wetted at 5kPa (DO)	2
$A4_{(DO\text{-}5)}$	16.9	0.99	45.0	250	759	Wetted at 5kPa (DO)	1
$B2_{(DO\text{-}5)}$	17.0	1.5	30.0	286	180		
$B2_{(SO\text{-}25)}$	16.6	1.49	29.5	286	180	Wetted at 25kPa (SO)	1
$B2_{(SO\text{-}50)}$	16.6	1.48	28.5			Wetted at 50kPa (SO)	1
$B2_{(SO\text{-}100)}$	16.6	1.49	29.5			Wetted at 100kPa (SO)	1
(1)	(2)	(3)	(4)	(5)	(6)	(7)	(8)

*: Initial matric suction was obtained using filter paper method

Table 4-2 Initial state of samples after compaction and wetting

Test	Moulding conditions			Volume of water used for wetting (mls)	Conditions at the start of the tests				Test details	No. of tests
	e_0	*w* (%)	*Sr* (%)		e	*w* (%)	*Sr* (%)	Estimated suction (kPa)		
$B2_{(CWC-66)}$	1.49	16.2	29	25.0	1.47	42.0	75.0	66	Constant water	2
$B2_{(CWC-148)}$				11.3	1.49	27.3	48.6	148	Constant water	2
$B2_{(CWC-252)}$				4.5	1.49	20.0	35.5	252	Constant water	2
$B2_{(CWC-286)}$				0.0	1.49	16.2	29.0	286	Constant water	2
(1)	(2)	(3)	(4)	(5)	(6)	(7)	(8)	(9)	(10)	(11)

4.3 EXPERIMENTAL TESTS RESULTS AND ANALYSIS

4.3.1 Compressibility behaviour

The results of single and double oedometer tests are presented in terms of void ratio versus log of vertical stress. To ensure repeatability of results, group A tests were repeated up to three times as shown in Table 4.1. For group B tests, only tests B3 was repeated. Repeatability and uncertainty in B1 and B2 were analysed by comparing the results of single oedometer tests (SO) with corresponding constant water content tests (DO-CWC) between 0 to 200kPa. Single odometer test from 0-200kPa is a repeat of constant water content test for the same stress range. Table 4.2 and 4.3 shows the standard deviation, mean and variance for the void ratios at 400kPa and 200kPa for group A and B respectively. The standard errors shown in Table 4.3 indicate that the measurements are repeatable.

Table 4-3 Error analysis for standard oedometer tests (e_0 = 1.0)

Tests	No of Obs.	Vertical stress (kN/m^2)	Final void ratio				Std. error
			Mean	Std dev.	Coeff. of variation	Variance	
$A1_{(SO)}$	2	400	0.7335	0.0007	0.0964	0.0000	0.0005
$A1_{(DO-CWC)}$	2	400	0.9366	0.0035	0.3775	0.0000	0.0025
$A1_{(DO-5)}$	3	400	0.7029	0.0013	0.1811	0.0000	0.0009
$A2_{(SO)}$	2	400	0.7429	0.0007	0.0952	0.0000	0.0005
$A2_{(DO-CWC)}$	2	400	0.9321	0.0042	0.4552	0.0000	0.0030
$A2_{(Do-5)}$	2	400	0.7049	0.0028	0.4013	0.0000	0.0020
$A3_{(SO)}$ & $A3_{(DOCWC)}$		200	0.9811	0.0088	0.8937	0.0001	0.0062

Table 4-4 Error analysis for standard oedometer tests (e_0 = 1.5)

Tests	No of Obs.	Vertical stress (kN/m^2)	Final void ratio				Std. error
			Mean	Std dev.	Coeff. of variation	Variance	
$B1_{(SO)}$ &$B1_{(DO-CWC)}$		200	1.2469	0.0113	0.9073	0.0001	0.0080
$B2_{(SO)}$ &$B2_{(DO-CWC)}$		200	1.4065	0.0154	1.0960	0.0002	0.0109
$B3_{(SO)}$ &$B3_{(DO-CWC)}$		200	1.4325	0.0001	0.0099	0.0000	0.0001
$B3_{(Do-5)}$	2	400	0.8715	0.0020	0.2272	0.0000	0.0014

The void ratios presented in the graphs were calculated from the average of the repeated measurements. To facilitate comparison of results and to account for small variations in the initial void ratio of the individual samples, all test data on the same graph were normalised to a common initial void ratio. Correction factor Δe (see Eq. 4.1) was applied to each result being compared to correct for differences in initial void ratio. The correction factor ranged between (-0.02 – 0.003) for A1, (-0.003 – 0.007) for B1 & B2 and (-0.004 – 0.02) for B3.

$$\Delta e_0 = e_0 - e_{avg} \qquad \textbf{4-1}$$

where e_0 is initial void ratio of the individual sample

e_{avg} is average void ratio

Figs. 4.2, shows the single and double oedometer test results obtained for samples at e_0 = 1.0 and 1.5. From Fig. 4.2(a-c), the samples in tests $A1_{(Do-5)}$, $A2_{(Do-5)}$ and $A3_{(Do-5)}$ at a void ratio of 1.0 experienced expansion on wetting at 5kPa. Void ratio e increased by 0.07 in Test $A1_{(Do-5)}$, 0.09 in $A2_{(Do-5)}$ and 0.16 in $A3_{(Do-5)}$. The observed expansion was greatest for Test $A3_{(Do-5)}$.

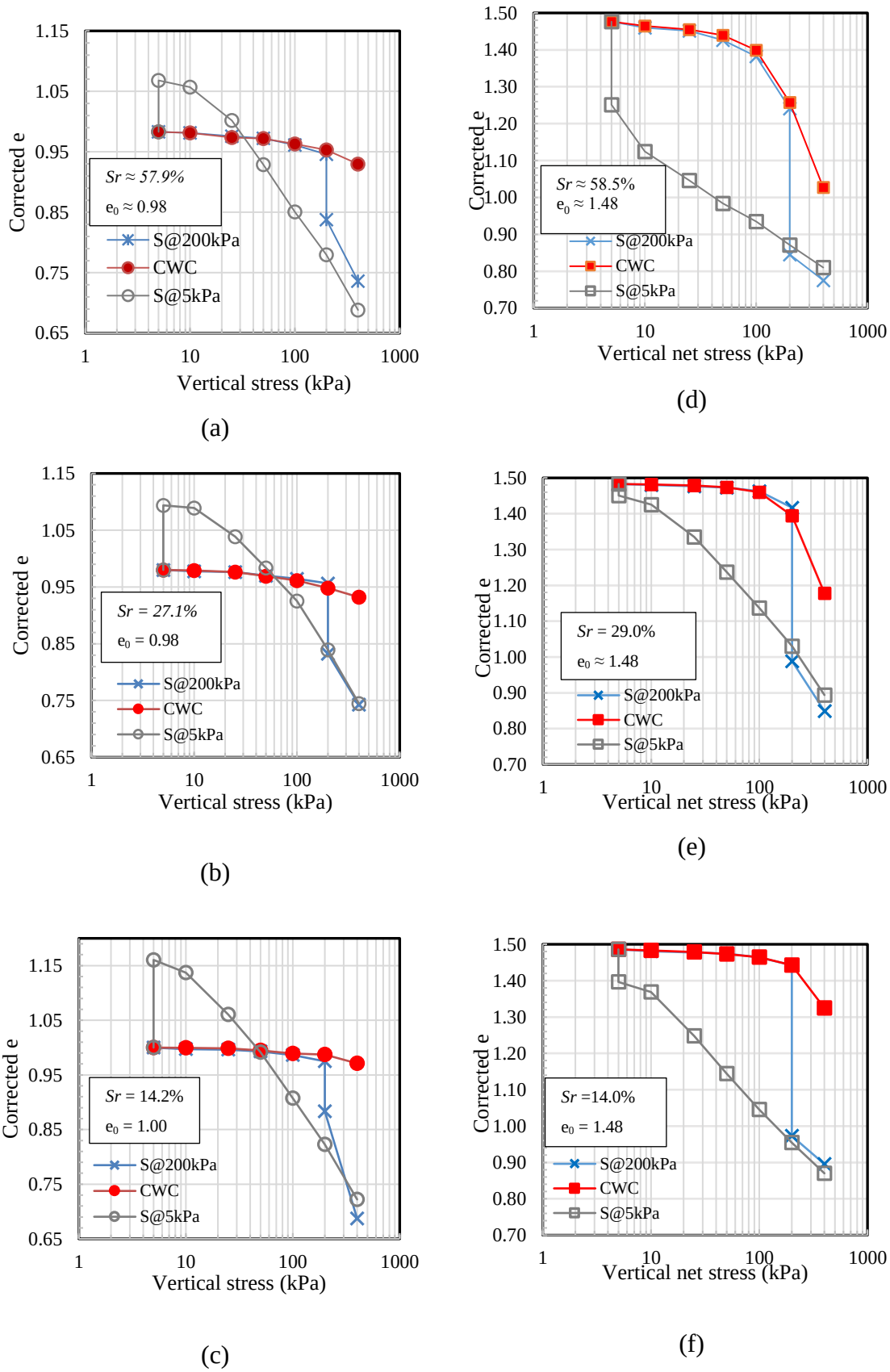

Figure 4-2 Double and single oedometer tests results (a) A1; e_0 = 0.98, *Sr* = 57.9% (b) A2; e_0 = 0.98, *Sr* = 27.1% (c) A3; e_0 = 1.0, *Sr* = 14.2% (d) B1; e_0 = 1.48, *Sr* = 58.5% (e) B2; e_0 = 1.48, *Sr* = 29% (f) B3 e_0 = 1.48, *Sr* = 14%

In contrast to group A tests, $B1_{(Do-5)}$, $B2_{(Do-5)}$ and $B3_{(Do-5)}$ exhibited collapse on wetting (see Fig. 4.2 d- f). Void ratio e decreased by 0.23 in $B1_{(Do-5)}$, 0.03 in Test $B2_{(Do-5)}$ and 0.084 in $B3_{(Do-5)}$. The different behaviours indicate that soil behaviour on wetting is dependent on the initial void ratio/density. The observed volumetric behaviours of both groups are consistent with the observations of Lawton et al. (1989); Sivarkumar & Wheeler (2000) and Montanez (2002). In Sivarkumar & Wheeler (2000), kaolin clay samples that were compacted to void ratios of 1.201 and 0.976 exhibited collapse and expansion respectively on wetting at a mean net stress of 50kPa. From Fig. 4.2, as load was increased after wetting from 5kPa to 400kPa, the volume changes in samples at e_0 = 1.0 could be seen to change from expansion to collapse, while samples at e_0 = 1.5 maintained collapse behaviour. Further analysis of the results later in the chapter will consider the influence of degree of saturation.

The volumetric behaviour of clay soils on wetting (expansion or collapse) is influenced by the type of clay mineral that constitutes the soil, the soil structure, initial density and imposed stress state (Sivarkumar & Wheeler, 2000; Ng & Menzies, 2007; Sun et al., 2007). Regarding the clay mineral, soils with 2:1 clay minerals e.g. smectite and montmorillonite, have been reported by numerous authors to swell on wetting at low value of applied stress (Grim, 1962; Jones & Jefferson, n.d.; Rao & Thyagaraj, 2003). Soils with a high content of loess generally collapse on wetting (Barden et al., 1973; Houston et al., 1988; Munoz-Castelblanco, 2011; Liu et al., 2016). Expansion on wetting generally occurs at low applied stress (Jotisankasa et al., 2007; Sivarkumar & Wheeler, 2000). It is worth mentioning that expansive soils can collapse on wetting at low applied stress depending on the initial dry density of the soil (Montanez, 2002). Collapse of expansive soils is possible at low initial dry density. For the presented results in Fig. 4.2, the soil type and the applied stress at which samples at e_0 = 1.0 (group A) and 1.5 (group B) were wetted, are the same. The different volumetric behaviour on wetting of samples A and B can be attributed to varying void ratios, due to compaction to different dry densities. From Sec. 2.3.3, evidence has shown that compaction to different dry densities affect the size of the macro pores (Lloret et al., 2003). However, it is not possible to infer how the relative sizes of the pores influenced the volumetric behaviour on wetting, since microstructural studies were not conducted on the samples. Given no microstructural investigation, the collapse and expansion on wetting observed in group A and group B can be explained based on different dry densities. Group A samples have an initial density of 1.34Mg/m^3 while group B samples have an initial dry density of 1.11Mg/m^3.

Tests $A1_{(DO\text{-}cwc)}$, $A2_{(DO\text{-}cwc)}$, $A3_{(DO\text{-}cwc)}$, $B1_{(DO\text{-}cwc)}$, $B2_{(DO\text{-}cwc)}$ and $B3_{(DO\text{-}cwc)}$ at constant water content were accompanied by a reduction of void ratio, as vertical stress was increased from 5kPa to 400kPa. Fig. 4.2 indicates that compressibility increased as initial void ratio increases. The vertical deformation in samples at $e_0 \approx 1.0$ (Fig. 4.2 a-c) is small relative to the deformation in samples at $e_0 \approx 1.5$ (Fig. 4.2 d-f). For instance, at a degree of saturation of approximately 58%, increase in vertical stress from 5kPa to a final value of 400kPa resulted in $\Delta e = 0.048$ in test $A1_{(DO\text{-}cwc)}$ and $\Delta e = 0.302$ in $B1_{(DO\text{-}cwc)}$. This observation is consistent with the finding of Haghighi (2011). He also observed an increase in compressibility, with an increase in initial void ratio. In relation to soil density, compaction of soils to relatively low density (high void ratio) will result in an open structure formation (Alonso et al., 2013) with large macro pores. Increasing vertical net stress will then cause instability and collapse of the soil grains into the open structure and thus increase in compressibility. If the soil density is high, the size of the macro pores will be relatively small, thus, the compressibility associated with increasing vertical net stress will be comparatively small.

For tests, $A1_{(so)}$, $A2_{(so)}$, $A3_{(so)}$, $B1_{(so)}$, $B2_{(so)}$ and $B3_{(so),}$ samples at $e_0 \approx 1.0$ and 1.5 were loaded incrementally from 5kPa to 200kPa and wetted at this value of applied vertical stress. From Figs. 4.2, both group A and B samples exhibited wetting induced collapse, irrespective of swelling previously observed in group A samples, when wetted at 5kPa. The single oedometer test is a repeat of the constant water content test up to the value of vertical stress at which wetting occurred (200kPa in this case). From Fig. 4.2 (a-f), it could be seen that the single oedometer and constant water content curves are in alignment between 5kPa and 200kPa, indicating that the repeatability is good. The wetting induced expansion and collapse of group A samples at 5kPa and 200kPa respectively agree with the findings (Lloret & Alonso, 1980) in which they reported that suction decrease (i.e. wetting) does not necessarily lead to swelling or collapse, but depends on the intensity of applied vertical stress. The collapse behaviour observed in group A at 200kPa is because the stress level is high enough to resist the swelling tendency (Bell & Culshaw, 2001). This explains why lightweight structures on expansive clays are susceptible to cracking due to wetting induced expansion of the soil. The swelling tendency is overcome when the weight of the structure is more than the swelling pressure of the soil. Subsequent discussion of the results will consider the influence of degree of saturation on the volumetric behaviour and compressibility parameters.

In Fig. 4.3a, tests $A1_{(DO\text{-}cwc)}$, $A2_{(DO\text{-}cwc)}$ and $A3_{(DO\text{-}cwc)}$ at Sr of 58%, 27% and14.2% respectively, and e_0 = 0.99, are compared to investigate the influence of degree of saturation on the compressibility of the samples. Fig. 4.3a shows that loading of the samples at constant water content was accompanied by relatively small reductions in void ratios for all three samples: max Δe at 400kPa is 0.053±0.003, 0.048±0.003 and 0.029 for Sr 58%, 27% and 14.2% respectively (note that the results were corrected based on the average initial void ratio of the three samples). *Sr* of 58% and 27% exhibited higher compressibility than *Sr* of 14%, within the vertical stress range of 50kPa to 400kPa. Inspection of Fig. 4.3a shows that the samples in tests $A1_{(DO\text{-}cwc)}$, $A2_{(DO\text{-}cwc)}$ and $A3_{(DO\text{-}cwc)}$ yielded at some point with increasing vertical applied stress. This will be discussed in details in the next section.

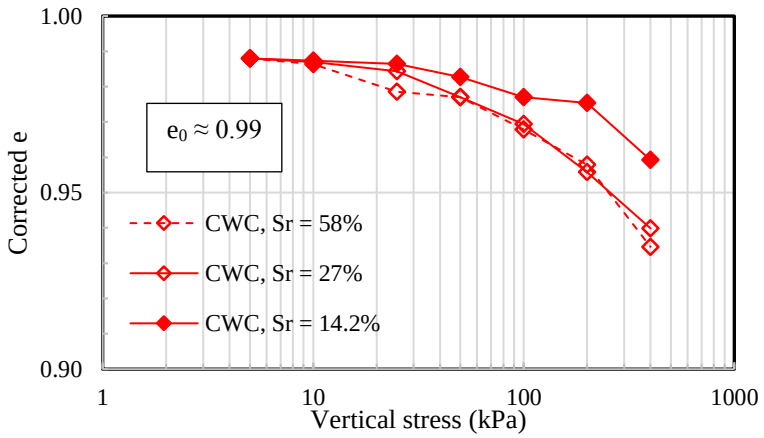

a

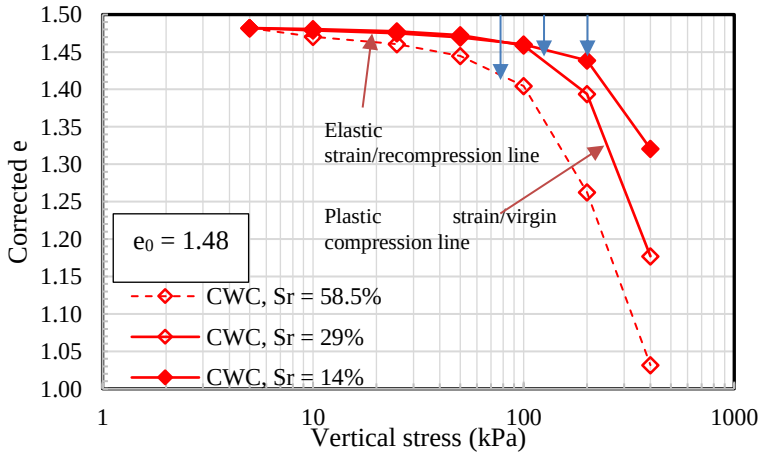

b

Figure 4-3 Void ratio versus vertical stress for constant water content tests (DO-CWC) at *Sr* = 58, 27, and 14.2% (a) e_0 = 0.99 (b) e_0 = 1.48

In terms of suction, increase in degree of saturation reduces suction. Since suction increases the soil rigidity and shear srength, thereby making the soil less compressible (Matyas & Rahakrishina, 1968; Barden & Sides, 1970; Alonso et al., 1990), it was expected that an increase in initial degree of saturation will increase compressibility. From Table 4.1, *Sr* of 14.2, 27 and 58% have corresponding initial matric suction of 1112, 628 and 212kPa respectively; therefore, *Sr* of 14.2% should be comparatively rigid and less compressible. This was confirmed by the data in Fig. 4.3a; the curve for Sr of 14% continuously plotted above the curves for Sr of 27 and 58% from 10kPa to 400kPa. This is consistent with the findings of Montanez (2002) in which compressibility increased with increasing water content (decreasing matric suction). Sr of 58% with the least value of matric suction (212kPa), was expected to exhibit higher compressibility than Sr of 27%, on the assumption that the degree of saturation increases monotonically in both samples with increasing vertical applied stress. However, no explanation could be given for the similar compressibility observed in Sr of 27% and 58%.

In terms of elasto-plastic behaviour, elastic strains are apparent in the three samples at Sr of 14, 27 and 58% (Fig. 4.3a); however, there is no clear evidence of plastic strains because the normal compression lines were not clearly established within the stress considered. It is possible that the virgin compression lines would be well defined if more loading steps were added or that the samples are so stiff that increasing vertical net stress will not have an impact. The strain along the recompression line, i.e. pre-yield strain, is elastic and reversible, whereas the strain along the normal compression line (post yield) is plastic. Elastic strains in soils are caused by elastic deformation of soils because of changes in inter-particle forces. Plastic strains on the other hand, are caused by inter-particle slippage or damage of soil particles (Wheeler, 2010). Compression of samples at e_0 = 1.0, produced by increasing vertical net stress, can be attributed mainly to change in inter-particle forces, since the observed strains were mostly elastic strains as can be seen from Fig. 4.3a, as the virgin compression lines were not established.

In Fig. 4.3b, tests $B1_{(DO\text{-}cwc)}$, $B2_{(DO\text{-}cwc)}$ and $B3_{(DO\text{-}cwc)}$ at *Sr* = 58.5%, 29% & 14% and e_0 =1.48 are compared to also investigate the influence of degrees of saturation on compressibility. From the figure, the compression curves for the three tests have similar shapes, with the individual values of the void ratios being the only differentiating characteristic. The void ratios reduced with increasing vertical stress. Inspection of the figure shows that compressibility increases with an increase in the initial degree of saturation, consistent with the compressibility behaviour of samples at e_0 = 1.0. For

instance, at maximum vertical net stress (400kPa), void ratios for *Sr* of 58, 29, 14% are 1.032, 1.177, and 1.321 respectively. For *Sr* of 29% and 14%, the compressibility values in the two samples were equal from 5kPa to 100kPa. The yield points, indicated by arrows on the curve, are apparent in all the tests; they increased with decreasing initial degree of saturation or increasing initial matric suction. The behaviour is in line with expectations, showing the stabilising effect of suction and the effect of increased compaction pressure on yield stress. The compaction pressures, as shown in Table 4.1, for *Sr* of 58%, 29% and 14% are 57, 180 and 280kPa respectively. It was expected that the yield stress will be equivalent to the compaction pressure and will increase accordingly, since the compaction pressure is the previous maximum stress a sample has been subjected to (Burton et al., 2014). The increase in yield stress with decreasing initial degree of saturation is in line with the findings of Sivarkumar & Wheeler (2000), Montanez (2002) and Haghighi (2011). In the study by Sivarkumar & Wheeler, a sample of kaolin compacted to a void ratio of 1.97 at *Sr* of 68.1% yielded a higher value of vertical net stress relative to a sample at *Sr* of 79.8%, void ratio of 1.95. It is worth mentioning that the initial water contents were varied in the samples used in this study, as shown in Table 4.1, as well as compaction pressure to achieve the initial degree of saturation. The initial matric suction created by compaction is usually determined by the compaction water content, based on the principle that the higher the water content the lower the initial suction, with dry density having a relatively small effect (Gens et al., 1995) although Tarantino (2009) has provided evidence to show that suction can change significantly with variation in dry density alone. A detrimental effect of an increase in compaction water content is reduction in rigidity, due to suction reduction and reduction in the elastic region from an elastoplastic point of view (Wheeler & Sivarkumar, 1995). It is however difficult to point out which of the two variables (initial matric suction or compaction pressure) is influencing the yield stresses in tests $B1_{(DO\text{-}cwc)}$, $B2_{(DO\text{-}cwc)}$ and $B3_{(DO\text{-}cwc)}$. Because of this, tests $B2_{(cwc\text{-}66)}$, $B2_{(cwc\text{-}148)}$ $B2_{(cwc\text{-}252)}$ and $B2_{(cwc\text{-}286)}$ were performed and presented in Sec. 4.3.2 to clearly show the influence of initial matric suction on yield stress. In this case, the initial water contents and compaction efforts were the same for the three samples. Fig. 4.3b shows that once the yield stress was exceeded, the soil state fell along the virgin compression line, also known as the normal compression line, which differs for each test. In other words, the normal compression lines are clearly established in group B samples unlike in group A. Both elastic (reversible) and plastic (irreversible) strains were observed in group B. Loading to yield pressure marked the onset of plastic strain, which increased significantly along the virgin compression line.

In Fig. 4.4a, tests $A1_{(DO-5)}$, $A2_{(DO-5)}$ and $A3_{(DO-5)}$ at e_0 = 0.99 and different *Sr* (14, 27 and 58%) are compared. The data are represented to clearly show the influence of degree of saturation on wetting induced expansion. As explained earlier, upon wetting at 5kPa, all samples with e_0 = 0.99 expanded with *Sr* of 14% having the highest magnitude of expansion (void ratio typically increased by 0.159). Sample at *Sr* of 27% expanded by 0.114. The smallest magnitude of expansion was observed in *Sr* of 58% with an increase of 0.085. The observed behaviour indicates that expansion of the sample increases with decreasing initial degrees of saturation. This corresponds with the findings from other researchers (Chen, 1975; Lawton et al., 1989; Montanez, 2002). It is worth mentioning that the different degrees of saturation in the samples were achieved by varying the compaction water content.

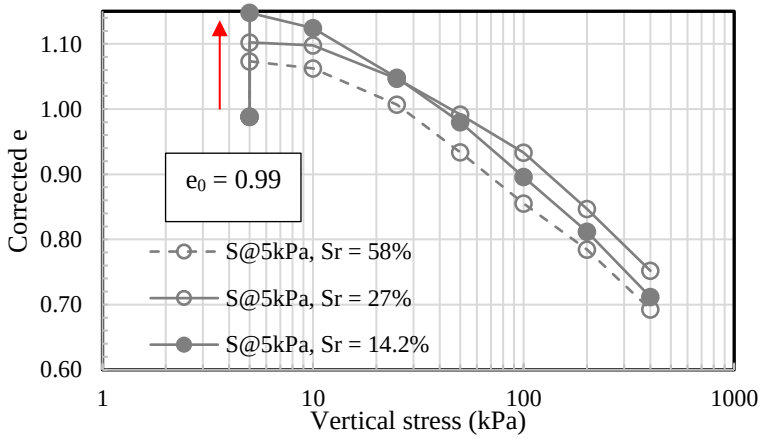

a

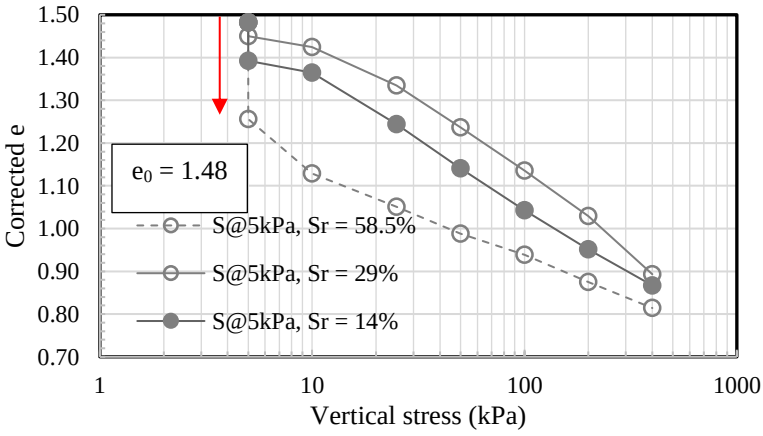

b

Figure 4-4 Wetting test results at *Sr* = 58%, 27%, 14% (a) e_0 = 0.99 (b) e_0 = 1.48

Per Chen (1975), a decrease in initial water content will increase the magnitude of swelling, but the swelling pressure will be unaffected by the initial water content. This was based on observations on remoulded samples of claystone shale found in Southeast Denver. A similar observation was made by Lawton et al. (1989). In their study, they observed that a decrease in compaction water content was inversely related to both the maximum swelling and collapse.

Wetting induced swelling of non-expansive clays is categorised as inter-crystalline swelling (Grim, 1962). In relatively dry and densely compacted clays, the soil particles are held together by water under tension due to capillary forces. On getting access to free water, the capillary forces relax, causing the clay to expand. In this case, water absorption is limited to the void spaces and external crystal surfaces.

In Fig. 4.4b, tests $B1_{(DO-5)}$, $B2_{(DO-5)}$ and $B3_{(DO-5)}$ at $e_0 \approx 1.48$ and *Sr* of 14, 29 and 58% are also compared to show the influence of degrees of saturation on wetting induced collapse. All the samples were wetted at vertical net stress of 5kPa. On wetting, all the samples exhibited collapse, as shown in Fig. 4.4b, which is because of compaction to low dry density as explained previously and as observed by Montanez (2002); Abbeche et al. (2007); Alonso et al. (2010). A decrease in void ratio by 0.226 was observed in *Sr* of 58%, 0.090 in *Sr* of 14% and a decrease of 0.032 in *Sr* of 29%. The collapse increased with a decreasing initial degree of saturation, as seen in *Sr* of 29% and 14%. This outcome was expected and agrees with published literature (e.g. Lawton et al., 1989). These researchers reported that the magnitude of collapse on wetting in compacted clays increases with decreasing initial degree of saturation. As could be seen from the figure, the sample with *Sr* of 58% ($B1_{(DO-5)}$) collapsed to a void ratio of 1.256 on wetting under 5kPa. The high magnitude of collapse observed in the sample at *Sr* of 58%, relative to *Sr* of 14% and 29%, is due to the unstable and open structure of the sample (see Fig. 4.5). It was the intention to prepare all group B samples at the same dry density (1.11mg/m^3) but at 60, 30 and 15% degrees of saturation. The water content required to achieve *Sr* of 60% at the proposed dry density is approximately 32.3%, as shown in Table 4.1. Preparing a sample at a water content of 32% and void ratio of approximately 1.5 resulted in an aggregated sample, as described by Koliji et al. (2010), or formation of macro-pods (Lawton et al., 1992) with large void spaces, as shown in Fig. 4.5 (B1). Samples B2 and B3 as can be seen in Fig. 4.5 have small void spaces that appear to be uniformly distributed. Consequently, wetting of sample ($B1_{(DO-5)}$) resulted in rearrangement of the

particles and closing of the large void spaces, resulting in the high magnitude of collapse shown in Fig. 4.4b.

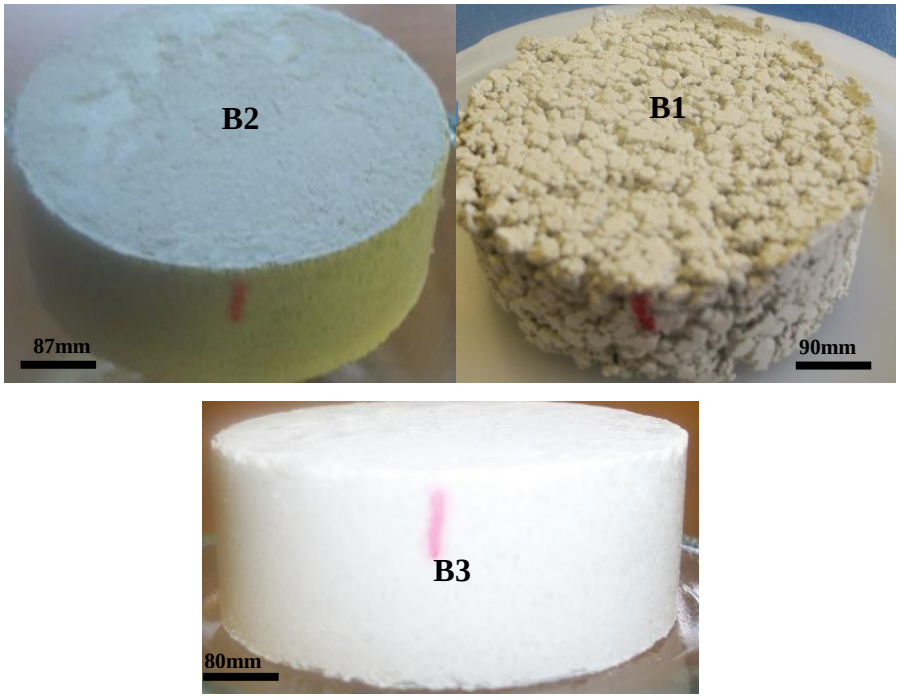

Figure 4-5 Sample B1 (*Sr* = 58%, e_0 = 1.48), B2 *(Sr* = 29%, e_0 = 1.48), B3 (*Sr* = 14%, e_0 = 1.48)

The collapse mechanism in clays compacted at low densities is explained by the model of Hodek & Lovell (1979 in Lawton et al., 1992). In the model, clay aggregates soften on absorption of water, collapse then occurs as the soil rearranges into a denser state of packing because of the softened aggregates.

From Fig. 4.4b, increase in vertical net stress after saturation was accompanied by compression, with the void ratios for *Sr* of 14% and 29% converging at maximum applied vertical net stress (400kPa).

Rahardjo & Fredlund (2003) observed that when samples are prepared to be in the same initial state, a unique compression line would be established at similar void ratios and corresponding vertical net stress, irrespective of the path taken and if the final stress state for the samples are identical. To examine this, single oedometer tests ($B2_{(SO-25)}$, $B2_{(SO-50)}$, $B2_{(SO-100)}$, $B2_{(SO-200)}$) were performed with four samples of similar initial conditions (e_0 = 1.49, Sr = 29%). $B2_{(SO-25)}$, $B2_{(SO-50)}$, $B2_{(SO-100)}$, and $B2_{(SO-200)}$ were loaded to a vertical stress of 25, 50, 100 and 200kPa respectively and saturated under this value of applied vertical stress.

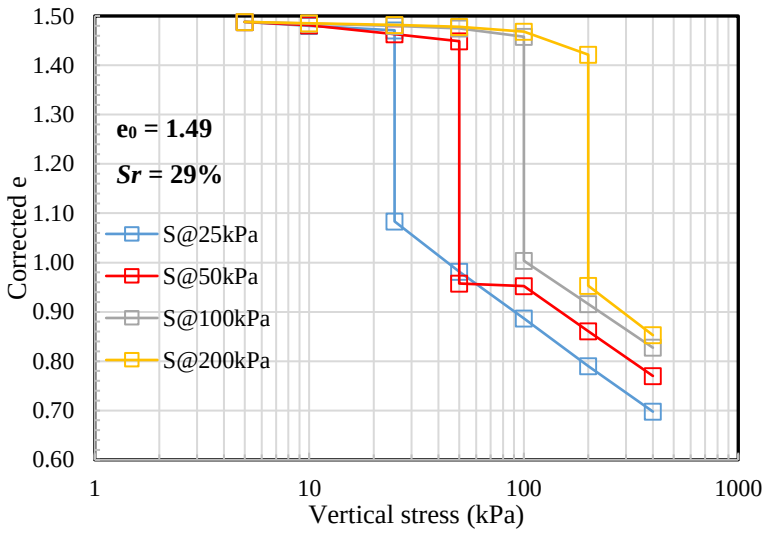

Figure 4-6 Single oedometer test results, with wetting at different stresses

The results from the tests are shown in Fig. 4.6 in terms of void ratio versus vertical stress. As shown in the figure, initial loading prior to saturation was not accompanied by a significant reduction in void ratios of the individual samples. On wetting, however, all the samples exhibited collapse, which increased with an increase in applied stress in consistent with the observations of Monroy (2005) on London clay saturated under constant applied stress between 276 to 442kPa. On subsequent loading in a fully saturated state, the samples experienced a further reduction in void ratio. It was expected that the compression lines after saturation will converge into a single line. From Fig. 4.6, the samples did not arrive at the same void ratio and a unique compression line was not established in the range of applied stress (maximum vertical net stress of 400kPa). It is possible that additional loading steps might lead to the convergence of the void ratios and compression lines.

Tests $A4_{(DO\text{-}5)}$ and $B2_{(DO\text{-}5)}$ were performed to investigate if the compression lines of samples at different e_0 (1.0 and 1.5) but the same water content (≈17%) will converge towards a single unique line. Rios et al. (2012) observed a unique CL for samples of cemented silty sand at different initial void ratios but similar water content. With Rio's observation, it appears that the same initial water content is the major factor that determines if a unique CL will be established. Tests $A4_{(DO\text{-}5)}$ and $B2_{(DO\text{-}5)}$ were performed in an oedometer cell following a wetting path at 5kPa and loaded incrementally afterwards to a maximum vertical net stress of 800kPa. The void ratio versus vertical net stress plot of the results are shown in Fig. 4.7.

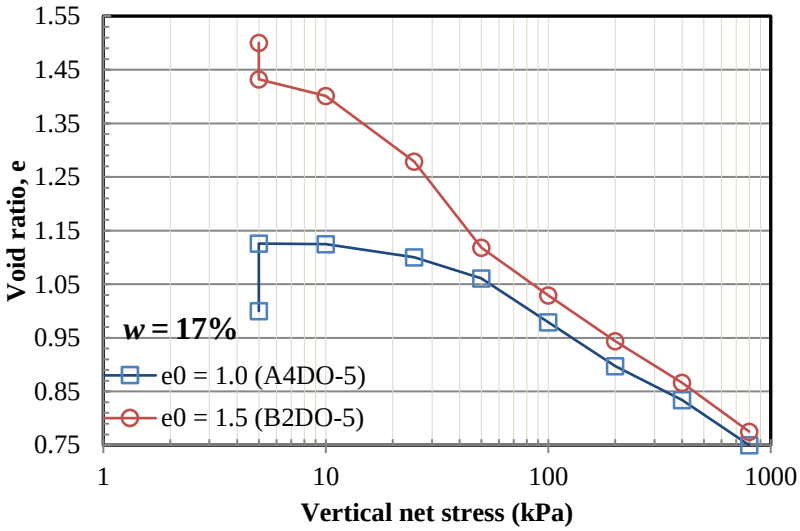

Figure 4-7 Void ratio versus vertical stress for samples at e_0 = 1.0 and 1.5; *w* = 17%

As shown in the figure, samples $A4_{(DO-5)}$ and $B2_{(DO-5)}$ experienced wetting induced expansion and collapse respectively. On subsequent loading in a fully saturated state, both samples experienced collapse. The compression lines could be seen tending towards a single compression line, which was evident from a vertical net stress of 50kPa. This indicates that the compression line of samples of the tested kaolin clay compacted to the same water content, but different void ratios would converge at some point upon loading in a saturated state. These outcomes indicate that compaction of the samples at the same water content but different void ratios will result in a change of initial state as also reported by Wheeler & Sivakumar (1995). Compression of soils to very high stress levels will result in a path that is asymptotic to a void ratio of zero or specific volume of one (Shipton & Coop, 2012). From Fig. 4.7, an asymptote was not achieved at the stress levels considered.

4.3.2 Yielding behaviour

Figs. 4.8a-c compare the compression curves of Tests $A1_{(DO-cwc)}$, $A2_{(DO-cwc)}$, $A3_{(DO-cwc)}$ and $B1_{(DO-cwc)}$ $B2_{(DO-cwc)}$ $B3_{(DO-cwc)}$ with the aim of investigating the influence of void ratio on yielding. The yield stress was estimated using Butterfield method (log e +1 – log σ'), which is the point of intersection of the two linear segments of the consolidation curve plotted in terms of log e+1 versus log σ. The merit of this method is that the plot of log e+1 – log σ' results in two distinct straight lines along the recompression and virgin compression curves, which makes estimation of yield stress easier and relatively accurate

when compared to Casagrande method. Other methods that can be used to estimate the yield stress are; Schmertmann method (e – log σ'), Janbu method (ΔH/H - σ'), Burmister method. These listed methods involve graphical construction of tangential lines along the recompression and virgin compression curves and estimation of the yield stress as the intersection of the lines. Leonards & Ramiah (1959) explained that it is difficult to rate the performance of the methods, since no reliable method exists for the determination of in-situ yield stress. However, Jose et. al (1989) demonstrated that Butterfield method estimates the yield stress better than Casagrande method. In their study, the deviation from the real pre-consolidation pressure obtained by Casagrande method is 15 to 50%, whereas the deviation in Butterfield method is 2 to 20%.

From the Figs. 4.8, increase in vertical net stress resulted in yielding of the soil at some point. The figures show that under the same initial *Sr*, samples at void ratio of ≈1.5 yielded before samples at void ratio of ≈1.0. For instance, from Fig. 4.8a, sample $B1_{(DO-cwc)}$ at e_0 = 1.48 yielded at a vertical net stress of 130kPa whereas sample $A1_{(DO-cwc)}$ at e = 0.99 yielded at 160kPa. The increase in yield stress associated with Group A samples can be attributed to high compaction dry density in A (1.34mg/m^3) relative to B (1.11mg/m^3). Sivarkumar & Wheeler (2000) explained this as a beneficial effect because samples compacted to high density will sustain a wide range of applied stress before yielding occurs. The yield curve for samples A will expand to a greater extent than the corresponding yield curve for B. This implies that samples A will have a wider elastic region than corresponding sample B when presented in an elastoplastic framework.

Fig. 4.9 shows variation of yield stress with initial degree of saturation *Sr*. The figure indicates that yield stress decrease with increasing degree of saturation. For each sample group, *Sr* was varied by compacting at different water content as shown in Table 4.1, therefore, the result can be explained in terms of water content. At low water content, the soil is stiff because of strong bond at interparticle contacts and can sustain high magnitude of stress before yielding. As water content is increased to achieve the same void ratio, the bond weakens; the magnitude of stress than can be sustained before yielding decreases. It is also worth mentioning that the compaction pressure required to achieve the pre-defined void ratio increases with decreasing water content. Additional, increase in compaction pressure will delay yielding.

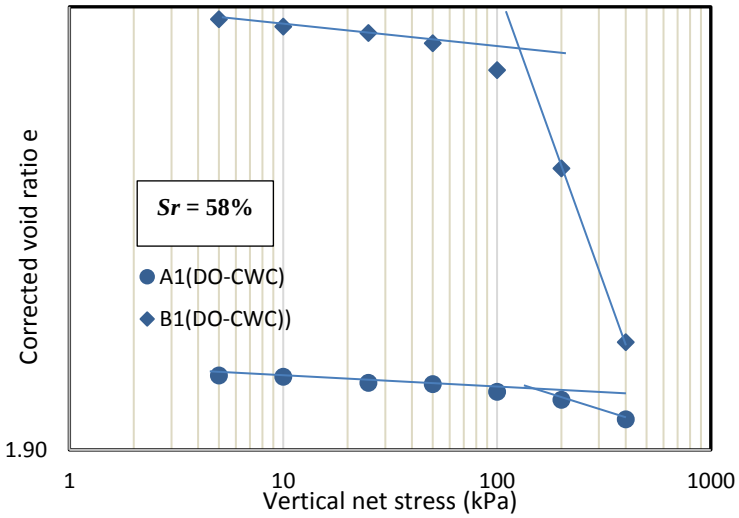

a

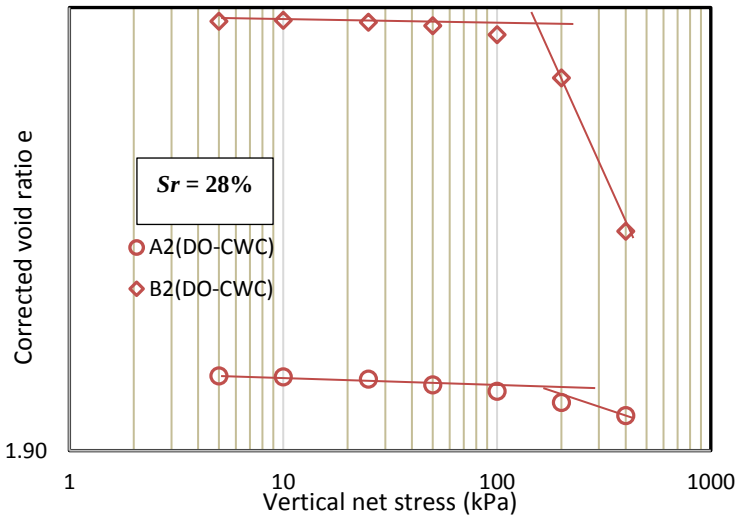

b

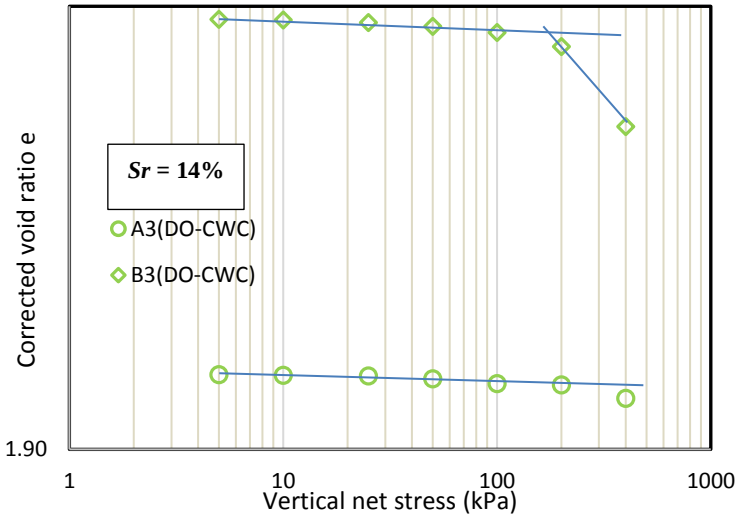

c

Figure 4-8 Comparison of compression curves at $e_0 \approx 1.0$ and 1.5: (a) *Sr* = 58% (b) *Sr* = 28% (c) *Sr* = 14%

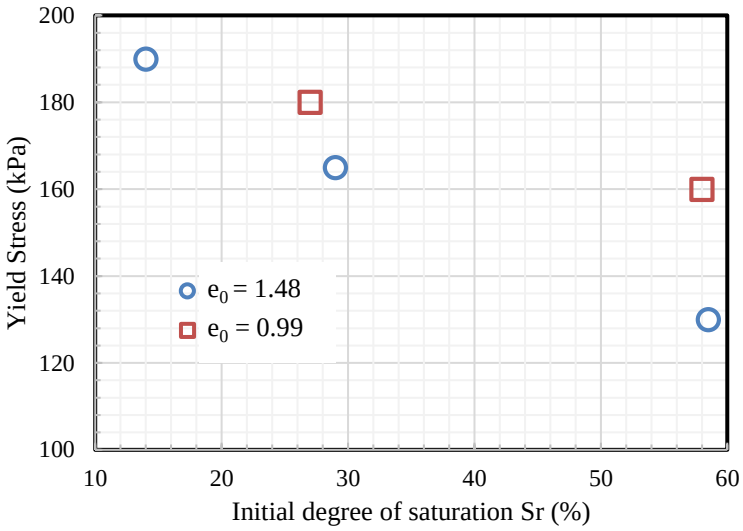

Figure 4-9 Variation of yield stress with degree of saturation

As explained by Sivarkumar & Wheeler (1995), the soil state after the yield stress is along the normal consolidation line defined by Eq. 4.2.

$$V = N - \lambda Ln \frac{p'}{p_{at}} \qquad \textbf{4-2}$$

Where N and λ are the intercept and the slope of the line respectively, p_{at} is atmospheric pressure. λ = Cc/ln10, where Cc is compression index.

The NCL are not well established in $A1_{(DO\text{-}cwc)}$, $A2_{(DO\text{-}cwc)}$, $A3_{(DO\text{-}cwc)}$, hence the discussion will be limited to tests $B1_{(DO\text{-}cwc)}$, $B2_{(DO\text{-}cwc)}$ and $B3_{(DO\text{-}cwc)}$.

Fig 4.10 shows the normal compression lines (NCL) of tests $B1_{(DO\text{-}cwc)}$, $B2_{(DO\text{-}cwc)}$ and $B3_{(DO\text{-}cwc)}$. Eq. 4.2 has been used to fit the experimental data along the virgin compression line to obtain the NCLs. It is worth mentioning that the equation was developed from an isotropic stress state, but has been used in a one-dimensional stress state herein. As expected, each sample had a different normal compression line, which is related to the initial degree of saturation. The slope of the normal compression line (λ) increased with increasing degrees of saturation, as shown in Table 4.5. The NCL presented are not parallel; they diverge with increasing vertical net stress. This behaviour agrees with the predictions and observations of Alonso et al. (1990) and Estabragh et al. (2004) but does not agree with the prediction of Wheeler & Sivarkumar (1995) which states that the NCLs converge with increasing vertical net stress. It is worth mentioning that suction was

controlled in the studies by Alonso et al. (1990), Estabragh et al. (2004) and Wheeler & Sivarkumar (1995) but was not controlled in tests $B1_{(DO\text{-}cwc)}$, $B2_{(DO\text{-}cwc)}$ and $B3_{(DO\text{-}cwc)}$. Suction controlled tests will be presented in the next chapters.

The NCLs have been presented in an *e versus log vertical stress* (see Fig. 4.10). It has been reported that normal compression line presented in *e versus log* stress might be curved (Butterfield, 1979; Pestana & Whittle, 1995), but that presenting the NCL in either *log v versus* stress or *log e versus* stress would achieve linearity. An attempt was made to present the NCLs using the proposed *log e versus* stress, the NCL at *Sr* = 58% was found to be curved.

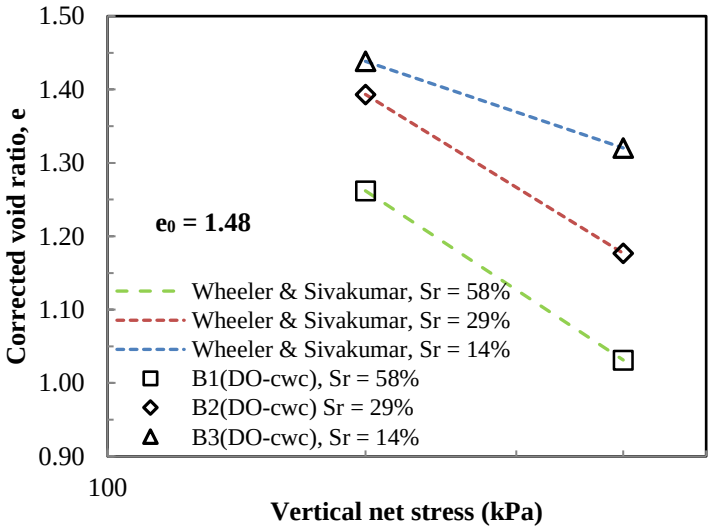

Figure 4-10 Normal compression lines of tests $B1_{(DO\text{-}cwc)}$, $B2_{(DO\text{-}cwc)}$ and $B3_{(DO\text{-}cwc)}$ fitted with the model of Wheeler & Sivakumar (1995)

Table 4-5 Yield parameters of the tested kaolin clay

Test	Initial degree of saturation (Sr) %	Slope of NCL (λ)	Yield stress σ'_p (kPa)	Compaction stress (kPa)
A1	57.6	-	160	679
A2	27.3	-	180	939
A3	14.2	-	-	999
B1	58.6	0.33	130	57
B2	29.0	0.31	165	180
B3	14.2	0.17	190	280

4.3.3 Collapse potential

Fig. 4.11 shows the collapse potential of samples at e_0 = 1.49 with initial degrees of saturation of approximately 59, 29 and 14.2%. The collapse potential was calculated as explained in Sec. 2.8.4 at each value of applied vertical net stress. Also on the figure is data on collapse potential obtained from the single oedometer tests. The figure indicates that the collapse potential in the three tests increased with increasing vertical net stress up to a maximum value (19.6, 18.7 and 14.7% in Sr of 14.2%, 59% and 29% respectively), beyond which further increase in vertical net stress resulted in a decrease in collapse potential. This is consistent with the findings of Lawton et al. (1989, 1992), Medero et al. (2003), Sun et al. (2007), Abbeche et al. (2007), El-Howayek et al. (2011), Liu et al. (2016). The stress level at which the collapse potential is at maximum is known as the critical stress. Lawton et al. (1989) expressed critical stress in terms of the pre-stress induced in the soil during compaction. In their study on clayey sand at 80% relative compaction and 10% water content, they observed that the critical stress corresponded to the yield stress. In Fig. 4.11, the critical stress for Sr of 14. 2% and 29% is 200kPa, but their yield stresses, as shown in Table 4.6, are 180kPa and 160kPa respectively, showing that the critical stresses of the samples are not dependent on pre-consolidation pressure. The collapse potential from single and double oedometer tests for *Sr* of 14.2 and 59% were found to be close. For Sr of 29%, the CP from the single oedometer was significantly higher (17.3%) than CP from the double oedometer (14.7%).

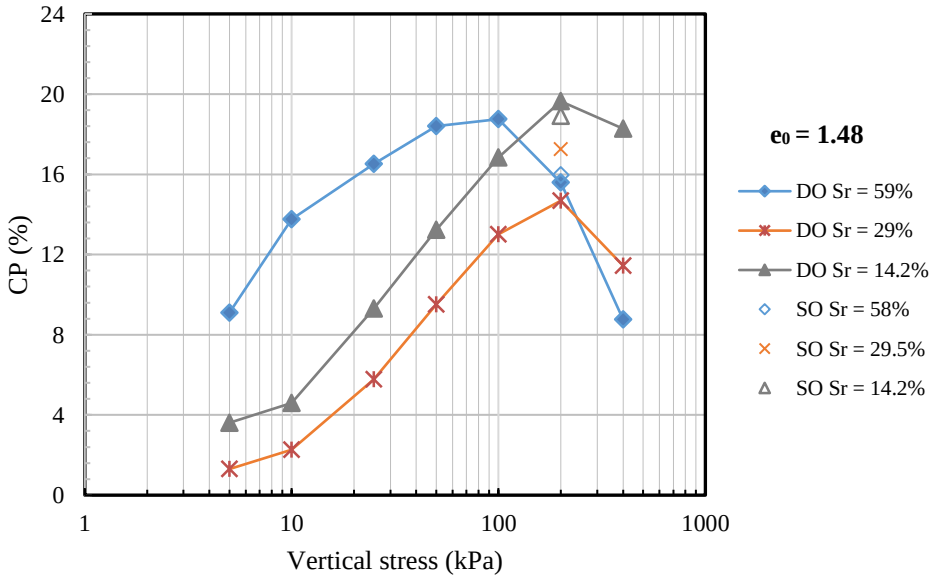

Figure 4-11 Collapse potential for samples at e_0 = 1.48

The CP curves for *Sr* of 14% and 29% show that collapse potential increases with decreasing compaction water content. These observations agree with those made by Lawton et al. (1989, 1992), Abbeche (2007) and El-Howayek (2011). From Table 4.1, the initial water content for group B samples compacted at *Sr* of 14% and 29% are approximately 8 and 16%. The curve for *Sr* 14% consistently plots above the curve for *Sr* 29%, indicating higher CP in *Sr* of 14%. The reason for the decrease in collapse potential with increasing water content is that wetter soils are more compressible and would have experienced loading-induced collapse before saturation. As mentioned earlier in Sec. 4.3.1, sample B1 (*Sr* = 58%) is significantly different from B2 and B3; *Sr* of 14% and 29% respectively. Within the stress range of 5 - 100kPa, the collapse potential for sample B1 is higher that the collapse potential in B2 and B3. This is attributed to the aggregated nature of sample B1 as explained in Sec. 4.3.1. Thus, sample B1 will not be compared with B2 and B3 in terms of collapse potential.

The maximum CP is also dependent on initial water content; increasing with decreasing initial water content as could be observed in Fig. 4.11. The maximum CP in *Sr* of 14% (*w* = 8%) is 19.6% while the maximum CP in *Sr* 29% (*w* = 16%) is 14.7%. The initial water content does not have any effect on the critical stress. The critical stress is the same (200kPa) for *Sr* 14% and 29%, as shown in Fig. 4.11.

The decrease in collapse potential beyond the critical stress is caused by densification and increase in degrees of saturation associated with increasing vertical net stress (Lawton et al., 1992). Medero et al. (2003) attributed this decrease in collapse potential beyond the critical stress to breakdown of the meta-stable structure associated with collapsible soil.

Fig. 4.12 shows collapse potential of group A samples, e_0 = 0.99 at *Sr* of 58, 27 and 14%. The figure shows two regions with different volumetric strain behaviour (negative and positive collapse potential). The soil behaviour in the negative region is expansion, showing that the void ratios, from compression curves obtained from saturated tests, were larger than void ratios at constant water content at corresponding vertical net stress. In the positive region, the soil behaviour is collapse; saturated samples had smaller void ratios than corresponding samples tested at constant water content. The transition from swelling to collapse occurred at an applied stress of 50kPa for *Sr* of 14 and 27%, indicating that the samples are susceptible to expansion between 5 - 50kPa and susceptible to collapse above 50kPa. For *Sr* of 58%, the transition occurred at approximately 35kPa,

showing that the range of vertical net stress at which the sample is susceptible to swelling is 5 - 35kPa and will collapse above 35kPa.

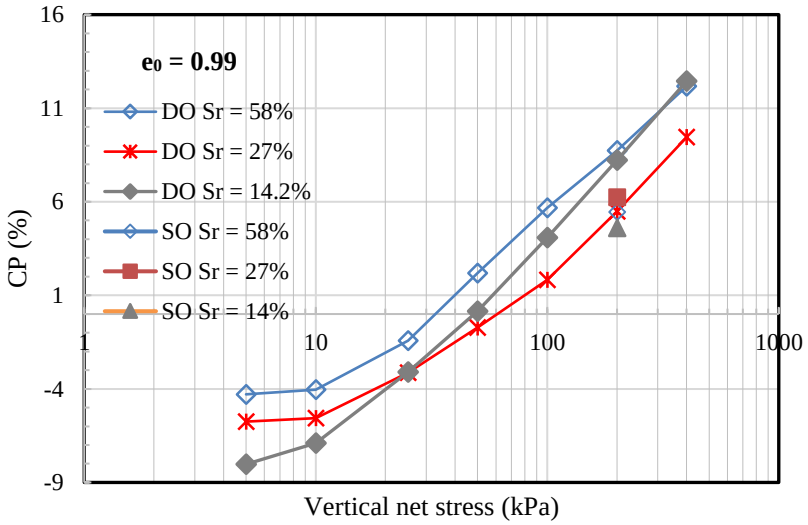

Figure 4-12 Swell and collapse potential for samples at e_0 = 0.99

From Fig. 4.12, the influence of the initial degree of saturation is not apparent in the collapse region. It was expected that the swell and collapse potential will increase with decreasing degrees of saturation. From Table 4.6, in the expansion region, the observed expansion increased with decreases in degrees of saturation or water content; *Sr* of 14% exhibited the highest magnitude of expansion CP = -8.0%, followed by Sr of 27% (-5.8%). In the collapse region, however, although *Sr* of 14% exhibited the highest magnitude of collapse (CP = 12.45%), the obtained value is close to CP for test at *Sr* of 58% (≈12.2%). Several authors e.g. Lawton et al. (1989) and Abbeche et al. (2007) have demonstrated that the swelling and collapse potential increases with decreasing initial water content. An explanation cannot be given for the similar CP values obtained in *Sr* of 14% and 58%. As observed in group B, collapse potential increases with increasing vertical net stress up to a maximum value (maximum CP), and decreases beyond this value as vertical stress is increased. For the range of vertical net stress under consideration, the peak collapse potentials were not established in group A as shown in Fig. 4.12. The maximum collapse potential was taken as that corresponding with the maximum applied vertical stress. However, it is possible that a clear peak would be established with additional loading steps.

Table 4-6 Maximum swell and collapse with corresponding critical applied stress

Sample	Maximum collapse (%)	Maximum swell (%)	Critical applied stress (kPa)
A1	12.17*	-4.3	400
A2	9.45*	-5.8	400
A3	12.45*	-8.0	400
B1	18.80	-	100
B2	14.70	-	200
B3	19.60	-	200

*: Collapse at maximum applied vertical stress

4.3.4 Effect of initial matric suction on yield stress and representation of result on loading collapse (LC) yield curve

In section 4.3.1, the yield stresses in tests $B1_{(DO\text{-}cwc)}$, $B2_{(DO\text{-}cwc)}$ and $B3_{(DO\text{-}cwc)}$ were found to increase as the initial degree of saturation decreases. However, it was not clear if this was due to an increase in matric suction resulting from decreasing compaction of water content (for the different degree of saturation) or an increase in compaction pressure associated with compacting samples at different water content to the same void ratio. To clearly show the effect of increasing initial matric suction on yield stress, four sets of constant water content oedometer tests ($B2_{(cwc\text{-}66)}$, $B2_{(cwc\text{-}148)}$, $B2_{(cwc\text{-}252)}$, $B2_{(cwc\text{-}286)}$), as shown in Table 4.2, were performed. All the samples were prepared and compacted to similar initial conditions ($e \approx 1.5$ and $w \approx 17\%$). Initial matric suction in each sample was varied before testing as explained in Sec. 4.2.

Variations in void ratios with vertical net stress for the tests are shown in Fig. 4.13. The figure shows that compressibility increases with decreasing initial matric suction. For instance, the final void ratio for sample $B2_{(cwc\text{-}66)}$ with an initial suction of 66kPa is 0.831 at maximum applied vertical net stress (400kPa) while the final void ratio for $B2_{(cwc\text{-}286)}$ with initial suction of 286kPa is 1.175 at corresponding stress value.

The yield stresses as shown in Table 4.7 decreases with decreasing initial matric suction. The behaviour is in line with expectations, and shows the stabilizing effect of an increase in matric suction. This is attributed to an increase in the number of meniscus water

associated with an increase in matric suction (Wheeler, 2010) and will be discussed in detail in Chapter 5.

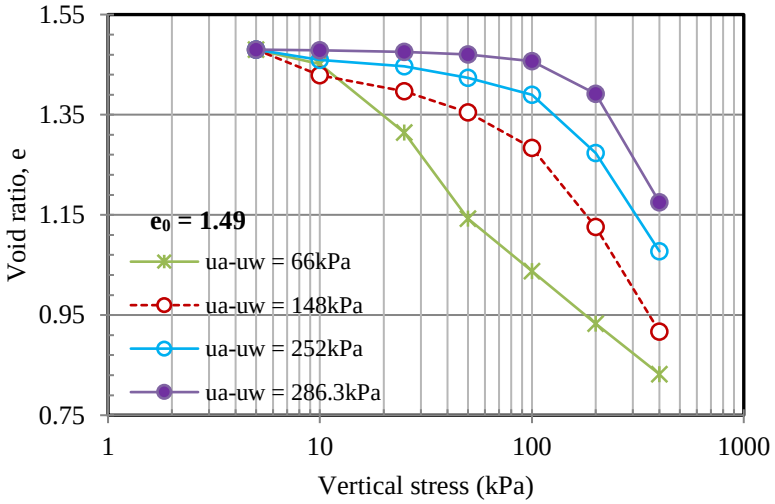

Figure 4-13 Compression curves for test B2 (cwc-66), B2 (cwc-148), B2 (cwc-252) and B2(cwc-286)) at different initial matric suctions

Table 4-7 Variation in yield stress with initial matric suction

Sample	Initial suction (kPa)	Yield stress (kPa)
B2 (cwc-66)	66	11
B2 (cwc-148)	148	92
B2 (cwc-252)	252	125
B2 (cwc-286)	286	165

The obtained results were further explained using the LC model. Alonso et al. (1987, 1990) formulated an elasto-plastic model for the stress strain behaviour of unsaturated soils. The model assumes that plastic volumetric strains commence once the yield surface has been reached, while volumetric strains prior to the yield are elastic strains. Typical behaviour classified as elastic strains include the following: strains on loading prior to yielding, strains due to swelling on wetting involving a decrease in suction, and strains resulting from unloading from a previous stress level. The stress paths for elastic volumetric behaviours are located inside the yield surface. At any point, the path taken

by any soil must be inside a yield curve. If the path goes beyond the primary yield curve, there would be expansion to a secondary yield surface. All paths inside the primary yield surface are marked by elastic strain, while the paths outside the primary yield surface are marked by plastic irreversible strain. A loading collapse (LC) yield curve similar to the yield surface was developed for isotropic stress state. In the LC model, yield stress increases with suction from saturated state (zero suction), as shown in Fig. 4.14. Subsequent increases in stress, or decreases in suction, once a stress path reaches the LC yield curve, will result in expansion of the yield curve and this is associated with large plastic volumetric strain known as plastic compression (Sivakumar & Wheeler, 2000). Volumetric strains that occur on wetting at high values of vertical net stress (collapse) are modelled in the same process as plastic compression.

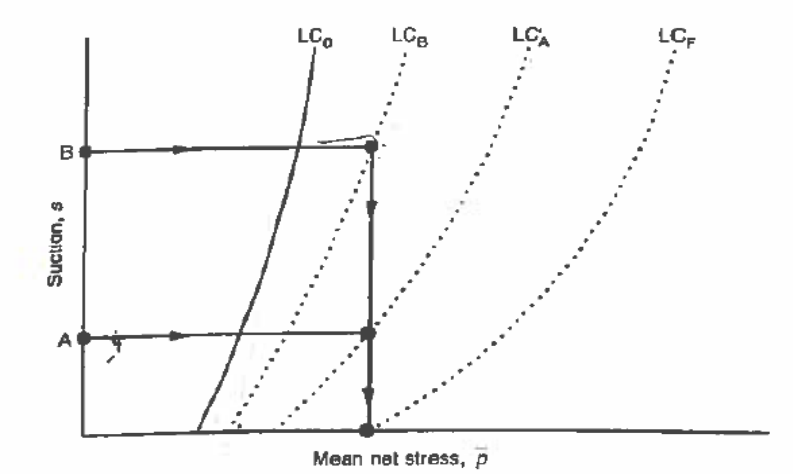

Figure 4-14 LC yield curve showing influence of suction (Sivakumar & Wheeler, 2000)

The stress paths for B2 (cwc-66), B2 (cwc-148), B2 (cwc-252), B2 (cwc-286) are explained in the light of the LC curve. The yield stress for each test was estimated from the compression curves in Fig. 4.13, using the Butterfield method. The estimated values of yield stresses at different initial matric suction values were used to plot the primary LC curve AB in Fig. 4.15. The secondary yield curves are shown as CD and EF. Only the stress paths for tests B2 (cwc-148) and B2 (cwc-252) are shown on the model. For the stress paths shown on the model, all the samples experienced both elastic and plastic volumetric compression, with the elastic portion of the compression inside the primary yield curve (paths 1-2 and 4-5) for B2(cwc-252) and B2(cwc-148) respectively (see Fig. 4.15). The plastic portions of the

volumetric compression are located outside the primary yield curve; path 2-3 for B2 $_{(cwc-252)}$ and path 5-6-7 for B2 $_{(cwc-148)}$. Plastic compression commenced once the path reached the primary yield curve, resulting in expansion of the yield curve to curves CD and EF for paths 1-3 and 4-7 respectively. Test B2$_{(cwc-148)}$ conducted at a matric suction of 148kPa yielded at a stress of 92kPa, while test B2$_{(cwc-252),}$ at a matric suction of 252kPa, yielded at 125kPa. This result agrees with previously discussed findings: yield stress increases with increasing suction (Alonso et al., 1987; Wheeler & Sivarkumar, 2000). It is worth noting that matric suction was not controlled during loading and was assumed to be constant.

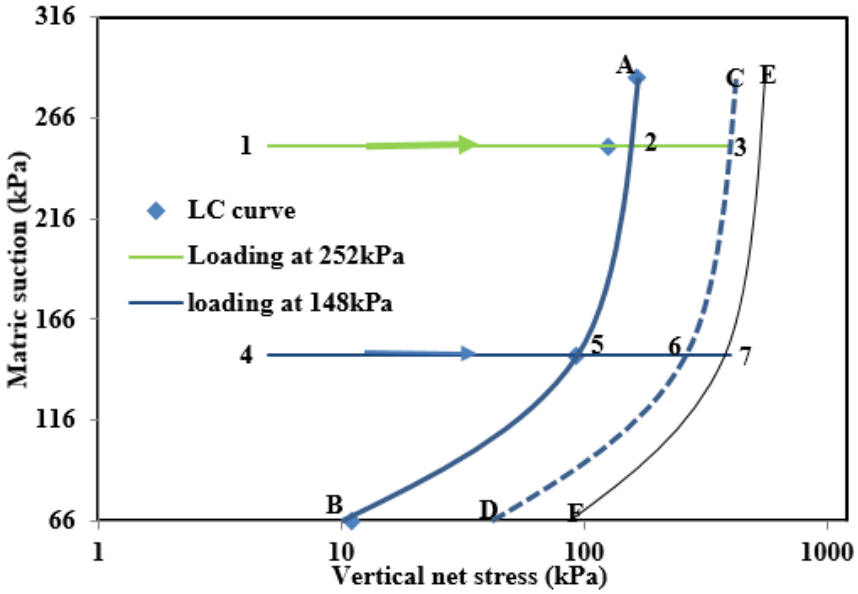

Figure 4-15 Representation of loading tests at different suction (252kPa and 148kPa) on LC curve

The collapse potentials at different matric suction levels (148kPa, 252kPa and 286kPa) were calculated from the results of tests B2$_{(Do-5)}$, B2$_{(cwc-148)}$, B2$_{(cwc-252)}$, and B2$_{(cwc-286)}$. In Fig. 4.16 the variation of collapse potential with vertical stress at the matric suction levels cited above is presented. The figure shows that collapse potential increases with increasing matric suction in agreement with the observations of Lawton et al. (1992), Rabbi et al. (2014). This indicates that at high values of matric suction, samples exhibit increased stability (less compressibility on loading) due to the influence of meniscus

water. On wetting, the stability reduces significantly. Consequently, the vertical distance between the saturated and unsaturated compression curves is high, hence increase in collapse potential.

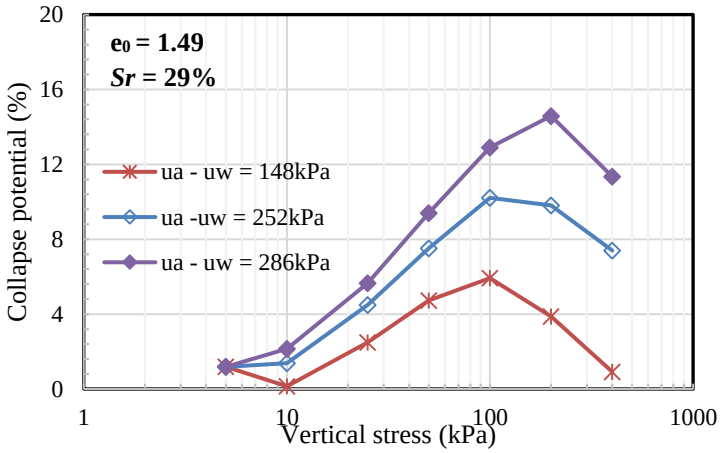

Figure 4-16 Collapse potential at different suction (148, 252 and 286kPa) for samples at e_0 = 1.49, *Sr* = 29%

4.4 CONCLUSION

The hydro-mechanical behaviour of compacted kaolin clay at e_0 = 1.5 (group A) and 1.0 (group B) has been studied through single and double oedometer tests to understand the volume change behaviour upon wetting and loading. The influence of degree of saturation on the volumetric behaviour was investigated by testing samples prepared at *Sr* = 60, 30, 15%. Additionally, it was sought to understand if change in initial water content will result in change of initial state or completely different sample. Furthermore, the influence of initial matric suction on yield stress was also investigated.

Some of the observed behaviours were in line with behaviours reported in literature. Upon loading, both group A and B samples experienced compression. The magnitude of compression increased with initial degree of saturation. The compressibility parameters were also influenced by initial degree of saturation. The slope of the normal compression line λ increased with increasing *Sr* while the yield stress decreased with increasing *Sr*. On wetting, group A and B samples exhibited different volumetric behaviour; expansion and collapse respectively. The direction of volumetric behaviour on wetting was influenced by the void ratio. Expansion on wetting was observed in samples at e_0 = 1.0 (dry density = 1.34mg/m^3) while collapse was observed in samples at e_0 = 1.5 (dry density

= 1.11mg/m^3). The uniqueness of the compression line was investigated. It was observed that samples compacted at the same water content (≈17%), but different void ratios (1.0 and 1.5) converged to a unique compression line on loading in a saturated state. This indicates that compaction to different void ratio but similar water content is only a change of initial state. Increase in matric suction was observed to delay the onset of yield and expand the elastic region of a compression curve.

CHAPTER FIVE

5 THERMO-MECHNICAL BEHAVIOUR OF KAOLIN CLAY

INTRODUCTION

In this chapter, experimental test results obtained from temperature and suction controlled oedometer tests are presented and discussed. Using the obtained data, the influence of temperature and suction on the compressibility parameters; λ and P^0 and coefficient of volume compressibility were evaluated. Also presented are experimental test results obtained from thermal loading and wetting paths under constant temperature and vertical net stress. The influence of temperature on the main features of the stress-strain behaviour in these tests are discussed.

5.1 STUDIED SAMPLES AND TEST CONDITIONS

An initial study was carried out to study the effect of temperature on the volumetric behaviour of statically compacted kaolin clay without suction imposition. This was done by characterizing the volume change at 50^{o}C, following loading upon wetting and loading at constant water content, using a standard oedometer. The results were then compared with corresponding results at room temperature as presented previously in Chapter 4. The study was then extended using a suction controlled oedometer to investigate in detail the influence of temperature on volume change and compressibility properties of statically compacted kaolin clay, at a water content dry of optimum. Most of the studies found in the literature have focused on slurred samples of kaolin clay, but this study focused on statically compacted kaolin clay at the dry side of optimum. The tests were performed at 25^{o}C and 50^{o}C following loading, thermal loading and drying paths, as will be explained later in this section. Most of the samples for these further investigations were limited to an initial water content of ≈17% and initial void ratio of ≈1.5. An exception was the thermal loading path, where samples with an initial water content of 32% were also tested. The initial plan was to test only samples with w = 17% in the thermal loading tests, but the results obtained indicated negligible volume change. Samples with w = 32% were then tested to examine if an increase in water content will be accompanied by a substantial volume change following a thermal cycle.

Three test series were performed with the suction controlled oedometer apparatus. The initial conditions of the samples, and each of the test's details, are summarised in Table 5.2. Details of each test are outlined in Chapter 3. Volume changes, in terms of vertical deformation, were monitored in all the tests. Test series 1: $L1_{(25)}$, $L1_{(50)}$, $L2_{(25)}$ and $L2_{(50)}$ involved a loading path at constant suction of 30kPa and 210kPa and constant temperature of 25ºC and 50ºC. The stress paths followed in the loading tests are schematically shown in Chapter 3 (Fig. 3.10). Test series 2: $NI1_{(30)}$, $NI1_{(100)}$, $NI2_{(30)}$ and $NI2_{(100)}$ involves thermal paths (heating and cooling paths) at constant vertical net stress (55kPa) and constant suction (30kPa and 100kPa). The stress paths followed in Test set 2 are shown in Fig. 3.9. The term *'heating and cooling path'* is used interchangeably with *'non-isothermal path'*. Test series 3: $D1_{(25)}$ and $D1_{(50)}$ involves drying paths at constant vertical net stress (55kPa) and constant temperatures (25ºC and 50ºC), following an initial decrease in suction to 30kPa. The stress paths followed in Tests $D1_{(25)}$ and $D1_{(50)}$ are shown schematically in Fig. 3.12 in Chapter 3.

The two groups of samples (A and B), explained in Chapter 4, were also tested under temperature control, using standard oedometer tests following the steps detailed in Chapter 3. Initial states of the samples prior to testing are shown in Table 5.1. The numeric value in subscript is the set temperature. The term '*heated samples'* is used for samples tested at 50ºC.

Table 5-1 Initial state of tested samples and test descriptions for temperature controlled standard oedometer tests

Tests	Initial states				Compaction pressure (kPa)	Temperature (ºC)	Test description	No. of tests
	Water content (%)	Void ratio e_0	Degree of saturation S_r (%)	Matric suction (kPa)				
$A2_{cwc(50)}$	11.0	1.00	29.2	628	939	50	CWC	1
$A2_{cwc(19)}$	10.1	0.98	27.3			19	CWC	1
$A2_{DO\text{-}5(50)}$	11.3	1.00	30.0			50	Wetted at 5kPa	2
$A2_{DO\text{-}5(19)}$	10.1	0.98	27.2			19	Wetted at 5kPa	1
$B1_{SO(50)}$	32.2	1.47	58.0	109	57	50	Wetted at 200kPa	1
$B1_{SO(19)}$	32.2	1.47	58.0			19	Wetted at 200kPa	1
$B1_{cwc(50)}$	32.3	1.47	58.2			50	CWC	1
$B1_{cwc(19)}$	32.7	1.48	58.6			19	CWC	1
$B1_{DO\text{-}5(50)}$	32.1	1.47	57.9			50	Wetted at 5kPa	1
$B1_{DO\text{-}5(19)}$	32.8	1.48	58.8			19	Wetted at 5kPa	1
$B2_{SO(50)}$	16.2	1.48	29.0	286	180	50	Wetted at 200kPa	1
$B2_{SO(25)}$	16.6	1.49	29.5			25	Wetted at 200kPa	1
$B2_{cwc(50)}$	16.1	1.48	28.8			50	CWC	2
$B2_{cwc(25)}$	15.7	1.48	28.1			25	CWC	1
$B2_{DO\text{-}5(50)}$	16.1	1.48	28.8			50	Wetted at 5kPa	1
$B2_{DO\text{-}5(25)}$	15.9	1.48	28.5			25	Wetted at 5kPa	1

Table 5-2 Initial state of tested samples and test descriptions for suction and temperature controlled oedometer tests

Tests	Initial states			Matric suction (kPa)	Vertical net stress (kPa)	Temperature (ºC)	Test description	No. of tests	No. of days
	Water content (%)	Void ratio e_0	Degree of saturation S_r (%)						
$L1_{(25)}$	16.9	1.49	30.0	30	-	25	Loading at constant temperature and suction	2	
$L1_{(50)}$	17.0	1.50	30.0		-	50		1	
$L2_{(25)}$	16.7	1.48	29.9	210	-	25		1	
$L2_{(50)}$	16.7	1.48	29.9		-	50		1	
$NI1_{(30)}$	16.7	1.49	29.6	30	55	-	Heating and cooling at constant suction and vertical net stress	2	
$NI1_{(100)}$	16.1	1.48	28.8	100		-		1	
$NI2_{(30)}$	32.5	1.47	58.6	30		-		1	
$NI2_{(100)}$	32.5	1.47	58.6	100		-		1	
$D1_{(25)}$	16.8	1.49	29.9	-	55	25	Increasing suction at constant temperature and vertical net stress	1	
$D1_{(50)}$	17.0	1.50	30.0	-		50		1	

Table 5-3 Error analysis for temperature controlled standard oedometer tests

Tests	No. of Obs.	Vertical net stress kN/m^2	Final void ratio				Std. error
			Mean	Std. dev.	Coeff. of variation	Variance	
$A2_{DO\text{-}5(50)}$	2	400	0.7449	0.0013	0.1709	0.0000	0.0009
$B1_{SO(19)}$ & $B1_{CWC(19)}$		200	1.2461	0.0120	0.9590	0.0001	0.0084
$B1_{SO(50)}$ & $B1_{CWC(50)}$		200	1.1623	0.0310	2.6647	0.0010	0.0219
$B2_{SO(25)}$ & $B2_{CWC(25)}$		200	1.4049	0.0156	1.1124	0.0002	0.0111
$B2_{CWC(50)}$		400	1.2509	0.0373	2.9847	0.0014	0.0264

EXPERIMENTAL TESTS RESULTS AND ANALYSIS

5.2 TEMPERATURE CONTROLLED STANDARD OEDOMETER TESTS

Table 5.3 shows the error estimation for the temperature controlled oedometer test results. The estimation was based on repeated measurement for test $A2_{DO\text{-}5(50)}$. The error in the final void ratio which corresponds to 400kPa was estimated, as this was considered the critical value. For the other tests shown in Table 5.3, errors were calculated at 200kPa because the analyses were based on result of single oedometer and constant water content double oedometer tests obtained under the same condition. From Table 5.3, the maximum error is ±0.0223, with a percentage uncertainty of 1.7%. This was obtained from B2 tests at 50^{o}C, the void ratio at 200kPa for $B2_{cwc50}$ is 1.3262±0.0223.

5.2.1 Compressibility behaviour at different temperatures

Fig. 5.1 shows the variation of void ratios with vertical stress of Tests $A2_{cwc(50)}$, $A2_{cwc(19)}$, $A2_{DO\text{-}5(50)}$, $A2_{DO\text{-}5(19)}$ (e_0 = 0.99, Sr = 28.4%). The figure shows results obtained at constant water content and on wetting at 5kPa. To enable comparison of results, the average initial void ratio from all the tested samples was used to adjust the individual test results, as explained in Sec. 4.3.1. By comparing the test results at 50^{o}C and the test results at 19^{o}C as previously presented in Chapter 4, the influence of temperature on volume change behaviour of the sample was investigated.

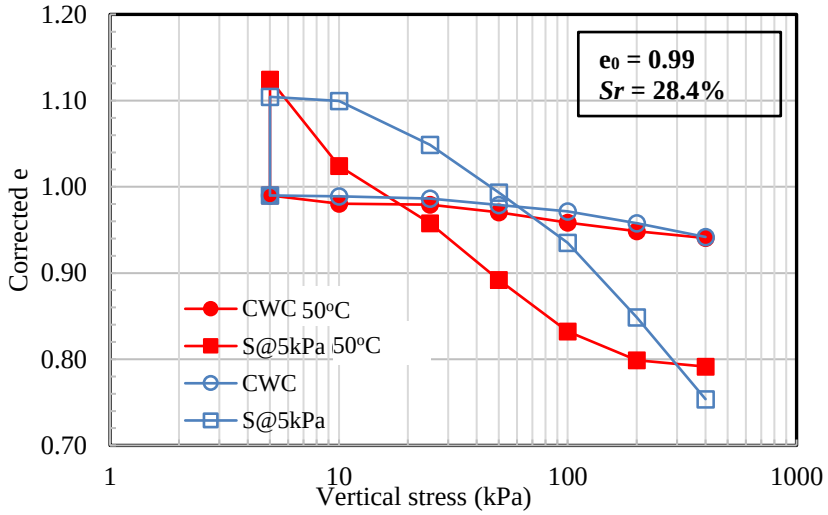

Figure 5-1 Double oedometer test results for sample A2 (e_0 = 0.99, Sr = 28%) at 50°C and room temperature (19°C)

For samples tested at constant water content, the figure shows that the compressibility of the sample slightly increased with an increase in temperature from 19°C to 50°C. The compression curve at 50°C continuously plots below the compression curve at =19°C for vertical stresses between 10kPa to 200kPa. At 400kPa, convergence of the compression curves at 50°C and 19°C was observed. The change in void ratio, due to an increase in temperature to 50°C, is relatively small. The maximum change Δe_{max} is 0.013 at 100kPa, a change considered to be negligible and within the error margin as shown in Table 5.3. Therefore, an increase in temperature to 50°C had a negligible influence on the volume change of sample A2 following a loading path at constant water content. Like the test 19°C, the normal compression line at 50°C was not fully established at the stress level considered.

For the tests following a wetting path (Fig. 5.1), assuming that the repeatability of the results is within an acceptable limit (final void ratio is 0.7449±0.0009), the difference in both curves is attributed to the difference in temperature. On wetting, an increase in temperature resulted in a slight increase in the magnitude of measured expansion, consistent with the findings of Romero (1999) and Romero et al. (2005) on heated Boom clay (80°C) subjected to wetting at constant vertical net stress (0.025, 0.085, 0.30 and 0.55MPa). The value of void ratio on wetting at 5kPa is 1.10 at 19°C, but the value increased slightly to 1.14 at 50°C. This value is also considered negligible. Following initial expansion on wetting, subsequent increases in vertical net stress (from 5kPa to 400kPa) was accompanied by compression. The change from expansion to compression

is gradual in samples tested at 19°C, but sharp in samples at 50°C and an explanation cannot be given for this. The effect of an increase in temperature during loading of the saturated sample was to produce an increase in the measured deformation, resulting in a shift of the compression curve at 50°C below the compression curve at 19°C, between the range of 10kPa to 200kPa vertical net stress. This indicates that an increase in temperature resulted in a denser sample; an outcome consistent with the findings of Cekerevac (2003), Francoise (2008) and Haghighi (2011) on saturated kaolin and silty clay. Pons et al. (1994 in Cekerevac, 2003), Leroueil & Marques (1996) reported that the mechanism responsible for thermal densification of clay soils is thermally induced decomposition and rearrangement of clay structures. Heating breaks down the bond between particles, thereby enhancing denser packing of clay soils on loading.

In Figs. 5.2a & 5.2b, the compression curves for Tests $B1_{SO(50)}$, $B1_{SO(19)}$, $B1_{cwc(50)}$, $B1_{cwc(19)}$, $B1_{DO\text{-}5(19)}$ & $B1_{DO\text{-}5(50)}$ (e_0 = 1.47, Sr = 58.3%) and Tests $B2_{SO(50)}$, $B2_{SO(25)}$, $B2_{cwc(50)}$, $B2_{cwc(25)}$, $B2_{DO\text{-}5(25)}$ & $B2_{DO\text{-}5(50)}$ (e_0 = 1.48, Sr = 28.8%) following double and single oedometer tests are presented. The results at room temperature (19°C), 25°C and 50°C are compared in both figures. Inspection of the tests at constant water content; curves A, A' and B, B' in Figs. 5.2a & 5.2b respectively show a shift of the compression curves to the left at 50°C. This indicates increased compressibility, due to an increase in temperature within the stress range of 10kPa to 200kPa.

At 400kPa, the compressibility observed in heated samples was smaller than observed in non-heated samples. For instance, in Test $B1_{cwc(50)}$, the void ratio at 400kPa (50°C) was 1.25, whereas the void ratio for Test $B1_{cwc(19)}$ at room temperature at the same stress level was 1.18. This was not expected; it was expected that the void ratios at 50°C would consistently be less than the void ratios at 19°C. Inspection of the final water content values showed that the samples used in tests B1 and B2 at room temperature and 25°C respectively maintained their initial water content during testing, yielding final water contents of 30.7% and 15.1% respectively. The samples were sealed with plastic membranes to prevent evaporation of water during testing. However, water content decreased significantly in samples tested at 50°C, with final water contents 24.6% and 11.2% for $B1_{cwc(50)}$ and $B2_{cwc(50)}$ respectively; even though the samples were also sealed during testing. The decrease in the water contents of the heated samples seems to have increased the stiffness of the samples against an external load, resulting in reduced compressibility at 400kPa.

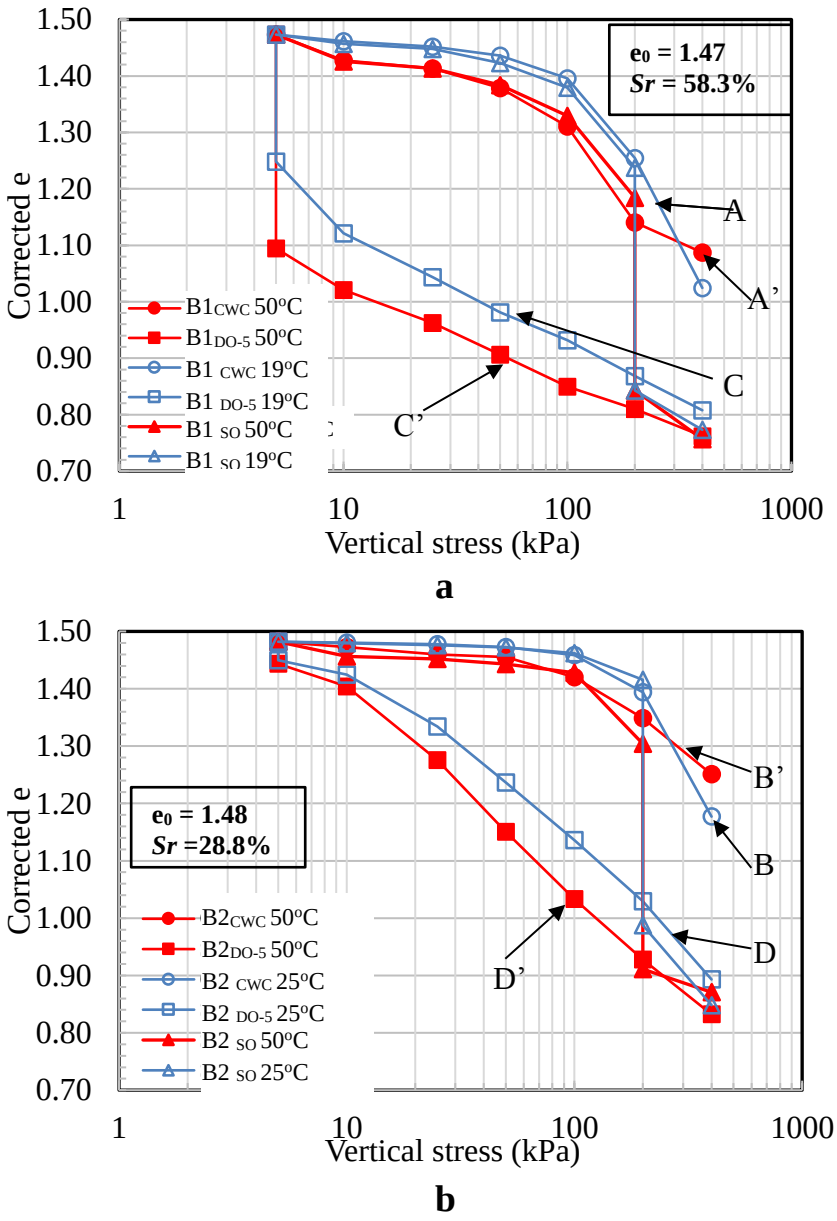

Figure 5-2 Double oedometer test results for group B samples at 50°C, 25°C and room temperature (19°C) (a) Sr = 58%; 50 & 19°C (b) Sr = 29%; 50 & 25°C

For wetting tests $B1_{DO\text{-}5(50)}$, $B1_{DO\text{-}5(19)}$, $B2_{DO\text{-}5(50)}$ and $B2_{DO\text{-}5(19)}$ at 5kPa, collapses of the samples were observed following initial wetting at 19°C and 50°C (see curves C, C' and D, D' in Fig. 5.2a & 5.2b respectively) contrary to expansion observed in samples A2 presented previously. Inspection of curves C, C' and D, D' indicates that the compressibility of the samples varied with temperature, with the compression curves at 50°C lying below the compression curves recorded at 25°C (D) and 19°C (C). This also shows that compressibility of samples B1 and B2 increased with an increase in temperature, following a wetting path as observed in sample A2. From the result, it could be said that increase in temperature enhanced densification of the samples.

5.2.2 Yielding behaviour at different temperatures

To clearly show the effect of temperature on yield stress, the compression curves obtained at constant water contents are replotted, as shown in Fig. 5.3 and Fig. 5.4. The value of yield stress was estimated, using Butterfield method, which is the intersection of tangent lines drawn on the virgin compression and recompression lines plotted in log e+1 – log σ_v. The compression curves at the same degree of saturation are plotted together.

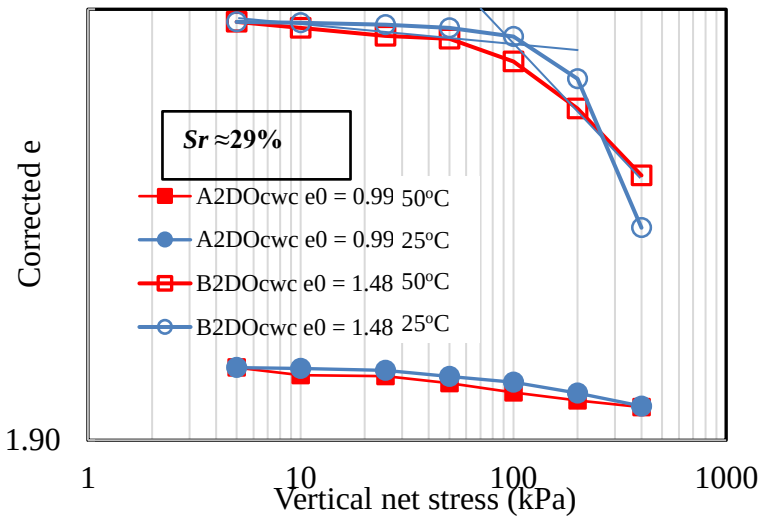

Figure 5-3 Identification of yield stresses at different temperatures for samples at *Sr* = 29%, e_0 = 0.99 and 1.48

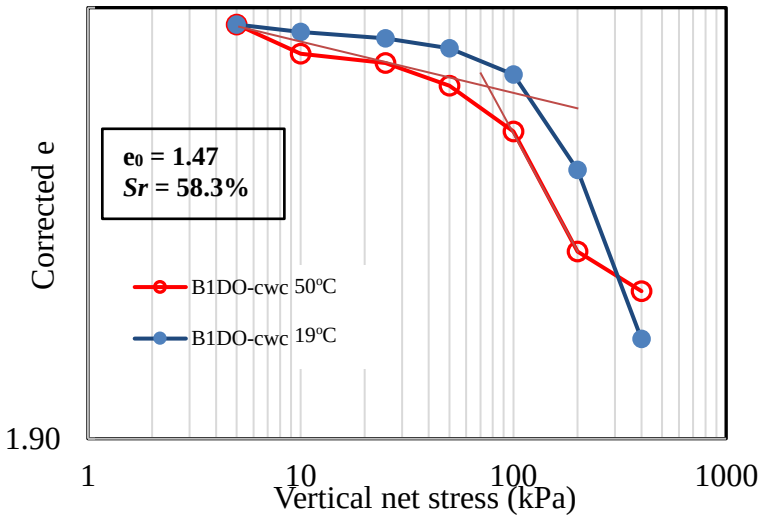

Figure 5-4 Identification of yield stresses at different temperatures for samples at *Sr* = 58%, e_0 = 1.47

Fig. 5.3 shows that the yield stress increases with a decrease in initial void ratio for the same *Sr*, as stated in Sec. 4.3.2. It should be noted that compaction to a different void ratio at the same *Sr* is possible, due to compaction at different water contents, as explained in Chapter 4. The estimated values of yield stress at each temperature for the different void ratios are plotted in Fig. 5.5. The figure shows that the yield stresses of B1 and B2 decreased with an increase in temperature, from 130 to 80kPa for B1 and 165 to 100kPa for B2; data consistent with the findings of Haghighi (2011) and Folly (2004) on kaolin clay. The yield stress of A2 was unaffected by temperature.

The normal compression lines were not established in Tests $A2_{cwc(50)}$, $A2_{cwc(19)}$ for the range of vertical net stress considered during testing as explained in Chapter 4. Comparison of the normal compression lines at 50°C and room temperature for B1 and 50°C and 25°C for B2, shows that the lines are not parallel. In fact a change in the slope of the normal compression line was observed in $B2_{cwc(50)}$ at 50°C between 200kPa and 400kPa, resulting in smaller measured void ratio of the heated sample when compared to the non-heated sample. Perhaps this outcome may be attributed to loss of water in sample B2 during testing, as explained earlier, and a wrong assumption of constant water content, resulting in the stiffness of the sample. The slope of the normal compression lines decreased with an increase in temperature; from 0.33 – 0.25 in B1 and from 0.31 – 0.14 in B2 as shown in Table 5.4. This does not agree with the findings in the literature. The compressibility parameters are either insensitive to temperature (Romero et al., 2005; Tang et al., 2008; Haghighi, 2011) or, in some cases, increase with temperature increase (Romero et al., 2003).

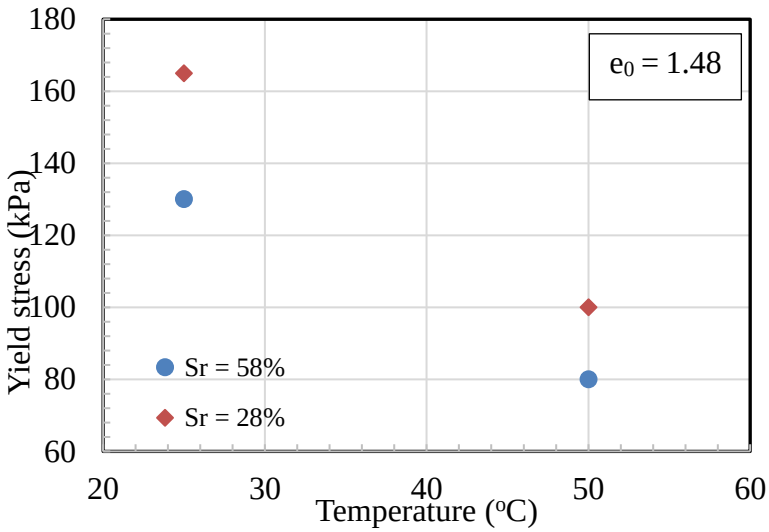

Figure 5-5 Variation of yield stress with temperature for B1 and B2; $e_0 \approx 1.5$

Table 5-4 Yield parameters at 50ºC, 25ºC and room temperature (19ºC)

Test	Initial Sr (%)	Temperature (ºC)	Yield stress (kPa)	Slope of NCL (λ)
A2	29.2 27.3	50 19	180 180	
B1	58.2 58.6	50 19	80 130	0.25 0.33
B2	28.8 28.1	50 25	100 165	0.14 0.31

5.2.3 Collapse potential of double oedometer tests at 50ºC, 25ºC and room temperature

In Fig. 5.6, the collapse potentials of sample A2 (e_0 = 0.99) at 50ºC and room temperature are compared. From the figure, it could be observed that the effect of an increase in temperature is a shift of the CP curve to the left, within vertical stress of 5kPa to 200kPa. This indicates an increase in collapse potential with an increase in temperature. For instance, at 5kPa, an increase in temperature to 50ºC shifted the negative collapse potential to a higher value of -5.1% from a value of -5.7%, observed at room temperature at the same applied stress. Another effect of temperature, observed from the figure, is that the vertical stress at which the transition from swelling to collapse occurred was reduced from 60kPa to 25kPa. This indicates that an increase in temperature reduces the stress range at which the sample is susceptible to expansion (5kPa – 25kPa) and increases the stress range at which the sample is susceptible to collapse (25kPa – 200kpa). The influence of an increase in temperature on the maximum collapse potential is a decrease in the maximum collapse potential to 7.5% (50ºC) from 11.5% (19ºC). The figure also shows a shift in the critical stress to the left, with an increase in temperature (from 400kPa to 200kPa). The peak CP is clearly established at 50ºC, but not established at 19ºC. Perhaps this might be because of increased consolidation associated with an increase in temperature (Cekerevac, 2003).

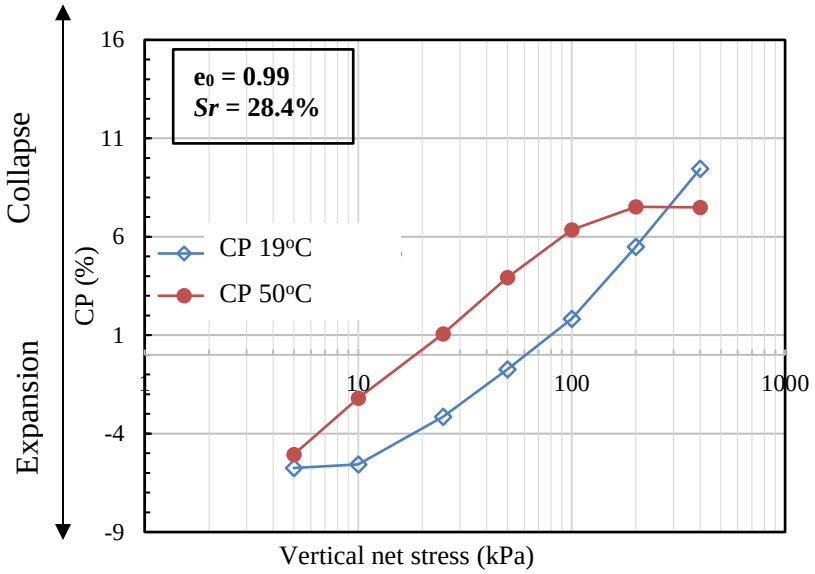

Figure 5-6 Variation of collapse potential with vertical net stress at 50°C and room temperature (19°C) e_0 = 0.99, *Sr* = 28.4%

To investigate the influence of temperature on the collapse potential of sample B1 (e_0 = 1.47, Sr = 58.3%) and B2 (e_0 = 1.48, Sr = 28.8%), the collapse potentials at 50°C, 25°C and room temperature were plotted together as shown in Fig. 5.7a & 5.7b. Fig. 5.7a shows that collapse potential increased at 50°C, relative to the collapse potential at room temperature, between applied vertical stress of 5kPa and 100kPa, and then decreased subsequently up to applied stress of 200kPa.

Between 200kPa and 400kPa, the collapse potential at 50°C unexpectedly became constant. This could be linked to the fact that compressibility of the sample between 200 to 400kPa vertical stress became constant, as explained in Sec. 5.2.1, due to loss of water from the sample and the erroneous assumption of constant water content in the sample. Contrary to sample A2, the maximum collapse potential increased from 18.7% (19°C) to 19.1% (50°C). The critical stress at which maximum collapse occurred also shifted to the left, from 100kPa (19°C) to 50kPa (50°C), as observed in A2.

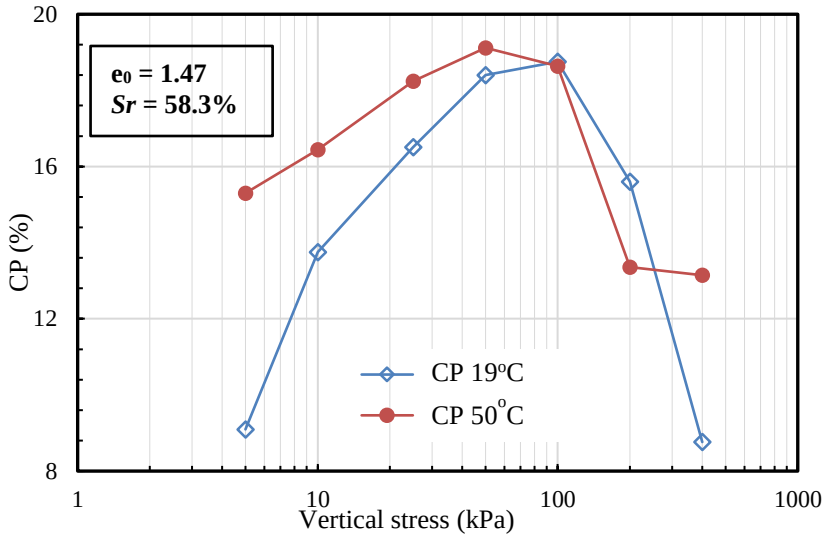

a

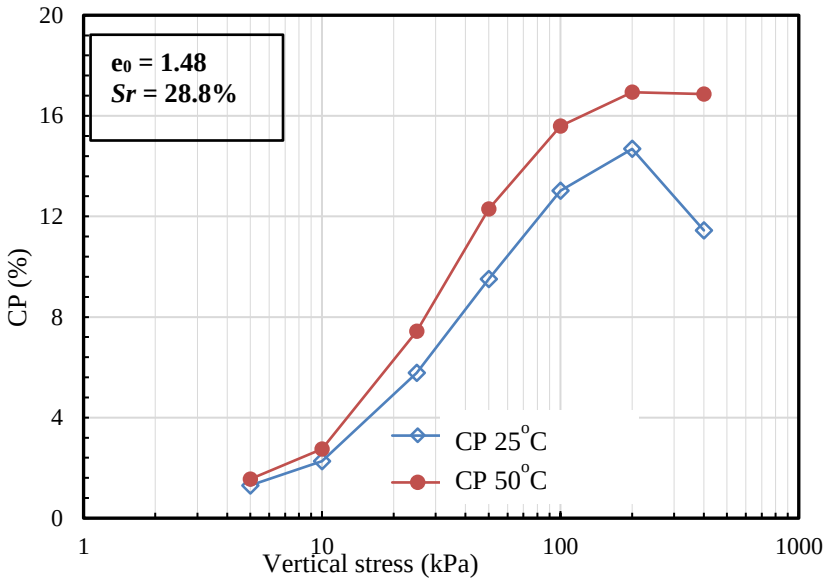

b

Figure 5-7 Variation of collapse potential with vertical stress for B1 and B2 at different temperatures (a) B1; *Sr* = 58.3% (b) B2; *Sr* = 28.8%

In Fig. 5.7 b, the collapse potentials of sample B2 at 50°C and 25°C are presented. The curve at 50°C, continuously plotted above and to the left of the curve at 25°C for all values of applied stress, indicating increased compressibility because of an increase in temperature for both loading test at constant water content and on wetting at 5kPa. This does not agree with the findings of Haghighi (2011) on kaolin clay and Kholgihfard et al. (2014) on residual granite. In both studies, the collapse potential decreased with an increase in temperature. Inspection of test results presented in Kholgihfard et al. (2014) indicated that compressibility increased with temperature on loading at constant water

content, but decreased with temperature on loading following wetting, a finding contrary to this study. Thus, the collapse potential decreased with an increase in temperature in their study. In this study, however, compressibility increased with temperature for both loading at constant water content and loading on wetting paths. The critical stresses at the two temperatures are the same (200kPa), while the maximum collapse potential increased from 14.7% to 16.9% because of an increase in temperature to 50^{o}C (see Fig. 5.7b).

From the results obtained from A2, B1 and B2, it can be concluded that an increase in temperature increased the collapse potential. In addition, an increase in temperature results in an increase in the maximum collapse potential of a collapsible sample. Although reduction in expansion region was observed with an increase in temperature, the effect on expansive samples cannot be concluded when based on the result obtained from A2 alone.

5.3 TEMPERATURE AND SUCTION CONTROLLED OEDOMETER TESTS

5.3.1 Loading at constant temperatures (25^{o}C and 50^{o}C) and constant matric suction (30kPa and 210kPa)

i) Compressibility behaviour

In Tests $L1_{(25)}$, $L1_{(50)}$, $L2_{(25)}$ and $L2_{(50)}$, statically compacted kaolin clay samples ($e_0 \approx$ 1.495, Sr = 30%) were subjected to one-dimensional loading at a constant suction of 30kPa and 210kPa. For Tests $L1_{(25)}$ and $L1_{(50)}$, the samples were tested at a constant matric suction of 30kPa (path 1 Fig. 3.13a), while in Tests $L2_{(25)}$ and $L2_{(50)}$ the samples were tested at a constant matric suction of 210kPa (path 1 in Fig.3.13b). In Tests $L1_{(25)}$ and $L2_{(25)}$ the samples were loaded at a constant temperature of 25^{o}C (path 2 Fig. 3.13a), while in Tests $L1_{(50)}$ and $L2_{(50)}$, the samples were loaded at 50^{o}C (path 2 in Fig. 3.13b). The test results are presented in Fig. 5.8 and Fig. 5.9 for matric suction 30kPa and 210kPa respectively in terms of void ratio and vertical net stress. Tests L1 and L2 had an average initial void ratio of 1.495±0.003 and 1.480 respectively. For repeatability, data points between 0 - 55kPa vertical net stress were repeated twice. The repeated measurements were limited to 55kPa due to time constrain. Table 5.5 shows the error associated with the measured points. From the Table, the maximum percentage uncertainties are 2.9, 2.0, 1.2 and 1.1% in $L1_{(50)}$, $L1_{(25)}$, $L2_{(50)}$ and $L2_{(25)}$ respectively.

Table 5-5 Measurement errors in Tests $L1_{(25)}$ and $L1_{(50)}$; $u_a - u_w$ = 30kPa

Tests	No. of Obs.	Vertical stress	void ratio				Std. error
		(kN/m^2)	Mean	Std. dev.	Coeff. of variation	Variance	
$L1_{(50)}$	2	0	1.4781	0.0069	0.4688	0.0000	0.0049
$L1_{(50)}$	2	4.2	1.4434	0.0594	4.1151	0.0035	0.0420
$L1_{(50)}$	2	20	1.3640	0.0170	1.2442	0.0003	0.0120
$L1_{(25)}$	2	0	1.4830	0.0064	0.4291	0.0000	0.0045
$L1_{(25)}$	2	4.2	1.4508	0.0011	0.0780	0.0000	0.0008
$L1_{(25)}$	2	20	1.3796	0.0074	0.5330	0.0001	0.0052
$L1_{(25)}$	2	55	1.2910	0.0361	2.7934	0.0013	0.0255

Table 5-6 Measurement errors in Tests $L2_{(25)}$ and $L2_{(50)}$; u_a - u_w = 210kPa

Tests	No. of Obs.	Vertical stress	Final void ratio				Std. error
		(kN/m^2)	Mean	Std. dev.	Coeff. of variation	Variance	
$L2_{(50)}$	2	4.2	1.4779	0.0246	1.6650	0.0006	0.0174
$L2_{(50)}$	2	20	1.4415	0.0163	1.1282	0.0003	0.0115
$L2_{(50)}$	2	55	1.4054	0.0075	0.5333	0.0001	0.0053
$L2_{(25)}$	2	4.2	1.4701	0.0238	1.6161	0.0006	0.0168
$L2_{(25)}$	2	20	1.4498	0.0139	0.9559	0.0002	0.0098
$L2_{(25)}$	2	55	1.4092	0.0129	0.9132	0.0002	0.0091

The initial path followed in Tests L1 and L2 were reductions in matric suction from 286kPa to 30kPa and 210kPa respectively (path 1 in Fig. 3.10), to achieve the constant matric suction at which loading was carried out. A decrease in matric suction to 30kPa resulted in a slight reduction in void ratio due to collapse (1.483 and 1.478 in Tests $L1_{(25)}$ and $L1_{(50)}$ respectively). For Test $L2_{(25)}$ and $L2_{(50)}$, a decrease in matric suction to 210kPa (paths 1 Fig.3.10b) resulted in negligible reduction in void ratio. In Haghighi (2011), marked reductions in void ratios were also observed on reconstituted kaolin clay prepared at wet side of optimum (e_0 = 1.5, w = 51%), following suction imposition to 100kPa, 300kPa and 500kPa (see Fig. 5.10). The reduction in void ratio achieved in Haghighi's study increased with increasing matric suction, whereas in this study the reduction in void ratio increased with a decrease in matric suction. It is worth noting that reductions in void ratio observed by Haghighi (2011), and this study, were due to different phenomenon: shrinkage and collapse. In Haghighi's study, the reduction in void ratio on imposing

matric suction was due to shrinkage of the samples, whereas the reduction in void achieved in this study was due to collapse. The reason for the difference is that the samples used by Haghighi were reconstituted samples and is located on the wet side of optimum of a compaction curve and thus, an initial increase in matric suction was achieved along a drying path. In this study, statically compacted samples were used and initial suction imposition was achieved on a wetting path. The reductions in void ratios associated with decreases in matric suction in $L1_{(25)}$ and $L1_{(50)}$ are not shown in Fig. 5.8. They occurred at 0kPa value of vertical net stress and zero values cannot be shown on a logarithmic scale. Hence, only the loading paths (paths 2 & 4 in Fig. 3.13a & b respectively) are shown in Fig. 5.8 and Fig. 5.9.

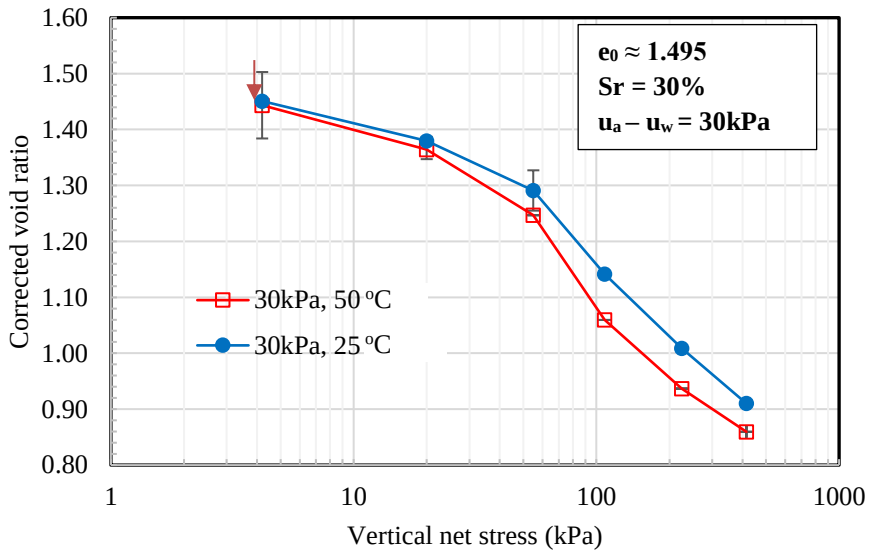

Figure 5-8 Void ratio versus vertical net stress at constant matric suction of 30kPa

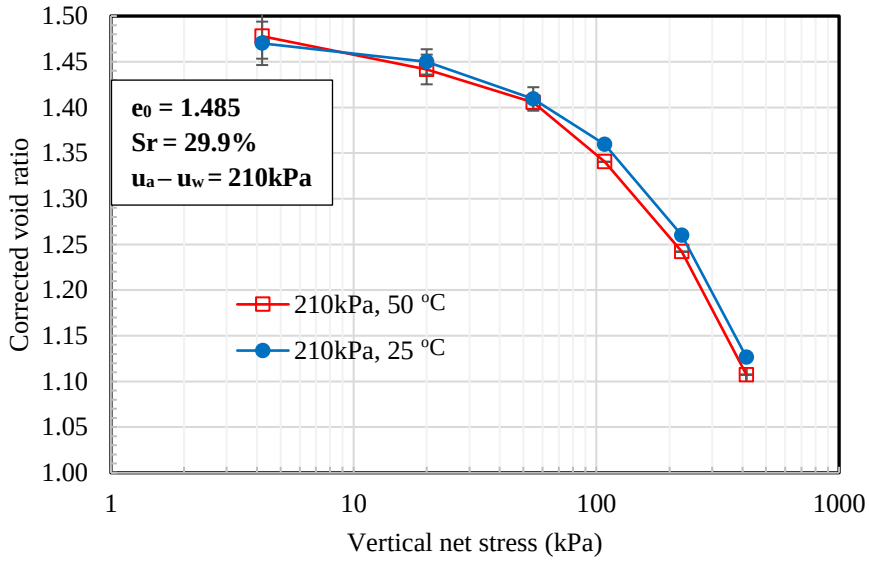

Figure 5-9 Void ratio versus vertical net stress at constant matric suction of 210kPa

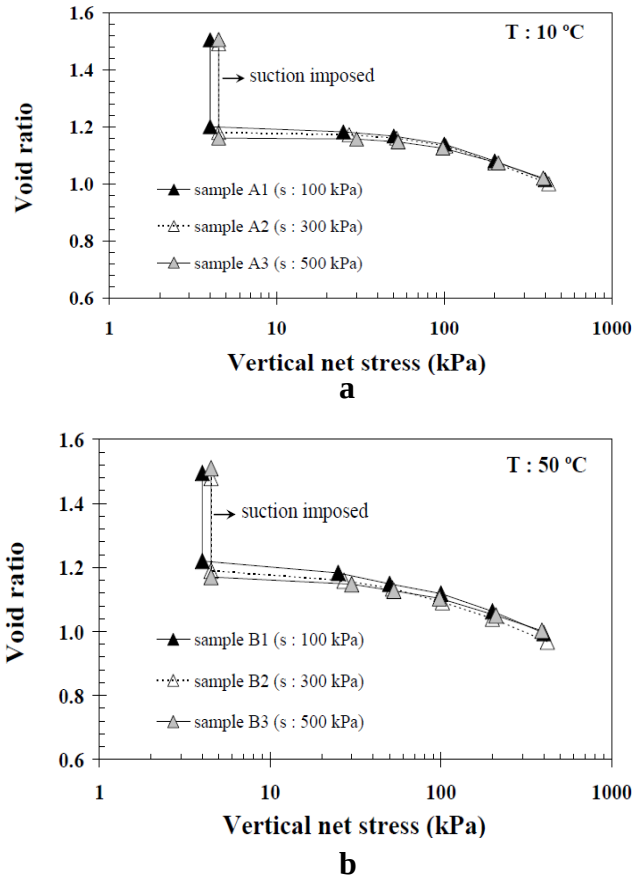

Figure 5-10 Oedometer compression curves at matric suction 100kPa, 300kPa and 500kPa (Haghighi, 2011)

In Fig. 5.8, the compression curves at 25°C and 50°C have the same shape; the recompression lines are inclined, indicating a relatively fast yield. The normal compression lines are steep, indicating an increase in compressibility of the tested samples with increasing vertical net stress. NCLs at 25°C and 50°C are not parallel to each other. This is evident from the different λ values estimated for each line and will be discussed later in this section. Inspection of the compression curves at 25°C and 50°C shows high compressibility at 50°C, relative to 25°C; an outcome in line with previously presented results on tests without suction control (A2, B1 and B2). The curve at 50°C continuously plots below the curve at 25°C at all values of vertical net stress. If repeatability of results was within acceptable limits (±0.02 for $L1_{(50)}$, ±0.04 for $L1_{(25)}$), the difference in compressibility of the two curves is attributed to an increase in temperature to 50°C. Similar increases in compressibility with increasing temperatures were observed by Di Donna & Laloui (2015) on natural silty clay; as well as Haghighi (2011) and Folly (2001) with kaolin clay.

In Fig. 5.9, the shape of the compression curves at 25^{o}C and 50^{o}C are similar. No significant difference was observed in the two curves along the recompression line (from 4kPa to 55kPa vertical net stress), indicating that an increase in temperature from 25^{o}C to 50^{o}C did not influence the compressibility behaviour of the samples along the recompression line. This agrees with the findings of Di Donna & Laloui (2015) on natural silty clay tested at 20^{o}C and 40^{o}C. Along the normal compression zone (from 55kpa to 415kPa), a slight increase in compressibility was observed at 50^{o}C relative to 25^{o}C. For instance, at maximum applied stress (415kPa), the void ratio at 50^{o}C is 1.11, whereas at 25^{o}C the void ratio at the same stress is 1.13. This translates to a Δe of 0.02 which is within the uncertainty range. Hence it can be concluded that a negligible thermal volume change was observed on test at 210kPa. The NCLs are parallel, a result consistent with the observations by Cekerevac & Laloui (2004), Romero et al. (2005), Tang et al. (2008) and Haghighi (2011). This is evident from the estimated slopes of the normal compression lines, which are similar; 0.220 at 50^{o}C and 0.218 at 25^{o}C (see Table 5.7).

Tests $L1_{(25)}$ and $L1_{(50)}$ are presented in Fig. 5.11 in a vertical net stress, versus compressive strain, format. Similar trends were observed in the two tests i.e. compressive linear elastic strain, followed by compressive plastic strain, after the quasi elastic limit; points A and B for 50^{o}C and 25^{o}C respectively. An increase in maximum strain (from 23% to 25%) was observed due to an increase in temperature from 25^{o}C to 50^{o}C, indicating thermal softening of the soil (Uchaipichat & Kalili, 2009; Haghighi, 2011). The observed behaviour agrees with some findings in the literature: Romero (1999) on highly porous bentonite samples heated from 22^{o}C to 80^{o}C; Folly (2001) on saturated kaolin clay heated from 25^{o}C to 60^{o}C; Villar & Lloret (2004) on compacted bentonite; Haghighi (2011) on saturated kaolin clay at 10^{o}C and 50^{o}C. The studies by Folly (2001) and Haghighi (2011) were carried out following a loading path at similar imposed constant matric suction values; 100kPa, 300kPa. In their observations, the magnitude of strain increased with an increase in temperature. Thus, the position of the yield stress was different in heated sample (shifted to the left) relative to non-heated sample. In Fig. 5.12, the strain observed on testing at 50^{o}C is like the strain at 25^{o}C, indicating that an increase in temperature to 50^{o}C had only a negligible effect on the straining of the samples tested at a constant suction of 210kPa.

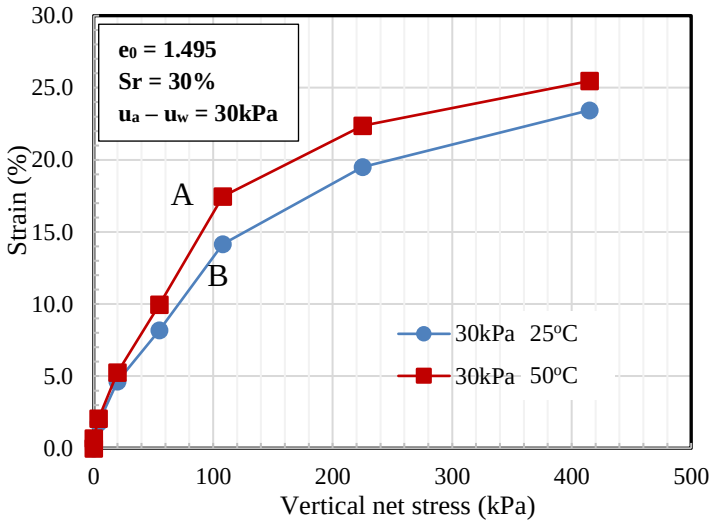

Figure 5-11 Strain versus vertical net stress at constant matric suction of 30kPa

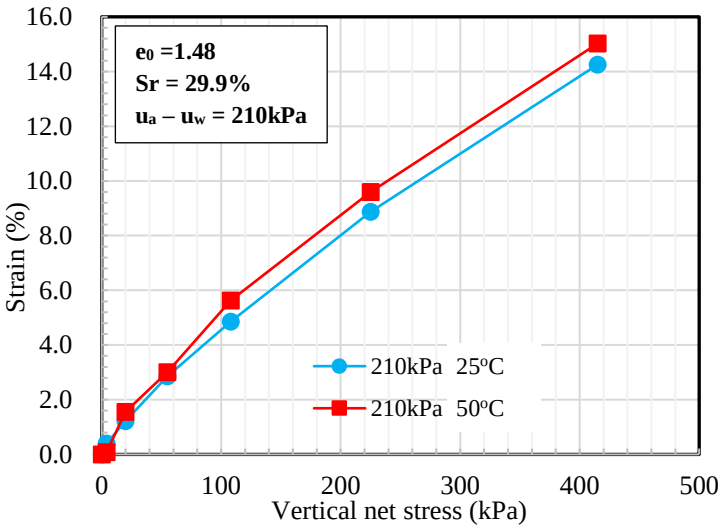

Figure 5-12 Stress versus vertical net stress at a constant matric suction of 210kPa

ii) Yielding behaviour

In Figs. 5.13a & 5.13b, the compression curves for Tests $L1_{(25)}$, $L1_{(50)}$, $L2_{(25)}$, $L2_{(50)}$, $B2_{cwc(50)}$, $B2_{cwc(25)}$, $B2_{DO\text{-}5(25)}$ and $B2_{DO\text{-}5(50)}$, are plotted together at their corresponding temperatures, to assess the effect of suction on the compressibility parameters; yield stress and the slope of the normal compression line λ. Table 5.7 shows the compressibility parameters at their corresponding temperatures. In Tests $B2_{cwc(50)}$ and $B2_{cwc(25)}$, the initial matric suction is 286kPa. Tests $B2_{DO\text{-}5(25)}$ and $B2_{DO\text{-}5(50)}$ were saturated tests and matric suction at saturation is 0kPa (Fredlund & Rahardjo, 1993). Inspection of the figures

shows a shift of the normal compression lines to the left, with decreasing matric suction and increasing temperature (see also Table 5.7), which is consistent with the findings of Haghighi (2011), Folly (2004) and Romero (1999). The normal compression lines at 30kPa and 0kPa converged at 100kPa vertical net stress. The slope of the normal compression lines λ, used for modelling the soil response along the normal compression, was estimated from the compression curves. The slopes λ were obtained within the stress range of 55kPa – 415kPa and presented in Table 5.7, together with their corresponding matric suction values and temperatures. Table 5.7 shows that the compressibility parameter λ, at 210kPa matric suction, was not affected by temperature, because of the negligible effect of temperature on the sample tested at 210kPa. The compression curves at 25^{o}C and 50^{o}C were similar for tests at 210kPa. The observed behaviour agrees with the findings of Haghighi (2011), Tang et al. (2008) and Cekerevac & Laloui (2004). In the study by Haghighi (2011) on saturated kaolin clay, he observed no significant difference in the λ values of samples tested at 10^{o}C and 50^{o}C for all values of imposed matric suction (100, 300 and 500kPa). It is worth noting that most studies that reported that λ was insensitive to temperature, reported that compressibility was sensitive to temperature (e.g. Cekerevac & Laloui, 2004; Romero, 2005; Hagihighi, 2011). At a matric suction of 30kPa and 0kPa, the compressibility parameters increased with temperature increase, as shown in Table 5.7. From 0.148 to 0.161 at 0kPa and from 0.221 to 0.277 at 30kPa indicating a steeper slope and an increased rate of consolidation. This is in line with the findings of Romero et al. (2003) on unsaturated boom clay. They reported that the post-yield compressibility parameters (stiffness parameter and slope of normal compression line) are temperature sensitive; they increase with temperature.

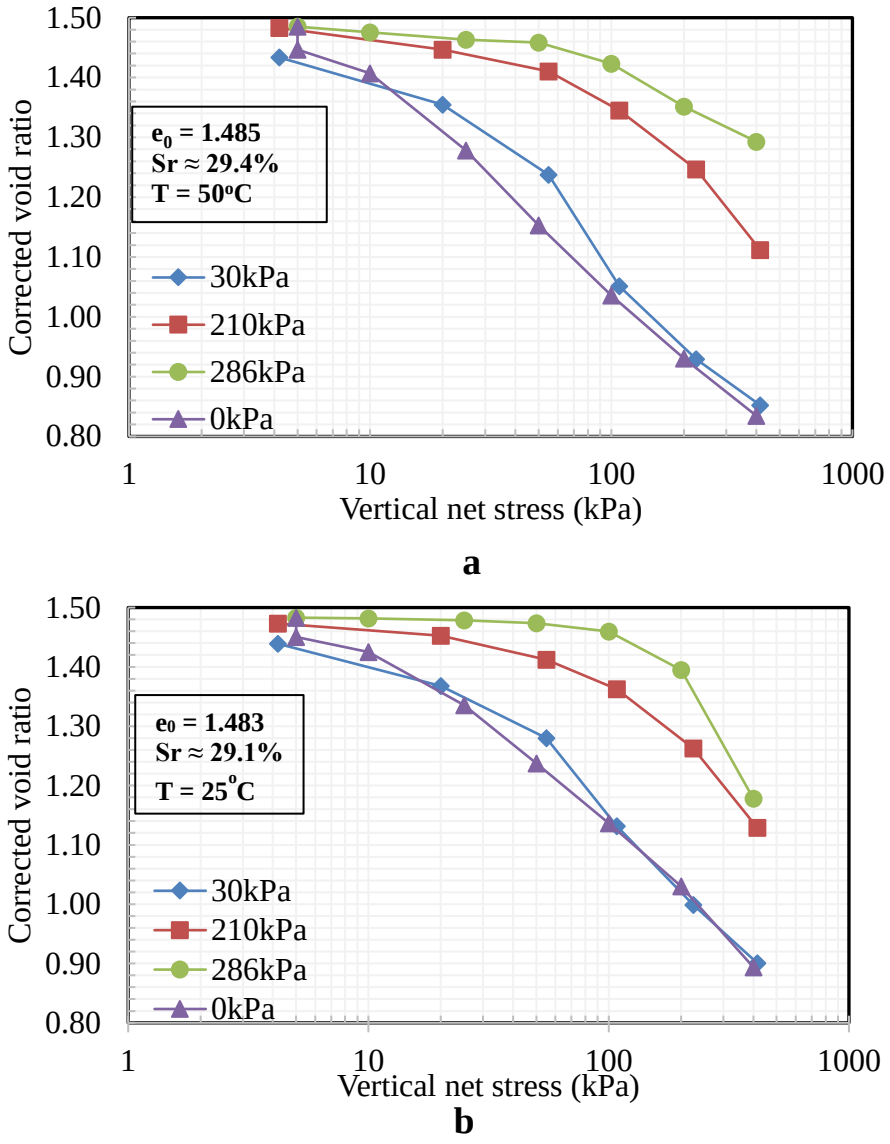

Figure 5-13 Compression curves at matric suction of 0, 30, 210 and 286kPa (a) 50°C (b) 25°C

For the test at a matric suction of 286kPa, λ decreased significantly with temperature increase (from 0.313 to 0.139). This was not expected and contradicts most of the reported literature except for Ye et al. (2012) who observed a decrease in λ with an increase in temperature on GMZ01 bentonite tested at 20°C and 60°C, but the difference between the λ values obtained at the two temperatures is relatively small (≈ -0.02). The huge difference in λ observed in the test at 286kPa matric suction can be linked to the wrong assumption of constant water content in the sample tested at 50°C, as explained in Sec. 5.2.1.

Table 5-7 Yield parameters at 25°C and 50°C

25°C			50°C		
Matric suction (kPa)	**Yield stress (kPa)**	**λ**	**Matric suction**	**Yield stress (kPa)**	**λ**
0	20	0.148	0	10	0.161
30	40	0.221	30	35	0.277
210	100	0.218	210	100	0.220
286	165	0.313	286	100	0.139

From the obtained results, it could be concluded that λ increased with temperature increase at low values of matric suction (0 - 30kPa), but was insensitive to temperature at relatively high matric suction (210kPa). There are doubts on the result obtained at matric suction of 286kPa. From Table 5.7 the compressibility parameter λ increased with increasing matric suction, consistent with the findings of Alonso et al. (1990).

In each test presented in Fig. 5.13 a & b, there is a clear indication of yield which did not correspond with the compaction pressure. The yield stress, which is the maximum stress a soil has been previously subjected to, was obtained by the log e+1 – log p method (Butterfield, 1979). Theoretically, yield stress is likened to elastic limit in Ohm's law (Wheeler, 2009). Prior to yield, samples exhibit elastic recoverable volume change, or negligible irrecoverable volume change in some cases (Wang & Frost, 2004). Sample behaviour after yield is classified as plastic irrecoverable volume change (Alonso et al., 1990). The zones before and after yield are known as the elastic and plastic domains, respectively. In Fig. 5.13, the yield stress varied with suction and temperature; increasing with increasing matric suction (in Fig. 5.13b and partly in Fig. 5.12a) and decreasing with increasing temperature (see also Table 5.7). In Fig. 5.13a (tests at 50°C), the increase in yield stress with suction was observed at 0kPa, 30kPa and 210kPa matric suction. At a matric suction of 286kPa, the estimated yield stress is 100kPa, which is the same as the yield stress at a suction level of 210kPa. Most literature (Wheeler & Sivarkumar, 1995; Francoise et al., 2007) reported that the yield stress increases with increasing suction. It was expected that the yield stress at 286kPa matric suction (T = 50°C) will be higher than the yield stress at 210kPa, at the same temperature. Apparently, this may be linked to the incorrect assumption of constant water content in the test at a matric suction level of 286kPa, as explained previously. At a matric suction of 210kPa, the yield stress was not

affected by temperature. This was expected because the influence of temperature on the compressibility of the samples was negligible.

As observed from the test results, and from other researchers (Ng & Zhou, 2014; Di Donna & Laloui, 2014; Haghighi, 2011; Uchaipichat & Khalili, 2009; Salager et al., 2008; Francoise et al., 2007; Folly, 2004), increase in temperature resulted in a reduction of the elastic domains and earlier onset of plastic behaviour. This also resulted in the shrinkage of the yield surface, through reduction in the yield stress. This condition is known as thermal softening. Conversely, increase in suction resulted in the expansion of the elastic domain and, therefore, the delay of plastic behaviour. This behaviour is known as suction hardening behaviour (Uchaipichat & Khalili, 2009; Wheeler & Sivarkumar, 2000). It is worth noting that the suction hardening reported by Uchaipichat & Khalili (2009) was observed on results of isotropic loading of compacted silty soil analysed in terms of effective stress. Their analysis in terms of net stress showed reduction in the elastic domain with increasing suction (softening), for suction values less than the air entry value of the sample. For suction, greater than the air entry values, Uchaipichat & Khalili (2009) reported that the elastic domain remained unchanged with increasing matric suction. The analysis in this study has been based on net stress; the suction hardening behaviour observed is consistent with other studies carried out in terms of net stress. Suction hardening phenomena are attributed to the stabilising effect, due to an increase in the normal force at inter-particle contacts associated with meniscus water (Wheeler & Karube, 1995). On the other hand, thermal softening is attributed to thermal dilation of mineralogical components of clay soil (Laloui, 1993) and thermal rearrangement of soil structure into a denser packing (Leroueil & Marques, 1996).

iii) Effect of temperature and suction on the coefficient of volume compressibility

The coefficient of volume compressibility M_v is an important parameter used in the calculation of maximum settlement of a soil on the application of vertical stress. The coefficient of volume compressibility ($M_v = [\delta e/\delta p]*[1000/1+e_1]$) was calculated at 25^{o}C and 50^{o}C, considering only the compression tests at constant matric suction of 30kPa, 210kPa, 286kPa, as shown in Fig. 5.14 and Fig. 5.15. From the figures, the influence of matric suction and temperature on the coefficient of volume compressibility, can be assessed.

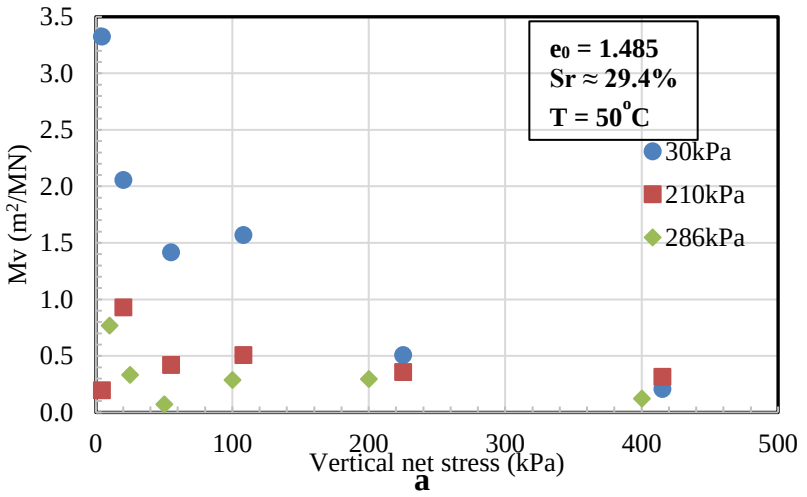

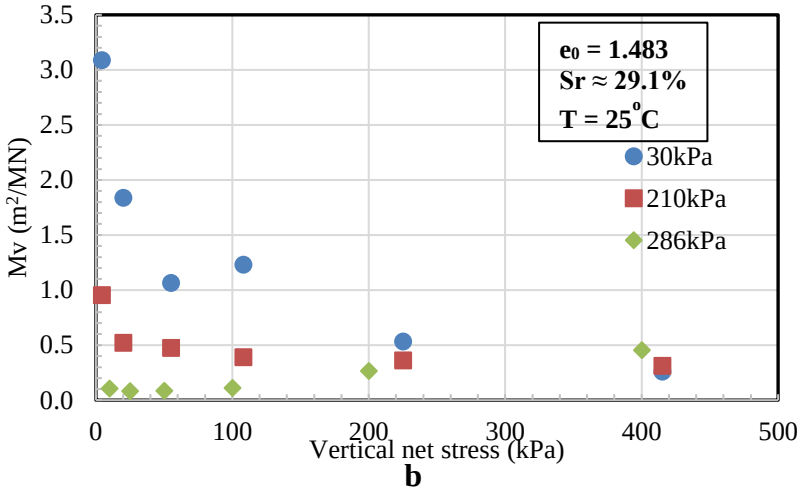

Figure 5-14 Variation of volume compressibility with vertical net stress at different matric suction: 30, 210 and 286kPa (a) 50°C (b) 25°C

Inspection of Figs. 5.14 shows that the coefficient of volume compressibility, at each value of vertical net stress, decreases with increasing matric suction between 0kPa and about 200kPa of applied stress. At high applied stress (200kPa - 415kPa), *Mv* was observed to be insensitive to increasing matric suction. This is expected, since increase in matric suction increases the stiffness of soils (Wheeler & Karube, 1995).

From Fig. 5.14, an increase in the coefficient of volume compressibility was observed with an increase in temperature at 30kPa matric suction, within the range of vertical net stress 0 – 225kPa. This observation is in line with the findings of Jefferson (1994), who observed an increase in *Mv* with an increase in temperature on reconstituted London clay. Convergence of the curves at 25°C and 50°C was observed at vertical net stresses above

225kPa. At matric suction of 210kPa and 286kPa, the influence of temperature on *Mv* is erratic. No clear trend was observed.

Information regarding the influence of temperature on *Mv* is conflicting in the literature. Ctori (1989), Jefferson (1994) reported increasing *Mv* with increasing temperature while Erikson (1989) reported that *Mv* is insensitive to temperature. The result from this study can confirm an increase in *Mv* with an increase in temperature at low suction value (30kPa).

iv) Effect of temperature and suction on collapse potential

In Fig. 5.15, variation of collapse potentials with vertical net stresses are presented. This was obtained from the difference in void ratio between the saturated test (0kPa) and the tests at matric suctions of 30kPa, 210kPa and 286kPa. The aim was to assess the influence of matric suction on the collapse potential of the tested samples.

Inspection of the figures indicated that the collapse potential increases with increasing matric suction as previously observed in Sec. 4.3.4. This agrees with the findings of Lawton (1986) who noted the collapse and swell potential of clayey sand increases with decreasing compaction water content (increasing matric suction) and Rabbi et al. (2014) in which they observed an increase in collapse potential with increasing matric suction. This is because wetter samples (at low matric suction) would have initially experienced loading induced compression, which would reduce the volume of the void spaces. Consequently, the magnitude of compression associated with loading on wetting is reduced. Thus, the difference in void ratios between initially loaded samples at constant water content and samples loaded after wetting, is less for wetter soils than for drier soils. It is worth noting that in Lawton (1989), matric suction was not controlled. However, compaction to different initial water content levels will result in samples with different initial matric suction; the suction increasing with decreasing water content.

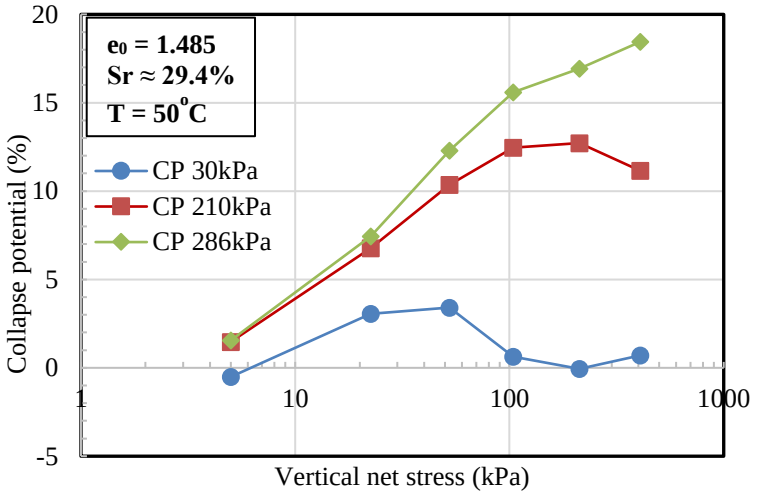

a

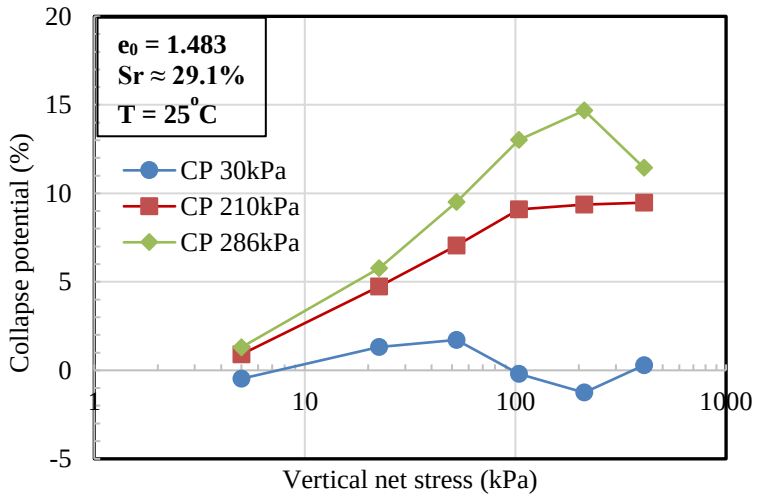

b

Figure 5-15 Variation of collapse potential with vertical net stress at different suction: 30, 210 and 286kPa (a) 50°C (b) 25°C

The influence of temperature on collapse potential is shown in Table 5.8. The maximum collapse potential increased with an increase in temperature (25°C to 50°C), at all values of matric suction, in line with previous observations in Sec. 5.2.3. The critical stress at which the maximum collapse occurred remained constant, with increase in temperature for suction values of 30kPa and 210kPa.

Table 5-8 Maximum collapse potential and critical applied stress at 50°C and 25°C

Suction (kPa)	50°C		25°C	
	CP Max (%)	Critical stress (kPa)	CP Max (%)	Critical stress (kPa)
30	3.4	52	1.72	52
210	12.72	212	9.36	212
286	18.45	405	14.68	212

At a suction value of 286kPa, the critical stress increased from 212kPa to 405kPa on an increase in temperature from 25°C to 50°C, contrary to previous observations in Sec. 5.2.3. In Haghighi (2011), a decrease in collapse potential was observed with an increase in temperature from 20°C to 50°C. He explained that this was due to a reduction in matric suction resulting from an increase in temperature. However, in this study, matric suction was imposed and controlled during testing, so it is less likely that suction would have been reduced because of an increase in temperature. The difference in the observed influence of temperature between this study and Haghighi (2011) may be linked to differences in soil structure resulting from different compaction water contents. The samples used by Haghighi were reconstituted samples, whereas the samples used in this study were statically compacted samples with open structure. The imposed suction in his study was obtained along a drying path. It is possible, that the difference in soil structure may have played a significant role in the observed thermal effect on collapse.

5.3.2 Heating and cooling at constant imposed matric suction and vertical net stress (Non-isothermal path)

Tests $NI1_{(30)}$, $NI1_{(100)}$, $NI2_{(30)}$ and $NI2_{(100)}$ were carried out to ascertain the volumetric behaviour of compacted kaolin clay during a thermal cycle under constant vertical net stress and suction. In tests $NI1_{(30)}$ and $NI1_{(100)}$, statically compacted samples of kaolin clay (e_0 = 1.490±0.014, Sr = 30%) were first subjected to matric suction of 30kPa and 100kPa respectively (path 1 in Fig. 3.12a & b). The samples were then loaded to a vertical net stress of 55kPa (path 2). Under the imposed matric suction and vertical net stress, the samples were subjected to a thermal cycle from 25°C to 50°C to 25°C (paths 3 and 4). The testing procedures are explained in Sec. 3.7.5a. The difference in terms of the stress path between $NI1_{(30)}$ and $NI1_{(100)}$ is the different imposed matric suction: 30kPa and 100kPa respectively. Test $NI1_{(30)}$ and $NI2_{(30)}$ were repeated twice to ensure repeatability

of the results. The maximum standard deviation obtained are 0.16, 0.18 and 0.17% in Tests $NI1_{(30)}$, $NI2_{(30)}$ and $NI2_{(100)}$ respectively.

In Fig 5.16, the result of the compressive strain observed in test $NI1_{(30)}$ is presented. The compressive strain, following imposition of matric suction, vertical net stress and thermal cycle, was calculated from the measured deformation ΔH during each step.

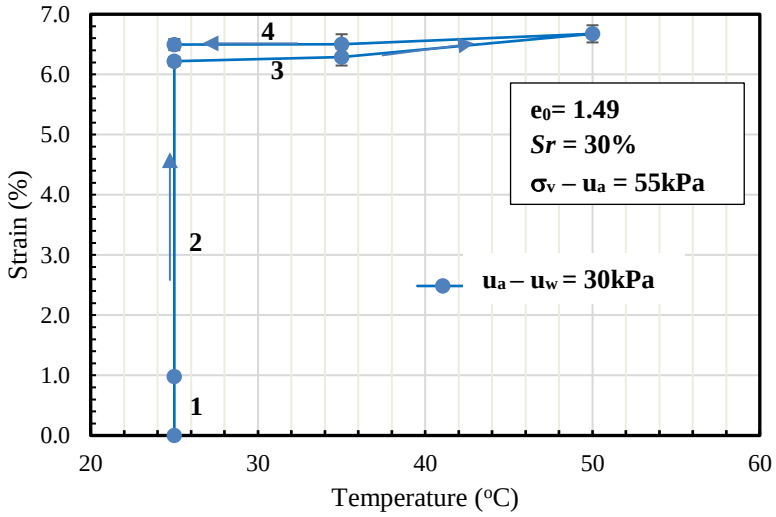

Figure 5-16 Compressive strain versus temperature for $NI1_{(30)}$

Inspection of Fig. 5.16 indicates that the sample experienced slight compressive strain (1.00±0.01%) due to the imposition of matric suction of 30kPa (path 1). Following an increase in vertical net stress to 55kPa (path 2), the sample experienced a compressive strain of 6.2±0.07%. On heating to 50°C (path 3), the sample experienced slight contraction (0.50±0.14% increase in strain). Similar observations were made by Tang et al. (2008) and Cui et al. (2013). They observed contraction of MX80 and GMZ01 bentonite respectively on heating at low suction values. From Fig. 5.16, the cooling process from 50°C to 25°C (path 4) was accompanied by negligible deformation. Thus, irrecoverable strain was observed on cooling, data consistent with the findings of Romero et al. (2003). Unfortunately, Test $NI1_{(100)}$ at a constant suction of 100kPa was inconclusive, due to a breakdown of the temperature chamber during the experiment; therefore, the result could not be compared with that at 30kPa.

If the observed strains are expressed in terms of void ratio, small change in void ratio would be observed on a complete temperature cycle, owing to the small contraction experienced by the sample on heating. However, considerable decrease in void ratio

occurred (1.46) after suction equalisation (path 1), and on application of vertical net stress (1.29) path (2). The reduction in void ratio was greatest on application of vertical net stress and was negligible on heating.

Because of the negligible volume change observed in Test $NI1_{(30)}$ and $NI1_{(100)}$ on heating, Test $NI2_{(30)}$ and $NI2_{(100)}$ were carried out on sample B1 to investigate if significant deformation will be observed on heating, due to relatively high compressibility and water content of the sample. Samples B1 with an initial degree of saturation and water content of 58.6% and 33% respectively, were observed to be highly compressible relative to other samples (see Sec. 4.3.1, Fig. 4.2d).

In Figs. 5.17a & b the results of $NI2_{(30)}$ and $NI2_{(100)}$ are presented in terms of compressive strain. Both samples experienced significant contraction (0.86±0.16% in $NI2_{(100)}$ and 0.96±0.18% in $NI2_{(30)}$) on heating; a change greater than experienced in Test $NI1_{(30)}$. The observed contraction was irrecoverable on cooling to 25°C. Cekerevac (2003) observed in his study on over-consolidated and normally consolidated kaolin clay, subjected to three thermal cycles (22°C to 90°C), that irreversible contraction is associated with the first thermal cycle and disappears with subsequent cycles. One thermal cycle was used in this study and irreversible contraction was observed on heating and cooling, consistent with the findings of Cekerevac (2003). Based on the number of cycles used during testing, this study cannot comment on the reported reversible behaviour observed by Cekerevac (2003) with 2nd and 3rd thermal cycles. The thermally induced irreversible behaviour is linked to structural rearrangement of particles at the macro-structural level, because of changes in the aggregate volume (Romero et al., 2003). Romero et al. (2005) explained that increase in temperature can result in either volume reduction or increase depending on the clay mineralogy. Whereas increase in volume which is usually observed in heating expansive clay is attributed to thermal expansion of mineral particles and absorbed water, reduction in volume is linked to the intra-aggregate water losses. Cui & Tang (2013) explained that the cooling process is elastic, because it involves contraction of the constituent elements, whereas thermal contraction is a plastic process. Comparison of Fig. 5.17a & b shows that the magnitude of strain observed on loading and heating decreased with an increase in matric suction.

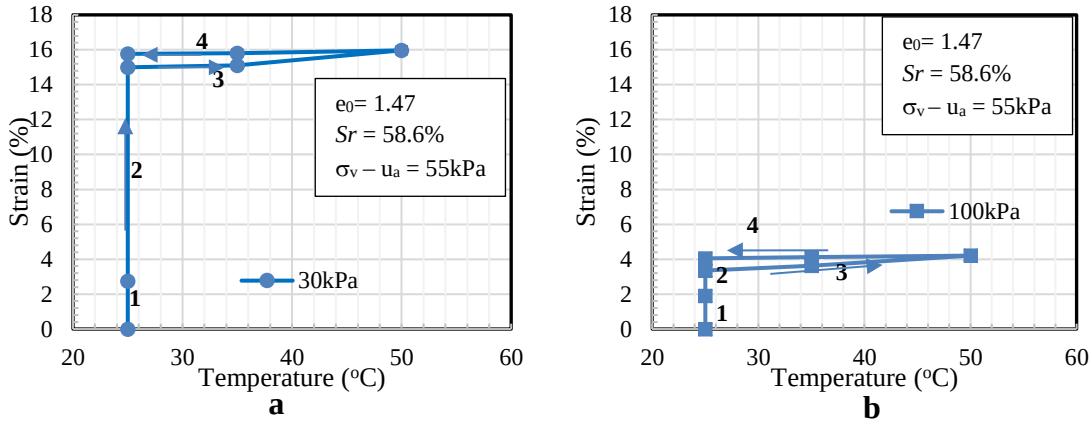

Figure 5-17 Compressive strain versus temperature (a) NI2$_{(30)}$ (b) NI2$_{(100)}$

For instance, it could be observed that the sample at a constant suction of 30kPa experienced a relatively higher strain (16%) than the sample at a matric suction of 100kPa (4.2%). A similar decrease in strain, with increase in suction, was also observed by Folly (2004) on reconstituted kaolin clay. The sample at a constant suction of 0kPa exhibited a higher magnitude of strain (≈ 0.24%) on heating to 60°C than the sample at a suction of 100kPa (0.16%) when heated to the same temperature. This result could be attributed to the reduction in normal force at inter-particle associated with a decrease in matric suction (Sivakumar & Wheeler, 2000), which also increases compressibility. In terms of void ratio, greater deformation of the samples was observed on application of vertical net stress and suction (paths 1 and 2) than on thermal cycles. The deformation was maximum on application of vertical net stress (path 2) as previously observed in NI1$_{(30)}$.

5.3.3 Increasing suction at constant temperature and vertical net stress

Tests D1$_{(50)}$ and D1$_{(25)}$ were carried out to investigate the influence of an increase in temperature (from 25°C to 50°C) on volume change of compacted kaolin following a drying path. In Tests D1$_{(50)}$ and D1$_{(25)}$, the samples were first subjected to a matric suction of 30kPa (path 1 Fig. 3.15). Following equalisation of suction, temperature was increased to 50°C (path 3, Fig. 3.15b) in D1$_{(50)}$ while D1$_{(25)}$ was maintained at 25°C. The samples were subjected to a vertical net stress of 55kPa (path 2 Fig. 3.15). Under the imposed temperature and vertical net stress, the samples were dried by increasing suction from 30kPa to 210kPa (paths 3 and 4 in Fig. 3.15a and Fig. 3.15b respectively).

Fig. 5.18 shows samples' responses with increasing matric suction at constant temperature and vertical net stress. The figure show initial straining, due to collapse

(7.2% and 6.3% in $D1_{(50)}$ and $D1_{(25)}$ respectively) of the samples, on reducing the matric suction (from 285 kPa to 30kPa) and on imposing a vertical net stress of 55kPa. The figure also shows straining of the samples on drying. In this case, the strain was due to shrinkage of the samples following increasing matric suction, contrary to collapse observed on reducing suction to 30kPa . The observed collapse and shrinkage were found to increase with temperature. The curve at 50°C continuously plotted above the curve at 25°C (Fig. 5.18). Similar findings were reported by Romero (1999) and Folly (2004), as shown in Fig. 5.19 a & b respectively. The shrinkage observed on drying was not accompanied by yield, as observed by Sharma (1998) during a drying path on a bentonite mixture.

Further on, it could also be observed that a greater percentage of the deformation occurred with the simultaneous reduction in matric suction and increase in vertical net stress than on drying.

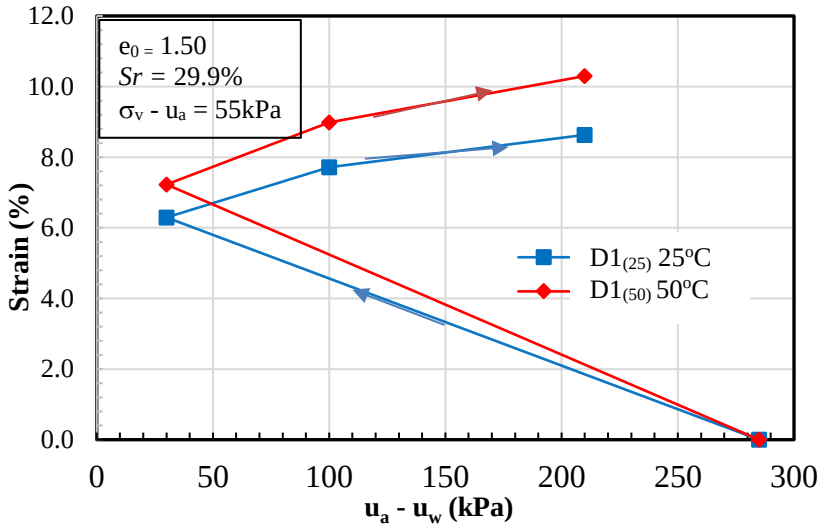

Figure 5-18 Strain versus matric suction at 50°C and 25°C of samples subjected to drying

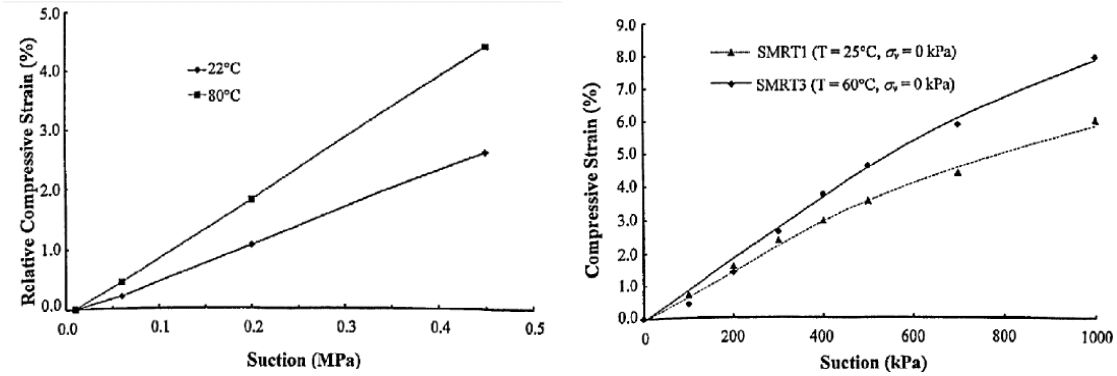

Figure 5-19 Effect of temperature on deformation behaviour following a drying path (a) Boom clay (Romero, 1999) (b) kaolin (Folly, 2004)

5.4 CONCLUSION

The effect of temperature on the volume change behaviour of statically compacted kaolin clay was studied through standard oedometer tests and suction controlled oedometer tests. Results obtained from the standard oedometer tests without suction control indicate that compressibility increases with temperature increase. For the suction, controlled tests, three testing paths were followed: loading at constant suction and temperatures; heating and cooling at constant suction and vertical net stress; and drying from 30kPa at constant temperature and vertical net stress. The results obtained following the loading path indicated that compressibility increases with an increase in temperature, resulting in a shift of the LC curve to the left, and then decreases with increasing suction. Additionally, slight volume changes (collapse) were observed in the samples on imposing suction as opposed high volume changes (shrinkage) reported by other authors e.g. Hagihigh (2011). With this evidence, the importance of considering the hydraulic history of a sample/soil when using experimental data to predict soil behaviour was highlighted. The heating and cooling tests showed contraction of the samples on heating, which was irrecoverable on cooling. An important observation under this stress path is that the magnitude of strain associated with loading to 55kPa is greater than wetting and heating combined. Finally, drying of samples at constant vertical stress resulted in shrinkage. The observed shrinkage increased with temperature.

CHAPTER SIX

6 TEMPERATURE EFFECT ON THE PRIMARY DRYING WATER RETENTION CURVE AND SUCTION OF KAOLIN CLAY

INTRODUCTION

In this chapter, the experimental results of the SWRC tests at 25^{o}C and 50^{o}C explained in Sec. 3.8 are presented. Experimental results from thermal cycle tests described in Sec. 3.9 are also presented. Additionally, results of correlation between the coefficient of permeability and soil suction, based on van Genuchten (1980) hydraulic model are also presented for the two temperatures of interest.

6.1 STUDIED SAMPLES AND TEST CONDITIONS

The first set of results presented are the drying paths of the SWRC which were obtained using both the axis translation (PP1, PP2) and vapour equilibrium (VE1, VE2) techniques. Summary of initial conditions of the samples and the test descriptions is shown in Table 6.1. Details of the testing procedures can be found in Chapter 3. Test PP1, PP2, VE1 and VE2 were repeated twice in most cases. The error and percentage uncertainty associated with each test are shown in Table 6.3. The estimated error was used during analysing, to ensure that the observed temperature effect is not within the error margin. The repeatability of tests $PP1_{25}$, $VE1_{25}$ and $PP1_{50}$, $VE1_{50}$ are plotted in Fig. 6.1. The figure indicates that the repeatability is reasonable.

The second set of results presented were obtained from monitoring suction (matric and total suction) and volume changes on specimens subjected to one cycle of heating and cooling (temperature was increased from 10^{o}C to 25^{o}C and subsequently to 50^{o}C and then decreased to 25^{o}C). The samples were unrestrained and statically compacted at two initial void ratios (e_0 = 1.0 and 1.5) and $Sr \approx$ 15, 30, 60% as shown in Table 6.2).

Table 6-1 Initial conditions of the tested samples and test descriptions for the SWRC tests (drying paths)

Tests	Initial states			Compaction pressure (kPa)	Temp. (ºC)	Testing path	No. of tests	Test Duration (days)	Testing Method
	Water content (%)	Void ratio e_0	Matric suction (kPa)						
$PP1_{25}$	17	1.0	250	759	25	Drying path 10 – 400kPa	10	70	Axis translation
$PP1_{50}$					50		9	70	
$PP2_{25}$		1.5	286	180	25		9	70	
$PP2_{50}$					50		9	56	
$VE1_{25}$	17*	1.0*	400	-	25	Suction values of 3000kPa, 4000kPa and 5000kPa.	5	56	Vapour equilibrium
$VE1_{50}$					50		5	14	
$VE2_{25}$		1.5*	400	-	25		6	14	
$VE2_{50}$					50		6	14	

*: initial conditions of the samples during axis-translation technique. For vapour equilibrium technique, off cuts from samples subjected to a matric suction of 400kPa with axis-translation technique were used.

Table 6-2 Initial conditions of the tested samples and test descriptions of thermal cycle tests

Tests	Initial states				Static compaction pressure (kPa)	Testing path	No. of tests	Test Duration (days)	Testing Method
	Water content w (%)	Void ratio e_0	Degree of saturation S_r (%)	Matric suction (kPa)					
A1	22.5	1.00	59.8	212	679	Thermal cycle; 10ºC - 25ºC - 50ºC - 25ºC	10	70	Filter paper
A2	11.3	1.00	30.0	628	939		10		
A3	4.8	0.98	13.0	1112	999		10		
B1	33.1	1.48	59.0	109	57	Thermal cycle; 10ºC - 25ºC - 50ºC - 25ºC	10	70	Filter paper
B2	16.7	1.49	29.7	286	180		10		
B3	8.1	1.49	14.5	691	280		10		

Table 6-3 Error and uncertainty associated with the SWRC

Test	No. of Obs.	Std. Deviation	Percentage uncertainty
$PP1_{25}$	2	0.015 - 1.368	0.02 - 2.52
$PP1_{50}$		0.491 - 1.700	0.74 - 4.16
$PP2_{25}$		0.308 - 2.206	0.22 - 6.06
$PP2_{50}$		0.032 - 1.386	0.07 - 2.76
$VE1_{25}$		0.020 - 0.557	0.09 - 2.46
$VE1_{50}$		0.031 - 0.913	0.20 - 5.39
$VE2_{25}$		0.179 - 0.809	1.23 - 6.01
$VE2_{50}$		0.467 - 0.840	4.22 - 6.62

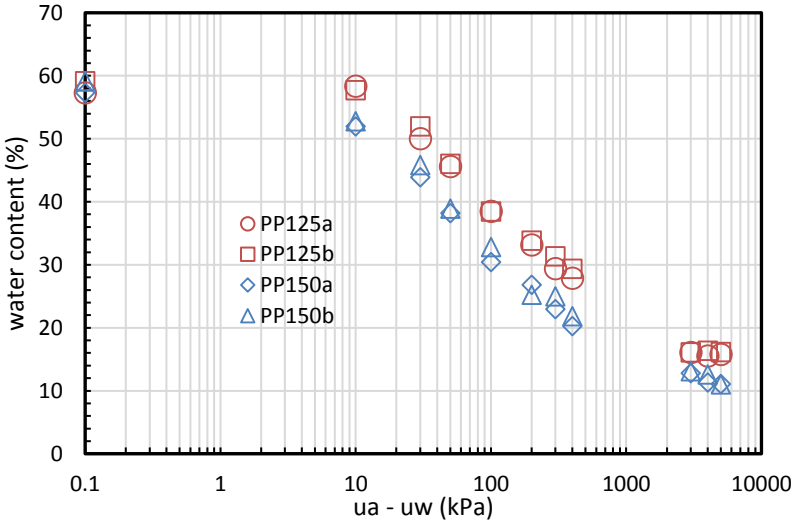

Figure 6-1 Repeatability of tests 25ºC and 50ºC (e_0 = 1.5)

6.2 EXPERIMENTAL TEST RESULTS AND ANALYSIS OF THE PRIMARY SWRC (DRYING PATHS)

The primary drying paths of kaolin clay, statically compacted to different void ratios (1.0 & 1.5) were obtained at 25ºC and 50ºC through tests PP1, PP2, VE1 and VE2 with the aim of assessing the influence of temperature and void ratio on the soil water retention. Tests PP1 and PP2 were carried out using a pressure plate apparatus (details of the testing procedure are explained in Chapter 3). Initial saturations of the samples were performed at a suction of 0kPa (path 1 in Fig. 3.19a & b). Samples $PP1_{50}$ and $PP2_{50}$ were then subjected to a temperature of 50ºC (path 2 Fig 3.19a) while samples $PP1_{25}$ and $PP2_{25}$ were subjected to 25ºC (2' Fig. 3.19b). This was followed by drying (increasing matric suction in steps) to a maximum matric suction of 400kPa (path 3 & 3'). Tests VE1 and VE2 (vapour equilibrium tests) were performed to define the curves at high suction ranges (> 400kPa). The same samples subjected to 400kPa matric suction in pressure plate tests were used for vapour equilibrium tests to ensure a continuous retention path.

6.2.1 Effect of temperature on the drying water retention curves of statically compacted kaolin clay

The drying curves at 25ºC and 50ºC are compared in Fig. 6.2a & b. The results are presented in terms of gravimetric water content versus matric suction/total suction. The data points obtained from vapour equilibrium method are total suction values. As will be

discussed later in the chapter, the SWRC models by van Genuchten (1980) and Fredlund & Xing (1994) were fitted to the experimental data.

For the test at 25^{o}C, immediately after saturation, the subsequent increase in suction up to the air entry point did not result in significant change in water content, resulting in a constant slope along the capillary fringe zone (0kPa – 10kPa). However, this was different for the tests at 50^{o}C; increasing suction from saturation resulted in a decrease in water content (e.g. from 58% - 52% for e_0 = 1.0) indicating a slightly inclined slope along the capillary fringe zone for the curve at 50^{o}C. It is worth mentioning that the curves at 50^{o}C and 25^{o}C originated from the same point (at the same water content and suction) as could be seen in Fig. 6.2. This is because the samples were first saturated at 25^{o}C before increasing the temperature. It is then likely that the capillary fringe zone for tests at 50^{o}C may have had a constant slope if the saturated water content was obtained at 50^{o}C.

Inspection of Fig. 6.2 showed that an increase in temperature from 25^{o}C to 50^{o}C resulted in a shift of the curve at 50^{o}C to the left, indicating a decrease in water content with an increase in temperature. The air entry values also known as bubbling pressures (Brooks & Corey, 1964) reduced with an increase in temperature from 15kPa to 10kPa (e_0 = 1.0) and from 13kPa to 10kPa (e_0 = 1.49) respectively (see also Table 6.4). These values were obtained graphically by extending a tangent line from the capillary and desaturation zone and then determining their point of intersection. Other researchers (e.g. Hopmans & Dane, 1986; Villar & Lloret, 2003; Villar & Gomez-Espina, 2008; Haghighi, 2011, Ye et al., 2014) have also observed a decrease in the air entry value with an increase in temperature. Conversely, the study by Folly (2000) reported an increase in air entry value with an increase in temperature from 25^{o}C to 60^{o}C based on observations on consolidated kaolin clay at a vertical net stress of 0kPa. But when the same soil was tested under a constant applied stress of 100kPa, a reduction in air entry value was observed with an increase in temperature.

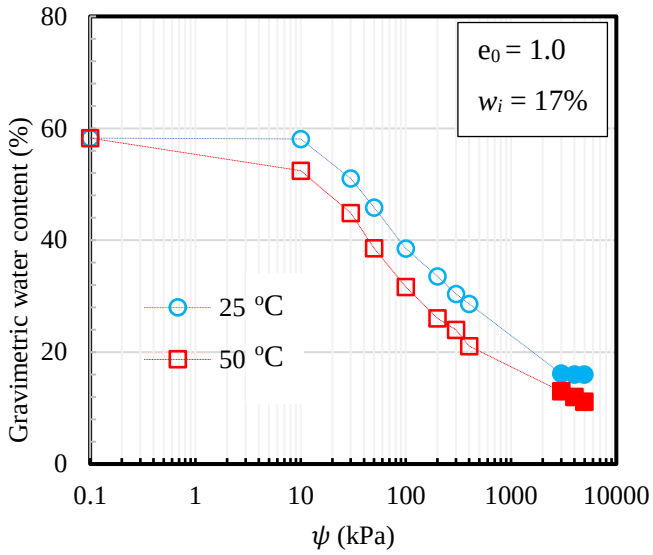

a

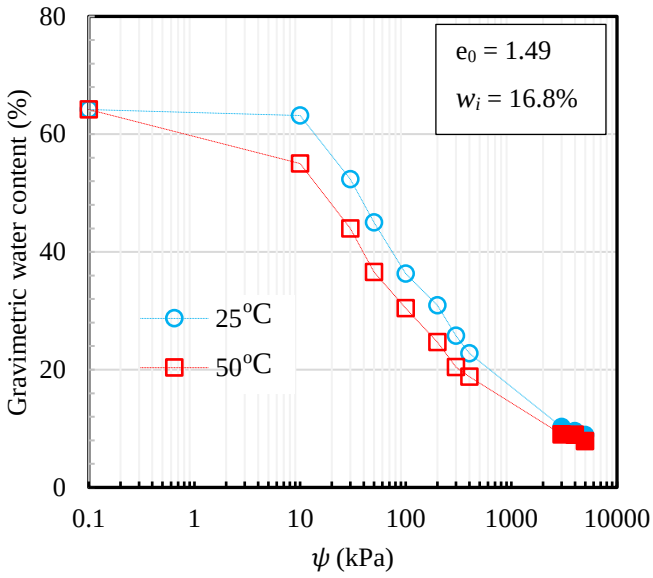

b

Figure 6-2 Primary drying curves at 25°C and 50°C (a) e_0 = 1.0: $PP1_{25}$, $PP1_{50}$ (b) e_0 = 1.49: $PP2_{25}$, $PP2_{50}$

The effect of temperature on soil water retention is linked to the surface tension dependence on temperature, because an increase in temperature reduces the surface tension (Nimmo & Millar, 1986; Bachmann, 2002). Review of different studies on temperature-soil water relationship by Grant & Bachmann (2002) concluded that the influence of temperature on surface tension is not enough to explain the dependency of soil water retention on temperature. They suggested that variation in contact angle, thermal expansion of entrapped air and liquid gas interfacial tension due to the solute effect are the possible influence. Additionally, Ma & Hueckel (in Villar et al., 2004)

pointed out that the transfer of tightly bound intra-aggregate water (meniscus water) to free inter-aggregate water (bulk water) because of an increase in temperature can also play a role in temperature dependence of soil water retention. In fact, Romero et al. (2001) in their study on Boom clay at 22°C and 80°C noted that the influence of temperature on soil water retention is dependent on the mechanism responsible for the water retention. At low suction/high water content region associated with inter-aggregate porosity, water retention is dominated by capillary mechanism. In this region, temperature influence on water retention can be linked to temperature dependence on surface tension, entrapped air and thermal dilation of water. However, in the high suction region associated with intra-aggregate pores, adsorption is the mechanism responsible for the water storage. Romero et al. (2001) further explained that temperature effect at high suction zone is also linked to thermal alteration of clay fabric and intra-aggregate fluid chemistry.

Table 6-4 Properties of the drying curves at 25°C and 50°C

Void ratio	Temperature (°C)	Slope	Air entry (kPa)
1.0	25	0.179	15.0
	50	0.189	10.0
1.49	25	0.229	13.0
	50	0.194	9.9

Comparison between the SWRC (drying path) at 25°C, e_0 = 1.5 from Haghighi (2011) Fig. 6.3 and the drying path at 25°C, e_0 = 1.49 from this study are shown in Table 6.5. From the Table, it could be observed that there is a significant difference in the air entry values, even though both studies were carried out on the same soil under similar testing conditions. The difference in air entry values can be attributed to different initial water contents and sample preparation methods resulting in different soil structures (Vanapalli et al., 1999). Haghighi's samples were prepared by tamping and at 51% water content and were not saturated afterward before drying. The samples used for this study were statically compacted (at 17% water content) and then saturated afterwards. Hence, the sample herein had a hydraulic history. From the compaction curve presented in Sec. 3.2.4, the position of the sample used by Haghighi (2011) is on the wet side of optimum, whereas the sample used in this study is located on the dry side of optimum. Samples at

the dry side of optimum have large pore spaces between soil aggregates or open void structure (Uchaipichat & Khalili, 2009). On the other hand, samples at the wet side appear homogenous without aggregated structure (Vanapalli, 1999). Because of this, the pore size distribution of wet and dry of optimum samples are different as explained in Sec. 2.3.3. This is the reason for the low air entry values obtained from the SWRC in this study relative to the values obtained by Haghighi. Since the sample at w = 17% has larger pore spaces than the sample at w = 51%, smaller suction will be required to desaturate the sample at w of 17% from a saturated state. The study of Ng & Pang (2002) on sandy clay and Gao et al. (2016) on silty clay made similar observation. They observed that the air entry values increased with increasing initial water content or the air entry value is higher for sample prepared at wet of optimum than sampled at dry of optimum.

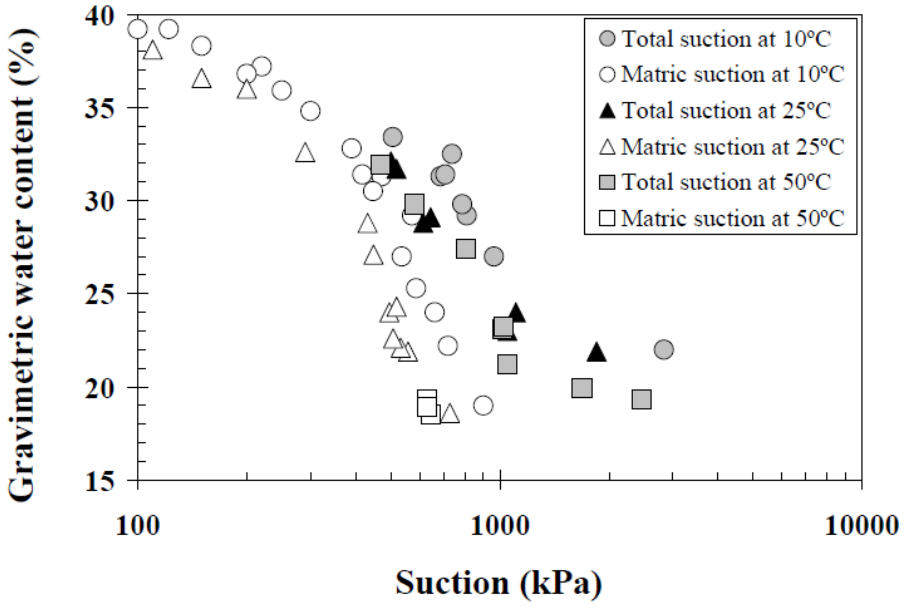

Figure 6-3 Drying paths at different temperatures 10, 25 and 50°C (Haghighi, 2011)

Table 6-5 Comparison of drying paths in Haghighi (2011) and this study

	Haghighi (2011)	Current study
Void ratio	1.5	1.49
Water content (%)	51	17
Temperature (°C)	25	25
Air entry value (kPa)	230	13

6.2.2 Effect of void ratio on the primary drying path

The drying curves at e_0 = 1.0 and 1.49 for the different temperatures (25°C and 50°C) previously presented are compared in Fig. 6.4. The aim was to ascertain the influence of void ratio on the primary drying paths of compacted kaolin clay. The two samples were compacted at the same initial water content (w = 17%) but different void ratios; e_0 = 1.0 & 1.49, with different compaction stress 759 and 180kPa respectively. From Fig. 6.4b it could be observed (as indicated by the arrows on the figure) that an increase in void ratio resulted in a decrease in air entry value (from 15kPa to 13kPa) for result at 25°C, consistent with some findings in literature (e.g. Tinjum et al., 1997: Tarantino, 2009). At 50°C, Fig. 6.4a, the air entry values of the two samples are similar (10kPa and 9.9kPa for e_0 = 1.0 and 1.5 respectively).

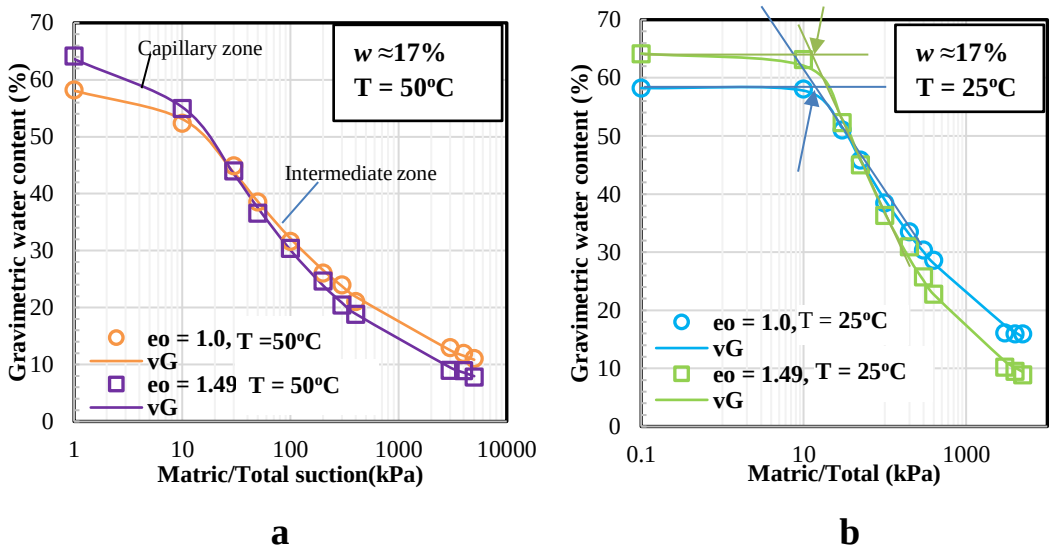

Figure 6-4 Comparison of the drying paths at different void ratios; e_0 = 1.0 and 1.49 (a) $PP1_{50}$, $PP2_{50}$ (b) $PP1_{25}$, $PP2_{25}$

The decrease in air entry value with an increase in void ratio can be attributed to large pores in e_0 = 1.49 relative to the size of pores in e_0 = 1.0. From Fig. 6.4a & b, at the two temperatures considered, samples at e_0 = 1.49 plotted above sample at e_0 = 1.0. This indicates higher water content along the capillary fringe zone (0kPa – 10kPa matric suction) and is attributed to high porosity of samples at e_0 = 1.49 compared with samples at e_0 = 1.0. Larger volume of water is required to fill up the large void spaces in sample at e_0 = 1.5 like the observation of Kasangaki (2012). However, along the intermediate zone (20kPa – 400kPa) and high suction zone (3000kPa – 5000kPa), the samples at e_0 =

1.0 exhibited higher water content with increasing matric suction than samples at e_0 = 1.49. This could be linked to the high rate of desorption of the sample at e_0 = 1.5 along the intermediate zone, which can be seen from the slope of the curves (Table 6.4). The samples at e_0 = 1.49 have larger pore spaces, interconnecting throats and pore radii than the samples at e_0 = 1.0. Larger pore spaces will drain faster than smaller pores, once the air entry value is exceeded. This can explain the reduction in water content observed in sample at e_0 = 1.49 relative to e_0 = 1.0 at the same suction value (at the intermediate and high suction zone). Several researchers (e.g. Tinjum et al., 1997; Romero & Vaunat, 2000; Romero et al., 2001; Jacinto, 2009; Tarantino, 2009) have studied the effect of void ratio on water retention. A general observation from their studies is that air entry suction will increase with a decrease in void ratio, in line with the capillary model that predicts an increase in air-entry suction with a decrease in the diameter of the primary pores. Tarantino (2009) demonstrated that an increase in air entry value was associated with a decrease in void ratio through water retention data plotted in terms of degree of saturation versus suction. Although when the results were plotted in terms of water ratio (V_w/V_s) versus suction, the influence of void ratio was less pronounced. In the study, the water retention of reconstituted and compacted Barcelona silt and kaolin clay, were obtained following a hydraulic path (removing or adding water to samples to vary their degree of saturation) and mechanical path (compressing samples at constant water content). Tarantino observed that the water retention curves obtained along a wetting path were independent of the mechanism by which degree of saturation was varied.

Romero & Vaunat (2000) observed an increase in water content with increasing void ratio at low suction values (0 - 2MPa) along the main drying curve. However, at high suction values (up to 200MPa), convergence of the curves (plotted in terms of water content versus suction) at different void ratios was observed. Their study was carried out on kaolinitic-illitic soil compacted at different void ratios. They explained that this was due to the intra aggregate voids being unaffected by compaction. Miller et al. (2002), Jacinto et al. (2009), also made similar observation on MX-80 bentonite tested at 60^{o}C. At high suction values, the intra aggregate water and clay mineralogy control the water retention behaviour of clays soils, while the inter-aggregate water is responsible for the water retention at low suction levels (Tarantino & De Col, 2008; Jacinto et al., 2009). Compaction of the same soil to different void ratio at the same compaction water content is associated with the compression of the inter-aggregate voids with the intra-aggregate voids unaffected. Convergence of the SWRCs is usually expected at high suction for

samples with the same water content, even if the initial void ratios were different. This is because, the intra-aggregate water of samples at the same initial water content is expected to be the same and is evident from the result shown in Fig. 4.7. Compaction to different void ratio but the same water content would result to changes in the inter-aggregate water only, with the intra aggregate water remaining the same. In this study, convergence of the curves at the e_0 = 1.0 and 1.5 was not observed at high suction, for the suction range considered. Convergence of the curve might be observed if the suction values are extended, but further data will be required to confirm this hypothesis.

6.2.3 Assessment of fitting parameters for the primary drying curve

Because of the difficulty associated with measuring the data points required to establish a full and continuous SWRC, mathematical models proposed for SWRC are usually best fitted to the limited experimental data to define a typical and continuous SWRC. The conventional SWRC models were reviewed in Chapter 2. The experimental data for the primary drying curves obtained at 25^{o}C and 50^{o}C were fitted with the SWRC models proposed by van Genuchten (1980); Equation 6.1 & 6.2 below and Fredlund & Xing (1994); Equation 6.3 (see Table 6.6).

The parameters w, w_s, and ψ were obtained from experimental data. The residual water content (w_r) was considered as the water content at 3000kPa suction, as that seems to mark the onset of residual condition. The consideration to adopt 3000kPa as the residual suction was based on van Genuchten (1980) definition of w_r, which he described as the water content at which the water retention curve becomes constant with increasing suction, resulting in zero gradient. van Genuchten (1980) recommended that w_r be treated as an independent fitting parameter in a case where it is difficult to measure w_r experimentally. Fredlund & Xing (1994) suggested that the residual water content can be taken as water content at 1500kPa. But this was not possible in this study, as there was no experimental data at 1500kPa. Initial fitting parameters were obtained from values reported by Ghanbarian-Alavijeh et al. (2013) for clay soils (m is between 0.34 – 0.02; α is between 50.3 – 0.01). The fitting parameters for the adopted models were finally determined using least square procedure as explained by van Genuchten (1978), Fredlund & Xing (1994), Leong & Rahardjo (1997), Wraith & Or (1998). This was done by altering the initial fitting parameters by iteration until the square differences between the measured and predicted data were minimised.

Table 6-6 vG (1980) and FX (1994) models for SWRC

No	Equation	Authors	Fitting Parameters
6.1	$w = w_r + \frac{(w_s - w_r)}{[1+(a_{vg}\psi)^{n_{vg}}]^{m_{vg}}}$	van Genuchten (1980) –Mualem (1976)	a_{vg}, n_{vg}, m_{vg}. The model is reduced to a close form by fixing m_{vg} (m_{vg} = 1-1/ n_{vg})
6.2	$w = \frac{w_s}{[1 + (\psi a_{vg})^{n_{vg}}]^{m_{vg}}}$	van Genuchten (1980)	a_{vg}, n_{vg}, m_{vg}
6.3	$w = C(\psi)\frac{w_s}{[\ln(e+(\frac{\psi}{a_f})^{n_f}]^{m_f}}$	Freudlund & Xing (1994)	a_f, n_f, mf, $C(\psi)$ $C(\psi)$ is a correction factor that causes the SWRC to pass through 10^6kPa at zero water content
6.4	$C(\psi) = \left[1 - \frac{\ln\left(1+\frac{\psi}{\psi_r}\right)}{\ln\left(1+\frac{1000000}{\psi_r}\right)}\right]$		

Where w is water content, w_r is residual water content, w_s is saturated water content, ψ is matric suction at low suction values (0 – 400kPa) and total suction at high suction values (3000kPa upwards from experimental data).

Fig. 6.5 - Fig. 6.7 show the drying curves at 25^{o}C and 50^{o}C fitted to van Genuchten (1980) with fixed parameter, van Genuchten (1980) without fixed parameter, Freudlund & Xing (1994). From the figures, the R^2 for all the models as shown in Table 6.7 are greater than 98% indicating an acceptable fit to the models. However, visual inspection of Fig. 6.5 shows that the van Genuchten Equation with two parameters did not fit perfectly at high suction zone (3000 – 5000kPa). Similar observation was made by Nimmo (1991), Ross et al. (in Assouline et al., 1998). In their studies, they observed that van Genuchten model with two parameters exhibited a good fit at high and medium water content, but fitted poorly at low water content (along the residual zone). In Eq. 6.1 (Table 6.6), the m parameter was related to n by the equation m = 1-1/n in an attempt to obtain a closed form equation, making the equation a two-parameter equation. This however has been reported to reduce the flexibility of the model (Fredlund & Xing, 1994) and may be the reason for the poor fit at the high suction zone, since a considerable fit was obtained at high suction zone using Eq. 6.2 (without fixed relationships between m and n). Consequently, the van Genuchten equation with two parameters will not be considered further. The focus will then be on van Genuchten's equation with three parameters (Eq. 6.2) and Fredlund & Xing (Eq. 6.3). As stated earlier, the two models exhibited satisfactory fit to the experimental data based on R^2 values in Table 6.7. The fitting parameters obtained from the two models are shown in Table 6.8. However, van Genuchten (1980) model was

adopted over Fredlund & Xing (1994) model because it is simpler to use for the estimation of hydraulic conductivity as will be shown later in this chapter. Additionally, the goodness of fit of the models was assessed using the Akaike Information Criterion. Surprisingly, van Genuchten (1980) exhibited better fit than Fredlund & Xing (1994) even though it has been reported that van Genuchten (1980) is best suited for cohesionless soils while Fredlund and Xing (1994) is best for cohesive soils (Leong et al., 1997). The values of AIC obtained with vG were lower than the values obtained with F & X as shown in Table 6.7.

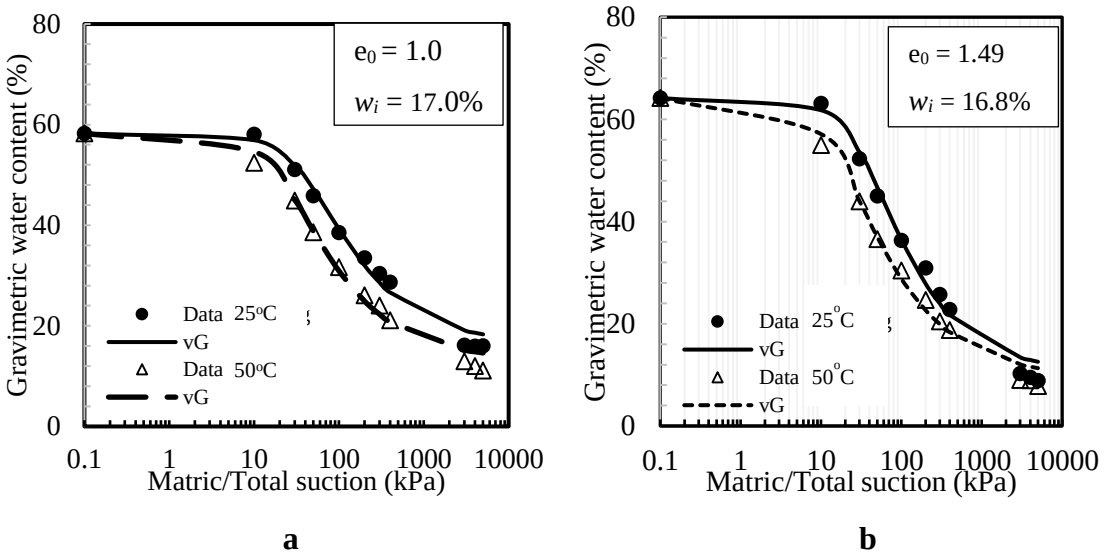

a **b**

Figure 6-5 Drying curves at 25°C and 50°C fitted with van Genuchten Equation with two fitting parameters (a) e_0 = 1.0 (b) e_0 = 1.49

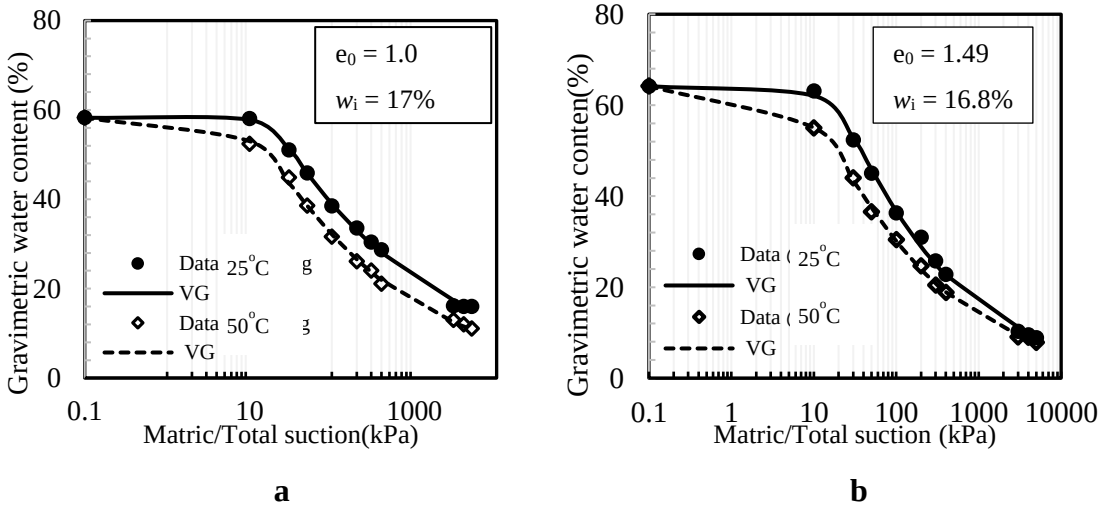

a **b**

Figure 6-6 Drying curves at 50°C and 25°C fitted with modified van Genuchten Equation with three fitting parameters (a) e_0 = 1.0 (b) e_0 = 1.49

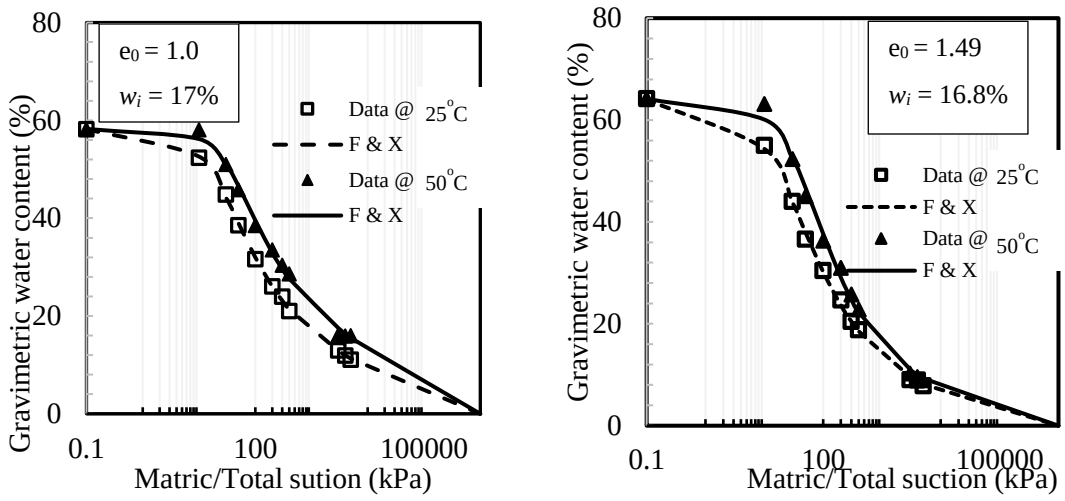

Figure 6-7 Drying curves at 50ºC and 25ºC fitted with Fredlund & Xing Equation (a) e_0 = 1.0 (b) e_0 = 1.49

Table 6-7 Assessment of goodness of fit of the SWRC models to the experimental data

Model	Temperature (ºC)	R^2 (%)		AIC (%)	
		e_0 = 1.49	e_0 = 1.0	e_0 = 1.5	e_0 = 1.0
vG	25	98.68	99.79	-	-
	50	98.89	99.68	-	-
vG without fixed parameters	25	99.94	99.98	7.53	3.6
	50	99.98	99.97	-8.96	-10.76
F & X	25	99.88	99.94	16.9	10.37
	50	99.94	99.98	2.6	-5.46

Table 6-8 Fitting parameters for vG (1980) and F &X (1994)

van Genuchten (1980) with three parameters					Fredlund &Xing (1994)				
Void ratio	Temperature (ºC)	Fitting parameters			Void ratio	Temperature (ºC)	Fitting parameters		
		a_{vg} (kPa)	n_{vg}	m_{vg}			a_f (kPa)	n_f	m_f
1.0	25	18	3.459	0.069	1.0	25	37	1.356	0.601
	50	12	1.630	0.171		50	24	1.137	0.818
1.49	25	20	2.094	0.167	1.49	25	43	1.148	1.030
	50	11	1.342	0.257		50	23	0.953	1.145

6.3 EXPERIMENTAL TEST RESULTS AND ANALYSIS OF THERMAL CYCLE TESTS

6.3.1 Effect of thermal cycles on suction values

Tests A1 – A3 ($e_0 \approx 1.0$) and B1 – B3 ($e_0 \approx 1.5$) in Table 6.2 were performed to study the influence of a thermal cycle (10°C - 25°C - 50°C - 25°C) on soil suction and volume change. Suction was measure through the filter paper method. The samples were subjected to a temperature of 10°C (path A Fig. 3.23) and allowed to equalise for 14days. The volume, water content and suction (total and matric suction) of the samples were obtained at the end of the equalisation (details are explained in Chapter 3). This was followed by a cycle of heating/cooling involving variation in temperature from 10°C to 25°C to 50°C (path C – D in Fig. 3.23) and then to 25°C from 50°C (path E). Each temperature step was also maintained for 14days for suction equalisation. The matric and total suction values after each temperature step were obtained from an average of 2 - 3 filter paper water content measurements. In some cases, the differences in value between individual data were up to 20%. In such situations, the standard deviation was employed for the selection of the most reliable data. The error and percentage uncertainty associated with each data point are shown in Tables 6.9 and 6.10. The repeatability of tests A2 for total and matric suction measurements are plotted in Fig. 6.8. The figure indicates that the repeatability is reasonable.

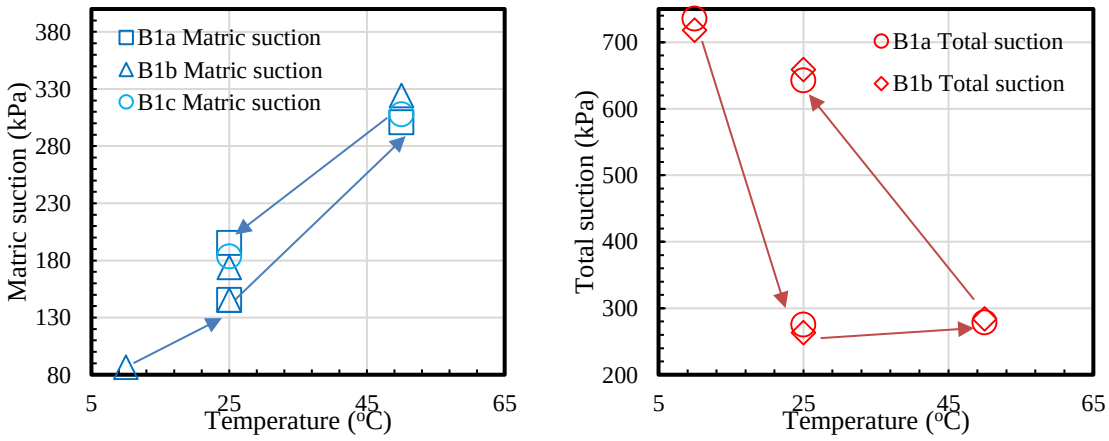

Figure 6-8 Repeatability of suction measurements with filter paper at different temperatures (a) Test B1 matric suction (b) Test B1 Total suction

Table 6-9 Errors associated with thermal cycle test (A); e_0 = 1.0

Test	T (°C)	Matric suction			Total suction		
		Mean	Std. error	% uncertainty	Mean	Std. error	% uncertainty
A1	10	300.40	5.40	1.80	4823.60	3.60	0.07
	25	229.00	2.00	0.87	421.40	6.40	1.52
	50	143.40	3.20	2.23	573.90	3.90	0.68
	25	273.40	5.40	1.98	578.00	4.00	0.69
A2	10	610.60	5.60	0.92	2262.90	7.40	0.33
	25	338.50	0.50	0.15	1156.60	5.70	0.49
	50	267.40	7.60	2.84	1265.60	5.20	0.41
	25	769.60	5.80	0.75	1559.50	0.00	0.00

Table 6-10 Errors associated with thermal cycle tests (B); e_0 = 1.49

Test	T (°C)	Matric suction			Total suction		
		Mean	Std. error	% uncertainty	Mean	Std. error	% uncertainty
B1	10	82.50	4.10	4.97	727.10	8.70	1.20
	25	145.50	0.00	0.00	269.30	6.03	2.24
	50	312.70	11.73	3.75	281.40	2.75	0.98
	25	184.60	10.70	5.80	650.70	8.20	1.26
B2	10	526.30	5.90	1.12	2448.70	17.40	0.71
	25	274.10	7.20	2.63	368.70	8.50	2.31
	50	118.10	0.00	0.00	737.40	11.00	1.49
	25	197.50	2.80	1.42	776.60	4.30	0.55

The filter paper calibration equations proposed by Haghighi (2011) were adopted and used to estimate the suction values from the measured filter paper water contents. The calibration equations were obtained at 10°C, 25°C and 50°C for Whatmann No. 42 filter paper using vapour equilibrium and axis-translational techniques. The results obtained from test A1- A2 and B1 – B2 are shown in Table 6.11 and 6.12 respectively. Results from Test A3 and B3 were discarded because the suction values were suspicious; differences of more than 30% (in filter paper water content) were obtained in most cases between repeated measurements of each data point. It is likely that samples were too dry for any reasonable estimate of matric suction. From Table 6.11 and 6.12, it emerged that increasing temperature influenced the matric suction in the samples. For instance, in Table 6.11 (see also Fig 6.9), an increase in temperature from 10°C to 50°C resulted in a decrease in matric suction from 300.4±5.4kPa to 143±3.2kPa for sample A1 (e_0 = 1.0, Sr = 59.8%) and from 610±5.6kPa to 267±7.6kPa for A2 (e_0 = 1.0, Sr = 30%). In Table 6.12, an increase in temperature from 10°C to 50°C also resulted in a decrease in matric suction from 526±5.9kPa to 118kPa for sample B2 (e_0 = 1.49, Sr = 29.7%). On the

contrary, an increase in matric suction was observed with increasing temperature for sample B1 (e_0 = 1.48, Sr = 59.1%) from 82±4.1 to 312±11.7kPa. This could be linked to increased evaporation in the sample with increasing temperature due to large void spaces in the sample as explained in Sec. 3.2.5. Evaporative fluxes occur because of difference in vapour pressure between soil pores and surrounding air and increase with decreasing relative humidity and high porosity (Romero, 1999). The decrease in matric suction with increasing temperature exhibited by samples A1, A2, B2 are in consistent with the findings of Gardner (1955), Chahal (1964), Faybishenko (1983).

Table 6-11 Measured suction values following a thermal cycle for A1 and A2 (e_0 = 1.0)

Sample	e_0	*Sr* (%)	T (ºC)	Matric Suction (kPa)	Total Suction (kPa)	Osmotic suction (kPa)	e_f	Sr_f (%)
$A1_{10}$	1.00	59.8	10	300.4	4823.6	4523.2	1.08	57.4
$A1_{25}$			25	229.0	421.4	192.3	1.03	56.9
$A1_{50}$			50	143.4	573.9	430.5	1.09	28.2
$A1_{25}$			25	273.4	578.0	304.7	1.07	26.3
$A2_{10}$	1.00	30	10	610.6	2262.9	1652.3	1.07	28.0
$A2_{25}$			25	338.5	1156.6	818.1	1.10	18.49
$A2_{50}$			50	267.4	1265.6	998.2	1.20	2.6
$A2_{25}$			25	769.6	1559.5	789.9	1.17	0.7

Table 6-12 Measured suction values following a thermal cycle for B1 and B2 (e_0 = 1.49)

Sample	e_0	Sr_i (%)	T (°C)	Matric Suction (kPa)	Total Suction (kPa)	Osmotic suction (kPa)	e_f	Sr_f
$B1_{10}$	1.48	58	10	82.5	727.1	644.6	1.20	68.6
$B1_{25}$			25	145.5	269.3	123.7	1.35	55.0
$B1_{50}$			50	312.7	281.4	-31.3	1.33	38.5
$B1_{25}$			25	184.6	650.7	466.1	1.30	34.6
$B2_{10}$	1.48	30	10	526.3	2448.7	1922.4	1.52	38.4
$B2_{25}$			25	274.1	368.7	94.6	1.52	38.3
$B2_{50}$			50	118.1	737.4	619.4	1.53	38.6
$B2_{25}$			25	197.5	776.6	579.0	1.55	38.8

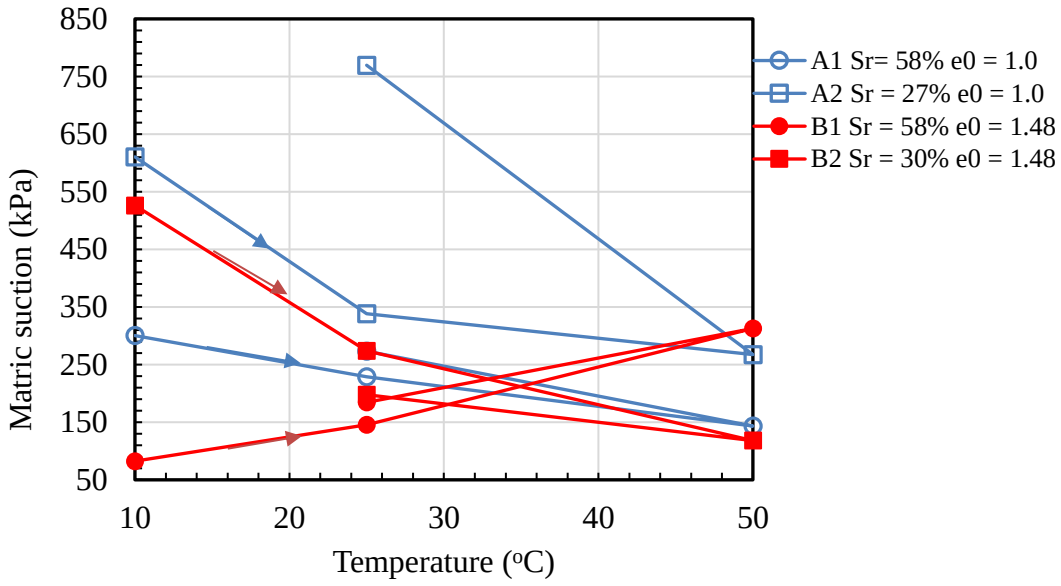

Figure 6-9 Variation of matric suction with temperature for A (e_0 = 1.0) and B (e_0 = 1.48)

Earlier soil scientists, e.g. Gardner (1955), Philip & de Vries (1957), Chahal (1964), have studied the influence of temperature on matric suction or capillary pressure extensively. A common conclusion from their studies is that matric suction decreases with increasing temperature. More recently, Jacinto et al. (2009) in an attempt to investigate the effect of temperature on the water retention of compacted MX 80 bentonite (at two densities; 1600 and 1750kg/m^3) observed decrease in matric suction with increasing temperature at the

two dry densities. Temperature effect was obvious at low suction values. Shuai et al. (2002), in an attempt to quantify the effect of temperature on the calibration curve of a thermal conductivity sensor also observed a decrease in matric suction with increasing temperature (8 – 23^{o}C). The influence of temperature on matric suction is attributed to the relationship between surface tension and temperature (Nimmo & Miller, 1986; Bachmann, 2002). From Kelvin's capillary model, matric suction is directly proportional to surface tension. Surface tension on the other hand is highly sensitive to temperature; as it decreases with increasing temperature (Kaye & Laby, 1973 in Fredlund et al., 2012). Through Kelvin's model, matric suction will decrease with increasing temperature because of the decrease in surface tension with temperature increase. However, evidence has shown that the effect of temperature on matric suction is greater than would be expected from surface tension alone (Bachmann, 2002). Other factors such as change in contact angle with change in temperature, thermal expansion of trapped air and water and the influence of solute on surface tension are attributed to the temperature dependency of matric suction (Peak, 1960; King, 1981; Hopman & Dane, 1986; Nimmo & Miller, 1986; Chahal, 1995, Haghighi, 2011). Of all the listed factors, Bachmann (2002) demonstrated that the solute effect on surface tension and temperature induced changes in contact angles are the major factors that contribute to temperature dependency of matric suction.

During the cooling stage, from 50^{o}C to 25^{o}C, an increase in matric suction was observed in sample A1, A2 and B2 as shown in Table 6.11 and 6.12 respectively (see also Fig. 6.10). Conversely, a decrease in matric suction was observed in sample B1 on cooling. Similar studies by Gardner (1955) and Haghighi (2011) observed a slight decrease in matric suction on cooling. A possible explanation for the increase in matric suction observed on cooling might be drying out of the samples and the filter papers. From Fig. 6.13 a & b, presented and discussed later in this chapter, it could be observed that all the samples experienced significant decrease in water content on heating and cooling. For example, sample A1 experienced about 50% decrease in water content on heating to 50^{o}C. It is possible that total suction values rather than matric suction were obtained on cooling due to dry samples. In all the samples, the matric suction values did not revert to the initial values on cooling. Gardner (1955 in Bachmann, 2002) also observed from coarse sand that matric suction was irreversible, even with two cycles of heating and cooling (between 0 – 50^{o}C). Faybishenko (1983) observed reversibility of matric suction in loam soil after a temperature cycle (0 - 20^{o}C). The results obtained in this study cannot draw

strong conclusion on whether the matric suction will be reversible with numerous thermal cycles, as samples were subjected to one thermal cycle.

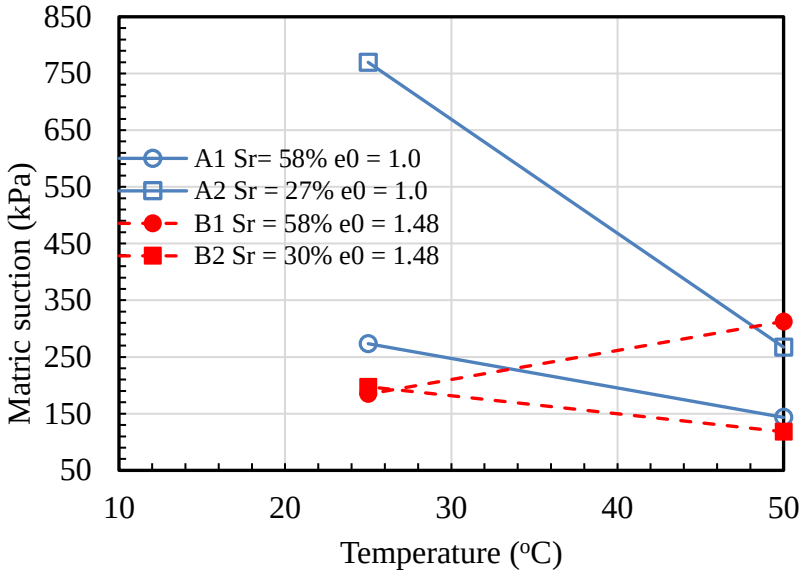

Figure 6-10 Matric suction measurement on cooling from 50°C to 25°C

Total suction values at varying temperatures (10-25-50-25°C) estimated from filter paper suspended on top of the samples are presented in Fig. 6.11 and in Table 6.11 and 6.12. From the Figure, it could be observed that temperature changes influenced the values of measured total suction, but the results do not show a definite trend. For instance, an increase in temperature from 10°C to 25°C, resulted in a decrease in total suction of samples A1, A2, B1and B2 with initial water contents of 22, 10, 32 and 17% respectively. However, on heating from 25°C to 50°C an increase in total suction was observed in all the samples. E.g. A1 had a total suction value of 4823.6±3.6kPa at 10°C. An increase in temperature from 10°C to 25°C resulted in a reduction of total suction to 421.4±6.4kPa. Further increase in temperature to 50°C resulted in an increase in the measured total suction by 36% (574kPa). This was not anticipated and does not agree with other findings. It was expected based on theory that an increase in temperature will increase the relative humidity around the sample and in turn decrease total suction. Romero et al. (2001) and Yang et al. (2013) observed a decrease in total suction with an increase in temperature on compacted Boom clay and Bentonite samples respectively. However, the results obtained in this study are consistent with the findings of Haghighi (2011). He observed a decrease in total suction of compacted kaolin clay by 310kPa when heated from 10 to 25°C and an increase by 2100kPa when heated from 25°C – 50°C.

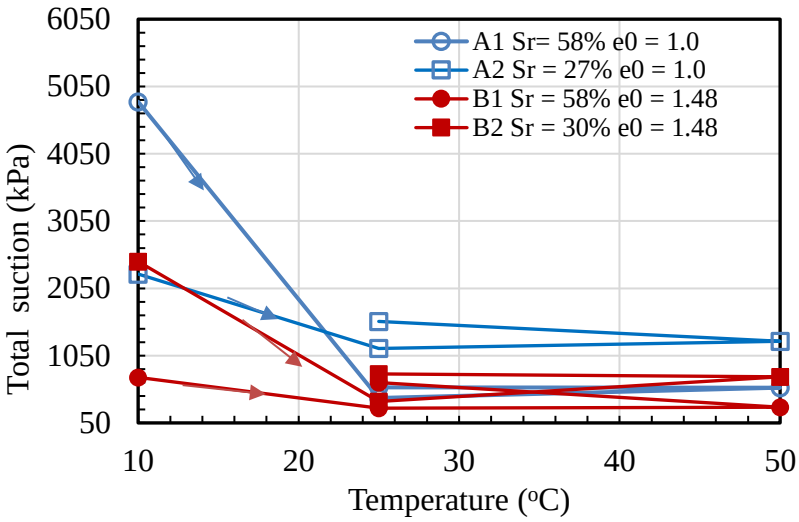

Figure 6-11 Variation of total suction with temperature for samples A (e_0 = 1.0) and B (e_0 = 1.48)

Fig. 6.12 shows the measured total suction values on cooling from 50°C to 25°C. From the figure, it emerged that total suction of A1 (Sr =59%, e_0 =1.0) and B2 (Sr = 30%, e_0 =1.48), seems unaffected on cooling. Sample A2 (Sr = 30%, e_0 =1.0) and B1 (Sr = 59%, e_0 =1.48) showed a substantial increase in total suction; $\Delta\psi_T$ = 294kPa (A2), $\Delta\psi_T$ = 370kPa (B1). From the obtained results, the effect of cooling on total suction is not clear. The only clear observation is that the total suction values were irreversible on cooling. Finally, from the results obtained, it could be inferred that temperature variation altered the values of suction in statically compacted kaolin clay for the initial conditions considered in this study.

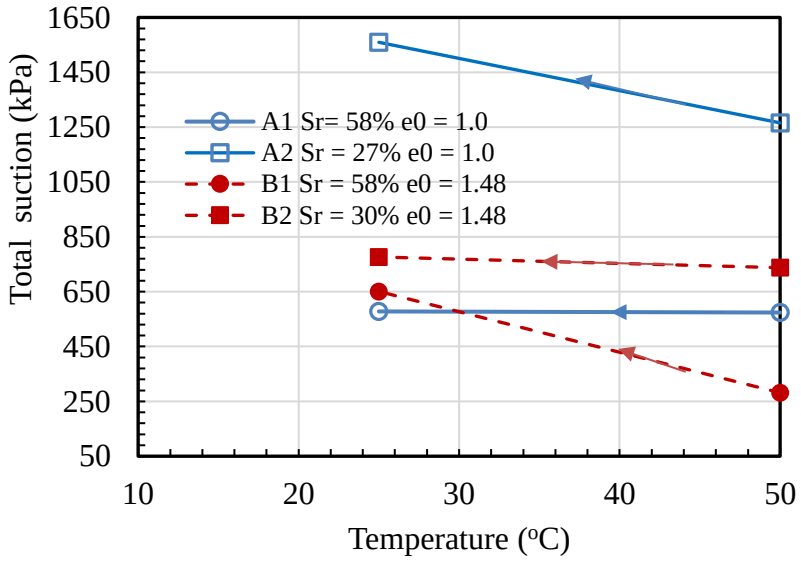

Figure 6-12 Total suction measurement on cooling from 50°C - 25°C

6.3.2 Effect of thermal cycles on water content and volume change

Fig. 6.13a & b show variation in water content of samples A1(e_0 = 1.0, *Sr* = 58%), A2(e_0 = 1.0, *Sr* = 27%), B1(e_0 = 1.48, *Sr* = 58%) and B2(e_0 = 1.48, Sr = 29%) with temperature. A notable decrease in moisture contents was observed in A1, A2, B1 and B2 during heating (from 10°C to 50°C), indicating that at a given void ratio, water content decreases with increasing temperature. In addition, the curves for A2, B1 and B2 tend to have a constant slope, while there was a change in slope of the A1 curve (Fig. 6.13a) on heating from 25°C to 50°C. Result from A1 shows that water content was almost constant on heating from 10°C to 25°C (Δ_w = 1.1%), while water content decreased significantly on heating from 25 to 50°C (Δ_w = 10.5%). Decreases in water contents with increasing temperature were also reported by other researchers; Romero et al. (2001), Romero (1999) and Wan (1996). In particular, Romero et al. (2001) subjected statically compacted Boom clay to four different temperatures (22, 40, 60 and 80°C). The samples were prepared at low water content and compacted to different initial dry densities (14.7 to 20.6kN/m^3). Total suction was imposed on each sample through vapour equilibrium method and then allowed to equilibrate at the specified temperatures. It is worth mentioning that changes in water content in Romero et al. (2001) were driven not only by temperature, but also suction flux whereas in this study, they were driven by temperature alone. The decrease in water content on heating may be linked to evaporation in the sample. From earlier discussion, it was explained that an increase in temperature will increase the rate of evaporation resulting in the reduction of water content of the samples.

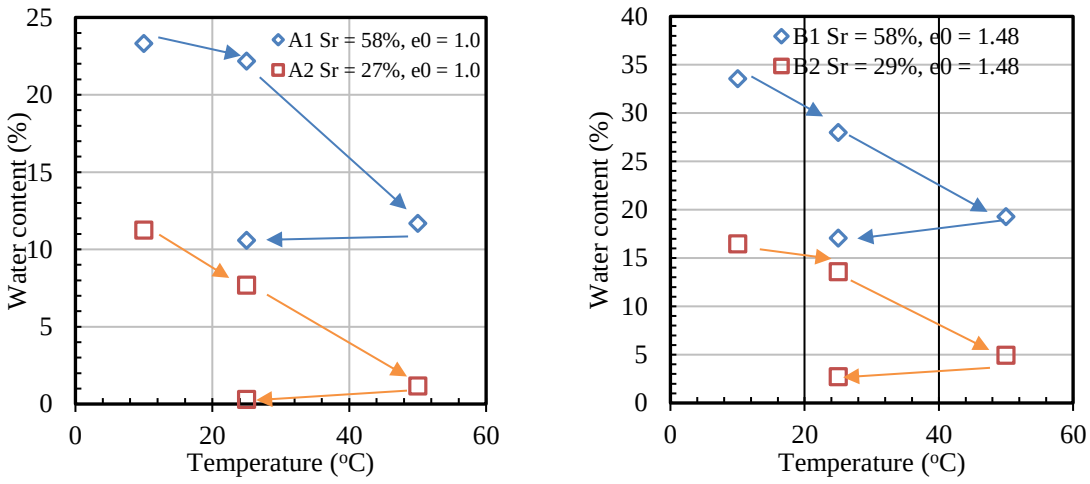

a **b**

Figure 6-13 Variation in sample water content with temperature (a) e_0 = 1.0; A1, A2 (b) e_0 = 1.48; B1, B2

Cooling (50°C – 25°C) was associated with a small decrease in water content. This was not expected and an explanation could not be given for it. It was expected that water content will increase or remain the same on cooling. The effect of temperature on water content was significant on heating than on cooling, as small changes in water content were observed on cooling (e.g. $\Delta w_{\text{max cooling}}$ = 2.23% in B1).

The dimensions of the samples used for the thermal tests were measured at the end of every temperature step. Fig. 6.14, shows variation of final void ratio with temperature. The results indicate that volume change occurred in the samples because of temperature change, but strong inference could not be drawn from the obtained results due to considerable scatter in experimental points.

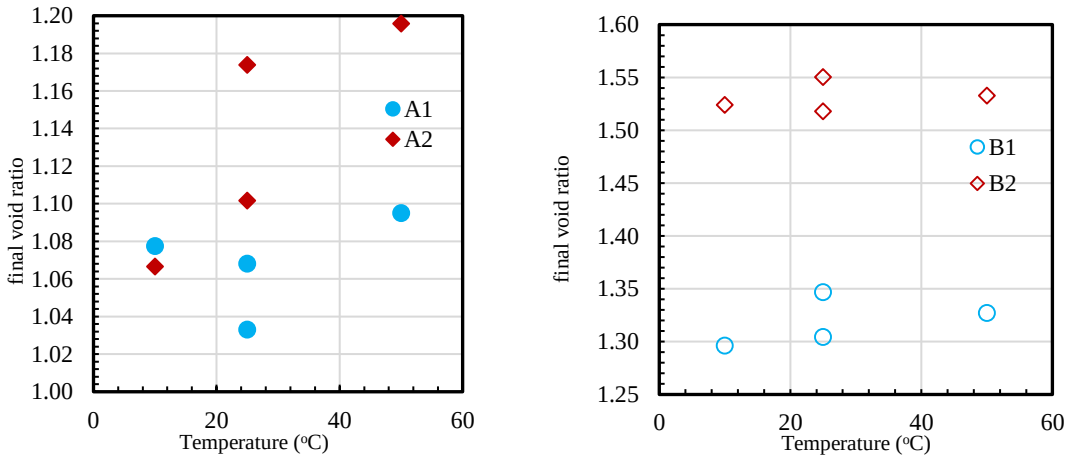

Figure 6-14 Variation in final void ratio with temperature

6.4 ANALYSIS AND PREDICTION OF UNSATURATED PERMEABILITY

In this Section, the results of saturated coefficient of permeability and the prediction of unsaturated coefficient of permeability from SWRC are presented. The coefficient of permeability is required in the design of many geotechnical and geo-environmental structures such as retaining walls, earth dams and pavements to analyse flow problems (Lobbezoo & Vanapalli, 2002). Unlike other properties of soils such as shear strength and volume change, the coefficient of permeability varies widely up to ten orders of magnitude for soils ranging from coarse grain to fine grained soil (Fredlund et al., 2012). For compacted fine grained soil, it can vary from three to six orders of magnitude for suction between 0 and 500kPa (Lobbezoo & Vanapalli, 2002). According to Fredlund et

al. (1994), the broad range of coefficient of permeability is the major difficulty associated with analysing seepage problems.

6.4.1 Result of saturated coefficient of permeability

Falling head permeability tests were performed to determine the saturated permeability coefficient of preheated kaolin clay samples statically compacted to two different void ratios (1.0 and 1.5). The samples were preheated at 25^{o}C and 50^{o}C. Each test was repeated twice and an average of the test results was taken. The obtained results are shown in Table 6.13. The Table indicates that permeability increases with increasing void ratio. For instance, the sample compacted at e_0 = 1.5 and preheated to 25^{o}C had higher permeability (1.17 x 10^{-8}m/s) than the sample at e_0 = 1.0 (5.04 x 10^{-9}m/s) at corresponding temperature. This is expected because sample with greater void ratio will have larger pore spaces for water to travel through. Samples preheated at 50^{o}C exhibited higher permeability than samples preheated at 25^{o}C. This seems reasonable because heating to 50^{o}C may have caused invisible cracks in the samples through which water can flow.

Table 6-13 Saturated permeability for samples at e_0 = 1.0 and 1.5

Void ratio	Permeability (m/s)	
	Preheated to 25^{o}C	Preheated to 50^{o}C
1.5	1.17 x 10^{-8}	4.50 X 10^{-8}
1.0	5.04 x 10^{-9}	6.67 x 10^{-9}

6.4.2 Unsaturated coefficient of permeability function

The unsaturated coefficient of permeability can be obtained directly through experimental procedure, e.g. steady state method, one step out flow method (Gardner, 1956), infiltration tests (Ye, 2010) or can be estimated indirectly from the SWRC and saturated permeability coefficient (K_s). Like the SWRC, experimental procedures to obtain the unsaturated coefficient of permeability is costly and time consuming. Indirect method is usually adopted to obtain the unsaturated coefficient of permeability. The indirect methods are grouped into four categories, namely; empirical, regression, correlation and statistical method. The common models for indirect estimation of the unsaturated coefficient of permeability are shown in Table 6.14 (Eq. 6.5 – 6.8). Equation 6.5 is a

statistical model obtained from Burdine (1953) model in conjunction with van Genuchten SWRC equation. By relating van Genuchten fitting parameters n_{vb} and m_{vb} ($m_{vb} = 1-2/n_{vb}$) and using it in Burdine's model, a closed form equation (Eq. 6.5) was obtained, which is commonly known as van Genuchten-Burdine permeability equation. The equation is simple to use because it does not require the complexities of integration (Fredlund et al., 2012). Equation 6.6 is a statistical model obtained by substituting van Genuchten (1980) SWRC equation in Mualem (1976) integration model. In this case, van Genuchten's equation was reduced to a two-parameter equation, by relating the fitting parameters n_{vm} and m_{vm} in the form $m_{vm} = 1-1/n_{vm}$. This was then substituted into Mualem's statistical model to obtain a closed form equation commonly called van Genuchten-Mualem permeability equation (van Genuchten, 1980; Fredlund et al., 2012). This equation also has the advantage of being simple to use. Equation 6.7 is Fredlund et al. (1994) model and was obtained by substituting Fredlund & Xing (1994) SWRC equation into Childs & Collis-George (1950) model. The equation is not a closed form equation and involves the complexities of numerical integration. Nonetheless, prediction of permeability coefficient with the model has been compared with experimental data and showed close agreement (Fredlund et al., 2012). Equation 6.8 is a correlation equation developed by Leong & Rahardjo (1997). The equation is simple, but its accuracy depends on the fitting parameter q obtained from fitting measured permeability data.

Table 6-14 Equations for evaluating unsaturated hydraulic conductivity

No	Equation	Authors	Parameters
6.5	$k_r(\Psi) = \frac{k_w(\Psi)}{k_s} = \frac{1-(a_{vb}\Psi)^{n_{vb}-2}[1+(a_{vb}\Psi)^{n_{vb}}]^{-m_{vb}}}{[1+(a_{vb}\Psi)^{n_{vb}}]^{2n_{vb}}}$	Burdine (1953), van Genuchten (1980)	m_{vb} = fitting parameter set equal to $1\text{-}2/n_{vb,}$ n_{vb} = fitting parameter from van Genuchten (1980) equation best fit to the SWRC, k_w = unsaturated coefficient of permeability, k_s = saturated permeability coefficient ψ = soil suction, a_{vb} = fitting parameter related to inverse of air entry value
6.6	$k_r(\Psi) = \frac{\{1-(a_{vm}\Psi)^{n_{vm}-1}[1+(a_{vm}\Psi)^{n_{vm}}]^{-m_{vm}}\}^2}{[1+(a_{vm}\Psi)^{n_{vm}}]^{0.5}}$	Mualem (1976), van Genuchten (1980)	m_{vm} = fitting parameter set equal to $1\text{-}1/n_{vm,}$
6.7	$k(\theta) = k_s \int_{\theta_L}^{\theta} \frac{\theta - x}{\psi^2(x)} dx \Big/ \int_{\theta_L}^{\theta_s} \frac{\theta_s - x}{\psi^2(x)} dx$	Fredlund et al. (1994b)	ψ = soil suction as a function of volumetric water content θ, x = dummy variable of integration representing water content, θ = volumetric water content, θ_s = volumetric water content at saturation, θ_L = lower limit for volumetric water content
6.8	$k_r(\psi) = k_s[\Theta_d(\psi)]^q$	Leong & Rahardjo (1997a)	$\Theta_d(\psi)$ = dimensionless water content form θ/θ_s for SWCC, q = correlation-based soil fitting parameter.

6.4.3 Prediction of relative permeability function at different temperatures and void ratios

Relative permeability functions of the statically compacted kaolin clay samples were predicted from the drying SWRC using van Genuchten-Mualem permeability model (Eq. 6.6). The permeability functions were estimated at 25°C and 50°C for the two void ratios; 1.0 and 1.49. Fitting parameters a_{vm} and n_{vm} obtained by fitting the van Genuchten (1980) SWRC model to the experimental data were used in Eq. 6.6 to predict the relative permeability function. The reason for analysing the data in terms of relative permeability function is because the saturated permeability tests were not conducted under controlled temperature, rather the samples were pre-heated to 25 and 50°C and then tested at room temperature. To obtain unsaturated permeability coefficient, the relative permeability function is multiplied by the saturated permeability coefficient as can be seen from Eq.

6.5. The fitting parameters a_{vm} and n_{vm} were obtained in terms of suction versus water ratio. This is because the permeability model requires fitting parameters obtained in terms of volumetric water content. Since the water retention data were obtained in terms of gravimetric water content, the SWRCs were re-analysed in terms of water ratio e_w by multiplying the gravimetric water content by the specific gravity $e_w = wGs$ (Tarantino & De Col, (2008). The use of volumetric water content in the analysis of SWRC is linked to the dependence of capillary forces on particle volume (which influences the pore size) rather than particle density (Kasangaki, 2012). Water ratio is used in some cases in place of volumetric water content (e.g. Tarantino, 2009; Romero et al., 2011; Kasangaki, 2012) since it also compares system volume rather than density.

The obtained results plotted in terms of relative permeability function versus suction are shown in Fig. 6.15. The results indicate that the permeability function decreases with increasing suction within the suction range of 1 – 1000kPa and becomes constant with increasing suction between 3000kPa – 5000kPa. For instance, at a temperature of 25^{o}C and e_0 = 1.49, the result indicates that as suction is increased from 10kPa to 3000kPa, the relative permeability function, decreased from 1.588 x 10^{-2} to 3.80 x 10^{-4} and becomes constant with subsequent suction increases. This indicates that permeability is significant at low suction region with the predominance of inter-aggregate pores and bulk water. This trend agrees with the study of Folly (2001) on kaolin clay using Gardner's one-step outflow method, Cui et al. (2008), Loiseau (2001) on a mixture of Kunigel bentonite & Houston sand, Ye et al. (2012) on GMZ01. The findings of Cui et al. (2008), Loiseau (2001) and Ye et al. (2012) showed that unsaturated hydraulic conductivity increases with an increase in suction at high suction region and then decreases with suction increase at low suction region. For instance, in Loiseau (2001), the decrease in permeability with increasing suction was observed at suction values less than 23MPa. In Ye et al. (2012), decrease in permeability with increasing suction was observed at suction values lower than 20MPa (similar to the finding of this study) then becomes constant between 20MPa and 55MPa as shown in Fig. 6.16. At suction value between 55MPa – 80MPa a slight increase with increasing suction was observed resulting in a U-shaped permeability versus suction curve. The results of this study are in line with the studies of both Loiseau, (2001) and Ye et al., (2012) within the range of suction considered (1kPa – 5000kPa).

From Fig. 6.15a & b, the effect of void ratio on relative permeability function can be observed. The figures indicate that as void ratio increases, relative permeability function increases. This is clearly seen in the tests at 50^{o}C, the curve at e_0 = 1.49 plotted above

the curve at e_0 = 1.0 between 1 – 400kPa suction with both curves converging from suction of 3000kPa. This is expected and agrees with other studies (e.g. Romero et al., 2001). Two possible explanations are given for this behaviour. Firstly, high void ratio is associated with large void spaces that offers less resistance to the flow of water, thereby resulting in high permeability as observed on sample at e_0 = 1.49. Secondly, it is considered that the swelling tendency of sample at e_0 = 1.0 (as reported in Sec. 4.3.1) may have caused resistance to the flow of water by reducing the size of the macro-pores.

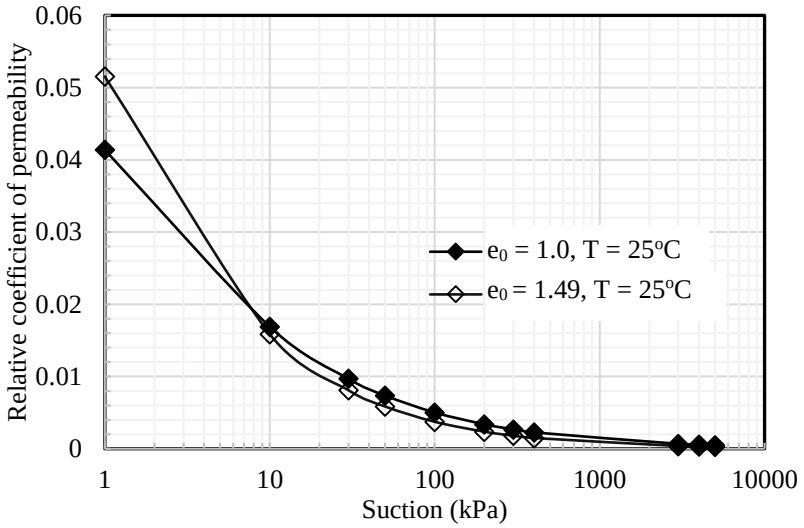

a

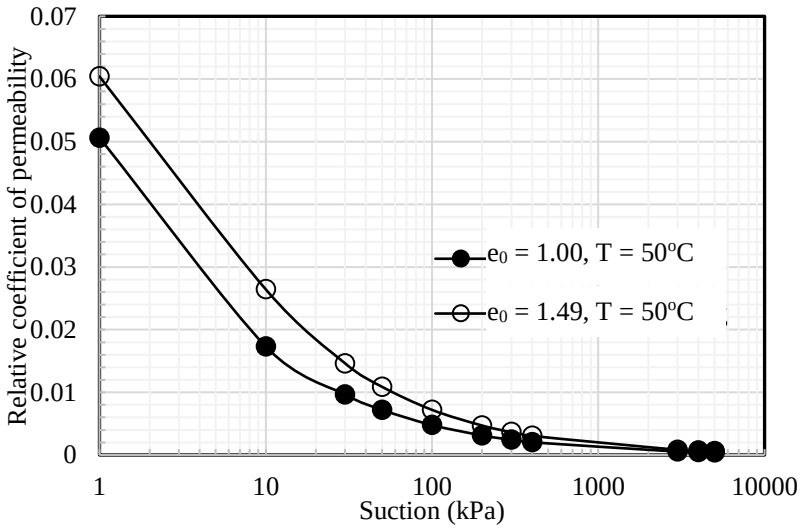

b

Figure 6-15 Relative coefficient of permeability versus suction at e_0 = 1.0 and 1.49 (a) T = 25ºC (b) T = 50ºC

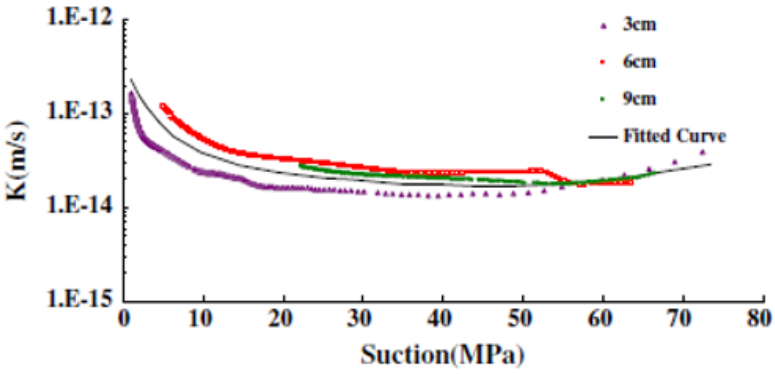

Figure 6-16 Coefficient of permeability function versus suction for GMZ01 (Ye et al., 2012)

To investigate the influence of temperature on relative coefficient of permeability, the estimated relative coefficient of permeability at 25^{o}C and 50^{o}C were compared as shown in Fig. 6.17a & b. From the figures, it could be observed that the relative coefficient of permeability increased with temperature increase. This is obvious at suction values between 1kPa - 10kPa for sample at e_0 = 1.0 and between 1kPa - 400kPa for sample at e_0 = 1.5. This indicates that the relative permeability of compacted kaolin is sensitive to temperature in the near saturation zone associated with bulk water and insensitive to temperature at high suction zone. This is consistent with the findings of Cho et al. (1999), Romero (1999) on bentonite.

The influence of temperature on saturated permeability is attributed to the dependence of permeability on viscosity (Cho et al., 1999). However, for unsaturated soils, Romero (2001), Zhang et al. (2013) observed small temperature dependence of permeability than could be predicted from temperature influence on viscosity and suggested thermal alteration of clay fabric due to thermo-chemical interactions as a possible influence. In this study, the influence of temperature on the relative permeability of kaolin clay is small especially at e_0 = 1.0. From the obtained results, the factor responsible for temperature dependence of permeability cannot be identified. Macro-structural studies will be needed to gain a better understanding of this.

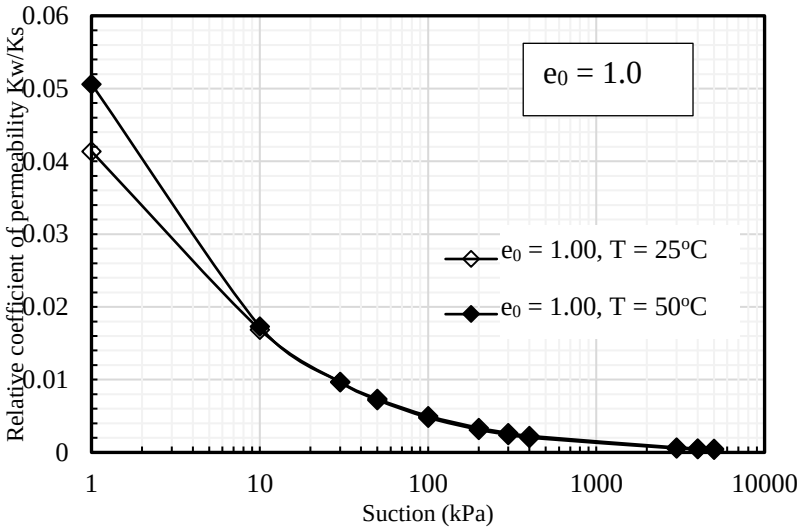

a

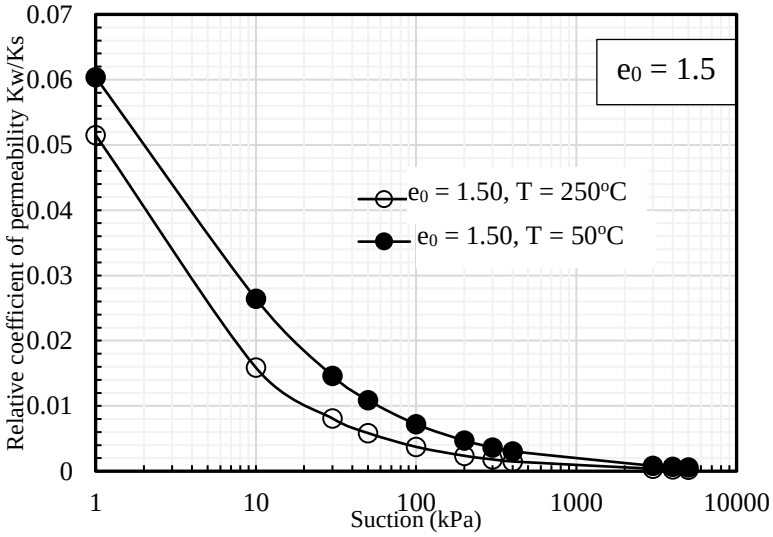

b

Figure 6-17 Relative coefficient of permeability versus suction at 25°C and 50°C (a) e_0 =1.0 (b) e_0 = 1.5

6.5 CONCLUSION

In this chapter, the influence of temperature on water retention, hydraulic conductivity and suction of compacted kaolin clay at e_0 = 1.5 and 1.0 were studied. The obtained results indicated that an increase in temperature affects the water retention capability by reducing it. The air entry values estimated from the SWRC were significantly different from those reported on kaolin clay prepared wet of optimum. Void ratio was found to influence the SWRC. In the inter-porosity region, samples at a void ratio of 1.5 had higher retention capability. In the intra-porosity region, however, samples at 1.0 displayed

higher water retention capability due to increased rate of desaturation of sample at e_0 = 1.5. Furthermore, soil suction was found to be affected by temperature increase; matric suction decreased with temperature, but total suction displayed no clear trend. The influence of temperature on relative permeability was found to be significant in the intra-porosity region with the predominance of bulk water in line with other studies.

CHAPTER SEVEN

7 DISCUSSION OF RESULT FINDINGS

7.1 MICRO AND MACRO STRUCTURAL CHANGES ASSOCIATED WITH DIFFERENT TESTING PATHS

In an attempt to demonstrate that an increase in temperature will influence the volume change and hydraulic behaviour of kaolin clay without hydraulic history differently, temperature controlled tests under different stress paths were carried out on statically compacted kaolin clay. A better understanding of the influence of temperature on kaolin clays will help to predict their behaviour accurately.

In this study, volume change and water retention of samples were measured in a suction and temperature controlled oedometer tests under the following stress paths: loading at constant suction and temperature; increasing temperature at constant suction and vertical net stress; drying at constant temperature and vertical stress. Through consolidation based analysis, it was identified in Secs. 5.2.1 and 5.3.1 that an increase in temperature to 50^{o}C increased the compressibility associated with loading, an outcome known as thermal softening. The results are in line with other findings in the literature (e.g. Di Donna & Laloui, 2015; Haghighi, 2011; Folly, 2001). The behaviour associated with thermal softening are explained from macrostructural point of view. The structure of a compacted kaolin clay as explained in Sec. 2.3.3 is made of intra-aggregate and inter-aggregate pores, with absorbed water located in the intra-aggregate pores and usually considered as part of the soil skeleton (Hueckel 2002). Generally, temperature affect the soil through the water in the void spaces. Various researchers attempted to explain thermal softening of clay soils using diffused double layer theory, which was based on the physico-chemical repulsive and attractive forces at particle contacts. While some researchers, e.g. Dixon (1993) reported that increase in temperature reduces the thickness of double layers in clay through reduction of the repulsive forces, Mitchell (1993) demonstrated that double layer was not affected by temperature. However, the thermal softening observed in Secs. 5.2.1 and 5.3.1 can be explained based on changes in the absorbed water and inter-particle contact. A general observation regarding macrostructural changes associated with increasing vertical net stress is the reduction of macro pores (Delage & Lefebvre, 1984; Juang & Holtz, 1986; Romero, 1999; Koliji et al., 2005). Micro pores are only affected when all the macro pores have been completely closed on loading. Increase in

temperature on loading results in loss of absorbed water (Paaswell, 1967; Huang et al., 1994) and breaking of bonds at inter particle contacts (Pons et al., 1994). These changes result in increased compressibility and a denser packing of soil skeleton and account for the additional volume change observed on loading heated samples as reported in Sec. 5.2.1 and 5.3.1.

Additionally, it was identified in Sec. 5.3.1(ii) that compressibility reduced with increasing suction, in agreement with the findings of Romero et al. (2003), Estabragh & Javadi (2013). This can also be explained by considering the structural changes associated with increasing suction. For non-active clays like kaolin, changes in suction modify only the macro-structure (Simms & Yanful, 2001). At high suction (210kPa in this study), the stability of soil is increased through the meniscus water at the inter-particle contacts (Wheeler et al., 2003). Meniscus water produces additional normal force at the inter-particle contact that inhibit sliding and rearrangement of the macrostructure (Romero, 1999). This explains the observation in Sec. 5.3.1. As suction increased, the inter particle contacts were influenced by meniscus water, thereby giving the sample extra rigidity against sliding, thus, volume change on loading was less because the sample gained rigidity from suction increase.

In Sec. 5.3.1, it was also observed that the magnitude of volume change associated with the suction imposition prior to loading was small compared to the value reported by Haghighi for kaolin clay, under similar conditions (Fig. 5.8 – 5.10). The difference was linked to different phenomena; shrinkage in Haghighi (2011) and collapse in this study. Both samples have the same initial void ratio (1.5) but the sample used in this study could be described as an unsaturated sample with bimodal pore size distribution while the sample used by Haghighi could be explained as saturated with the unimodal pore size distribution. Although similar values of suction were imposed, the water retention path in each case was different; drying path for shrinkage and wetting path for collapse. Wheeler and Karube (1996) explained that there are different arrangements of soil water in the voids for drying and wetting path and these affect the mechanical behaviour of soils in different ways. This may explain the huge difference in the magnitude of volume change. Simms and Yanful (2001) demonstrated that drying (increasing suction) will result in a progressive increase in micro-pore due to reduction in macro-pores. This finding was also confirmed by Romero (2011). Regarding the macrostructural behaviour associated with wetting, Suriol et al. (1998) and Thom et al. (2007) demonstrated that wetting results in the reduction of macro-pores or fusing of aggregates due to loss of

rigidity, but in this case, the bimodal pore size of compacted clay was not broken down. If wetting only changes the volume of macro-pores without converting them to micro pores, then this explains the small magnitude of strain observed in Fig. 5.8 and 5.9. Increase in micro-pores due to reduction in macro-pores that is associated with drying, implies that the macro pores have been reduced to the sizes of micro-pores which resulted in significant volume change. This explains the high magnitude of strain reported by Haghighi (2011).

In Sec. 5.3.2, results of thermally induced volume change at constant suction and vertical net stress were presented. The results showed that the compacted kaolin clay samples subjected to a thermal cycle at a constant suction and vertical net stress experienced volume reduction. The behaviour of the samples under each stress path is associated with different macro/micro structural changes. For instance, in Fig. 5.16, the sample was subjected to an initial suction of 30kPa. This was considered a wetting process, because the initial suction was 286kPa. Subsequent stress path involved an increase in vertical net stress to 55kPa. Both stress paths will affect the macro-pores (Suriol & Lloret, 2007; Thom et al., 2007). Whereas wetting to 30kPa will reduce the sizes of macro-pores but not necessarily reduce them to the sizes of micro-pores, increase in vertical net stress to 55kPa may reduce the macro-pores to micro-pores. However, additional research is required to confirm to what extent the macro-pores will be reduced due to the loading to 55kPa. Under the applied suction and vertical net stress, temperature was increased from 25^{o}C to 50^{o}C. Shrinkage was observed under this path and is linked to reduction in micro-pores due to water losses (Romero, 2005).

7.2 COMPRESSIBITY IN TERMS OF LC YIELD CURVES

The influence of matric suction and temperature on the volumetric response of kaolin clay presented in Sec. 5.3.1 is discussed in the light of LC yield curves. Fig. 7.1 shows paths taken by Tests $L1_{(25)}$ and $L2_{(25)}$ during loading at constant matric suctions (30kPa and 210kPa) and temperature (25^{o}C). From the testing paths presented in Fig. 3.13, the matric suction in the two tests were reduced to 30kPa and 210kPa in Test $L1_{(25)}$ and $L2_{(25)}$ respectively along wetting paths. The suction reduction paths are not shown on the LC curves. At the imposed suction and temperature points, the sample was loaded up to 415kPa. Since the samples used in $L1_{(25)}$ and $L2_{(25)}$ had the same initial state, their yield stresses were part of the same primary yield curve and shown as curve LCc in Fig. 7.1.

The inclination of the curve shows increase in yield stress with increasing matric suction. The responses of the samples agree with those reported in literature; that increase in suction increases yield stress *p0* (Alonso, et al., 1987; Sivarkumar & Wheeler, 2000) and delays the onset of plastic straining. This could be seen in paths A (30kPa) and B (210kPa) at constant suction loading. Path A reached the yield curve; LC_C before B, showing an earlier onset of plastic straining in A and a relatively small magnitude of elastic strain. On reaching the primary yield curve LC_C, the yield curve expanded to LC_A and LC_B for paths A and B respectively. Similar behaviour was observed in Tests $L1_{(50)}$ and $L2_{(50)}$ conducted at 50°C, as shown in Fig. 7.2. The yield stress increased with suction. In Path E, $L2_{(50)}$ at a suction of 210kPa yielded at 100kPa vertical net stress, whereas in path D, $L1_{(50)}$ tested at a suction of 30kPa yielded at 35kPa. The difference in the yield stresses resulted in an inclined primary yield curve LC_C, as shown in Fig. 7.2. The influence of an increase in suction is eminent from the figure. In path E, at a matric suction of 210kPa, the magnitude of elastic compression (path 1-2) was greater than the plastic compression (path 2–3). Conversely, in path D, at 30kPa matric suction, the observed plastic compression (path 5-6) was greater than the elastic compression (path 4-5). In all, an obvious effect of loading at high suction, is a decrease in the magnitude of plastic strain and an increase in the yield stress, also known as suction induced hardening (Ng & Zhou, 2014).

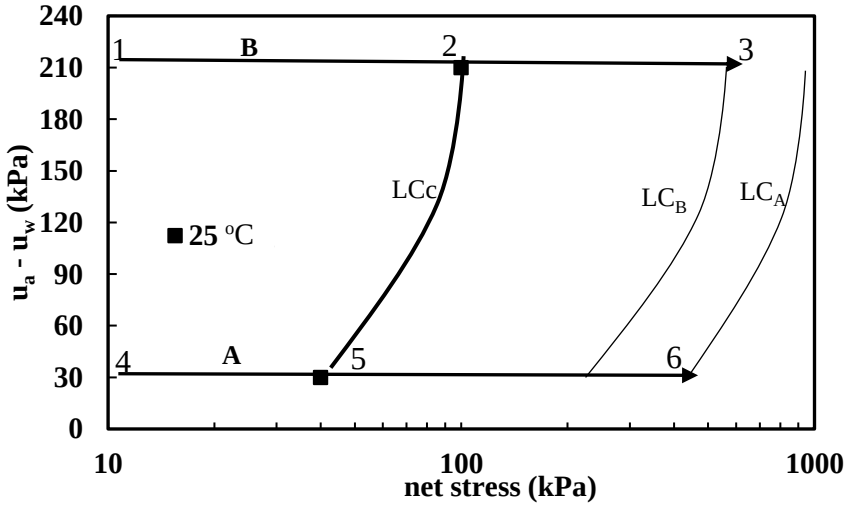

Figure 7-1 Tests $L1_{25}$ and $L2_{25}$ (e_0 = 1.5) represented in LC curve

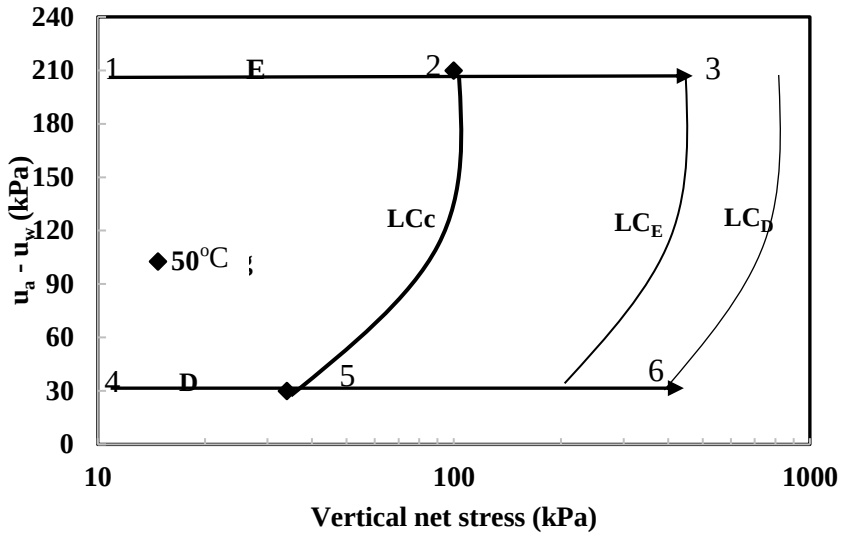

Figure 7-2 Test $L1_{50}$ and $L2_{50}$ represented in LC curve (e_0 = 1.48)

Finally, the effect of temperature on the compression behaviour of statically compacted kaolin clay is presented with an LC curve, as shown in Fig. 7.3. From the figure, an increase in temperature resulted in contraction of the yield curve (at low matric suction 30kPa) and a change in the curve's position i.e. a shift to the left consistent with Ileme et al. (2016). This is like the effect of a decrease in compaction stress, as reported by Sivakumar & Wheeler (2000). However, the result does not completely agree with previous findings. Other researchers have reported a shift of the yield curve to the left with temperature at all values of suction. For instance, Ng and Zhou (2014) demonstrated that the yield curve of a compacted silty clay soil shifted to the left with an increase in temperature (20 – 40°C) at all values of suction (0, 30 and 60kPa). Similar finding was also made by Haghighi (2011) on kaolin clay tested at 10 and 50°C at suction values of 0, 300 and 500kPa. The inconsistency may be explained by variation in sample structure from mode of sample preparation. It is possible that the suction level of 210kPa was high enough to resist the influence of temperature. However, this cannot be confirmed, as it requires additional data at temperature values higher than 50°C, which is above the range of temperature that can be achieved with the testing equipment.

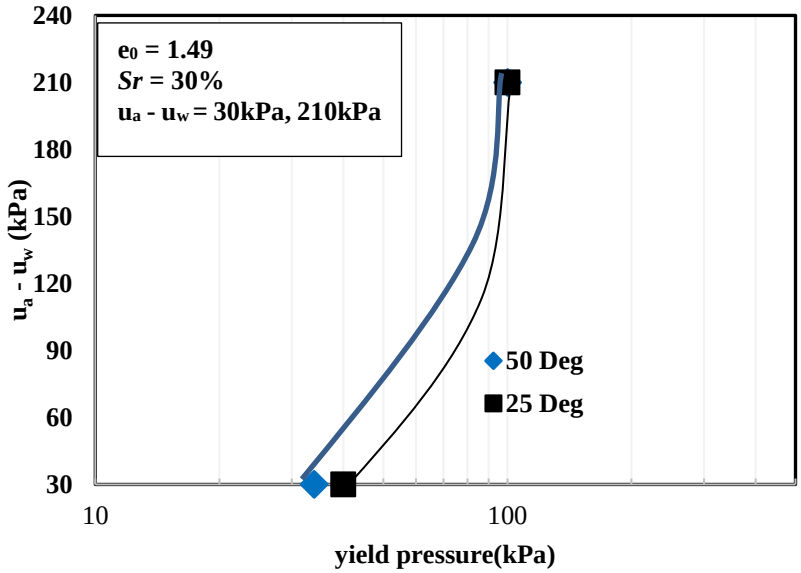

Figure 7-3 LC curves at 25°C and 50°C

7.3 SWRC AND RELATIVE PERMEABILITY COEFFICIENT

In Sec. 6.2, the influence of temperature and void ratio on the SWRC was investigated by considering a drying SWRC obtained at 25 and 50°C; e_0 = 1.5 and 1.0. The mathematical models of van Genutchen (1980) and Fredlund & Xing (1994) were fitted to the experimental data. The values of R^2 obtained which were between 98.7 - 99.8% for both models showed good fit to the data. Since the R^2 values for both models indicated acceptable fit, additional measure of fit known as Akaike information criterion (AIC) was used to assess the goodness of the fit. The AIC gives an estimate of information lost when a model is used to represent an experimental process or used as a means of generating data. The calculations of AIC were made with a computer software known as "SWRC fit". The values of the AIC for the individual data are presented in Table 6.6. In all cases, it was found that values of AIC obtained from van Genuchten (1980) were lower than the values obtained for Fredlund & Xing (1994), making vG model a better fit to the data. Leong and Rahardjo (1994) have reported that F & X model is best suited for fine grain soils while vG model is best for coarse grain soils. However, the AIC result and some other evidences in literature (e.g. Alonso et al., 2013; Yang & You, 2013) have shown that vG model can be fitted satisfactory on SWRC data obtained from a clay soil. For the fitting parameters, the values obtained for m_{vg} and n_{vg} are within the range reported for clay soils (Ghanbarian-Alavijeh et al., 2013). In Sec. 6.2, the influence of temperature on the SWRCs under a drying path were analysed. The analysis indicated that an increase in temperature reduces the water retention capability of the sample. In all the results, an

increase in temperature resulted in a reduction of the air entry suction value and a shift of the water retention curve to the left, consistent with the literature (Hopmans & Dane, 1986; Villar & Lloret, 2003; Villar & Gomez-Espina, 2008; Haghighi, 2011, Ye et al., 2014). A typical water retention curve is characterised by intra-porosity and inter-porosity regions and temperature influence are associated with different mechanisms depending on the region (Romero et al., 2001). The inter-porosity which is the region at high water content is characterised by a capillary storage mechanism which may be in the form of bulk water depending on the void ratio. The influence of temperature on water retention in this region is linked to temperature dependence on surface tension, thermal expansion of entrapped air (Hopmans & Dane, 1989, Nimmo & Millar, 1989). This suggests that an increase in temperature will increase the water drainage rate, and explains the lower air entry value obtained at 50^{o}C relative to 25^{o}C (Fig. 6.2). The intra- porosity region is characterised by adsorption storage mechanism. Zhang et al. (1993) explained that temperature induced changes on water retention in this region is caused by thermo-chemical disturbances that alter the clay fabric.

In terms of void ratio, the results presented in Fig 6.4 indicate that water retention increases with an increase in void ratio in the inter-porosity region and decreases at some point before the intra-porosity region. The sample at a void ratio of 1.5 is characterised by larger void spaces compared to samples at void ratio of 1.0, thus the curve at 1.5 plotted above the curve at 1.0, indicating higher water retention. However, as suction is increased, these large void spaces will offer less resistance to drainage, thus, a reversal in the trend was observed and the curve at 1.0 plotted above. The reversal in trend is not an inherent characteristic of all SWRC, it is highly dependent on the soil structure and rate of desaturation with increasing temperature. For instance, Romero et al. (2001) demonstrated that the SWRC of Boom clay at 13.7kN/m^3 consistently plotted above the SWRC of Boom clay at 16.7kN/m^3.

In the introduction, one of the hypothesis of this study is to explore if an increase in temperature will have the same effect on kaolin clay regardless of the hydraulic history. In Sec. 6.2, it was pointed out that the effects of temperature on water retention behaviour of soil with and without hydraulic history are quantitatively different. This was achieved by comparing the SWRCs from current study with SWRCs from Haghighi's study at corresponding temperatures. An obvious difference between the SWRCs from this study and those from Haghighi's study is higher air entry values and larger spread of data in

Haghighi's study. This difference indicates the importance of considering hydraulic history when attempting to predict the water retention properties of a soil.

The relative permeability coefficients at 25 and 50^{o}C were predicted from van Genuchten's hydraulic model. The obtained results indicated that the influence of temperature on permeability was significant in the inter-porosity region, with predominance of bulk water (Romero, 1999). The relative coefficient of permeability increased with increasing temperature in this region.

7.4 THERMALLY INDUCED SUCTION AND VOLUME VARIATION

In an effort to investigate the influence of temperature on soil suction and volume without controlling load and suction, unrestrained samples were subjected to a temperature cycle; total suction, matric suction and volume changes were measured from the samples. In Sec. 6.3, it was demonstrated that an increase in temperature affects the values of matric and total suction in the soil. The result obtained from Tests A1, A2 and B2 indicated that matric suction decreased with increasing temperature (Table 6.11 and 6.12). This was expected and agrees with reported literature e.g. Gardner (1955), Chahal (1964), Faybishenko (1983), Shuai et al. (2002), Jacinto et al. (2009). Decrease in matric suction with temperature is due to the influence of temperature on surface tension occurring from changes in contact angle and the concentration of solute. However, the result obtained from tests B2 opposed the trend reported in literature, an increase in matric suction was observed with increasing temperature. This may be explained by increased evaporative flux in the sample due to high porosity (Romero, 1999). As explained earlier in Sec. 4.3.1, B2 is an aggregated sample with relatively large void spaces. Evaporation was confirmed during testing from condensation of water observed on the top cap of the glass jar used for testing.

In case of total suction, the obtained results showed non-linear variation of total suction with temperature (see Fig. 6.11). Total suction decreased with an increase in temperature from 10 to 25^{o}C, but increased when the temperature was raised to 50^{o}C. The results are not in agreement with some previously reported effect of temperature on total suction, which is decrease in total suction with an increase in temperature (e.g. Romero et al., 2001; Yang et al., 2013). Total suction changes because of variation in relative humidity around the environment of a soil. The lack of trend in the observed effect of temperature on total suction may represent variation in relative humidity with temperature fluctuation.

Fredlund & Krhan (1972) reported that a temperature control within ± 0.001 must be maintained during total suction measurements. However, temperature data obtained from a back-up thermocouple used during thermal cycle tests showed temperature fluctuation at some points during testing.

7.5 APPLICATION OF RESEARCH FINDINGS

The result presented in this study has highlighted the effect of temperature on the mechanical and hydraulic behaviour of compacted kaolin clay. The findings of this study will enhance the understanding of the Geotechnical community on the effect of temperature on the volume change and water retention behaviour of compacted soils. Additionally, the results can be used to model or predict deformation and soil water retention of compacted inactive clays at 25 and 50^{o}C. However, the results presented in this study have been obtained from compacted kaolin clay samples with inherent structure and are not representative of all soil structure. Numerous researchers have demonstrated that soil structures greatly influence the mechanical and hydraulic behaviour of soils (e.g. Wheeler & Sivarkumar, 1995; Gao et al., 2016). Therefore, the result of this study can only be extended to inactive clays having similar structure. Additionally, the influence of temperature on SWRC investigated in this study was based on the drying path, therefore, the result can only be used to predict behaviour along a drying path. The results from this current study can be used over a limited range of suction; 0, 30, 210 and 286kPa for compressibility problems; 0 – 5000kPa for SWRC.

CHAPTER EIGHT

8 CONCLUSIONS AND RECOMMENDATIONS

8.1 CONCLUSIONS

This study has focused on the influence of temperature on the volumetric behaviour and compressibility properties of statically compacted kaolin clay, as well as identifying the effect of increasing matric suction on the compressibility of the soil. The study has investigated the effect of increasing temperature on the volume change behaviour of kaolin clay following loading, wetting/loading, wetting/drying paths. Furthermore, the study has investigated the influence of an increase in temperature on the water retention and hydraulic conductivity of compacted kaolin clay following a primary drying path. The study has also sought to find out whether earlier observed volume change, following a heating cycle, will revert on cooling. The impact of temperature cycle on measured suction, volume and water content was also explored. The findings in the literature on the influence of temperature increase on unsaturated clay soils are contradictory and soil specific; probably due to differences in mineralogical compositions and initial states of the soils. Previous studies on the influence of temperature on kaolin clay have been limited to reconstituted samples from slurry or samples prepared at wet side of optimum, without considering compacted samples on the dry side of optimum. Many studies have demonstrated that the behaviour of samples prepared wet of optimum is fundamentally different from compacted samples at dry of optimum. Given the increasing use of experimental data from kaolin clay for predicting the behaviour of inactive clays, it was considered important to investigate the effect of temperature on statically compacted kaolin clay. The study has sought to answer the following questions: will change in temperature affect the magnitude of volume change under a specific stress path? Is the influence of elevated temperature on soil water retention curve of compacted soils with hydraulic history the same as reported influence on soils without hydraulic history?

The conclusions drawn from various aspects of the study are summarised below.

8.1.1 Standard oedometer tests

Influence of void ratio and degree of saturation on volume change behaviour.

1) For samples at e_0 = 0.99 (group A), a negligible volume change was observed following a loading path. However, samples at e_0 = 1.48 (group B) experienced higher volume change on loading than samples at e_0 = 0.99, consistent with the observations of Estabragh (2004), Hagihigh (2011). For instance, at maximum vertical net stress (400kPa), the maximum change in void ratio for group B samples is 0.44. The higher volume change observed in group B samples relative to A can be linked to higher void ratio of the samples relative to group A samples. Compaction of soils to low density will result in an open structure formation (Alonso et al., 2013) or a soil with large inter aggregate voids (Delege et al., 1996). Increasing vertical net stress will then cause instability and collapse of the soil grains into the open structure and thus increase in compressibility. From macro-structural point of view, increase in vertical stress will result in the reduction of the macro-pores and sometimes micro-pores. But this is usually at a high level of stress when all macro-pores have closed (Delage & Lefebvre, 1984). The observed volume change in group B samples increased with increasing degree of saturation.
2) The influence of void ratio was clear on wetting at 5kPa. Swelling was observed on samples at e_0 = 0.99, which increased with decreasing degrees of saturation; an outcome consistent with the observations of Lawton (1989). Collapse on wetting at 5kPa was observed on samples at e_0 = 1.48. The observed collapse also increased with decreasing degrees of saturation. The swelling on wetting observed on samples at e_0 = 0.99 is linked to higher the dry density of the samples (1.34Mg/m^3) relative to samples at e_0 = 1.48 (1.11Mg/m^3). This type of expansion is categorised as inter-crystalline expansion, because water adsorption is limited to the void spaces and external crystal surfaces since the kaolin clay does not have an active clay mineral. Similar observations; collapse and expansion on wetting of loosely and densely compacted clays respectively have been reported by Lawton (1989), Sivarkumar & Wheeler (2000) and Montanez (2002).
3) From single oedometer tests, collapse behaviours were observed in the samples at e_0 = 0.99 and 1.48 on wetting at 200kPa. The applied stress was high enough to resist the expansion previously observed on samples at e_0 = 0.99 when wetted at 5kPa vertical stress. This indicates that the volume changes of samples at e_0 = 0.99 are dependent on the saturation stress; expansion at low stress values and collapse at high stress values. This is consistent with the observations of Monroy (2005).

4) Single oedometer tests in which samples at e_0 = 1.48 were wetted at different vertical stresses (25, 50, 100, 200kPa) showed that collapse on wetting increased with increasing applied vertical stress.
5) The normal compression lines for samples prepared at the same water content (w =17%) but different void ratios of e_0 = 1.5 and 1.0 coincided from a vertical stress of 50kPa following a loading after wetting path. This indicates that preparation of the samples to different void ratios, but the same water content may be explained as change in initial state.

Influence of void ratio and degree of saturation on yield, compressibility parameter λ and collapse potential (standard oedometer tests)

1) From constant water content oedometer tests, samples at e_0 = 0.99 and 1.49 yielded on loading. Irrespective of the initial void ratio, the yield stress decreased with increasing initial degrees of saturation or decreasing compaction effort, consistent with the findings of Sivarkumar & Wheeler (2000). The value of yield stress obtained in samples at e_0 = 0.99 (group A) for each degree of saturation was higher than the value obtained in samples at e_0 = 1.49 (group B) at corresponding degrees of saturation. This was linked to high dry density of group A relative to group B, which Sivarkumar & Wheeler (2000) explained as a beneficial effect, because increase in dry density delays yielding of samples and onset of plastic strain.

2) The soil state after yield stress is along a normal compression line because the maximum stress, which the soil has initially been subjected to has been exceeded. The normal compression lines were not observed in group A samples at the stress range considered, but were observed in group B samples and were not parallel. They were found to be divergent, with increasing initial matric suction consistent with the findings of Alonso et al. (1990) and Estabragh et al. (2004).
3) The slopes of the normal compression lines λ were observed to increase with increasing initial degrees of saturation.
4) Based on double and single oedometer tests obtained at e_0 = 1.49 with different initial degrees of saturation (59%, 29% and 14.2%), the collapse potential was found to increase with applied vertical stress to a maximum value (maximum collapse) and to decrease with further increases in vertical stress beyond the maximum collapse. This agrees with observations of Lawton et al. (1989),

Medero et al. (2003) and El-Howayek et al. (2011). The decrease in collapse potential beyond the maximum collapse is attributed to the breakdown of the meta-stable structure associated with collapsible soil Medero et al. (2003). The collapse potential from single and double oedoemeter tests was found to coincide for samples at *Sr* of 14.2 and 59%, but did not coincide for the sample at *Sr* = 29%. At all values of applied stress, the collapse potential was observed to increase with decreasing initial degrees of saturation or water content as expected and as noted by Lawton (1992). The stress values at which the maximum collapses occurred (also known as critical stress) were found to be independent of the initial degree of saturation.

5) Expansion followed by collapse was observed on samples at $e_0 = 0.99$, at different initial degrees of saturation. The transition from swell to collapse was within the stress range of 5 – 50kPa for the samples. Typical features of a CP curve (decrease in collapse potential beyond a critical value) were not observed at the stress levels considered. The observed expansion increased with a decrease in initial degrees of saturation, an outcome consistent with the observations of Lawton et al. (1989); Abbeche et al. (2007).

Influence of suction on yield, compressibility parameter λ and collapse potential (standard and suction controlled oedometer tests)

1) Loading of samples brought to initial matric suction values of 66kPa, 148kPa, 252kPa was accompanied by yielding. The yield stress was observed to increase with increasing initial matric suction, suggesting the stabilizing effect of suction. Yield stresses obtained from the tests defined a primary yield curve in a suction versus vertical net space (LC curve).
2) Loading tests, in which suction was maintained constant using an axis-translational technique, also revealed that at the studied temperature values (25 and 50^{o}C), the yield stress increased with increasing suction. This is similar to the observations of Haghighi (2011). An exception was the sample at matric suction of 286kPa tested at a temperature of 50^{o}C. The yield stress was observed to be lower than the yield stress of the sample at a matric suction of 210kPa at corresponding temperature. This reduction was due to a change in slope of the normal compression line and the fact that the stiffness of the sample increased at some point during testing, because of loss of water from the sample. The slopes

of the normal compression lines were found to be dependent on matric suction; they increased, with increasing matric suction as reported by Alonso (1990).

3) From suction controlled oedometer tests, collapse potential was found to increase with increasing matric suction in agreement with the observations of Rabbi et al. (2014).
4) The coefficient of volume compressibility *Mv*, was found to decrease with increasing matric suction between vertical net stress of 0 to 200kPa, suggesting the stabilizing effect of matric suction. Between 200kPa to 415kPa applied vertical net stress, *Mv* was insensitive to increasing matric suction.

8.1.2 Temperature and suction controlled oedometer tests

1) Initial reductions in suction from an initial suction of 286kPa to 30kPa and 210kPa were accompanied by collapse associated with wetting, as opposed to shrinkage phenomenon observed by Haghighi (2011) which is linked to drying. This outcome is due to the differences in structure between the samples used in this study (dry of optimum) and those used by Haghighi (2011) (wet of optimum). From macro-structural point of view, the collapse behaviour is linked to the reduction in the sizes of macro-pores, while shrinkage is associated with conversion of macro-pores to micro-pores (Simms & Yanful, 2001; Suriol & Lloret, 2007).
2) The influence of temperature on volume change of compacted kaolin clay has been demonstrated by the difference in the compressibility curves obtained at 25^{o}C and 50^{o}C from Tests $L1_{(25)}$ and $L1_{(50)}$ respectively on loading at a constant suction of 30kPa. The sample in test $L1_{(25)}$ yielded at a higher vertical net stress than the sample in test $L1_{(50)}$, indicating thermal softening. This is consistent with the observations of Folly (2004), Haghighi (2011), Di Donna & Laloui (2014) and Ng & Zhou (2014). Thermal softening is attributed to loss in adsorbed water and bond at the inter-particle contacts. The loss of bond is linked to thermal dilation of mineralogical components of clay soils (Laloui, 1993). Loading tests at a constant suction of 210kPa and temperatures of 25^{o}C and 50^{o}C (tests $L2_{(25)}$ and $L2_{(50)}$ respectively) showed a negligible difference in compressibility at the two temperatures. This suggests that the stabilizing influence of suction outweighed thermal dilation.
3) The slopes of the normal compression lines λ were found to be influenced by temperature at low suction (0 and 30kPa) but were insensitive to temperature at

high suction (210kPa); these outcomes are in line with the findings of Cekerevac & Laloui (2004) and Tang et al. (2008). The slopes λ at constant matric suction of 0 and 30kPa were found to increase with an increase in temperature from 25^{o}C to 50^{o}C.

4) The loading test at a constant suction of 30kPa, showed that temperature influenced the coefficient of volume compressibility *Mv* within the vertical net stress of 5 - 225kPa. *Mv* increased with an increase in temperature (from 25 – 50^{o}C). The significance of this is that in the field, soil subjected to high temperature and low suction will settle at a faster rate than corresponding soil at low temperature and at the same value of suction. At matric suction levels of 210kPa and 286kPa, the results were erratic and no clear trend was identified.
5) Collapse potential was found to increase with an increase in temperature at all values of suction.
6) Based on standard double oedometer tests, a shift of the critical stress towards lower value of vertical stress was observed with an increase in temperature; from 100kPa to 50kPa for the sample at e_0= 1.47, *Sr* =58.3% and from 400 to 200kPa for the sample at e_0 = 0.99, *Sr* = 28.4%. The maximum collapse potential was found to increase with temperature (up to 2%) in most cases, except in a case where the collapse was preceded by expansion (see Sec. 5.2.3)
7) An explanation of the temperature and suction controlled loading tests in the light of the LC model proposed by Alonso et al. (1990), indicated that the yield points derived from the loading paths at constant suction of 30kPa and 210kPa, were part of the same yield curve, for corresponding temperature. At matric suction of 30kPa, a contraction of the yield curve by a shift to the left was observed with an increase in temperature to 50^{o}C. This is like the effect of a decrease in compaction stress (Sivakumar & Wheeler, 2000). The position of the yield curve at 210kPa was unaffected by an increase in temperature.
8) Tests in which samples were loaded at a constant suction, and subsequently subjected to a thermal cycle under the imposed suction and vertical stress, revealed thermally induced strain on heating; a strain which was irreversible on cooling. Straining was greatest on loading, compared to imposing suction and heating combined. The observed strains on loading and heating were found to increase with an increase in initial water content, and to decrease with an increase in imposed matric suction.

9) Wetting (decreasing suction) and drying (increasing suction) tests at constant temperature and vertical stress, indicated the collapse of samples on wetting and shrinkage on drying. The collapse and shrinkage on wetting and drying respectively increased with an increase in temperature to 50^{o}C and was not accompanied by yield.

8.1.3 Soil water retention curve and hydraulic tests.

1) An increase in temperature was found to influence the water retention capacity of compacted kaolin at initial void ratios of 1.0 and 1.5 following a drying path. An increase in temperature to 50^{o}C shifted the drying water retention curve to low suction. SWRC at 50^{o}C lies to the left of SWRC at 25^{o}C suggesting a decrease in water content with an increase in temperature. The air entry values were found to decrease with an increase in temperature consistent with the findings of Villar & Lloret (2003), Villar & Gomez-Espina (2008), Haghighi (2011) Ye et al. (2014), whereas the slope of the water retention curve increased with increased temperatures.
2) The positions of the drying water retention curves were found to be affected by the initial void ratios. The water storage capacity of the samples increased with a decrease in void ratio along the intermediate and residual zone, and increased with an increase in void ratio in the capillary zone. The air entry suction was found to decrease with an increase in the void ratio as also observed by Tinjum et al. (1997), Tarantino (2009).
3) The Fredlund & Xing (1994), van Genuchten (1980) equations were found to provide a satisfactory fit to the SWRC data based on the values of R^2 obtained from the least square method. An additional method; AIC was used to check the goodness of fit. Based on the AIC values, van Genuchten (1980) equation performed better and was adopted.
4) Falling head permeability tests on samples (e_0 = 1.5 and 1.0) pre-heated to 25^{o}C and 50^{o}C, indicated that the coefficient of permeability increases with an increase in void ratio and preheated temperature. This is expected because an increase in void ratio is associated with larger void spaces.
5) The relative permeability function, predicted from the drying water retention curve using the van Genuchten-Mualem permeability equation, indicated that the permeability function increases with decreasing matric suction, which is

consistent with the finding of Folly (2001). The relative coefficient of permeability was found to increase with increasing temperature.

8.1.4 Thermal cycle tests

1) Matric suction in samples A1, A2 (e_0 = 1.0) & B2 (e = 1.5) subjected to a thermal cycle were found to decrease as temperature increases. This is consistent with the findings of Gardner (1955), Chahal (1965) and Faybishenko (1983). An exception to this is sample B1, in which an increase in matric suction was observed with increasing temperature. This was linked to increased rates of evaporation in the sample with an increase in temperature. On cooling from 50^{o}C to 25^{o}C, matric suction was observed to increase in samples A1, A2 and B2, but decreased in B1 (see Sec. 6.3.1).
2) Heating from 10^{o}C to 25^{o}C was accompanied by a decrease in total suction, whereas heating from 25^{o}C to 50^{o}C, was accompanied by an increase in total suction. This is contrary to thermodynamics theory and observations reported in literature (e.g. Romero et al., 2001; Yang et al., 2013). Theoretically, total suction decreases with increases in temperature. On cooling, the total suction values of A1 and B2 were not affected by temperature change, but total suction increased in A2 and B1.
3) Heating and cooling produced a net variation in overall volume of samples. However, there was a considerable scatter of the data and a definite trend could not be identified.

This current study has noted that while using experimental data to predict the behaviour of a soil, it is important to consider the hydraulic history of the soil, to ensure accurate prediction.

8.2 RECOMMENDATIONS

- The influence of temperature on water retention of compacted kaolin clay was observed only on a drying path. The wetting path of a SWRC is significantly different from the drying path, due to hydraulic hysteresis. It is recommended that the influence of temperature on the wetting path of compacted kaolin clay be studied at higher temperature values than was the case in this current study.

- This research was carried out on a narrow range of suction and temperature values, due to the limitations of the testing equipment. Extension of this work to higher temperature and suction ranges is recommended.
- Soil fabric plays a tremendous role in the behaviour of most soils and, in most cases, new fabric evolves with a change in stress path. Consequently, it is recommended that further studies be carried out to investigate the evolution of fabric associated with an increase in temperature of compacted kaolin especially at low suction values. Additionally, existing studies have demonstrated that loading results in the reduction of macro-pores and eventually micro-pores when all the macro-pores have closed. The macro-structural changes associated with the loading of the compacted kaolin clay need to be understood. The stress levels at which loading will affect the micro-pores need to be known.
- The relative hydraulic conductivity of compacted kaolin was estimated from SWRC using van Genuchten's hydraulic model. It is recommended to conduct saturated permeability tests at 50^{o}C to extend the data in terms of unsaturated permeability function.

REFERENCES

Abbeche, K., Hammoud, F. & Ayadat, T. (2007). Influence of relative density and clay fraction on soils collapse. *Experimental Unsaturated Soil Mechanics* [C], Springer Proceedings in Physics, 112, pp. 3-9.

Akesson, M., Jacinto, A. C., Gatabin, C., Sanchez, M. & Ledesma, A. (2009). Bentonite THM behaviour at high temperatures: experimental and numerical analysis. *Geotechnique.* 59(4), pp. 307-318.

Al-Homoud, A. S., Basma, A. A., Husein Malkawi, A. L. & Al Bashabsheh, M. A. (1995). Cyclic swelling behaviour of clays. *Journal of Geotechnical Engineering,* 121(7), pp. 562-565.

Alonso, E. E., Gens, A. & Hight, D.W. (1987). Special problem soils. General report: *Proc. 9th Eur. Conf. Soil Mech. and Foundation Eng. Dublin* 3, pp. 1087-1146.

Alonso, E.E., Gens, A. & Josa, A. (1990). A constitutive model for partially saturated soils. *Géotechnique,* 40(3), pp. 405-430.

Alonso, E.E., Lloret, A. Gens, A. & Yang, D. Q. (1995). Experimental behaviour of highly expansive double structure clay: *1st International conference on Unsaturated Soils, Paris*. 1, pp. 11-16.

Alonso, E.E., Romero, E., Hoffmann, C. & Garcia-Escudero, E. (2005). Expansive bentonite-sand mixture in cyclic controlled-suction drying and wetting. *Engineering Geology,* 81, pp. 213-226.

Alonso, E. E., Pinyol, N. M. & Puzrin, A. M. (2010). Geomechanics of Failures. Advanced Topics. [Online]. London: Springer. [10 January 2016]. http://link.springer.com/book/10.1007%2F978-90-481-3538-7.

Al Rawas, A. A. (1999). The factors controlling the expansive nature of the soils and rocks of northern Oman. *Engineering Geology, 53*, pp. 327 – 350.

Assouline, S., Tessier, D. & Bruand, A. (1998). A conceptual model of soil water retention curve. *Water Resource Research* 34(2), pp. 223-231.

Bachmann, J., Horton, R., Grant, S.A. & van der Ploeg, R. R. (2002). Temperature dependence of water retention curves for wettable and water repellent soils. *Soil Sci. Soc. Am. Journal*, 66(1), pp. 44-52.

Baker, R. & Frydman, S. (2009). Unsaturated soil mechanics critical review of physical foundations. *Engineering Geology*. 106: pp. 26-39.

Baldi, G., Hueckel, T. & Pellegrini, R. (1988). Thermal volume changes of mineral-water system in low porosity clay soils. *Canadian Geotechnical Journal*, 25, pp. 807-825.

Barbour, S.L. (1998). Nineteenth Canadian Geotechnical Colloquium: The soil-water characteristic curve: a historical perspective. *Canadian Geotechnical Journal*, 35, pp. 873-894.

Barden, L. & Sides, G. R. (1970). Engineering behaviour and structure of compacted clay. *Proceedings of American Society of Civil Engineers*, 9, pp. 1171-1200.

Barden, L., McGown, A. & Collins, K. (1973). The collapse mechanism in partly saturated soil. *Engineering Geology*, 7, pp. 49-60.

Bell, F. G., & Culshaw, M. G. (2001). Problem soils: a review from British perspective. In: *Proc. Symp. on Problematic Soils*, Nottingham Trent University, Thomas Telford, London, pp. 1-35.

Bishop, A. W. (1959). The principle of effective stress. *Teknik Ukeblad.* 39, pp. 859-863.

Bishop, A. W. & Donald, I. B. (1961). The experimental study of partly saturated soil in the triaxial apparatus. *Proceedings of 5th Int. Conf. on Soil Mechanics and Foundation Engineering, Paris*, 1, pp. 13 – 21.

Bishop, A. W. & Blight, G. E. (1963). Some aspects of effective stress in saturated and partly saturated soils. *Geotechnique*, 13(3), pp. 177 – 197.

Blatz, J., Cui, Y. J. & Oldecop, L. (2008). Vapor equilibrium and osmotic technique for suction control. *Geotechnical and Geological Engineering*, 26(6), pp. 661 – 673.

Brackley, I. J, (1975). A model for unsaturated clay structure and its application to swell behaviour. *Proceedings of 6th Regional Conference for Africa on Soil Mechanics and Foundation Engineering*, 1, pp. 71-79.

BRE (1993). Low-rise buildings on shrinkable clay soils: BRE Digest CRC, London, (240), pp. 241-242.

Brooks, R. H. & Corey, A.T. (1964). Hydraulic properties of porous medial, *Hydrology Paper 3*, Colorado State University.

Bulut, R., Lytton, R. L., & Warren, W. K. (2001). Suction measurements by filter paper method. *American Society of Civil Engineers, Geotechnical Special Publication*, 115, pp. 243-261.

Bulut, R. & Leong, E.C. (2008). Indirect measurement of suction. *Geotech. Geol. Eng.* 26, pp. 633-644.

Burland, J. B. (1964). Effective stress in partly saturated soils. *Geotechnique,* 14, pp. 64-68.

Burland, J. B. (1990). On the compressibility and shear strength of natural soils. *Geotechnique*, 40(3), pp. 329-378.

Burland, J.B. & Ridley, A. M. (1996). The importance of suction in soil mechanics, Keynote address. *Proceedings of the 12th Southeast Asian Geotechnical Conference*, 2, pp. 27 – 49.

Burton, G. J., Sheng, D. & Airey, D. (2014). Experimental study on volumetric behaviour of Maryland clay and the role of degree of saturation. *Canadian Geotechnical Journal*, 51, pp. 1449-1455.

Butterfield, R. (1979). A natural compression law for soils. *Geotechnique*, 29(4) pp. 469 -480.

Campanella, R. G. & Mitchell, J. R., (1968). Influence of temperature variation on soil behaviour. *Journal of Soil Mech. Found. Div., ASCE*, 94 (3), pp. 709-734.

Carter, M. & Bentley, S. P. (1991). Correlations of soil properties. *Pentech Press, London.*

Casagrande, A. (1936). The determination of the pre-consolidation load and its practical significance. *Proc. Of the First International Conference on Soil Mechanics and Foundation Engineering, Cambridge,* 3, pp. 60-64.

Cekerevac, C. (2003). *The thermal effects on the mechanical behaviour of saturated clays: an experimental and constitutive study*. PhD thesis. Ecole Polytechnique Federale de Lausanne.

Cekerevac, C. & Laloui, L. (2004). Experimental study of thermal effects on the mechanical behaviour of a clay. *International Journal for Numerical and Analytical Methods in Geomechanics.* 28(3), pp. 209-228.

Cekerevac, C. & Laloui, L. (2010). Experimental analysis of the cyclic behaviour of kaolin at high temperature. *Géotechniqu,* 60(8), pp. 651–655.

Chahal, R. S. (1964). Effect of temperature and trapped air on the energy status of water in porous media. *Soil Science,* 98, pp. 107-112.

Chahal, R. S. (1995). Effect of temperature and trapped air on matric suction. *Soil Science.* 100, pp. 262-266.

Chandler R.J. & Gutierrez C.I., (1986). The filter paper method of suction measurement, *Géotechnique*, 36(2), pp. 265-268.

Chandler, R. J., Crilly, M. S. & Montgomery-Smith, G. (1992). A low-cost method of assessing clay desiccation for low-rise buildings. *Proceedings Institute of Civil Engineering*, 92, pp. 82-89.

Chen, F. H., (1975). Foundations on expansive soils. 1st Edition, Elsevier, New York.

Childs, E. C. & Collis-George, N. (1950). Permeability of porous materials. *Proceedings of the Royal Society,* London. 201, pp. 392-405.

Cho, W. J., Lee, J. O. & Chun, K. S. (1999). The temperature effects on hydraulic conductivity of compacted bentonite. *Pllied Clay science*, 14, pp. 47-58.

Clarke, E. C. W. & Glew, D. N., (1985). Evaluation of the thermodynamic functions for aqueous sodium-chloride from equilibrium and calorimetric measurements. *J. Phys. Chem. Ref. Data*, 14, pp. 489-610.

Croney, D. (1952). The movement and distribution of water in soils. *Géotechnique*, 3(1), pp. 1-16.

Ctori, P. (1989). The effect of temperature on the physical properties of cohesive soils. *Ground Engineering,* 22(6), pp. 26-27.

Cunningham, M. R. (2000). *The mechanical behaviour of a reconstituted unsaturated soil*. PhD Thesis. Imperial College, University of London.

Cui, Y. J. & Delage, P. (1996). Yielding and plastic behaviour of unsaturated compacted silt. *Géotechnique,* 46, pp. 291-311.

Cui, Y. J., Sultan, N. & Delage, P. (2000). A thermo-mechanical model for saturated clays. *Can. Geotech. J.* 37(3), pp. 607–620.

Cui, Y. J., Yahia-Aissa, M. & Delage, P. (2002). A model for the volume change behaviour of heavily compacted swelling clays. *Engineering Geology,* 64, pp. 233-250.

Cui, Y. J., Tang, A. M., Loiseau, C. & Delage, P. (2008). Determining the unsaturated hydraulic conductivity of a compacted sand-bentonite mixture under constant volume and free-swell conditions. *Phys Chem. Earth, 33*, pp. 462-471.

Cui, Y. J. & Tang, M. J. (2013). On the chemo-thermo-hydro-mechanical behaviour of geological and engineered barrier. *Journal of Rock Mechanics and Geological Engineering,* 5, pp. 169-178.

Cuisinier, S. & Laloui, L. (2004). Fabric evolution during hydro-mechanical loading of compacted silt. *International Journal for Numerical and Analytical Methods in Geomechanics*, 28(6), pp. 483-499.

Cuisinier, O. & Masrouri, F. (2005). Hydro-mechanical behaviour of compacted swelling soil over a wide suction range. *Engineering Geology,* 81, pp. 204-212.

Davies, J. T. & Rideal, E. K. (1963). Interfacial Phenomena. *New York Academic*.

Delage, P. & Lefebvre, G., (1984). A study of structure of a sensitive Champlain clay and of its evolution during consolidation. *Canadian Geotechnical Journal,* 21(1), pp. 21-35.

Delage, P., Audiguier, M., Cui, Y. J. & Howat, M. (1996). Microstructure of a compacted silt. *Canadian Geotech. J.*, 33, pp. 150-158.

Delage, P., Howat, M. & Cui, Y. J. (1998). The relationship between suction and swelling properties in a heavily compacted unsaturated clay. *Eng. Geology*, 50(1-2), pp. 31-48.

Delage, P., Sultan, N. & Cui, Y. J. (2000). On the thermal consolidation of Boom clay. *Canadian Geotechnical Journal.* 37, pp. 343-354.

Delage, P., Cui, Y. J. & Antoine, P. (2005). Geotechnical problems related to loess deposits in Northern France. *Proceedings of International Conference on Problematic Soils, Famagusta, Cyprus. Pp.* 1-24.

Delage, P., Cui, Y. J. & Tang, A. M. (2010). Clays in radioactive waste disposal. *Journal of Rock Mechanics and Geotechnical Engineering,* 2(2), pp. 111-123.

Di Donna, A. & Laloui, L. (2015). Response of soils subjected to thermal cyclic loading: Experimental and constitutive study. *Engineering Geology*, 190, pp. 65-76.

El-Howayek. A, Huang, P., Bienett, R. & Santagata, M.C. (2011). *Identification and behaviour of collapsible soils*. JTRP Technical Report. Purdue University, Indiana.

Eriksson, L. G. (1989). Temperature effects on consolidation properties of sulphide clays. *Proceedings of the 12th International Conference on Soil Mechanics & Foundation Engineering,* Rio de Janeiro, Brazil, 3, pp. 2087-2090.

Estabragh, A. R., Javadi, A. A. & Boot, J.C. (2004). Effect of compaction pressure on consolidation behaviour of unsaturated silty soils. *Canadian Geotechnical Journal,* 41(3), pp. 540-550.

Estabragh, A. R., Pereshkafti M. R. S., Parsaei, B. & Javadi, A. A. (2013). Stabilised expansive soil behaviour during wetting and drying. *International Journal of Pavement Engineering*. 14(4), pp. 418 – 427.

Farulla, C. A., Ferrari, A. & Romero, E., (2010). Volume change behaviour of compacted scaly clay during cyclic suction changes. *Canadian geotechnical journal*, 47, pp. 688–703.

Faybishenko, B. (1983). Effect of temperature on moisture content, entropy and water pressure in loam soils. *Pochvevedenie,* 12.

Feng, M. & Fredlund, D. G. (1999). Hysteretic influence associated with thermal conductivity suction measurements. *Proceeding from Theory to the Practice of Unsaturated Soil Mechanics*, pp. 14-20.

Folly. W.P.J. (2001). *Thermo-hydro-mechanical behaviour of unsaturated soils: an experimental study.* PhD Thesis, Cardiff University.

Folly, J. P. W. & Rees, S. W. (2001). One dimensional testing of partly saturated soils at elevated temperatures. Preliminary results. *Geo-environmental Impact Management, Thomas Telford, London.*

Francoise, B., Salager, S. & El Youssoufi, M.S. (2007). Compression tests on sandy silt at different suction and temperature levels. *ASCE Geotech. Spe. Publ.,* 157, pp. 1-10.

Francios, B. (2008). *Thermo plasticity of fine grained soil at various saturation states: application to nuclear waste disposal*. PhD Thesis. Universite de Liege.

Fredlund, D. G. & Morgenstern, N. R. (1976). Constitutive relation for volume change in unsaturated soils. *Canadian Geotech. J,* 13, pp. 261-276.

Fredlund, D. G. & Morgenstern, N. R. (1977). Stress state variables for unsaturated soils. *J. Geotech. Eng. Div., ASCE*. 103(5), pp. 447-466.

Fredlund, D. G., Morgenstern, N.R. & Widger, R. A. (1978). Shear strength of unsaturated soils. *Canadian Geotechnical Journal,* 15, pp. 313-321.

Fredlund, D. G., (1985). Soil mechanics principles that embrace unsaturated soils. *Proc. 11th Int. Conf. Soil Mech. Found. Eng., San Francisco*. 2, pp. 465-472.

Fredlund, D. G. & Rahardjo, H. (1993). Soil mechanics for unsaturated soils. *John Wiley and Sons*.

Fredlund, D. G. & Xing, A. (1994). Equations for the soil-water characteristic curve. *Canadian Geotechnical Journal,* 31(4), pp. 521-532.

Fredlund, D.G., Xing, A., Fredlund, M. D. & Barbour, S.L. (1996). The relationship of the unsaturated soil shear strength to the soil-water characteristic curve. *Canadian Geotech. J.*, 33(3), pp. 440-448.

Fredlund, M.D., Fredlund, D.G. & Wilson, G.W. (1997). Prediction of the soil water characteristic curve from grain-size distribution and volume mass properties. *Proceeding of the 3rd Brazilian Symposium on unsaturated soils*, Rio de Janerio, Brazil, 1, pp. 13-23.

Fredlund, D. G. (2000). The Implementation of unsaturated soil mechanics into geotechnical engineering. *Canadian Geotechnical Journal*, 37, pp. 963-986.

Fredlund, D. G., Rahardjo, H., Leonge, E. C. & Ng, C. W. W. (2001). Suggestions and recommendations for the interpretation of soil-water characteristic curves. *Proc. 14th Southeast Asian Geotech. Conf.* Hong Kong, (1), pp. 503-508.

Fredlund D. G. (2002). Use of soil water characteristic curve in the implementation of unsaturated soil mechanics. *Proceeding Third International Conference on Unsaturated Soils. Recife Brazil*, 3, pp.1-16.

Fredlund, D. G., Sheng, D. & Zhao, J. (2011). Estimation of soil suction from soil-water characteristic curve. *Canadian Geotechnical Journal.* 48(2), pp. 186-198.

Fredlund, D. G., Rahardjo, H. & Fredlund, M.D. (2012). Unsaturated soil mechanics in Engineering practice. *John Wiley and Sons*.

Gallage, C., Kodikara, J. & Uchimura, T. (2013). Laboratory measurement of hydraulic conductivity functions of two unsaturated sandy soils during drying and wetting. *Soils and Foundations*, 53, pp. 417-430.

Gallipoli, D., Gens, A., Sharma, R. & Vaunat, J. (2003). An elastoplastic model for unsaturated soil incorporating the effect of suction and degree of saturation on mechanical behaviour. *Geotechnique*, 53, pp. 123-136.

Gao, Y., Sun, D. & Zhou, A. (2016). Hydromechanical behaviour of unsaturated soil with different specimen preparations. *Canadian Geotechnical Journal*, 53(6), pp. 909-917.

Gardner, W. R. (1955). Relation of temperature to moisture tension of soil. *Soil Science*,79, pp. 257-265.

Gardner, R. (1958). Some steady state solutions of unsaturated moisture flow equations with applications to evaporation from a water table. *Soil Science Journal*, 85, pp. 228-232.

Gens, A. & Alonso, E. E., (1992). A framework for the behaviour of unsaturated expansive clays. *Canadian Geotechnical Journal,* 29, pp. 1013-1032.

Gens, A., Alonso, E.E., Suriol, J. & Lloret, A. (1995). Effect of structure on the volumetric behaviour of compacted soils. *Proc. Ist Int. Conf. on Unsaturated Soils, Paris*. Pp. 83-88.

Gens, A., Vaunat, J., Gatitte, B. & Wileveau, Y. (2007). In situ behaviour of a stiff layered clay subjected to thermal loading: Observation and interpretation. *Geotechnique*, 57(2), pp. 207-228.

Grim, R.E. (1962). *Applied clay mineralogy,* McGraw-Hill, New York.

Haghighi, A. (2011). *Thermo-Hydro-Mechanical behaviour of kaolin Clay*. PhD Thesis. Heriot-Watt University.

Head, K. H. (2006). Manual of soil laboratory testing. (1) *Whittles Publishing, Caithness, Scotland.*

Hopman, W. J. & Dane, J.H. (1986). Temperature dependence of soil water retention curves. *Soil Science of American Journal,*50, pp. 562-567.

Houston, S. L., Houston, W. N. & Spadola, D. J. (1988). Prediction of field collapse of soils due to wetting. *Journal of Geotechnical Engineering,* 114, pp. 40-50.

Houston, S.L., Houston, W.N. & Wagner, A. (1994). Laboratory filter paper suction measurements. *Geotechnical Testing Journal*, 17, pp. 185-194.

Houston, S. L. Houston, W. N. Zapata, C. E. & Lawrence, C. (2001). Geotechnical engineering practice for collapsible soils. *Geotechnical and Geological Engineering,* 19, pp. 333 – 355.

Hilf, J. W., (1956). An investigation of pore water pressure in compacted cohesive soils. *Technical Memorandum, United States Department of the interior Bureau of Reclamation, Design and Construction Division*. Denver. No 65.

Hu, Y. & Liu, X. (2003). Chemical composition and surface property of kaolin. *Minerals Engineering,* 16, pp. 1279-1284.

Ileme, O.M., Medero, G.M. & Woodward, P.K. (2016). Effect of temperature on volume change behaviour of statically compacted kaolin clay. In: *3rd European Conference on Unsaturated soil*, Paris.

Jacinto, A.C., Villar, M.V., Gomez-Espina, R. & Ledesma, A. (2009). Adaptation of the van Genuchten expression to the effects of temperature and density for compacted bentonites. *Applied Clay Science*, Elsevier, 42, pp. 575-582.

Jefferson, I. (1994). *Temperature effects on clay soils*. PhD Thesis, Loughborough University of Technology.

Jennings, J. E. B. & Knight, K. (1957). Prediction of total heave from the double oedometer test. *Proc. Symp. Expansive Clays South African Inst. of Civil Engineers*, Johannesburg, 7(9), pp. 13-19.

Jennings, J. E. B. & Burland, J. B. (1962). Limitations to the use of effective stresses in partly saturated soil. *Géotechnique*. 12(2), pp. 125-144.

Jones, L. D. & Jefferson, L. (n.d). Expansive soils: Institute of Civil Engineers Manual series, [Online], Available: https://core.ac.uk/download/files/79/386982.pdf [26 February 2016]

Josa, A., Balmaceda, A., Gens, A. & Alonso, E. E. (1992). An elastoplastic model for partially saturated soils a maximum of collapse. *Proc. 3rd International Computational Plasticity, Barcelona*, pp.815-826.

Jotisankasa, A. (2005). *Collapse behaviour of compacted silty clay*. PhD thesis. Imperial College London.

Jotisankasa, A., Ridley, A. & Coop, M. (2007). Collapse behaviour of compacted clay in suction monitored oedometer apparatus. *J. Geotech. Geoenviron. Eng.*, 133(7), pp. 867-877.

Jotisankasa, A., Coop, M. & Ridley, A. (2009). The mechanical behaviour of unsaturated compacted silty clay. *Geotechnique*, 59, pp. 415–428.

Juang, C. H. & Holtz, R. D. (1986). Fabric, pore size distribution and permeability of sandy soils. *J. Geotech. Engng, ASCE.* 112(9), 855–868.

Karube, D., Kato, S., Hamada, K. & Honda, M. (1995). The relationship between the mechanical behaviour and the state of pore-water in unsaturated soil. *Journal of Japanese Society of Civil Eng.,* 535, pp. 83-92.

Karube, K., & Kawai, D. (2001). Role of pore water in mechanical behaviour of unsaturated soil. *Geotechnical and Geological Engineering*, pp. 211-241.

Kasangaki, G. J. (2012). *Experimental study on the hydro-mechanical behaviour of granular soils.* PhD Thesis, Heriot-Watt University.

Kennedy, J. (2011). *A full-scale laboratory investigation into railway track substructure performance and ballast reinforcement*. PhD Thesis, Heriot-watt University.

Khalili, N., Geiser, F. & Blight, G. E. (2004). Effective stress in unsaturated soils: Review with new evidence. *International Journal of Geomechanics.* 4(2), pp. 115-126.

Kholghifard, M., Ahmad, K., Ali, N., Kassim, A., Kalatehjari, R. & Babakanpour, F. (2014). Temperature effect on compression and collapsibility of residual granite soil. *GRADEVINAR*, 66(3), pp. 1-10.

Kim, B. S., Shibuya, S., Park, S.W. & Kato, S. (2010). Application of suction stress for estimating unsaturated shear strength of soils using direct shear testing under low confining pressure. *Canadian Geotechnical Journal.* 47, pp. 955-970.

Koliji, A., Laloui, L., Cusinier, O. & Vulliet, L. (2010). Suction induced effect on the fabric of a structured soil. *Transport in Porous Media* 64: pp. 261- 278.

Koliji, A., Vulliet, L. & Laloui, L. (2010). Structural characterisation of unsaturated soils. *Canadian Geotechnical Journal* 47: pp. 297-311.

Krahn, J., and Fredlund, D. G. (1972). On total matric and osmotic suction. *Journal of Soil Science Journal*, 114(5), pp. 339–348.

Krenz, J., Lee, B. & Owens, P. (n.d), Swelling clays and septic system, [Online], Available: https://www.extension.purdue.edu/extmedia/rw/rw-3-w.pdf [26 February 2016]

Laloui, L., Francois, B., Nuth, M., Peron, H. & Koliji, A. (2008). A thermo-hydro-mechanical stress-strain framework for modeling the performance of clay barriers in

deep geological repositories for radioactive waste. *Proceedings of the 5th International Conference on Unsaturated Soil, Barcelona*, pp. 63-80.

Lawton, E. C., Fragaszy, R. J. & Hardcastle, J. H. (1989). Collapse of compacted clayey sand. *J. Geotech. Engrg., 115(9)*, pp. 1252 – 1267.

Lawton, E. C., Fragaszy, R. J. & Hetherington, M. D. (1992). Review of wetting induced collapse in compacted soil. *J. Geotech. Engrg., 118(9)*, pp. 1376 – 1394.

Leong, E.C. & Rahardjo, H., (1997). Review of soil-water characteristic curve equations, *Journal of Geotechnical and Geoenvironmental Engineering, ASCE*, 123(12), pp. 1106-1117.

Leong, E. C., He, L. & Rahardjo, H. (2002). Factors affecting the filter paper method for total and matric suction measurements. *Geotechnical Testing Journal*, 25(3), pp. 322-333.

Leroueil, S. & Vaughan, P.R. (1990). The general and congruent effect of structure in natural soils and weak rocks. *Geotechnique*, 40(3), pp. 467-488.

Leroueil, S. & Marques, M.E.S. (1996). Importance of strain rate and temperature effects in geotechnical engineering (State-of the-art). *ASCE Geotechnical Publication*, 61, pp. 1-59.

Li, X. & Zhang, L. M. (2009). Characterization of dual-structure pore-size distribution of soil. *Can. Geotech. J.*, 46, pp. 129-141.

Liu, Z., Liu, F., Ma, F., Wang, M., Bai, X., Zheng, Y., Yin, H. & Zhang, G. (2016). Collapsibility, composition and microstructure of Loess in China. *Canadian Geotechnical Journal*, 53, pp. 673-689.

Lloret, A., & Alonso, E. E. (1980). Consolidation of unsaturated soils including swelling and collapse behaviour. *Geotechnique*, 30(4), pp. 449–477.

Lloret, A., Villar, M. V., Sa´nchez, M., Gens, A., Pintado, X. & Alonso, E. E. (2003). Mechanical behaviour of heavily compacted bentonite under high suction changes. *Geotechnique*, 53, pp. 27–40

Lloret, A. & Villar, M. V. (2007). Advances on the knowledge of thermo-hydro-mechanical behaviour of heavily compacted FEBEX bentonite. *Physics and Chemistry of the Earth,* 32, pp. 701–715.

Lobbezoo, J.P. & Vanapalli, S.K**.** (2002). A simple technique for estimating the coefficient of permeability of unsaturated soils. *Proceedings of the 55th Canadian Geotechnical Conference*, Niagara Falls, pp. 1277-1284.

Loiseau, C. (2001). *Water transfers and hydro-mechanical couplings in engineered barriers.* PhD Thesis, CERMES/ENPC, France.

Lu, N. and Likos, W.J. (2004). Unsaturated Soil Mechanics. John Wiley and Sons.

Malaya, C. (2011). A laboratory procedure for measuring high soil suction. *Geotechnical Testing Journal*, 34, pp. 396.

Marinho, F.A.M. and Oliveira, O.M. (2006). Filter paper method revisited. *Geotechnical Testing Journal*, 29, pp. 250-258.

Marihno, F.A.M., Take, W.A. & Tarantino, A. (2008). Measurement of matric suction using tensiometric and axis translation techniques. *Journal of Geotechnical and Geological Engineering,* Springer, 26, pp. 615-631.

Marinho, F. A. M. & Da Silva Gomes J. E. (2012). The effect of contact on the filter paper method for measuring soil suction. *Geotechnical Testing Journal*, 35(1).

Matyas, E. L. & Radhakrishna, H. S. (1968). Volume change characteristics of partially saturated soils. *Geotechnique,* 18(4), pp. 432-448.

Medero G.M., Schnaid F., Gehling W.Y.Y. & Gallipoli D. (2003). Analysis of the mechanical response of an artificial collapsible soil. *Proc. From Experimental Evidence towards Numerical Modelling of Unsaturated Soils, Berlin*, pp. 135-145.

Medero, G. M., Schnaid, F. & Gehling, Y. Y., (2009). Oedometer behaviour of an artificial cemented highly collapsible soil. *Journal of Geotechnical and Geoenvironmental Engineering,* 135, pp. 840–843.

Miller, C. J., Yesiller, N., Yaldo, K. & Merayyan, S. (2002). Impact of soil type and compaction conditions on soil water characteristic. *Journal of Geotechnical and Geoenvironmental Engineering,* 9, pp. 733–742.

Miranda-Trevino, J. C. & Coles, C. A. (2003). Kaolinite properties, structure and influence of metal retention on pH. *Applied Clay Science,* 23, pp.133–139.

Mitchell, J. K. (1993) Fundamentals of Soil Behaviour. *John Wiley & Sons,* New York

Monroy, R., Zdravkovic, L. & Ridley, A. (2007). Fabric changes in compacted London due to variations in applied stress and suction. *Experimental Unsaturated soils; Springers Proceeding in Physics,* 112, pp. 41– 47.

Monroy, R. Zdravkovic, L. & Ridley, A. (2005). Fabric changes in compacted London clay due to variations in applied stress and suction. *Experimental Unsaturated Soil Mechanics*, Springers, pp. 41-48.

Monroy, R. Zdravkovic, L. & Ridley, A. (2010). Evolution of microstructure in compacted London clay during wetting and loading. *Geotechnique,* 60(2), pp. 105 – 119.

Montanez, J. E. C. (2002). *Suction and volume changes of compacted sand-bentonite mixtures*. PhD Thesis. Imperial College London.

Mualem Y. (1976). A new model for predicting the hydraulic conductivity of unsaturated porous media, *Water Resources Research,* 12, pp. 513-522.

Munoz-Castelblanco, J., Delage, P., Pereira, J.M. & Cui, Y.J. (2011). Some aspects of the compression and collapse behaviour of an unsaturated natural loess. *Geotechnique Letters,* 1, pp. 17-22.

Nam, S., Gutierrez, M., Diplas, P., Petrie, J., Wayllace, A., Lu, N. & Muñoz, J. J. (2010). Comparison of testing techniques and models for establishing the SWCC of riverbank soils. *Engineering Geology,* 110, pp. 1-10.

Navaneethan, T., Sivakumar, V., Wheeler, S. J. & Doran, I. G. (2005). Assessment of suction measurements in saturated clays. *Proceedings of the ICE - Geotechnical Engineering,* 158(1), pp. 15 – 24.

Navarro, V & Alonso, E. E. (2000). Modelling swelling soils for disposal barriers. *Computer and Geotechnics,* 27, pp. 19 – 43.

Ng C.W.W., Menzies B., 2007. Advanced unsaturated soil mechanics and engineering, *Taylor and Francis,* Abingdon, United Kingdom.

Ng, C. W. W. & Zhou, C. (2014). Cyclic behaviour of unsaturated silt at various suction and temperature. *Geotechnique,* 64(9), pp. 709–720.

Nimmo, J.R. & Miller, E.E. (1986). The temperature dependence of isothermal moisture vs. potential characteristics of soils. *Soil Sci. Soc. Am. J.* 50, pp. 1105-1113.

Nimmo, J. R. (1991). Comment on the treatment of residual water content in "A consistent set of parametric models for the two-phase of immiscible fluids in the subsurface. *Water Resource Res.,* 27, pp. 661-662.

Noorany, I. (1992). Stress ratio effect on the collapse of compacted clayey sand-discussion. *Journal of Geotechnical Engineering,* ASCE, 118(9), pp. 1472-1473.

O'Sullivan, D. & Quigley, P. (2003). Geotechnical engineering and some environmental aspects of clay liners for landfill projects. *Fehily Timoney & Co. & Irish* [online] *Geotechnical Services Ltd.* Available at: http://citeseerx.ist.psu.edu/viewdoc/pdf [Accessed:23 March 2017].

Paaswell, R. E. (1967). Temperature effects on clay soil consolidation. *Journal of Soil Mechanics and Foundation Division, ASCE,* 93(3), pp. 9 – 22.

Peak, A. J. (1960). Change of moisture tension with temperature and air pressure: theoretical. *Soil Science,* 89, pp. 303-310.

Pestana, J. M. & Whittle, A. J. Compression model for cohesionless soil. *Geotechnique,*45(4), pp. 611-631.

Pham, H. Q., Fredlund, D. G. & Barbour, S. L. (2003). A practical hysteresis model for the soil-water characteristic curve for soils with negligible volume. *Geotechnique,* 53(2), pp. 293-298.

Pham, H. Q., Fredlund, D. G. & Barbour, S. L. (2005). A study on the hysteresis models for the soil-water characteristic curve. *Canadian Geotechnical Journal,* 42(6), pp. 1548-1568.

Philip, J.R. & de Vries, D.A. (1957). Moisture movement in porous materials under temperature gradients. *AGU Transactions,* 38, pp. 222-232.

Pintado, X., Lloret A. & Romero, E. (2009). Assessment of the use of the vapour equilibrium technique in controlled-suction tests. *Can. Geotech. J.*,46, pp. 411- 423

Pintado, X., Lloret, A. & Romero, E. (2014). Assessment of the use of vapour equilibrium technique in controlled-suction tests. *Can. Geotech. J. 46,* pp. 411–423.

Pusch, R. (1980). Permeability of highly compacted bentonite. SKB Technical Report. *Swedish Nuclear Fuel and Waste Management.* pp. 29-30

Pusch, R., Moreno, L. (2001). Saturation and permeation of buffer clay. *Proc. 6th Int. Workshop Key Issues in Waste Isolation Research, Paris,* pp. 71–81.

Rabbi, A.T.M.Z, Cameron, D.A. & Rahman, M.M. (2014). Role of matric suction on wetting-induced collapse settlement of silty sand. In: *International Conference on Unsaturated Soils: Research & Applications, Sydney, Australia.*

Rahardjo, H. & Fredlund, D. G. (2003). Ko volume characteristic of an unsaturated soil with respect to various loading paths. *ASTM Geotechnical Testing Journal,* 26(1), pp. 79–91.

Randy Rainwater, N. (2012). Measurement of total soil suction using filter paper: Investigation of Common Filter Papers, Alternative Media, and Corresponding Confidence, pp. 35: 1

Rao, S. M. & Thyagaraj, T. (2003). Lime slurry stabilisation of an expansive soil. *Proceedings of the Institute of Civil Engineering: Geotechnical Engineering,* 156, pp. 139-146.

Raveendiraraj, A. (2009). *Coupling of mechanical behaviour and water retention behaviour in unsaturated soils*. PhD Thesis. University of Glasgow.

Ridley, A. M. & Burland, J. B. (1993). A new instrument for measurement of soil suction. *Geotechnique,* 43, pp. 321–324.

Ridley, A. M. & Burland, J.B. (1995). Measurement of suction in materials which swell. *Appl. Mech. Rev.,* 48(9), pp.727-732.

Ridley, A. M., Dineen, K. & Burland, J. B. & Vaughan, P. R. (2003). Soil matrix suction: some examples of its measurement and application in geotechnical engineering, *Géotechnique,* 53(2), pp. 241-253.

Rios, S., Viana da Fonseca A. & Baudet, B. A. (2012). Effect of porosity/cement ratio on the compression of cemented soil. *Journal of Geotechnical and Geo-Environmental Engineering*, 138, pp. 1422-1426.

Romero, E. (1999). *Characterisation and hydro-mechanical-behaviour of unsaturated Boom clay: an experimental study*. PhD Thesis. Universitat Politecnica De Catalunya.

Romero, E. & Vaunat, J. (2000). Retention curves of deformable clays. In: *Experimental Evidence and Theoretical Approaches in Unsaturated Soils.* Rotterdam: Balkema, pp. 91-106.

Romero, E., Gens, A. & Lloret, A. (2001). Temperature effects on the hydraulic behavior of an unsaturated clay. *Geotechnical and Geological Engineering,* 19, pp. 311– 332.

Romero, E., Gens, A. and Lloret, A. (2003). Suction effects on compacted clay under non-isothermal condition. *Geotechnique*, 53, pp. 65–81.

Romero, E., Villar, M. V. & Lloret, A. (2005). Thermo-hydro-mechanical behaviour of two heavily overconsolidated clays. *Engineering Geology*, 81, pp. 255–268.

Romero, E., Della Vecchia, G. & Jommi, C. (2011). An insight into the water retention properties of compacted clayey soils. *Geotechnique*, 61(4), pp. 313–328.

Rowe, P.W. (1972). The relevance of soil fabric to site investigation. *Geotechnique* 22(2), pp. 195-200.

Salager, S., Francois, B., El Youssoufi, M. S., Laloui, L. & Saix, C. (2008). Experimental investigation of temperature and suction effects on compressibility and preconsolidation pressure of a sandy silt. *Soils and Foundations*, 48(4), pp. 453-466.

Sharma, S. R. (1998), *Mechanical behaviour of unsaturated highly expansive clay.* PhD thesis. University of Oxford.

Sharma, S. R. & Wheeler, S. J. (2000). Behaviour of unsaturated highly expansive clay during cycles of wetting and drying. *In Unsaturated Soils for Asia*, pp. 721-726.

Sherwood, P.T. & Ryley, D. M. (1968). An examination of cone-penetration methods for determining the liquid limit of soils. *TRRL Report LR233, Transport and Road Research Laboratory*, Crowthorne, Berks.

Shipton, B. & Coop, M. R. (2012). On the compression behaviour of reconstituted soils. *Soils and Foundations* 52(4), pp. 668-681.

Shuai, F. Clements, C., Ryland, L. & Fredlund, D. G. (2002). Some factors that influence soil suction measurements using a thermal conductivity sensor. *Proceedings of the Third International Conference on Unsaturated Soils,* Recife, Brazil, pp. 325-329.

Simms, P. H. and Yanful, E. K. (2001), Measurement and estimation of pore shrinkage and pore distribution in a clayey till during soil-water characteristic curve tests. *Can. Geotech. J.* 38(4), pp. 741–754.

Sivakumar, V. (1993). *A critical state framework for unsaturated soil*. PhD thesis. University of Sheffield.

Sivakumar, V. & S. J. Wheeler, (2000). Influence of compaction procedure on the mechanical behaviour of an unsaturated: Wetting and isotropic compression. *Geotechnique,* 50(4), pp. 359-368.

Skempton, A. W. & Bjerrum, L. (1957). A contribution to settlement analysis of foundations on clay. *Geotechnique,* 7(4), pp. 168-178.

Skempton, A.W. (1985). Residual strength of clays in landslides, folded strata and the laboratory. *Geotechnique* 35(1), pp. 1-18.

Spark, A. D. W. (1963). Theoretical considerations of stress equation for partially saturated soils. *Proc. 3rd African Conf. Soil Mech. Found. Eng., Salisbury, Rhodesia.* 1, pp. 215-218.

Sun, D. Sheng, D. & Xu, Y. (2007). Collapse behaviour of unsaturated compacted soil with different initial densities. *Canadian Geotechnical Journal,* 44, pp. 673-686.

Suriol, J., Gens, A. & Alonso, E.E. (1998). Behaviour of compacted soils in suction controlled oedometer. *Proc. 2nd Int. Conf. on Unsaturated Soils,* Beijing 1, pp. 463 - 443.

Tang A., Cui, Y. & Nathalie, B. (2008). Thermo-mechanical behaviour of a compacted swelling clay. *Geotechnique,* 58(1), pp. 45–54

Tarantino, A. & Mongiovi, L. (2000). Experimental investigations on the stress variables governing unsaturated soil behaviour at medium to high degrees of saturation. *Proc. Of an International Workshop, Trento, Italy*. Rotterdam.

Tarantino, A. & Tombolato, S. (2005). Coupling of hydraulic and mechanical behaviour in unsaturated compacted clay. *Geotechnique*, 55, pp. 307–317.

Tarantino, A. & De Col, E. (2008). Compaction behaviour of clay. *Geotechnique*, 58(3), pp. 199–213.

Tarantino, A. (2009). Water retention model for deformable soil. *Geotechnique*, 59, pp. 751–762.

Terzaghi, K. (1936) The shearing resistance of saturated soils and the angle between the planes of shear. *Proc. Ist Int. Conf. Soil Mech. Fnd. Eng., Cambridge.*

Thom, R., Sivakumar, R., Sivakumar, V., Murray, E.J. & Mackinnon, P. (2007). Pore size distribution of unsaturated compacted kaolin: the initial state and final state following saturation. *Geotechnique*, 57, pp. 469–474.

Tinjum, J. M., Benson, C.H. & Blotz, L. R. (1997). Soil water characteristic curve for compacted clay. *J. Geotech. Geoenviron,* 123, pp. 1060-1069.

Towhata, I., Kuntiwattanakul, P., Seko, I. & Ohishi, K. (1993). Volume change of clays induced by heating as observed in consolidation tests. *Soils and Foundations*,33(4), pp. 170-183.

Tsutsumi, A. & Tanaka, H. (2012). Combined effects of strain rate and temperature on consolidation behaviour of clayey soil. *Soils and Foundations,* 52(2), pp. 207-215.

Uchaipichat, A. & Khalili, N. (2009). Experimental investigation of thermo-hydro-mechanical behaviour of unsaturated silt. *Geotechnique*, 59, pp. 339–353.

van Genuchten, M.Th. (1980). A closed form equation for predicting the hydraulic conductivity of unsaturated soils. *Soil Science Society of the America Journal*, 44, pp. 892-898.

Vanapalli, S. K., Fredlund, D. G. & Pufahl, D. E. (1996). The relationship between Soil-water characteristic curve and unsaturated shear strength of a compacted Glacial till. *Geotechnical Testing Journal,* pp.259-268.

Vanapalli, S. K. & Pufahl, D. E. & Fredlund, D. G. (1999). The influence of soil structure and stress history on the soil water characteristics of a compacted till. *Geotechnique,* 49, pp. 143-159.

Vanapalli, S.K., Nicotera, M.V. & Sharma, R.S. (2008). Axis translation and negative water column techniques for suction control. *Journal of Geotechnical and Geological Engineering*, pp. 645-660.

Vanoudheusden, E., Sultan, N. & Cochonat, P. (2003). Hydro mechanical behaviour of gassy soils: *1st International conference on Submarine Mass Movement and their Consequences*: Kluwer academic publishers, Netherlands, pp.145-153.

Venkatarama, Reddy, B. V. & Jagadish, K. S. (1993). The static compaction of soils. *Geotechnique,* 43(2), pp. 337-341.

Villar, M. V. & Lloret, A. (2004). Influence of temperature on the hydro-mechanical behaviour of a compacted bentonite. *Applied Clay Science.* 26(1), pp. 337-350.

Villar, M. V. & Gomez-Espina, R. (2007). Retention curves of two bentonites at high temperature. *In Experimental Unsaturated Soil Mechanics. Springer Proceedings in Physics, Berlin,* 112, pp. 267-274.

Walker, S.C, Gallipoli, D. & Toll, D.G. (2005). The effect of structure on the water retention of soil tested using different methods of suction measurement. *Advanced Experimental Unsaturated Soil Mechanics*. Taylor and Francis Group, London.

Wang, L. B. & Frost, J. D. (2004). Dissipated strain energy method for determining pre-consolidation pressure. *Canadian Geotechnical Journal,* 41(4), pp. 760-768.

Wersin, P., Johnson, L. H. & McKinley, I.G. (2007). Performance of bentonite barrier at temperature beyond 100^{o}C: a critical review. *Physics and Chemistry of Earth,* 32, pp. 780-788.

Westsik, J. H., Hodges, F. N, Kuhn, W. L. & Myers, T. R. (1983). Water migration through compacted bentonite backfills for containment of high level nuclear waste. *Nuclear and Chemical Waste Management*, 4, pp. 291-299.

Wheeler, S.J. (1986). *Stress-strain behaviour of soils containing gas bubbles*. PhD thesis, University of Oxford.

Wheeler, S. J. (1988). A conceptual model for soils containing large gas bubbles. *Geotechnique.* 38: 389-397.

Wheeler, S. J. & Sivakumar, V. (1995). An elasto-plastic critical state framework for unsaturated soil. *Geotechnique.* 45: 35-53.

Wheeler, S. J. & Karube, D. (1996). Constitutive modelling. *Proceedings of the First International Conference on Unsaturated Soils, Paris,* 3, pp.1323 -1356.

Wheeler, S. J. & Sivarkumar, V. (2000). The influence of compaction procedure on the mechanical behaviour of an unsaturated compacted clay: Part 1. *Geotechnique,* 50(4), pp. -368.

Wheeler, S. J. (2010). Mechanics of unsaturated soils. *Introduction to Geotechnical Engineering.* University of Strathclyde.

Wraith, J. M. & Or, D. (1998). Nonlinear parameter estimation using spreadsheet software. *J. Nat. Resour. Life Sci. Educ.*, 27, pp. 13-19.

Wroth, C. P. & Houslby, G. T. (1985). Soil mechanics: property characterization and analysis procedure. *Proc. 11th ICSMFE, San Francisco,* 1, pp. 1-55.

Yang, H., Rahardjo, H., Leong, E. C & Fredlund, D. G. (2004). Factors affecting drying and wetting soil-water characteristic curves of sandy soils. *Canadian Geotechnical Journal,* 41, pp. 908-920.

Yang, S. R., Lin, H. D., Kung, J. H. S. & Huang, W. H. (2008). Suction controlled laboratory testing on resilient modulus of unsaturated compacted subgrade soils. *Journal of Geotechnical and Geoenvironmental Engineering, ASCE,* 134(9), pp. 1375-1384.

Ye, W.M., Chen, Y.G., Chen, B., Wang, Q. & Wang, J. (2010). Advances on the knowledge of the buffer/backfill properties of heavily compacted GMZ bentonite. *Eng. Geo.* 116(1-2), pp. 12-20.

Ye, W. M., Wan, M., Chen, B., Chen, Y.G., Cui, Y. J. & Wang, J. (2012). Temperature effects on the unsaturated permeability of densely compacted GMZ01 bentonite under confined conditions. *Eng. Geo.*, 126, pp. 1-7.

Ye, W. M., Zhang, Y. W., Chen, Y. G. & Cui, Y. J. (2013). Experimental investigation on the thermal volumetric behavior of highly compacted GMZ01 Bent. *Applied Clay Science.* 83-84: pp. 210-216.

Yong, R. N. (1999). Overview of modeling of clay microstructure and interactions for prediction of waste isolation barrier performance. *Engineering Geology*. 54 pp. 83-91.

Zakaria, I. (1994). *Yielding of unsaturated soils*. PhD thesis. University of Sheffield.

Zhang, F., Zhang, Z. Z., Low, P. F. & Roth, C. B. (1993) The effect of temperature on the swelling of montmorillonite. *Clay Minerals*, 28, pp. 25 -31.

Zhang, M., Zhang, H. Zhou, L. & Jia, L. (2013). Temperature effects on unsaturated hydraulic property of bentonite-sand buffer backfilling mixture. *J. of Wuhan University of Technology-Mater, pp.* 487-490.